Swansea University
Prifysgol Abertawe

Targeting Ferroptosis in Tuberous Sclerosis cell line models

Thesis submitted for the degree of Doctor of Philosophy

2025

TASMIA TAHSIN

[redacted]

Declaration

This work has not been submitted in substance for any other degree or award at this or any other university or place of learning, nor is being submitted concurrently in candidature for any degree or other award.

Signed ……Tasmia Tahsin…….. (candidate) Date …23-06-2025…

STATEMENT 1

This thesis is being submitted in partial fulfilment of the requirements for the degree of **PhD**

Signed …… Tasmia Tahsin (candidate) Date ……23-06-2025……

STATEMENT 2

This thesis is the result of my own independent work/investigation, except where otherwise stated.

Other sources are acknowledged by explicit references. The views expressed are my own.

Signed … Tasmia Tahsin (candidate) Date …23-06-2025

STATEMENT 3

I hereby give consent for my thesis, if accepted, to be available online in the University's Open Access repository and for inter-library loan, and for the title and summary to be made available to outside organisations.

Signed … Tasmia Tahsin … (candidate) Date …23-06-2025

Acknowledgements

Pursuing a PhD has been both a challenging and rewarding experience. I am fortunate to have undertaken my PhD in collaboration with North Wales and South Wales (Swansea and Cardiff University Medical School). Throughout this project, I have received invaluable support from many individuals at the Maelor Academic Unit of Medical & Surgical Sciences (MAUMSS) lab, where I was based.

First and foremost, I would like to express my gratitude to my supervisors, Prof. Andrew Tee, Steve Conlan, Mr. David Davies, and Stephen Hughes, for their training, support, and guidance throughout my PhD journey. I am especially thankful to Prof. Andrew Tee and Mr. David Davies for their professional and personal support during the challenging moments of my studies. Their mentorship, encouragement, and friendship have been invaluable and went far beyond their roles as supervisors.

I would also like to thank KESS2 for funding this research and for being so understanding of the difficulties arising from the COVID-19 pandemic and my maternity leave afterwards.

A special thanks to Prof. Stephen Hughes for offering me the opportunity to undertake this research under his supervision at the Maelor Academic Unit of Medical & Surgical Sciences (MAUMSS) in Wrexham (North Wales). I am very grateful for the help, guidance, and friendship of my colleagues within the MAUMSS lab; it has been a pleasure working and researching with them.

I would like to acknowledge and thank Prof. Jeffrey MacKeigan for providing access to sequencing data from TSC lesions, Dr. Jesse Champion for NRF2 and FSP1 gene expression data, and Dr. Darius Mcphaill for repeating my western blot analysis during my maternity leave.

On a personal note, my deepest gratitude goes to my wonderful husband, Dr. Darren Sexton, whose unwavering love, support, and guidance have been my rock throughout these years. Thank you for looking after our baby while I wrote this thesis.

Table of contents

List of Figures and Tables

Figures

Tables

Abbreviations

Abbreviation	Full Form
3'	Three Prime
4E-BP1	Eukaryotic Translation Initiation Factor 4E-Binding Protein 1
5'	Five Prime
AAs	Amino Acids
ACC1	Acetyl-CoA Carboxylase 1
ACSL4	Acyl-CoA Synthetase Long Chain Family Member 4
ADHD	Attention Deficit Hyperactivity Disorder
ADP	Adenosine Diphosphate
AIFM2/FSP	Apoptosis-Inducing Factor Mitochondria Associated 2/Ferroptosis Suppressor Protein
AIFM	Apoptosis-Inducing Factor Mitochondria Associated
AKT	Protein Kinase B
AMBRA1	Activating Molecule in BECN1-Regulated Autophagy Protein 1
AML	Angiomyolipoma
AMP	Adenosine Monophosphate
AMPK	AMP-Activated Protein Kinase
ANGPTL4	Angiopoietin-Like 4
ANOVA	Analysis of Variance
A/O PI	Acridine Orange/Propidium Iodide
ARE	Antioxidant Response Element
ASD	Autism Spectrum Disorder
ATF3	Activating Transcription Factor 3
ATF4	Activating Transcription Factor 4
Atg101	Autophagy Related 101
Atg13	Autophagy Related 13
ATP	Adenosine Triphosphate
Baf	Bafilomycin
Bcl2	B-Cell Lymphoma 2
BECN1	Beclin 1
BiP	Binding Immunoglobulin Protein
BNIP3	BCL2 Interacting Protein 3
BSA	Bovine Serum Albumin
bZIP	Basic Leucine Zipper Domain
CAD	Coronary Artery Disease
CA9	Carbonic Anhydrase 9
CARS	Cysteinyl-tRNA Synthetase
CARS1	Cysteinyl-tRNA Synthetase 1
CASP	Caspase
CAT	Catalase
CBS	Cystathionine Beta-Synthase

CBD	Cannabidiol
cDNA	Complementary DNA
CDK	Cyclin-Dependent Kinase
CHMP1A	Charged Multivesicular Body Protein 1A
ChIP Seq	Chromatin Immunoprecipitation Sequencing
CHOP	C/EBP Homologous Protein
CK1	Casein Kinase 1
CKI	Casein Kinase Inhibitor
CISD1	CDGSH Iron Sulfur Domain 1
CISD2	CDGSH Iron Sulfur Domain 2
CO2	Carbon Dioxide
CoQ	Coenzyme Q
CoQ10	Coenzyme Q10
CoQ10H2	Reduced Form of Coenzyme Q10
COX-2	Cyclooxygenase-2
CReP	Constitutive Repressor of eIF2α Phosphorylation
CSE	Cystathionine Gamma-Lyase
CTD	C-Terminal Domain
CTSB	Cathepsin B
C11 BODIPY	C11 BODIPY lipid peroxidation probe
CM-H2DCFDA	5-(and-6)-chloromethyl-2',7'-dichlorodihydrofluorescein diacetate, acetyl ester
DFP	Deferiprone
DRAQ7	DRAQ7 far-red fluorescent probe
DCFDA	Dichlorofluorescein Diacetate
DEG	Differentially Expressed Gene
DEPDC5	DEP Domain Containing 5
Deptor	DEP Domain Containing MTOR-Interacting Protein
DFP	Deferiprone
DHFR	Dihydrofolate Reductase
DPP-4	Dipeptidyl peptidase 4
DMEM	Dulbecco's Modified Eagle Medium
DMNQ	2,3-Dimethoxy-1,4-Naphthoquinone
DMSO	Dimethyl Sulfoxide
DNA	Deoxyribonucleic Acid
Dox	Doxorubicin
DR5	Death Receptor 5
DTT	Dithiothreitol
eEF2	Eukaryotic Elongation Factor 2
eEF2K	Eukaryotic Elongation Factor 2 Kinase
EGF	Epidermal Growth Factor
eIF2α	Eukaryotic Initiation Factor 2 Alpha
eIF4A	Eukaryotic Initiation Factor 4A

eIF4B	Eukaryotic Initiation Factor 4B
eIF4E	Eukaryotic Initiation Factor 4E
ELISA	Enzyme-Linked Immunosorbent Assay
ELT3	Eker Rat Leiomyoma-Derived Cells
EMT	Epithelial-Mesenchymal Transition
EMP1	Epithelial Membrane Protein 1
ER	Endoplasmic Reticulum
ERAD	Endoplasmic Reticulum-Associated Degradation
ERα	Estrogen Receptor Alpha
ERK	Extracellular Signal-Regulated Kinase
ESCRT-III	Endosomal Sorting Complex Required for Transport-III
Eto	Etoposide
EXIST	Existence
FAD	Flavin Adenine Dinucleotide
FANCD2	Fanconi Anemia Group D2
FAT	Fatty Acid Translocase
FBS	Fetal Bovine Serum
Fer-1	Ferrostatin-1
FDA	Food and Drug Administration
FGF	Fibroblast Growth Factor
FINs	Ferroptosis Inducers
FKBP12	FK506 Binding Protein 12
FLCN	Folliculin
FPN1	Ferroportin 1
FRB	FKBP-Rapamycin Binding
FSC	Forward Scatter
FSP1	Ferroptosis Suppressor Protein 1
FTH1	Ferritin Heavy Chain 1
FTL	Ferritin Light Chain
G6PD	Glucose-6-Phosphate Dehydrogenase
GADD34	Growth Arrest and DNA Damage-Inducible Protein 34
GAP	GTPase-Activating Protein
GATOR	GAP Activity Toward Rags
GβL	G Protein Beta Subunit-Like
GCLC	Glutamate-Cysteine Ligase Catalytic Subunit
GCH1	GTP Cyclohydrolase 1
GEF	Guanine Nucleotide Exchange Factor
GLUT4	Glucose Transporter Type 4
GJIC	Gap Junction Intercellular Communication
GPX4	Glutathione Peroxidase 4
GRB2	Growth Factor Receptor-Bound Protein 2
GRP94	Glucose-Regulated Protein 94
GSDMD	Gasdermin D

GSH	Glutathione
GSHTracer	Glutathione fluorescent probe
GSSH	Glutathione Disulfide
H_2O_2	Hydrogen Peroxide
HBXIP	Hepatitis B Virus X-Interacting Protein
HCC	Hepatocellular Carcinoma
HER2	Human Epidermal Growth Factor Receptor 2
HIF	Hypoxia-Inducible Factor
HMGB1	High Mobility Group Box 1
HMG-CoA	3-Hydroxy-3-Methylglutaryl-Coenzyme A
HMOX1	Heme Oxygenase 1
HRP	Horseradish Peroxidase
HSF1	Heat Shock Factor 1
HSP90	Heat Shock Protein 90
HSPB1	Heat Shock Protein Beta-1
IκKβ	IκB Kinase Beta
IC50	Half-Maximal Inhibitory Concentration
ID	Inhibitor of Differentiation
IL-6	Interleukin 6
IPP	Isopentenyl Pyrophosphate
IRE-1α	Inositol-Requiring Enzyme 1 Alpha
JAK	Janus kinase
KEAP1	Kelch like ECH associated protein 1
LCN2	Lipocalin 2
LIP	Labile iron pool
LPCAT3	Lysophosphatidylcholine acyltransferase 3
Lipid-ROS	ROS-mediated Lipid Peroxidation
LPOX	Lipid peroxidation
LTF	Lactotransferrin
MAPK14	Mitogen-activated protein kinase 14
MDA	Malondialdehyde
MDM2	Murine double minute 2
MDMX	Murine double minute X
MEF	Mouse embryonic fibroblasts
MGST1	Microsomal glutathione S-transferase 1
MLKL	Mixed-lineage kinase domain-like pseudokinase
mLST8	Mammalian lethal with Sec13 protein 8
MP	Methyl pyruvate
MP1	MAPK scaffold protein 1
MPST	Mercaptopyruvate Sulfurtransferase
MTT	3-(4,5-Dimethylthiazol-2-yl)-2,5-Diphenyltetrazolium Bromide
MT1G	Metallothionein 1G
MUFAs	Monounsaturated fatty acids

NAPDH	Nicotinamide adenine dinucleotide phosphate
Nec-1	Necrostatin 1
NFE2L2/NRF2	Nuclear factor, erythroid 2 like 2
NQO1	Quinone oxidoreductase 1
PEBP1	Phosphatidylethanolamine binding protein 1
PERK	Protein kinase RNA-like endoplasmic reticulum kinase
PFKFB3	6-phosphofructo-2-kinase/fructose-2,6-biphosphatase 3
PGC1α	Peroxisome proliferator-activated receptor gamma, coactivator 1α
PI3K	Phosphoinositide 3-kinase
PIP3	Phosphatidylinositol-3, 4, 5-trisphosphate
PKCα	Protein kinase Cα
PML	Progressive multifocal leukoencephalopathy
PMSF	Phenylmethane sulfonyl fluoride
POR	Cytochrome P450 oxidoreductase
IC50	Half-maximal Inhibitory Concentration
LIP	Labile Iron Pool
MEF	Mouse Embryonic Fibroblasts
MFI	Median Fluorescent Intensity
mTORC1	Mechanistic Target of Rapamycin Complex
SSC	Side Scatter
SCD	stearoyl-CoA desaturase
SLC11A2	solute carrier family 11 member 2
SLC40A1	solute carrier family 40 member 1
SLC7A11	Solute carrier family 7 member 11,
SQSTM1/p62	Sequestosome 1
STING1	Stimulator of Interferon Response CGAMP Interactor 1
TF	Transferrin
TFR	Transferrin Receptor
TGFB1	Transforming Growth Factor Beta 1
TP53	Tumour Protein p53
UC	Untreated Control
Z-VAD-FMK	benzyloxycarbonyl-Val-Ala-Asp-fluoromethyl ketone

Abstract

Ferroptosis, an iron-dependent cell death mechanism characterized by oxidative damage to phospholipids and subsequent membrane damage, presents a promising target for cancer therapy. The TSC1-TSC2 complex is crucial in cellular signalling, regulating cell growth, proliferation, and metabolism. Mutations or loss of TSC2 lead to hyperactivation of mTORC1, implicated in various cancers. This research aimed to elucidate the role of TSC2 loss in ferroptosis and its contribution to drug resistance in TSC2-cell line models, potentially guiding the development of new therapeutic strategies.

Cytotoxicity testing within this study revealed that *Tsc2*-deficient cells have greater resistance to ferroptosis induction compared to *Tsc2*-positive cells. Notably, inhibition of mTORC1 did not reverse this resistance, whereas NRF2 antioxidant pathway inhibition and AMPK activation did, suggesting that resistance operates through mTORC1-independent pathways. Biochemical analysis identified altered ferroptosis markers in *Tsc2*-deficient cells, such as ROS-mediated lipid peroxidation, GPX4, GSH, and labile iron pools as key factors in this resistance.

Further investigations into NRF2 revealed significantly elevated nuclear translocation upon ferroptosis induction in *Tsc2*-deficient cells during ferroptosis induction, identifying the NRF2 pathway as a potential mediator of resistance. qPCR and RNAseq analyses confirmed significant dysregulation of NRF2 and its target genes between *TSC2*-deficient and *TSC2*-expressing tumours. Additionally, inhibition of ferroptosis suppressor protein 1 (FSP1) also counteracted the cell death resistance in *Tsc2*-deficient cells. These cells displayed a fourfold increase in mRNA levels of FSP1, which significantly enhanced their resistance to ferroptosis. Overall, this thesis establishes that the loss of TSC2 confers resistance to ferroptosis through mechanisms that are independent of mTORC1 overactivation but dependent on NRF2 activation. This study also provides a deeper understanding of ferroptosis and additional cellular signalling

pathways, such as those involving ROS regulation, lipid peroxidation, and iron metabolism, within the context of TSC2 loss. These insights will guide the development of future therapeutic strategies targeting ferroptosis in TSC2-deficient cancers.

Word count -69800

Chapter 1: General Introduction

1.1 Tuberous Sclerosis Complex (TSC)

Cancer cells exhibit a loss of homeostatic flexibility due to genetic mutations and the dysregulation of signalling pathways that are crucial for maintaining cellular equilibrium (Bou Antoun and Chioni, Gyamfi et al., 2022) . One significant pathway involves the TSC1/TSC2 complex, which is vital in regulating cell growth and metabolism through its inhibitory effect on mTORC1. In many cancers, mutations in *TSC1* or *TSC2* lead to the aberrant activation of mTORC1. This hyperactivation results in uncontrolled cell proliferation, enhanced survival mechanisms, and metabolic reprogramming, which collectively contribute to tumorigenesis and cancer progression (Mieulet and Lamb, 2010). However, TSC2 loss is known to impact various cellular pathways such as cell cycle and DNA damage response, reactive oxygen species (ROS) regulation, AMPK, and autophagy regulation, independent of mTORC1 signalling (Fidalgo da Silva et al., 2021, Brugarolas et al., 2003, Di Nardo et al., 2014). This thesis aims to enhance the understanding of mTORC1 signalling and other pathways disrupted by TSC2 loss, with the goal of contributing to the development of more effective therapies for TSC-driven cancers.

1.1.1 Overview of TSC

Tuberous Sclerosis Complex (TSC), historically referred to as Bournville-Pringle disease, is a genetic disorder characterized by the growth of benign tumours, seizures and intellectual disabilities in multiple organs caused by mutations in either the *TSC1* or *TSC2* genes (Radhakrishnan and Verma, 2011). *TSC1* encodes the protein hamartin, and *TSC2* encodes tuberin. Together, TSC1 and TSC2 proteins form TSC regulatory complex that negatively controls the mechanistic target of rapamycin complex 1 (mTORC1), a master regulator of cell growth and proliferation (Kwiatkowski, 2003). Disruption of this complex due to *TSC2*

mutations leads to uncontrolled mTORC1 activity, contributing to the growth of benign tumours (hamartomas) across various organs (Dodd and Dunlop, 2016).

1.1.2 TSC-Associated Lesions and Their Clinical Impact

TSC associated hamartomas commonly affect the brain, kidneys, skin, heart, and lungs (see Table 1.1) and can result in significant morbidity and mortality, depending on their size, location, and growth) (Northrup et al., 2021).

Renal angiomyolipomas (AMLs), present in approximately 80% of TSC patients, consist of a mixture of blood vessels, smooth muscle, and fat. These lesions can cause significant renal complications, including haemorrhage and progressive kidney function loss, which can lead to chronic kidney disease or end-stage renal failure if not properly managed (Martin et al., 2017). Renal lesions are highly vascularized with weak blood vessel walls prone to aneurysm, leading to severe haemorrhaging and potentially death (Yamakado et al., 2002). These lesions disrupt normal renal parenchyma, decreasing kidney function (Eijkemans et al., 2015). Renal complications remain a leading cause of mortality despite advancements in surveillance and treatment (Bjornsson et al., 1996).

Brain lesions, such as cortical tubers, subependymal nodules (SENs), and subependymal giant cell astrocytomas (SEGAs), are common in TSC and can cause severe neurological issues like epilepsy, intellectual disability, and autism spectrum disorder. These brain tumours pose a risk of life-threatening conditions due to potential blockage of cerebrospinal fluid pathways, leading to hydrocephalus and increased intracranial pressure. SENs are asymptomatic periventricular nodular lesions that can evolve into SEGAs during postnatal development and early adulthood. They are reported in 80% to nearly 100% of TSC patients and frequently exhibit early-stage

calcifications. These lesions are typically less than 1 cm in diameter and are better detected using computerized tomography (CT) (Çelenk et al., 2005; Hu et al., 2016; Zordan et al., 2018)

Skin manifestations, such as facial angiofibromas, hypomelanotic macules, shagreen patches, and ungual fibromas, are prevalent in TSC. While typically not life-threatening, these lesions can cause considerable psychological distress due to their impact on appearance(Ebrahimi-Fakhari et al., 2017).

Pulmonary lymphangioleiomyomatosis (LAM) is another severe manifestation of TSC, particularly affecting women, leading to progressive lung function decline and respiratory failure. This condition represents a significant cause of mortality in adult female TSC patients (Gupta and Henske, 2018)

1.1.3 Non-lesional neurological disorders in TSC

Non-lesional neurological disorders in TSC include a range of cognitive, behavioural, and psychiatric issues collectively known as TSC-associated neuropsychiatric disorders (TAND). These manifestations are not directly linked to visible brain lesions such as cortical tubers or subependymal nodules. Key aspects include epilepsy and seizures, which can be refractory and suggest a diffuse neural dysfunction; cognitive impairments ranging from mild to severe intellectual disability; a high incidence of Autism Spectrum Disorder (ASD) with social communication difficulties and repetitive behaviours; and various behavioural and psychiatric disorders such as hyperactivity, aggression, anxiety, and depression. Developmental delays and deficits in motor skills, language, and adaptive functioning are also common, often occurring independently of brain lesions. Emerging research points to neuroinflammation as a contributing factor to these neurological symptoms, further indicating a complex interplay of factors beyond structural abnormalities in the brain. Understanding the full spectrum of non-lesional neurological disorders in TSC is crucial for developing comprehensive treatment approaches

.

TABLE 1.1 TSC-ASSOCIATED LESIONS AND DISORDERS, DESCRIPTIONS, AND THEIR PREVALENCE AMONG TSC PATIENTS (PERCENTAGE FREQUENCY OBTAINED FROM (NORTHRUP ET AL., 2021) AND (KINGSWOOD ET AL., 2017)

Types	Lesions/Symptoms	Description	Percentage in Patients
TSC-associated lesions		**Cardiovascular**	
	Cardiacrhabdomyomas	Large or strategically located benign tumours can obstruct blood flow within the heart, leading to heart failure, arrhythmias, or valvular dysfunction	34.3%
		Dermatological	
	Facial Angiofibromas	These are small, reddish-pink papules that typically appear on the central face, especially the nose and cheeks. They can are very common in TSC patients and become confluent over time	57.3% 75.0%
	Hypomelanotic Macules	Also known as "ash leaf spots," these are white or hypopigmented patches that can appear anywhere on the body. They are usually present at birth or develop in early childhood.	66.8% 90%
	Shagreen Patches	These are thickened, irregularly textured skin patches, often found on the lower back. They can be flesh-coloured or slightly pigmented	27.4% 50%
	Ungual Fibromas	Also known as Koenen's tumours, these are fibrous growths that typically occur around or under the nails of fingers and toes	20-50%
	Fibrous Plaques	These plaques are usually found on the forehead and scalp, appearing as thickened, firm, skin-coloured patches	25%
		Ophthalmologic	
	Various Retinal Hamartomas	Retinal hamartomas, or astrocytic hamartomas, are the most common ocular manifestation in TSC, appearing as benign white or yellowish lesions in the retina. Typically do not result in visual complications	14.0% 30-50%
		Renal	
	Renal Angiomyolipomas (AMLs)	AMLs are most common benign tumours composed of blood vessels, smooth muscle, and fat. They are the most common renal manifestation in TSC	47.2% 80%
	Renal Cell Carcinoma (RCC)	RCC is a malignant tumour of the kidney that occurs at a higher incidence in TSC	2-4%

		patients compared to the general population, although it is less common than AMLs	
		Neurological	
	Cortical Tubers	These are areas of disorganised brain cortex. They are associated with seizure activity and cognitive impairments	82.2%, 90%
	SENs	These benign nodules located along the ventricular walls can sometimes grow into subependymal giant cell astrocytomas (SEGAs), which may obstruct cerebrospinal fluid flow and cause hydrocephalus	78.2%, 80%
	SEGAs	SEGAs are slow-growing tumours that can arise from SENs. They can lead to increased intracranial pressure, headaches, and obstructive hydrocephalus if they block cerebrospinal fluid pathways	24.4%, 5-15%
Non-lesional neurological disorders (TAND)		**Neurological (TAND)**	
	Epilepsy	Epilepsy is one of the most common neurological manifestations in TSC, affecting up to 90% of patients with multiple and prolonged seizure types	83.5%
	Autism Spectrum Disorder (ASD)	ASD is characterized by difficulties in social interaction, communication challenges, and repetitive behaviours	20.7%
	Attention-Deficit/Hyperactivity Disorder (ADHD)	Commonly observed in TSC patients, contributing to difficulties in academic and social settings	19.6%
	Intellectual Disability (ID)	Intellectual disability involves significant limitations in intellectual functioning and adaptive behaviour	54.9%
	Anxiety disorder	Anxiety disorders in TSC patients can manifest as generalized anxiety, social anxiety, or specific phobias	9.1%
	Depressive disorder	Depressive disorders include major depression and dysthymia, which can lead to persistent feelings of sadness and loss of interest in activities	6.1
	Behavioural difficulties	Behavioural issues in TSC include aggression, self-injury, temper tantrums, and sleep disturbances	35.6
	Academic difficulties	More than half of TSC patients show severe to mild c mild learning disabilities, which reflects on intellectual impairment and academic difficulties	

1.1.3 Current Treatments for TSC

mTORC1 Inhibitors

The primary pharmacological treatment for TSC involves mTORC1 inhibitors such as Rapamycin and Everolimus (Habib et al., 2016). These drugs have been effective in reducing the size of TSC-associated lesions and controlling seizures. Clinical trials like the EXIST studies have demonstrated significant reductions in the volume of SEGAs and AMLs and improvements in seizure control with Everolimus treatment (Franz et al., 2013). However, these drugs are not curative and require lifelong administration, with concerns about long-term side effects such as immunosuppression, decreased renal function, and hypercholesterolemia (Li et al., 2019b)

Cannabidiol (Epidyolex)

Recently, cannabidiol (Epidyolex) has been approved for treating seizures in TSC patients. Clinical trials have shown that cannabidiol can significantly reduce the frequency of treatment-resistant epileptic seizures. However, it is not effective for all patients, and drug-drug interactions with mTORC1 inhibitors can lead to increased serum levels and potential toxicity (Thiele et al., 2022, Ebrahimi-Fakhari et al., 2017).

Despite the progress made with mTORC1 inhibitors effectiveness in managing TSC-associated lesions, surgical intervention remains crucial for certain cases. For AMLs, surgery aims to prevent acute complications like haemorrhaging, necessitating elective resection or embolization of large, rapidly growing, or mTOR-resistant AMLs (Eijkemans et al., 2015). In treating SEGAs, symptomatic cases often require surgical resection, while mTOR inhibitors are recommended for asymptomatic or non-surgical SEGAs (Curatolo et al., 2015). However, SEGA resection carries significant risks, including infection and neurological deficits for TSC-associated epilepsy, surgery is viable when epileptogenic foci can be accurately identified

(Kotulska et al., 2014). A meta-analysis by (Zhang et al., 2013) found that 59% of patients achieved seizure freedom post-surgery, although long-term efficacy may decline over time .

1.2 Mammalian/mechanistic Target of Rapamycin (mTOR)

mTOR protein plays a pivotal role in the pathogenesis of TSC (Wataya-Kaneda, 2015). Understanding the function of mTOR, its complexes, regulatory mechanisms, and downstream signalling pathways is crucial for unravelling the molecular and cellular basis of TSC. This knowledge underpins why mTOR has become the primary target for therapeutic interventions aimed at managing the condition. Insights into mTOR's intricate network provide a comprehensive framework for developing effective treatments and improving patient outcomes in TSC.

1.2.1 The Structure of mTOR and Complexes

Mammalian/mechanistic target of rapamycin (mTOR), also known as FRAP (FKBP12-rapamcyin-associated protein), RAFT1 (rapamycin and FKBP12 target), RAPT 1 (rapamycin target 1), or SEP (sirolimus effector protein). It is a 289 kDa serine/threonine kinase and a member of the phospho-inositide 3-kinase (PI3K)-related protein kinases (PIKK) family (Figure 1) (Brown et al., 1994, Chen et al., 1994)

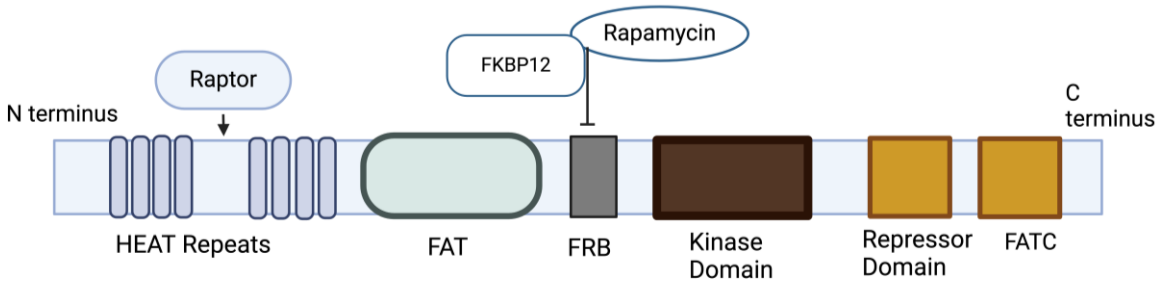

Fig. 1.1 Domain structure of mTOR.

The *N*-terminus of mTOR contains two tandem repeated HEAT motifs (protein interaction domains found in Huntington, Elongation factor 3, PR65/A and TOR), followed by a FAT (domain shared by FRAP, Ataxia telangiectasia mutated, and TRRAP, all of which are PIKK family members) domain, a FRB (FKBP12-rapamycin-binding site, found in all eukaryotic TOR orthologs) domain, a PtdIns 3-kinase related catalytic domain, an auto-inhibitory (repressor domain or RD domain), and a FATC (FAT *C* terminus) domain that is located at the *C*-terminus of the protein. The FRB domain forms a deep hydrophobic cleft that serves as the high-affinity binding site for the inhibitory complex FKBP12-rapamycin.

Dysregulation of the mTOR pathway, particularly mTORC1, has been associated with chemoresistance, as well as the development and progression of various types of cancer (Shaw and Cantley, 2006, Samuels et al., 2004, Li et al., 1997).

1.2.1.1 mTORC1

The mTOR protein serves as the catalytic core for two distinct complexes: mTOR complex 1 (mTORC1) and mTOR complex 2 (mTORC2)(Loewith et al., 2002, Sarbassov et al., 2004). These complexes can couple with different protein substrates, leading to the activation of unique signalling pathways and fulfilling varied roles in maintaining cellular balance (refer to Figure 2). mTORC1 is recognized as the central regulator of cellular growth, proliferation, and survival. In contrast, mTORC2 is involved in the organization of the cytoskeleton, cell movement, modulation of the cell cycle, and regulation of cell survival (Unni and Arteaga, 2019). The differentiation between mTORC1 and mTORC2 originated from their specific components and their varying responses to rapamycin, a macrolide antibiotic derived from *Streptomyces*

hygroscopicus, which selectively blocks mTOR activity (Seto, 2012) . Initially, mTORC1 was identified as sensitive to rapamycin, whereas mTORC2 was thought to be resistant (Ben-Sahra and Manning, 2017). However, it has since been discovered that extended rapamycin exposure can also results in the inhibition of mTORC2 (Sarbassov et al., 2005a, Ye et al., 2012). Both mTORC1 and mTORC2 are positioned within the PI3K/Akt signalling pathway, where mTORC2 lies upstream of Akt and mTORC1 lies downstream of Akt and the TSC1 and TSC2 proteins (Sarbassov et al., 2005b, Shimobayashi and Hall, 2014).

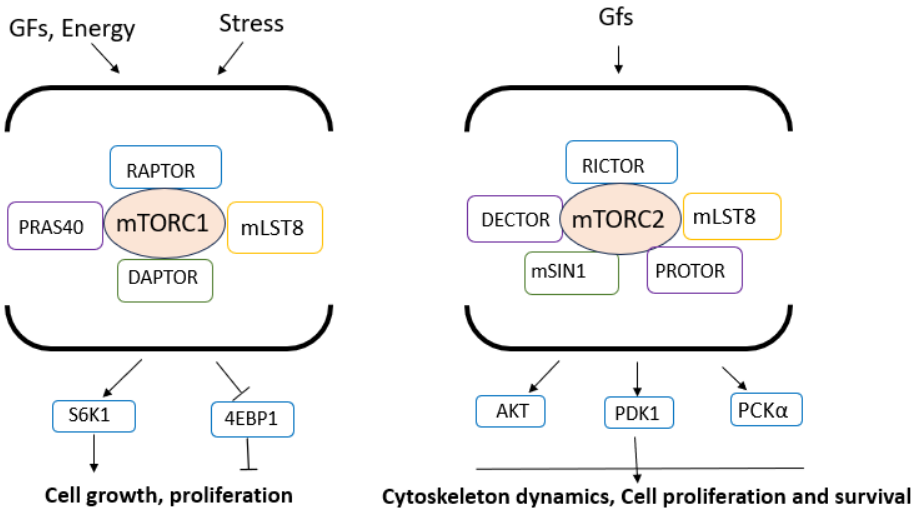

Fig. 1.2 Schematic representation of both mTOR complexes, mTORC1 and mTORC2, along with their upstream activating stimuli and downstream effectors.

In cellular physiology, mTORC1 serves as a central hub that integrates various signalling inputs to regulate cellular growth, translation, transcription and autophagy (Sulaimanov et al., 2017). Diverse stimuli, ranging from growth factors, nutrients, energy, and stress signals, activate mTORC1 through mitogen-activated protein kinase (MAPK) and phosphoinositide-3 kinase (PI3K) pathways (He et al., 2020). Upon activation, mTORC1 phosphorylates its two main downstream effectors, eukaryotic translation initiation factor 4E-binding protein 1 (4E-BP1) and inhibits ribosomal protein S6 kinase 1 (S6K1), which orchestrates a complex network of signalling events that regulate essential cellular functions, including mRNA translation, protein and lipid synthesis, glucose metabolism, cell cycle progression and growth (Lim et al., 2003, Schalm et al., 2003, Sonenberg and Gingras, 1998, Manning and Cantley, 2003) . mTORC1 also plays critical roles in autophagy (a catabolic process essential for cellular homeostasis and stress adaptation through its downstream regulation of the ULK1 complex (discussed later)(Ma et al., 2017b).

mTORC1 adopts a cage-like, dimeric architecture with the mTOR kinase domain located near the centre of the assembly (Ramlaul and Aylett, 2018). It consists of the mTOR catalytic subunit, mammalian lethal with sec-13 protein 8 (mLST8), DEP domain-containing mTOR interacting protein (DEPTOR), Tti/Tel2, regulatory-associated protein of mTOR (RAPTOR) and proline-rich Akt substrate 40 kDA (PRAS40) (refer to Figure 2) (Laplante and Sabatini, 2012).

Rapamycin inhibits mTORC1 via formation of a gain-of-function complex with 12-kDa FK506-binding protein (FKBP12), that binds to the FKBP12/rapamycin-binding (FRB) domain of mTOR in mTORC1 only (Ben-Sahra and Manning, 2017). When this occurs the rapamycin/FKBP12 complex causes dissociation of Raptor from the mTOR causing loss of contact between mTORC1 and its substrate, resulting in pathway shutdown (Ehninger et al., 2009, Chiarini et al., 2015). In signal transduction pathways, mTORC1 is activated through Rheb, a process counteracted by a GTPase-activating heterodimeric protein complex comprised of tuberous sclerosis complex (TSC) proteins, including Hamartin (TSC1) and Tuberin (TSC2) (Inoki et al., 2003). The components of mTORC1 that interact with mTOR are found in Table 1.2.

TABLE 1.2 COMPONENTS OF MTORC1 COMPLEX AND THEIR FUNCTION

Component	Description	Function	Reference
Regulatory associated protein of mammalian target of rapamycin (Raptor)	150 kDa scaffold protein, which is exclusive in mTORC1	Interacts with downstream substrates, S6K1 and 4E-BP1 – which will be discussed later in the chapter. mTORC1 substrates, contain mTOR signalling (TOS) motifs that helps with mTORC1-dependent phosphorylation of those substrate. Raptor is also needed to assist with the localization of the mTORC1 to the lysosome.	(Chong, 2015, Tee et al., 2016)
Proline-rich AKT substrate 40 kDa (PRAS40)	mTORC1 exclusive protein with a TOS motif that is a negative regulator of mTORC1.	PRAS40 interacts with Raptor and competitively binds to S6K1 and 4E-BP1. AKT phosphorylates PRAS40 causing PRAS40 to bind to protein 14-3-3 (causing PRAS40 inactivation) resulting in increased mTORC1 activity (Cho, 2011; Chong, 2015)	(Sancak et al., 2007, Oshiro et al., 2007)
mLST8		See Table 1.3	
Deptor		See Table 1.3	

1.2.1.2 mTORC2

The catalytic subunit of mTOR also contributes to the formation of another kinase complex known as mTORC2. mTORC2 consists of components such as rapamycin-insensitive companion of mTOR (RICTOR), protein observed with RICTOR-1 (PROTOR-1), stress-activated protein kinase-interacting protein 1 (mSIN1), and mLST8. As with mTORC1, mTORC2 is activated in response to growth factor stimulation, resulting in association with the ribosome. mTORC2 controls regulation of the actin cytoskeleton and has an involvement in cell survival (Dazert and Hall, 2011).

mTORC2 is located proximally to various cellular structures such as the endoplasmic reticulum (ER), mitochondria, mitochondria-associated ER-membrane (MAM), and the nucleus in mammalian cells. Initially characterized for its role in regulating cell skeletal organization, mTORC2 has since been implicated in promoting cell proliferation and survival through the phosphorylation of AKT (Fu and Hall, 2020, Boulbes et al., 2011). While rapamycin is known as an mTORC1 selective inhibitor (as rapamycin/FKBP12 complex does allosterically inhibit

mTORC2), it also affects inhibition of mTORC2 activity under certain conditions, such as prolonged exposure (>24 h), high concentrations, or variations in the expression levels of FK506 binding proteins, particularly FKBP12 and FKBP51 (Sarbassov et al., 2006, Efeyan and Sabatini, 2010).

TSC2 promotes mTORC2 activity in a Rheb-independent manner, potentially through direct binding to mTORC2 components and Akt activation, which in turn phosphorylates and activates downstream effectors (Huang et al. 2008). The components of mTORC2 (including mTOR) are found in Table 1.3.

TABLE 1. 3 COMPONENTS OF MTORC2 COMPLEX AND THEIR FUNCTION

Component	Description	Function	Reference
Rapamycin-insensitive companion of mTOR (Rictor)		An mTORC2 exclusive component that is involved in the activation of AKT via direct phosphorylation of Ser473, a priming site that enables PDK1 to phosphorylate Thr308	(Sarbassov et al., 2004)
Mammalian stress-activated protein kinase interacting protein (mSIN1)		A negative regulator exclusive to the mTORC2 complex that prevents mTOR kinase activity by interacting with and inhibiting the mTOR kinase domain. mSIN1 is regulated by PIP3	(Yu et al., 2022)
Protein observed with Rictor-1 (Protor-1)		Protor-1 is a Rictor-binding subunit required for the activation of serum- and glucocorticoid-induced protein kinase 1 (SGK1)	(Chong, 2015)
Mammalian lethal with Sec13 protein 8 (mLST8)		Also called G protein β-subunit like protein (GβL). mLST8 structurally has seven WD-40 repeats and is located on endosomal or Golgi membranes. mLST8/GβL associates with mTORC2 by binding to the kinase domain of mTOR and plays several roles in stability, assembly, and mTOCR2 activity towards AKT and protein kinase Cα (PKCα)	(Guertin et al., 2006)
DEP domain containing mTOR interacting protein (Deptor)		A negative regulator of mTORC2, which binds to the FAT domain of mTOR.	(Chong, 2015)

1.2.3 Activation and Regulation of mTORC1 Signalling

mTORC1 plays a central role in balancing cellular metabolism through both anabolic and catabolic regulation: (i) it promotes anabolic processes such as protein, lipid, and nucleotide synthesis by phosphorylating substrates including S6K and 4E-BP1; and (ii) it suppresses catabolic pathways by targeting ULK1, Atg13, and MiT-TFE transcription factors that regulate autophagy and lysosomal biogenesis (Deaver et al., 2020, Cheong and Klionsky, 2015, Asrani et al., 2019). mTORC1 activity is tightly regulated at multiple levels, including its localization and interactions with regulatory components(Ben-Sahra and Manning, 2017). Dysregulation of this pathway contributes to cancer, making it a key target for therapeutic intervention (Sato et al., 2010, Peng et al., 2022b).

1.2.3.1 Upstream regulators of mTORC1

The activation of mTORC1 is tightly regulated by a range of upstream signals, including growth factors, amino acid availability, and cellular energy status. These signals are sensed at the cell surface or within the cytoplasm and converge on intracellular regulators such as the TSC1/TSC2 complex, Rheb, and Rag GTPases to modulate mTORC1 activity (Hara et al., 1998).

Growth Factors

Growth factors such as insulin activate mTORC1 signalling through receptor tyrosine kinases (RTKs), which initiate two major intracellular pathways: PI3K/Akt and Ras/MAPK (Saxton and Sabatini, 2017). Upon activation, RTKs recruit adaptor proteins that activate PI3K, converting PIP2 to PIP3. This lipid product recruits PDK1 and Akt to the membrane, where Akt is phosphorylated and activated. mTORC2, also activated by PI3K, phosphorylates Akt at Ser473, enhancing its activity further (Fingar and Blenis, 2004). Activated Akt promotes mTORC1 activity by phosphorylating and inhibiting TSC2 and PRAS40, both of which normally repress mTORC1 (Tee et al., 2002).

Concurrently, the Ras/MAPK pathway activates ERK and its downstream effector RSK1, which also phosphorylate TSC2, further inhibiting the TSC complex and promoting mTORC1 activation (Ma et al., 2005). The mechanism by which TSC2 regulates mTORC1 will be discussed in more detail in the following section.

Activation by TSC1/TSC2 complex and Rheb

The TSC1/TSC2 complex functions as a central negative regulator of mTORC1 by acting as a GTPase-activating protein (GAP) for Rheb (Manning and Cantley, 2003). Rheb has low intrinsic GTPase activity, so it remains predominantly active unless regulated. The GAP activity of the TSC1/TSC2 complex converts Rheb-GTP to Rheb-GDP, thereby inhibiting mTORC1 signalling (Mazhab-Jafari et al., 2012). Mutations in TSC1 or TSC2 disrupt this inhibition, leading to sustained mTORC1 activation and promoting abnormal cell growth and tumorigenesis (Gao et al., 2002, Inoki et al., 2002). The nucleotide-bound status of Rheb is regulated by the TSC1/2 complex, thereby allowing TSC1/TSC2 to negatively regulate mTORC1 signalling through Rheb (Inoki et al., 2003, Tee et al., 2002).

The TSC complex consists of three subunits: TSC1, which stabilizes TSC2 and prevents its degradation; TSC2, which contains the GAP domain; and TBC1D7, which enhances the stability and function of the TSC1/TSC2 complex, adding an extra layer of control (Dibble et al., 2012).

Amino acids

Amino acids, particularly leucine and arginine, are essential activators of mTORC1. Unlike growth factors, amino acid signalling does not act directly through TSC1/TSC2. Instead, it controls mTORC1 activation via Rag GTPases (Frappaolo and Giansanti, 2023). In the presence of amino acids, the Rag GTPases (RagA/B and RagC/D) form heterodimers in an active conformation that recruit mTORC1 to the lysosomal membrane. This spatial positioning brings

mTORC1 into proximity with Rheb-GTP, enabling its activation. Without this lysosomal localization, mTORC1 remains inactive—even if Rheb is in its active form.

While early studies suggested a role for TSC1/2 and hVps34 (a class III PI3K) in amino acid sensing, more recent evidence supports a TSC-independent, Rag-dependent mechanism. Notably, mTORC1 can still respond to amino acid levels in TSC2-deficient cells, indicating the existence of TSC-independent regulation (Demetriades et al., 2016). Although, hVps34, a class III PI3K was proposed as a mediator of amino acid signalling to mTORC1, this role remains controversial, particularly in Drosophila (Backer, 2008).

Low Energy and Stress

Cellular energy status critically influences mTORC1 activity through the AMP-activated protein kinase (AMPK) pathway. Under low energy conditions (e.g., glucose deprivation), the AMP/ATP ratio increases, leading to the activation of AMP-activated protein kinase (AMPK), a central energy sensor. AMPK inhibits mTORC1 through two main mechanisms:

1. **Direct phosphorylation of Raptor**: AMPK phosphorylates Raptor, a core component of the mTORC1 complex, thereby reducing mTORC1 kinase activity (Shackelford and Shaw, 2009).
2. **Indirect inhibition via TSC2**: AMPK phosphorylates and activates TSC2, enhancing its GAP activity toward Rheb, which shifts Rheb to its inactive GDP-bound form and suppresses mTORC1 signalling (Inoki et al., 2002).

Energy sensing is further regulated by LKB1, which activates AMPK in response to increased AMP levels. This AMPK-LKB1-TSC2 axis ensures that mTORC1 is downregulated during energetic stress (Shackelford and Shaw, 2009).

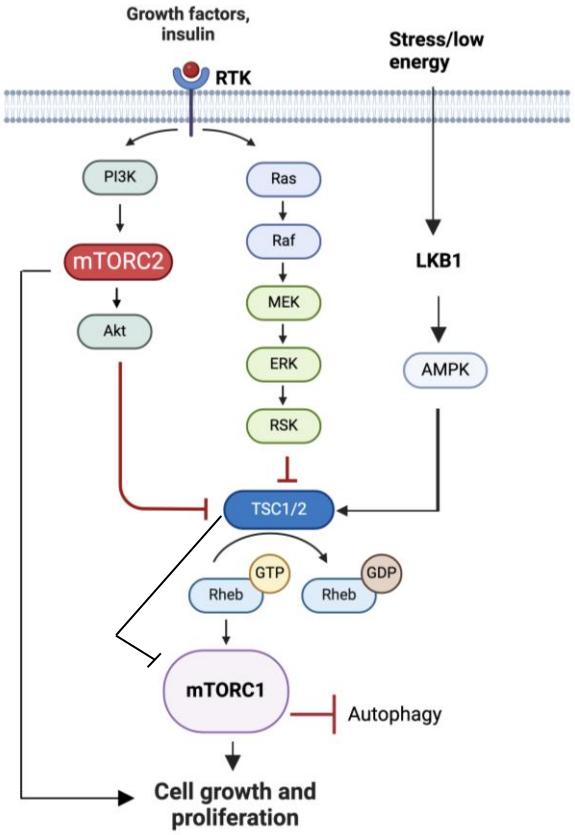

Fig 1.3 Molecular mechanism of mTOR signalling.

Growth factors such as insulin activate RTKs, stimulating PI3K/Akt and Ras/Raf/MEK/ERK pathways. Akt and ERK inhibit the TSC1/2 complex, enabling Rheb-GTP to activate mTORC1. mTORC2, activated by PI3K, enhances Akt phosphorylation at Ser473, amplifying mTORC1 signalling. Conversely, energy stress activates AMPK, which inhibits mTORC1 via TSC2 activation and Raptor phosphorylation. Activated mTORC1 promotes cell growth and proliferation, while simultaneously inhibiting autophagy.

Hypoxia

Interestingly, mTOR signalling pathway can also be influenced by hypoxia, a condition of low oxygen levels. Hypoxia induces changes in mTOR phosphorylation and its downstream targets

Hypoxia inhibits mTORC1 through both TSC-dependent and independent mechanisms (Kim et al., 2023). It induces expression of REDD1, which suppresses mTORC1 by promoting TSC2 activity (Kim et al., 2023). REDD1 expression is itself enhanced by AMPK during hypoxic stress, forming a feedback loop that ensures mTORC1 inhibition under adverse conditions (Schneider et al., 2008)

1.2.3.2 Downstream targets of mTORC1

As previously noted, mTORC1 regulates key cellular processes—including protein synthesis, lipid metabolism, cell growth, cell cycle progression, proliferation, and autophagy—through its downstream effectors, which will now be discussed in further detail

Protein Synthesis

In mammals, S6 kinases (S6Ks) and eukaryotic translation initiation factor 4E-binding proteins (4E-BPs) are key downstream targets of mTOR and crucial regulators of protein synthesis. mTORC1-driven phosphorylation of S6Ks promotes ribosomal protein S6 (rpS6) phosphorylation, thereby influencing translation by modulating the eIF3 initiation complex (Holz et al., 2021, Fingar and Blenis, 2004). In the absence of phosphorylation, 4E-BP1 binds tightly to eIF4E and inhibits translation initiation (Hinnebusch, 2012). In response to growth factors and nutrients, phosphorylation at multiple 4E-BP1 sites (T37, T46, S65, T70, S83, and S112) triggers its release from eIF4E. This permits eIF4E to associate with eIF4G, facilitating the assembly of initiation factors and the ribosome on mRNA (Showkat et al., 2014).

Lipid Metabolism and Cell Growth

mTORC1 exerts profound influence over lipid metabolism and cellular growth through its downstream effectors. Activation of mTORC1 promotes lipogenesis by enhancing the activity of lipin, a key regulator of lipid biosynthesis (Duvel et al., 2010). Additionally, mTORC1-mediated regulation of glycogen synthase contributes to cellular energy storage, supporting anabolic processes essential for cell growth and proliferation (Mao and Zhang, 2018).

Cell Cycle Progression and Proliferation

Central to cell cycle progression and proliferation are the regulatory roles played by mTORC1 downstream targets. Through modulation of cyclin-dependent kinase inhibitors such as p21Cip1 and p27Kip1, mTORC1 influences cell cycle transitions, ensuring coordinated progression through cell cycle phases (Wang et al., 2015). Moreover, mTORC1 activation promotes the expression of proteins involved in cell proliferation, including retinoblastoma protein (Rb) and signal transducer and activator of transcription 3 (STAT3) (Populo et al., 2012).

Autophagy Regulation

In addition to its anabolic functions, mTORC1 exerts significant control over catabolic processes such as autophagy. When active, mTORC1 suppresses autophagy through inhibition of the ULK1 complex, thereby limiting cellular self-degradation and promoting nutrient retention (Dunlop and Tee, 2014). Conversely, mTORC1 inhibition induces autophagy, facilitating the clearance of damaged organelles and protein aggregates to maintain cellular homeostasis (discussed later).

1.2.4 Dysregulation of mTORC1 by TSC2 Loss in Cancer

Many cancer cells exhibit sustained proliferation, often independent of normal growth-promoting signals and despite the presence of growth-inhibitory cues (Hanahan and Weinberg,

2011). In certain contexts, such as in cancers with TSC2 loss, this abnormal proliferative capacity can be driven in part by aberrant activation of mTORC1 (Tee et al., 2016). Hyperactive mTORC1 signalling, frequently driven by genetic alterations, leads to activation of S6K1, which in turn suppresses Akt signalling by phosphorylating and inhibiting Insulin Receptor Substrate (IRS) proteins (Zhang et al., 2008) (Browne and Proud, 2004). This creates a negative feedback loop that impairs PI3K/Akt signalling. In tumours with intact TSC2, this feedback inhibition can paradoxically restrain mTORC1 activity, as reduced Akt activity leads to reduced phosphorylation of TSC2, allowing it to inhibit Rheb and suppress mTORC1. However, in cancers with TSC2 mutations or deletions, this checkpoint is lost, and mTORC1 remains constitutively active despite reduced Akt signalling (Manning and Cantley, 2007).

Given its central role in tumour progression, mTORC1 has become a major therapeutic target. Inhibitors such as rapamycin and its analogues—CCI-779 (temsirolimus), RAD001 (everolimus), and AP23573—have demonstrated efficacy across various cancer types, although their clinical use is often limited by side effect (Ali et al., 2022, Habib et al., 2016). Hence, to enhance treatment outcomes and limit resistance, combination approaches co-targeting mTORC1 and upstream effectors such as IGF-1R or PI3K have been investigated (May et al., 2017, Fujimoto et al., 2020). For instance, mTOR inhibition has been shown to potentiate RSL3-induced cytotoxicity in PIK3CA-mutant colorectal cancer. Additionally, suppression of the AKT/mTORC1 pathway has been found to induce ferroptosis via autophagy-mediated GPX4 degradation in pancreatic cancer (Liu et al., 2021). These findings support the use of combinatorial mTOR-targeted therapies to overcome resistance and improve efficacy. Beyond cancer, TSC2 and mTORC1 play key roles in regulating cellular metabolism and stress responses. TSC2 integrates signals from the energy-sensing AMPK pathway; during low-energy conditions, AMPK phosphorylates TSC2, enhancing its GAP activity toward Rheb and thereby inhibiting mTORC1 (Inoki et al., 2002). This mechanism ensures mTORC1 is downregulated

during metabolic stress to conserve energy. Dysregulation of this axis contributes to a range of non-malignant disorders, including cardiac hypertrophy, type II diabetes, and obesity (Gollob et al., 2001, Kenerson et al., 2002, Kwiatkowski, 2003, Johnson and Tattersfield, 2002, Inoki et al., 2005).

In both cancer and metabolic diseases, the mTORC1 pathway emerges as a pivotal therapeutic axis. The success of mTORC1 inhibitors in cancers such as renal cell carcinoma, breast cancer, and glioblastoma highlights their clinical relevance. By targeting mTORC1-dependent survival pathways, these drugs offer a more precise therapeutic strategy. Using TSC-deficient models to study mTORC1 signalling continues to provide valuable insights for advancing cancer therapy(Park et al., 2020). Thus, leveraging TSC as a model system for studying mTORC1-related pathways provides crucial insights for developing advanced cancer therapies.

1.2.4 TSC2 and mTORC1 in Cellular Death Programs

The regulation of cellular metabolism is a critical determinant of cell fate, particularly in the context of various cell death programs such as apoptosis, necrosis, necroptosis, pyroptosis, and ferroptosis (Zhu et al., 2022a). These processes are essential for maintaining cellular homeostasis and are implicated in a wide range of physiological and pathological conditions, including cancer, neurodegenerative diseases, and genetic disorders like TSC. Recent studies have highlighted the intricate relationship between metabolic pathways and these cell death mechanisms underscoring their importance in the development and progression of these conditions (Green and Llambi, 2015, Peng et al., 2022a, Ouyang et al., 2012). Below we introduce, briefly, several salient cell death mechanisms and their links to metabolic control but a primary focus in subsequent sections will be ferroptosis and its metabolic regulation via perturbations in TSC2 and mTORC1.

Apoptosis

Apoptosis is a form of programmed cell death essential for removing damaged or unwanted cells. Hyperactivation of mTORC1 disrupts this balance, promoting survival and proliferation even in cells that should undergo apoptosis. Therapeutic inhibition of mTORC1 in TSC2-deficient cells can restore apoptotic pathways, enhancing the elimination of aberrant cells and reducing tumour growth. Studies have shown that mTORC1 inhibitors such as rapamycin and everolimus can induce apoptosis in cancer cells, providing a targeted approach to reducing tumour burden (Franz et al., 2013, Villar et al., 2017).

Autophagy

Autophagy is a cellular degradation process that helps maintain homeostasis by recycling cellular components. mTORC1 is a known inhibitor of autophagy, and its overactivation in TSC2-deficient cells suppresses this critical survival pathway. Therapeutic targeting of mTORC1 can restore autophagy, promoting the degradation of damaged organelles and proteins, thereby enhancing cell survival under stress conditions. This restoration is particularly relevant in neurodegenerative diseases and cancer, where autophagy plays a dual role in cell survival and death (Johnson and Tee, 2017, Tungsukruthai et al., 2021).

Necrosis

Necrosis often considered an unregulated form of cell death resulting from acute cellular injury, has been reevaluated with evidence of regulated forms such as necroptosis. Necroptosis is mediated by receptor-interacting protein kinases (RIPK1 and RIPK3) and the mixed lineage kinase domain-like protein (MLKL), linking metabolic stress to inflammatory responses (Lou et al., 2020)

Necroptosis and Pyroptosis

Necroptosis and pyroptosis are forms of programmed necrosis, often associated with inflammatory responses. Hyperactive mTORC1 signalling can influence these pathways by altering the expression of inflammatory cytokines and cell survival signals. Inhibiting mTORC1 in TSC2-deficient cells may modulate these inflammatory cell death pathways, reducing tissue damage and inflammation. This modulation is crucial in conditions where chronic inflammation contributes to disease progression, such as in certain cancers and autoimmune disorders (Bertheloot et al., 2021)

Ferroptosis

Ferroptosis is an iron-dependent form of cell death mechanism characterized by lipid peroxidation (Dixon et al., 2012). TSC2-deficient cells, with their hyperactive mTORC1 signalling, exhibit altered metabolic and redox states (Medvetz et al., 2015). By modulating lipid metabolism and enhancing oxidative stress, targeting mTORC1 overactivation can alter sensitivity of these cells to ferroptosis. This approach offers a promising strategy for overcoming resistance in cancer therapy, as ferroptosis inducers like RSL3 have shown efficacy in inducing cell death in mTORC1-hyperactive cells (Yang et al., 2014). Regulation and mechanisms of ferroptosis, along with the potential therapeutic benefits of these processes, will be explored in detail in the following section.

1.3 Ferroptosis

Ferroptosis, a relatively recent form of regulated cell death (RCD), was first characterized by its dependence on iron and the accumulation of toxic reactive oxygen species (ROS), leading to lipid peroxidation of the cell membrane (Dixon et al., 2012). Ferroptosis presents unique

morphological, biochemical, and genetic features compared to apoptosis, necroptosis, and autophagic cell deaths (Dolma et al., 2003, Tang et al., 2019).

The primary source of oxidative stress in ferroptosis originates from iron-driven Fenton reactions (non-enzymatic), mitochondrial ROS, and membrane-associated ROS driven by the NOX protein family (enzymatic) (Kuang et al., 2020). Poly-unsaturated fatty acid-containing phospholipids are the main substrates of lipid peroxidation in ferroptosis, regulated positively by ACSL4, LPCAT3, ALOXs, or POR enzymes (Yang et al., 2016). Increased iron levels in the cell, by autophagic degradation of the iron storage protein ferritin and the upregulation of haem-oxygenase 1 (HMOX1), contribute to ROS production and ferroptosis induction (Hou et al., 2016, Menon et al., 2022).

In contrast, mechanisms that prevent ferroptosis include the cystine/glutamate antiporter (System Xc-) also known as SLC7A11, glutathione peroxidase 4 (GPX4), and other antioxidants like coenzyme Q10 and tetrahydrobiopterin. The nuclear factor E2 related factor 2 (NRF2/NFE2L2) plays a crucial role in defending cells from ferroptosis by upregulating antioxidant and cytoprotective gene expression (Liu et al., 2022). Additionally, the cellular machinery of endosomal complexes required for transport (ESCRT-III) helps repair membrane damage caused by ferroptotic stimuli, leading to ferroptosis resistance (Dai et al., 2020). The detailed mechanisms of ferroptosis, including the signalling pathways involved and the defence mechanisms that regulate this process, will be discussed in the following section.

1.3.1 Core Molecular Mechanism and Regulation of Ferroptosis

Lipid peroxidation is the hallmark of ferroptosis and multiple oxidative and antioxidant systems along with their signalling pathways are involved in this process to induce ferroptosis (Yang and Stockwell, 2016). However, the main mechanism of ferroptosis induction is the

inhibition of the cellular antioxidant defence and facilitation of oxidative damage, which manifests via redox imbalance caused by disruptions in iron and lipid metabolism. The mechanism of initiating lipid peroxidation is not yet fully elucidated but can potentially occur by non-enzymatic process through iron metabolism and enzymatic processes by lipid metabolism (see Fig. 1.4)(Stockwell et al., 2017).

(A) (B)

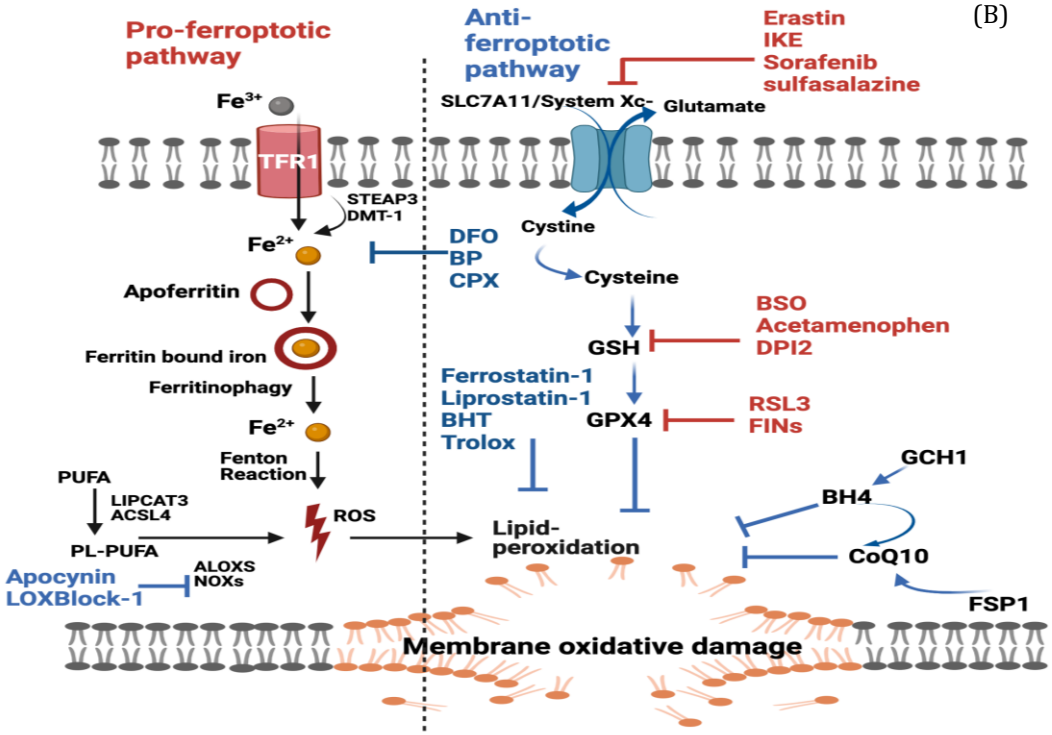

Fig. 1.4 The core mechanisms of ferroptosis regulation

(A) Induction of pro-ferroptotic iron metabolism and lipid peroxidation: Free iron (Fe^{2+})catalyses lipid peroxide accumulation via the Fenton reaction. Enzymatic peroxidation of polyunsaturated fatty acids (PUFAs) by LPCAT3, ACSL4, ALOX, and NOXs also contributes. These enzymes initiate reactions leading to lipid hydroperoxide generation, promoting ferroptotic cell death (Dixon et al., 2015, Yang et al., 2016). **(B) Inhibition of anti-ferroptotic antioxidant amino acid metabolism**: System Xc – inhibition reduces cellular cysteine, causing GSH depletion and GPX4 inactivation (Yang et al., 2014). Consequently, the cell loses its ability to neutralize lipid peroxides, making it susceptible to ferroptotic cell death. This figure was created based on the tools provided by Biorender.com.

(A) Pro-ferroptotic pathway

Dysregulation of iron metabolism

Iron has two oxidation states: ferrous (Fe^{2+}) or ferric (Fe^{3+}). The participation of Fe^{2+}/Fe^{3+} in the formation of ROS is one of the critical factors of ferroptosis. Circulating iron outside the cell is Fe^{3+}, which gets absorbed by the transferrin receptor (TFR) in the cell membrane and reduced to Fe^{2+} by the ferrireductase activity of STEAP3; and ferroportin can transfer iron inside of cells to the outside, and then into the circulatory system (Gao et al., 2021b, Hao et al., 2018). Eventually, divalent metal transporter 1 (DMT1) acts on the release of Fe^{2+} from the endosome into the cytoplasm (Yu et al., 2019). Iron can be stored in ferritin maintaining a non-toxic form known as the iron pool (IP) (Kwon et al., 2015). However, free Fe2+, forming a labile iron pool (LIP) within cells, is highly toxic. This form exhibits strong reactivity and readily interacts with hydrogen peroxide (H_2O_2) in cells (Cao and Dixon, 2016). Such interaction leads to the generation of hydroxyl free radicals through the Fenton reaction. These free radicals can extract oxygen atoms from PUFA diallyl carbon and induces PUFA-PLs peroxidation, which ultimately promotes oxidative damage to membrane lipids and destroys cell membrane (Yang et al., 2016). Additionally, overexpression of nuclear receptor coactivator 4 (NCOA4) can facilitate autophagic degradation of ferritin 'ferritinophagy' to the release of Fe^{2+} to mediate this process (Mancias et al., 2014). Interestingly, heme oxygenase-1 (HMOX1) has dual role in iron metabolism in ferroptosis. Firstly, it enzymatically breaks down heme into biliverdin, carbon monoxide, and free iron, which can contribute to ferroptosis by promoting lipid peroxidation and oxidative stress (McKie et al., 2001, Kovtunovych et al., 2010). On the other hand, overexpression of HMOX1 can activate NRF2 pathway, which upregulates the expression of various antioxidant enzymes and proteins, enhancing the cell's antioxidant capacity (discussed later) (Chiang et al., 2018). Additionally, RAS increases the intracellular iron concentration by upregulating transferrin receptor and downregulating ferritin, resulting in

the occurrence of ferroptosis. RAS mutations increase the ability of cellular resistance to ferroptosis (Yang and Stockwell, 2008, Schott et al., 2015).

In the cell, iron plays an important role as a cofactor in diverse biological processes such as oxygen transport, cellular respiration, and DNA synthesis and iron-sulfur protein production in mitochondria. Reduced iron–sulfur cluster biosynthesis by the depletion of NFS1 cysteine desulfurase triggers ferroptosis. Whereas the overexpression of the iron–sulfur cluster assembly enzyme (ISCU) blocks dihydroartemisinin (DHAN)-induced ferroptosis.

Lipid metabolism

Lipid metabolism plays a crucial role in ferroptosis by facilitating lipid peroxidation primarily through Fe2+ mediated oxidation of polyunsaturated fatty acids (PUFAs) to produce lipid peroxides, which are key inducers of ferroptosis (Lin et al., 2018) (Lim et al., 2024). Lipid peroxides, particularly phospholipid peroxides, accumulate during ferroptosis and contribute to cell death by damaging DNA, RNA, lipid molecules, and cell membranes. Key enzymes involved in this process include various isoforms of arachidonate lipoxygenase (ALOX), such as ALOX5, ALOX12, ALOX15, ALOX15B, and ALOXE3 (Wenzel et al., 2017, Li et al., 2020d). Additionally, cytochrome P450 oxidoreductase (POR) may mediate lipid peroxidation independently of ALOX (Zhou et al., 2020). The production of PUFAs for lipid peroxidation requires the activation of upstream lipid synthesis pathways, particularly the conversion of arachidonic acid (AA) to AA-CoA by acyl-CoA synthetase long-chain family member 4 (ACSL4); and arachidonic acid (AA) and docosahexaenoic acid (DHA) into phosphatidylcholine (PC) by Lysophosphatidylcholine acyltransferase 3 (LPCAT3)(Doll et al., 2017, Yuan et al., 2016). Upregulation of ACSL4 and LPCAT3 expression serves as a biomarker of ferroptosis sensitivity. Conversely, ACSL3-mediated production of monounsaturated fatty acids (MUFAs) can limit oxidative PUFA-mediated ferroptosis in certain cancer cells, indicating opposing roles for

ACSL4 and ACSL3 in ferroptosis (Magtanong et al., 2019). In addition, Nicotinamide Adenine Dinucleotide Phosphate (NADPH) Oxidases (NOX) contribute to the final step of lipid peroxidation by catalysing the production of reactive oxygen species (ROS), including superoxide radicals (O2•−), using NADPH as a substrate (Yang et al., 2016).

The process of lipid peroxidation

Lipid peroxidation, a critical process in ferroptosis, which undergoes three distinct phases: initiation, propagation, and termination. Initiation involves the formation of a phospholipid radical (PL•) from bis-allylic position methylene groups in polyunsaturated fatty acids (PUFAs) (Pope and Dixon, 2023). Subsequently, propagation occurs as a lipid peroxyl radical (LOO•) is generated through oxygenation, leading to the production of another lipid radical (L•) and lipid peroxide (LOOH) by removing hydrogen from another PUFA. This chain reaction continues until termination, where excessive free radicals are neutralized by antioxidants or reach saturation, forming stable non-radical species. Failure to neutralize oxidative stress from PUFAs leads to increased lipid peroxidation, facilitating ferroptosis by damaging the cell membrane (Li and Li, 2020).

(B) Anti-ferroptotic pathway

Ferroptosis can be induced by inhibiting cellular anti-oxidant system, such as Cystine-Glutamate Transporter System Xc−and GPX4 (Kuang et al., 2020).

Dysregulation of Amino Acid metabolism

Amino acid metabolism plays a critical role in ferroptosis by regulating cellular antioxidant defences, lipid metabolism, and redox balance (Habib et al., 2015). Perturbations in amino acid availability, particularly cysteine, plays a central role due to its significance in the synthesis of glutathione (GSH), the most abundant intra cellular antioxidant. Cysteine is derived from the

metabolism of methionine via transsulfuration pathways or from extracellular cystine uptake via the cystine/glutamate antiporter system Xc^-(Hayano et al., 2016). Once synthesized, GSH serves as a reducing agent to glutathione peroxidase 4 (GPX4), a selenium-dependent enzyme, to detoxify lipid hydroperoxides and prevent the accumulation of lipid peroxides in cell membranes. This reaction converts GSH into its oxidized form, glutathione disulfide (GSSG). The recycling of GSSG back to GSH is mediated by glutathione reductase, maintaining a pool of reduced GSH for continuous GPX4 activity (Mannes et al., 2011). Additionally, dysregulation of system Xc^- or alterations in GPX4 expression or activity can disrupt cellular antioxidant defences and exacerbate lipid peroxidation, leading to ferroptosis induction (Huang et al., 2005).

Interestingly, Transcriptional regulation of GPX4 expression can be influenced by various cellular signalling pathways, including the nuclear factor erythroid 2-related factor 2 (Nrf2) pathway, which controls the expression of antioxidant response genes. (Discussed later) (Liu and Wang, 2019). The inhibition of these antioxidant systems promotes the accumulation of toxic iron and reactive peroxides, which, in turn, triggers a series of lipid radical reactions that damage the cell membrane (Roh et al., 2017, Wu et al., 2024).

The regulation of ferroptosis involves additional antioxidant pathways beyond the canonical GSH/GPX4 and system Xc−, each playing a crucial role in maintaining redox balance and preventing lipid peroxidation. The NADPH pathway is essential for regenerating glutathione (GSH) and supporting antioxidant enzymes, thereby inhibiting ferroptosis (Fernandez et al., 2000). Nuclear factor erythroid 2–related factor 2 (NRF2), a transcription factor, upregulates genes involved in antioxidant defences, including GPX4 and system Xc−, to counteract oxidative stress (Habib et al., 2015, Roh et al., 2017). FSP1 (also known as AIFM2) reduces CoQ10 to ubiquinol, preventing lipid peroxidation and ferroptosis (Doll et al., 2019, Bersuker et al., 2019, Wu et al., 2024). The roles of NRF2 and FSP1 in ferroptosis regulation will be discussed in detail

in the next section. Additionally, the thioredoxin system maintains redox homeostasis by reducing protein disulfides and regenerating antioxidants, further protecting cells from ferroptosis (Hsieh et al., 2024). BH4, a cofactor with antioxidant properties, scavenges reactive oxygen species and modulates lipid metabolism, thereby inhibiting ferroptosis. Guanosine triphosphate cyclohydrolase 1 (GCH1) and its metabolic-derived tetrahydrobiopterin (BH4) also counteract ferroptosis by selectively preventing phospholipid depletion and lipid peroxidation, independently of the GPX4/GSH system (Kraft et al., 2020). These pathways collectively ensure cellular resistance to ferroptotic cell death.

1.3.2 Regulation of Ferroptosis by Noncanonical Antioxidant Pathways

a) NRF2-Mediated Antioxidant Response

Nuclear factor erythroid 2-related factor 2 (NRF2) is a master regulator of the cellular antioxidant response, controlling the expression of a wide array of cytoprotective genes involved in redox balance, detoxification, and metabolism. While NRF2 activation is protective in normal cells, providing defence against oxidative stress and inflammation, its persistent upregulation in cancer can drive tumour progression, therapeutic resistance, and poor clinical outcomes.

Under normal physiological conditions, NRF2 is tightly regulated by its cytoplasmic repressor KEAP1 (Kelch-like ECH-associated protein 1), which targets it for ubiquitin-mediated degradation. In response to oxidative stress or electrophilic compounds, NRF2 dissociates from KEAP1, translocates to the nucleus, and binds to antioxidant response elements (ARE) in the promoters of target genes, driving the expression of detoxifying enzymes such as glutathione S-transferases (GSTs), NAD(P)H, peroxiredoxins (PRDXs), and thioredoxin (TRX). These enzymes collectively work to detoxify reactive oxygen species (ROS) and maintain cellular redox homeostasis, protecting cells from oxidative damage (Itoh et al., 1997).

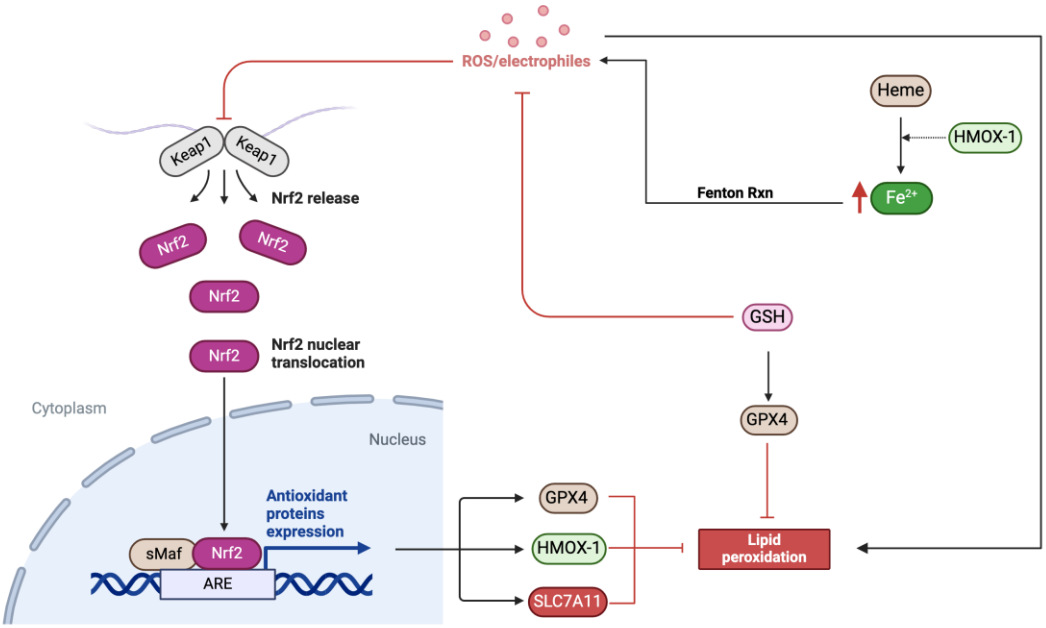

Fig. 1.5 Interaction between KEAP1 and Nrf2)

During oxidative stress, KEAP1 can no longer direct NRF2 towards degradation, stabilizing and accumulating NRF2 within the cell. NRF2 protects cells from ferroptosis by upregulating genes involved in iron metabolism, such as GPX4, HMOX1, and SLC7A11. This modulation prevents toxic iron (Fe^{2+}) generation and lipid peroxidation, key features of ferroptosis. The figure was generated by Biorender and modified from (Zhao et al., 2023a)

In many cancers, the NRF2-KEAP1 pathway is often dysregulated due to mutations in KEAP1, NFE2L2 (NRF2), or related signalling pathways, leading to persistent NRF2 activation. This constitutive activation enhances antioxidant defences, supports metabolic reprogramming, and promotes chemoresistance by upregulating genes involved in GSH biosynthesis, NADPH regeneration, and iron and lipid metabolism. These processes not only support tumour growth and survival but also play a critical role in ferroptosis resistance by maintaining redox balance and controlling iron levels (Chan and Kwong, 2000, Saha et al., 2020, Fraser et al., 2011).

Maintaining Redox Homeostasis Through Glutathione

NRF2 maintains redox homeostasis by regulating the expression of genes involved in the synthesis and recycling of GSH. NRF2 controls the expression of genes encoding glutamate-cysteine ligase catalytic (GCLC) and modulatory (GCLM) subunits, which are essential for GSH synthesis, and regulates glutathione synthetase (GSS) to further promote GSH production (Romero et al., 2017). NRF2 contributes to anti-ferroptotic pathway by upregulating SLC7A11, thereby enhancing cysteine import for GSH synthesis, which is essential for GPX4-mediated detoxification of lipid hydroperoxides (Chan and Kwong, 2000)). Beyond this, NRF2 broadly enhances cellular antioxidant capacity by inducing the expression of a wide range of antioxidant and detoxifying enzymes, thereby providing robust defence against oxidative stress. It activates genes encoding phase II detoxification enzymes, including glutathione S-transferases (GSTs) and NAD(P)H, which support cellular redox homeostasis (Saha et al., 2020).

Additionally, NRF2 regulates the expression of antioxidant enzymes like peroxiredoxins (PRDXs) and thioredoxin (TRX), which cooperate to reduce ROS levels and regenerate antioxidant molecules, maintaining cellular redox balance (Cuadrado et al., 2019).

Controlling Lipid Metabolism

In lipid metabolism, NRF2 regulates the transcription of glucose-6-phosphate dehydrogenase (G6PD) and other enzymes in the pentose phosphate pathway (PPP), as well as controlling the expression of malic enzyme 1 (ME1) and isocitrate dehydrogenase 1 (IDH1), both of which contribute to NADPH production (Mitsuishi et al., 2012). By reducing fatty acid generation and desaturation, NRF2 increases NADPH availability for detoxification processes rather than lipid synthesis. Additionally, NRF2 activation leads to the transcription of PPARγ and NR0B2, nuclear receptors that regulate cholesterol metabolism and mitigate lipid peroxide accumulation, further protecting cells from ferroptosis (Cho et al., 2010).

Controlling Iron Metabolism

NRF2 regulates iron metabolism to control iron levels and prevent ferroptosis, a process driven by the iron-catalysed formation of ROS through the Fenton reaction. It upregulates the expression of ferritin light chain (FTL) and heavy chain (FTH1), which stabilize and store iron, as well as haem oxygenase-1 (HMOX1), which degrades haem to release iron (Fraser et al., 2011). NRF2 activates HMOX1 expression in response to oxidative stress, providing cytoprotective effects by reducing ROS levels through biliverdin and bilirubin. HMOX1 degrades haem into biliverdin, free iron, and CO. While the antioxidant products inhibit ferroptosis, the free iron can promote ferroptosis by catalysing ROS production (Menon et al., 2022, Chiang et al., 2018). NRF2 also controls iron export by regulating ferroportin (FPN1/SLC40A1), the only known iron exporter, thus facilitating iron excretion and reducing intracellular iron levels (Kerins and Ooi, 2018). Additionally, NRF2 upregulates HERC2, an E3 ubiquitin ligase that degrades proteins involved in iron storage and release, such as NCOA4 and FBXL5, to maintain appropriate iron levels and prevent excessive ROS generation (Anandhan et al., 2023). Furthermore, NRF2 enhances cellular antioxidant capacity by upregulating a wide range of antioxidant and detoxifying enzymes, ensuring robust defences against oxidative stress (Saha et al., 2020)

Interestingly, dysregulation in PI3K/mTORC1 can promote glycolysis and fatty acid synthesis. Activation of the PI3K/AKT signalling pathway also enhances NRF2 nuclear translocation, triggering its antioxidant response independent of KEAP1 regulation (Vivanco and Sawyers, 2002, Li et al., 2006). This mechanism will be discussed in more detail later.

Pharmacological inhibitors of NRF2

Several pharmacological inhibitors, such as dexamethasone, clobetasol propionate, all-trans-retinoic acid, brusatol, luteolin, and wogonin, show potential but lack specificity. High-throughput screening identified ML385 as a promising inhibitor, though its selectivity is uncertain. Other inhibitors like halofuginone, AEM1, ochratoxin A, trigonelline, malabaricone-A, and ascorbic acid have shown efficacy in reducing NRF2 activity and sensitizing cancer cells to therapies. However, the main concern with these compounds is the lack of conclusive evidence for their selectivity in inhibiting NRF2 (Robledinos-Anton et al., 2019).

Trigonelline

Trigonelline exerts its inhibitory effects on NRF2 signalling through multiple mechanisms. Primarily, it disrupts the interaction between NRF2 and KEAP1, which prevents the ubiquitination and degradation of NRF2. This stabilization of NRF2 in the cytoplasm hinders its nuclear translocation and transcriptional activity, leading to a reduction in the expression of NRF2 target genes involved in antioxidant defence. Additionally, trigonelline can modulate NRF2 and KEAP1 stability and activity through post-translational modifications, including phosphorylation, acetylation, and ubiquitination. These modifications influence NRF2's transcriptional activity and overall antioxidant response (Srivastava et al., 2022). Trigonelline also affects the expression and function of upstream regulators like p62/SQSTM1 and cullin 3 (CUL3), further regulating NRF2 activation and downstream antioxidant gene expression (Liao et al., 2015)..

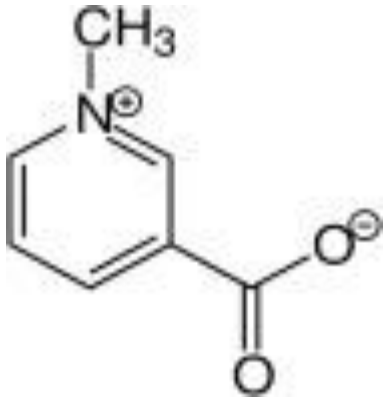

Fig. 1.6 Structural formula of trigonelline

Trigonelline-based therapies targeting NRF2 inhibition hold significant promise for cancer treatment, particularly in sensitizing cancer cells to ferroptosis-inducing agents. By reducing NRF2 activity, trigonelline enhances cancer cell susceptibility to oxidative stress and lipid peroxidation, both critical for ferroptotic cell death. This approach may overcome drug resistance and improve the efficacy of conventional chemotherapeutics (Roh et al., 2017). For instance, combining trigonelline with GPX4 inhibitors or iron chelators can synergistically promote ferroptosis in cancer cells, potentially reversing resistance to standard therapies (Shin et al., 2018). Additionally, Fouzder et al. (2021) reported that trigonelline inhibits non-small cell lung cancer (NSCLC) cell proliferation by downregulating NRF2 signalling and activating lipid peroxidation pathways, enhancing the efficacy of cisplatin in NSCLC xenograft models. These findings underscore the potential of trigonelline as a versatile adjuvant in overcoming resistance and enhancing ferroptosis in a variety of cancer types.

b) AIFM2/FSP1-CoQ10 Axis in Ferroptosis Suppression

Apoptosis-Inducing Factor Mitochondria-Associated 2 (AIFM2), also known as Ferroptosis Suppressor Protein 1 (FSP1), is a mitochondrial flavoprotein that protects against ferroptosis independently of the classical GPX4 (Doll et al., 2019). This alternative defence mechanism is particularly significant in cancer cells, where resistance to cell death can limit treatment efficacy.

Molecular Mechanisms of FSP1 in Antioxidant Defence

FSP1 mitigates ferroptosis by reducing coenzyme Q10 (CoQ10) to its active form, ubiquinol, which acts as a lipid-soluble antioxidant, preventing lipid peroxidation within cell membranes. This process requires FSP1 to be myristoylated, facilitating its association with lipid bilayers, and utilizes NAD(P)H as a co-substrate. Loss of FSP1 or inhibition of its myristoylation increases susceptibility to ferroptosis (Bersuker et al., 2019).

Additionally, NRF2 can transcriptionally upregulate FSP1, enhancing cellular resistance to ferroptosis by increasing CoQ10 levels and maintaining membrane integrity (Koppula et al., 2022). This NRF2-FSP1-CoQ10 axis forms a potent antioxidant defence network, particularly in KEAP1-deficient lung cancer cells (Taguchi and Yamamoto, 2017). Furthermore, in KRAS mutant cells, FSP1 upregulation confers resistance to ferroptosis, indicating that KRAS mutations activate NRF2, promoting FSP1 expression (Li et al., 2023).

The discovery and development of FSP1 inhibitors, such as iFSP1, represent a significant breakthrough in overcoming the resistance of certain cancers to ferroptosis.

FSP1 inhibitor (iFSP1)

Doll et al. (2019) screened conducted a large-scale screening of approximately 10,000 compounds to identify potent FSP1 inhibitors. This effort led to the discovery of iFSP1, a small

molecule that directly targets FSP1, thereby inducing ferroptosis in tumour cells. iFSP1 operates by inhibiting the enzyme's ability to reduce CoQ10, a critical antioxidant in the cell membrane that prevents lipid peroxidation. By blocking this pathway, iFSP1 significantly enhances the accumulation of lipid peroxides, driving cancer cells towards ferroptosis.

Interestingly, iFSP1 is particularly effective in cells with impaired GPX4 function. In GPX4-knockout cells that overexpress FSP1, iFSP1 induces robust ferroptosis, highlighting its potential to target cancers that have developed resistance to GPX4 inhibitors. Notably, Cheu et al. (2023) demonstrated that in hepatocellular carcinoma (HCC) cells, even with intact GPX4, iFSP1 effectively induces ferroptosis and significantly suppresses tumour growth. This suggests that targeting FSP1 alone is sufficient to trigger ferroptotic cell death in some contexts, broadening the therapeutic potential of iFSP1. Additionally, iFSP1 indirectly activates anti-tumour immune responses by upregulating chemokines like CXCL9 and CX3CL1, which recruit immune cells such as antigen-presenting dendritic cells, macrophages, and cytotoxic T cells to the tumour, promoting immune clearance of HCCs (Ozga et al., 2021). While iFSP1 enhances tumour cell sensitivity to ferroptosis, it is particularly effective when combined with immune checkpoint inhibitors (ICIs) like anti-PD-1 or anti-PD-L1, improving the efficacy of immunotherapy in drug-resistant cancers (House et al., 2020).

Moreover, combining iFSP1 with GPX4 inhibitors can further reduce tumour cell resistance, demonstrating promising results in treatments for cancers such as esophageal squamous cell carcinoma and osteosarcoma (Yamasaki et al., 2010). Interestingly, iFSP1 is effective specifically on human FSP1 and not on mouse Fsp1, highlighting a need for further research on its efficacy *in vivo* (Gao et al., 2024). Additionally, iFSP1 enhances the toxicity of RSL3 in FSP1-knockout human cancer cell lines and selectively induces ferroptosis in GPX4-knockout Pfa1 and HT1080 cells, sensitizing various cancer cell lines to ferroptosis inducers (Mishima et al., 2022). This raises the question of whether GPX4 is the sole target for RSL3 in ferroptosis

regulation or could involve off-target effects, compensatory pathways, or increased cellular sensitivity to lipid peroxidation when antioxidant defences like FSP1 are impaired.

Further research is needed to fully understand the upstream signalling pathways and transcriptional regulators of FSP1 to develop targeted therapies that modulate its activity, enhancing the efficacy of ferroptosis-based treatments.

c) Protective Roles of ESCRT-III, GCH1, and CoQ10

Beyond these classical antioxidant pathways, recent studies have identified the ESCRT-III complex, GTP cyclohydrolase 1 (GCH1), and CoQ10 as critical components in the maintenance of membrane integrity during oxidative stress.

ESCRT-III Machinery in Membrane Repair

The ESCRT-III complex, traditionally known for its role in endosomal sorting and membrane remodelling, has emerged as a critical player in membrane repair. It functions by excising peroxidized regions of the cell membrane, preventing complete rupture and consequent cell death. For instance, CHMP4B, a core component of the ESCRT-III complex, is recruited to sites of membrane damage where it facilitates the formation of membrane vesicles that bud off, removing damaged lipid regions and maintaining cell viability under oxidative stress (Skowyra et al., 2018; Conway et al., 2021).

GCH1 and CoQ10 in Membrane Protection

In parallel, GCH1 supports membrane integrity by enhancing the synthesis of CoQ10 through the production of BH2 and BH4. CoQ10, a product of the mevalonate pathway, acts as a potent lipophilic antioxidant, scavenging lipid peroxyl radicals and protecting membrane integrity. This dual approach, where ESCRT-III addresses physical membrane damage and CoQ10 neutralizes lipid peroxides, forms a protective network against ferroptosis, emphasizing the

critical role of noncanonical antioxidant pathways in maintaining cellular survival (Kraft et al., 2020).

d) Other Key Noncanonical Modulators

Dual role of Haem oxygenase-1 (HMOX1)

Although Haem oxygenase-1 (HMOX1) is commonly associated with promoting ferroptosis by increasing intracellular iron and reactive oxygen species (ROS), its function is highly context-dependent and, under certain conditions, it can also contribute to ferroptosis resistance (Adedoyin et al., 2018, Fraser et al., 2011). This dual behaviour reflects the complex balance between iron metabolism and antioxidant regulation, particularly in cancer cells with adaptive redox responses.

HMOX1 can promote resistance to ferroptosis through the upregulation of ferritin, an iron-storage protein. While HMOX1 increases the labile iron pool by degrading haem, its overexpression can induce ferritin, an iron-storage protein, which sequesters excess iron, thereby limiting the availability of labile Fe^{2+} for the Fenton reaction to generate ROS needed for ferroptosis (Wang et al., 2023a). Additionally, HMOX1 is a well-known transcriptional target of NRF2, a central regulator of oxidative stress responses. When activated, HMOX1 becomes part of a broader antioxidant program, which includes increased GSH synthesis and enhanced ROS detoxification—both critical for limiting ferroptosis (Chiang et al., 2018). Interestingly, while ferroptosis inducers like Erastin and RSL3 elevate HMOX1 expression, knockout or inhibition studies show conflicting roles, indicating that HMOX1 can also promote ferroptosis under certain stress conditions (Yang et al., 2021a, Tang et al., 2021). Chronic or excessive HMOX1 activity can shift the balance from promoting oxidative damage to limiting it, particularly in cancer cells or tissues with robust adaptive responses. This is evident in Erastin-

and Sorafenib-treated models, where inhibition of HMOX1 increases ferroptotic cell death, implying its protective role in these contexts (Zhu et al., 2022b).

Dual role of p53

p53 is a tumour suppressor gene activated under various stress stimuli and plays a complex role in ferroptosis. It promotes ferroptosis by repressing SLC7A11, a component of the cystine/glutamate antiporter system Xc−. This repression reduces cystine uptake and glutathione (GSH) synthesis, leading to increased lipid peroxidation and ferroptotic cell death (Liu and Gu, 2022). Additionally, p53 induces the expression of spermidine/spermine N1-acetyltransferase 1 (SAT1), which enhances lipid peroxidation and ferroptosis through metabolic reprogramming (Ou et al., 2016).

However, p53 can also inhibit ferroptosis by upregulating genes that increase the expression or activity of glutathione peroxidase 4 (GPX4), which neutralizes lipid peroxides, maintaining cellular redox balance and preventing ferroptotic cell death under certain conditions (Kang et al., 2019). p53 also induces p21, a cyclin-dependent kinase inhibitor that maintains GSH levels and reduces oxidative stress, providing further protection against ferroptosis (Tarangelo and Dixon, 2018).

1.3.2 Ferroptosis modulation by TSC2 loss

Ferroptosis drug resistance is modulated by various signalling pathways that regulate cellular responses to oxidative stress and lipid peroxidation. These pathways play crucial roles in modulating the expression of key proteins involved in antioxidant defences, iron metabolism, lipid homeostasis, and cell death. Here are some of the signalling pathways known to influence ferroptosis resistance.

1.3.2.1 *TSC2* Loss-Mediated mTORC1 Overactivation on Ferroptosis

The hyperactive mTORC1 signalling in *TSC2*-deficient cells which enhances anabolic processes and alters redox homeostasis exacerbates oxidative stress. Understanding how these changes affect the susceptibility of *TSC2*-deficient cells to ferroptosis provides valuable insights into potential therapeutic strategies.

Altered Redox Balance and Lipid Metabolism

Studies have shown that cells with heightened mTORC1 activity exhibit increased levels of reactive oxygen species (ROS), which eventually overwhelm the cellular antioxidant systems, leading to lipid peroxidation and cell death (Yang et al., 2016, Stockwell et al., 2017). Over time, this persistent oxidative stress can deplete their antioxidant defences, making them increasingly vulnerable to ferroptosis (Jiang et al., 2021a). For example, In *TSC2*-deficient cells, hyperactive mTORC1 signalling promotes the synthesis of proteins and glutathione through the activation of transcription factors such as ATF4. This elevated antioxidant capacity might initially confer resistance to oxidative stress (Torrence et al., 2021). Additionally, mTORC1 signalling upregulates the expression of SLC7A11 and glutathione peroxidase 4 (GPX4), both of which are vital antioxidants that negatively regulate ferroptosis by preventing the accumulation of lipid peroxides (Friedmann Angeli et al., 2014). The balance between these protective mechanisms and the pro-oxidant environment created by hyperactive mTORC1 determines the sensitivity of TSC2-deficient cells to ferroptosis.

The mTORC1 pathway also stimulates lipid synthesis and the incorporation of polyunsaturated fatty acids (PUFAs) into cellular membranes, which are substrates for lipid peroxidation. This makes TSC2-deficient cells more susceptible to the accumulation of lipid reactive oxygen species (L-ROS) and ferroptotic cell death. Studies have demonstrated that mTORC1 enhances lipogenesis through the activation of sterol regulatory element-binding proteins (SREBPs),

which in turn increase the synthesis of PUFAs (Peterson et al., 2011). This generation of higher levels of oxidizable lipids through metabolic reprogramming is critical in determining the susceptibility of *TSC2*-deficient cells to ferroptosis (Zhou and Huang, 2010).

mTOR Regulation of Intracellular Iron Homeostasis

mTOR also regulates iron metabolism by modulating the expression of iron transport proteins, such as transferrin receptor 1 (TfR1) and ferroportin (FPN), thus affecting cellular iron levels (Bayeva et al., 2012). Sustained mTORC1 activation can elevate the expression of haem oxygenase 1 (HMOX1), which releases iron from haem for ROS production, playing a dual role in ferroptosis induction and inhibition (discussed in 1.3.2.3). Additionally, environmental fluctuations like temperature changes, mTORC1 activates heat shock proteins (HSPs) by nuclear translocation to maintain cell structure. This activation negatively regulates ferroptosis through iron regulation. Phosphorylated HSPB1 acts as a negative regulator of ferroptosis by reducing cellular iron uptake and lipid ROS production. Inhibition of heat shock protein beta-1 (HSPB1) expression and phosphorylation *in vitro* and *in vivo* increases the anticancer activity of Erastin-mediated ferroptosis (Fuhrmann et al., 2020) . Moreover, Ferritinophagy, a form of autophagy, regulates ferroptosis through iron metabolism; impaired autophagy due to mTORC1 overactivation inhibits ferroptosis (Wei et al., 2020, Sui et al., 2019). Furthermore, mTOR regulates the other endogenous antioxidant defence systems, crucial for counteracting oxidative stress-induced lipid peroxidation. mTORC1 promotes NRF2 activation by phosphorylating p62, leading to Keap1 degradation and NRF2 nuclear translocation. This enhances cellular defence against oxidative stress and reduces susceptibility to ferroptosis (Ichimura et al., 2013).

1.3.2.2 Through mTORC1 Independent Mechanisms

Ferroptosis sensitivity in tumours is significantly influenced by various extrinsic stresses such as nutrient availability, temperature, hypoxia, and metabolic acidosis, independent of the

mTORC1 pathway. Intrinsic stresses, including energy, oncogenic, endoplasmic reticulum (ER), and genomic stress, also play critical roles. Understanding how these stresses affect ferroptosis in *TSC2*-deficient cells is crucial for developing therapeutic strategies.

Modulation by AMPK

AMPK plays a dual role in ferroptosis, particularly in TSC2 deficiency. Energy stress-activated AMPK can promote ferroptosis by inhibiting System Xc– activity, reducing cystine uptake, and glutathione synthesis (Song et al., 2018, Li et al., 2022c). Conversely, AMPK can inhibit ferroptosis by regulating lipid metabolism, reducing PUFA synthesis, and enhancing antioxidant defences (Li et al., 2020b, Lee et al., 2020).

Modulation by Hypoxia

In response to low levels of oxygen in tissues, termed hypoxia, cells undertake myriad changes in both gene transcription, translation and protein activity. Crucial to the response are the hypoxia-inducible factor family of transcription factors (HIFs) (Sun et al., 2020)). HIF1α stabilization triggers its nuclear translocation, resulting in de novo gene transcription and the modulation of cellular metabolic processes. This includes regulation of iron uptake and lipid peroxidation with a consequent impact on ferroptosis sensitivity; namely resistance to ferroptosis (Fuhrmann et al., 2020). HIF1a also influences ferroptosis through GSH depletion and activation of antioxidants through NRF2/HMOX1 signalling pathways. Vascular endothelial growth factor (VEGF), which is known to be important for neo-angiogenesis and tumour progression can be upregulated by HIF1a and has been identified as up regulated in *TSC2* deficient cells. This upregulation of VEGF has been reported as independent of the mTORC1 overactivation observed in TSC2 deficient cells (Coffey and Simon, 2024, Brugarolas et al., 2003).

Other stress factors

TSC2 deficiency also leads to increased stress granule formation, with proteins like HDLBP recruiting TSC2 to stress granules, crucial for tumour suppression (Kosmas et al., 2021). Long-term sorafenib treatment in HCC cells increases HDLBP levels, reducing the efficiency of ferroptosis-inducing agents and highlighting a mechanism of ferroptosis resistance (Feicht and Jansen, 2024).

1.3.2.3 Interplay Between TSC2 Loss and Antioxidant Pathways in Ferroptosis Regulation

The loss of TSC2 significantly modulates multiple antioxidant pathways, enhancing cellular resistance to ferroptosis. These pathways include GSH/GPX4 synthesis, iron metabolism, NRF2 activation, FSP1 upregulation, and membrane repair via ESCRT-III, collectively supporting cancer cell survival under oxidative stress (Zarei et al., 2019, Liu et al., 2021).

Importantly, the impact of TSC2 loss on ferroptosis resistance extends beyond mTORC1 hyperactivation. For instance, TSC2 deficiency can enhance antioxidant defences by upregulating MGST1, a key enzyme involved in lipid peroxidation detoxification, thereby reducing oxidative damage and protecting cells from ferroptosis (CHEN Yuting, 2023). Additionally, TSC2 plays a critical role in regulating autophagy, a process essential for clearing damaged organelles and maintaining redox balance. For example, NQO1 deficiency can activate autophagy via the AMPK/TSC2 pathway, reducing oxidative stress by facilitating the removal of dysfunctional mitochondria (Kim et al., 2016). This connection underscores the importance of mitochondrial quality control in ferroptosis resistance.

Moreover, TSC2 influences NRF2 activation through non-mTORC1 mechanisms. Sestrins promote NRF2 activation by degrading KEAP1, thereby increasing the expression of antioxidant proteins that protect against oxidative damage (Rhee and Bae, 2015). This NRF2-driven response supports the synthesis of GSH, a critical antioxidant that, in conjunction with GPX4, neutralizes lipid peroxides and suppresses ferroptosis (Rhee and Bae, 2015).

In addition to these antioxidant pathways, Ataxia Telangiectasia Mutated (ATM) regulates TSC2 in response to ROS, maintaining the balance between cell growth and antioxidant defences (Alexander et al., 2010). This connection highlights the importance of DNA damage responses in controlling ferroptosis sensitivity in TSC2-deficient cells.

Furthermore, the p62/SQSTM1 protein interacts with TSC2-related networks to regulate glutathione production, supporting mitochondrial integrity and protecting against ferroptosis (Lam et al., 2017). This finding underscores the importance of autophagy and mitochondrial quality control in ferroptosis regulation.

Notably, targeting FSP1 has been shown to sensitize TSC2-deficient cells to ferroptosis, indicating its critical role in maintaining ferroptosis resistance(Kosmas et al., 2021). This relationship highlights the interconnected nature of TSC2 signalling and antioxidant defences in ferroptosis regulation.

Collectively, these pathways enhance the cell's ability to manage oxidative stress and produce antioxidants, offering robust protection against ferroptosis. Understanding these modulators is critical for deciphering the pathways underlying ferroptotic resistance and developing strategies to overcome it, especially in cancer treatment where resistance to cell death pathways can lead to therapeutic failure.

1.3.3 Ferroptosis and Other Cell Death Mechanisms: Key Differences

As previously discussed, ferroptosis is a distinct form of regulated cell death that is dependent on iron and is both mechanistically and morphologically different from other forms such as apoptosis, autophagy, necroptosis, and pyroptosis. While the detailed mechanisms of these pathways have been discussed earlier, the comparison table below offers a concise overview of their key features, activation processes, and regulatory proteins. This overview highlights the

unique features of ferroptosis, particularly its reliance on lipid peroxidation and disruption of cellular redox balance. It also highlights how each cell death pathway contributes differently to cellular balance, immune responses, and disease progression. Understanding these differences is essential for identifying targeted therapeutic strategies, especially in the context of cancer and degenerative disorders.

TABLE 1.4 COMPARISON OF VARIOUS TYPES OF RCD (FERROPTOSIS, APOPTOSIS, AUTOPHAGY, PYROPTOSIS, NECROPTOSIS) MODIFIED FROM (MOU ET AL., 2019)

Features	**Ferroptosis**	**Apoptosis**	**Autophagy**	**Necroptosis**	**Pyroptosis**
Biochemical Features	GPX4 inhibition, plasma membrane damage by lipid peroxidation	Caspase activation, DNA fragmentation	Increased lysosomal activity	ATP depletion; activation of inflammatory cytokines; activation of RIP1, RIP3, and MLKL	Dependent on caspase-1 and release of proinflammatory cytokines
Morphological Features	Small mitochondria; change in density reduction or vanishing of mitochondria cristae; outer mitochondrial membrane rupture	Plasma membrane blebbing; cellular and nuclear volume reduction; nuclear fragmentation	Formation of double-membraned autolysosomes	Plasma membrane rupture; organelle swelling; moderate chromatin condensation	Karyopyknosis; cell swelling; membrane rupture
Immune Features	Pro-inflammatory	Mostly anti-inflammatory	Mostly anti-inflammatory	Mostly pro-inflammatory	Pro-inflammatory
Activation	Triggered by iron-mediated ROS	Induced by caspase activation	Caused by mTOR inhibition or nutrient deprivation	Triggered by specific signalling pathways (e.g., TNF receptor)	Initiated by Caspase 1 and 11
Regulation	Regulated by lipid peroxidation, GPX4, and iron metabolism	Regulated by Bcl-2 family proteins, caspases	Regulated by mTOR, AMPK, and autophagy-related genes	Regulated by RIPK1, RIPK3, and MLKL signalling	Caspases, PAMPs DAMPs, and cytosolic LPS
Key Genes	GPX4, NRF2, LSH, TFR1, xCT	Caspase, P53, Fas, Bcl-2, Bax	ATG5, ATG7, DRAM3, TFEB	LEF1, RIP1, RIP3	Caspase-1, IL-1β, IL-18

Inducers	Erastin, DPI2, BSO, SAS, lanperisone, SRS, RSL3, DPI7, DPI10, FIN56, sorafenib, artemisinin	FASL, DCC, UNC5B	Rapamycin, lithium, sodium valproate, carbamazepine, C2-ceramide	TNFα, zVAD-fmk, PAMPS	ZnO-NPs, Ivermectin
Inhibitors	Desferoxamine, vitamin E, U0126, ferrostatin-1, SRS, CA-1, cycloheximide, aminooxyacetic acid, Liproxstatin-1 HCl	XIAP, c-IAP1, c-IAP2, ILP-2, ML-IAP/livin, NAIP, Z-VADFMK	3-ME, LY294002, wortmannin, PIK-III, compound 31, SAR 405, Vps34-In1, MRT68921, Spautin-1, Bafilomycin A1, hydrochloroquin	Nec-1, NSA, Kongensin-A	Necrosulfonamide

1.3.4 Ferroptosis inducers

Ferroptosis inducers (FINs) play a pivotal role in cancer treatment by exploiting cancer cells' vulnerability to oxidative stress. They are classified into several groups based on their mechanisms of action. Class I inducers, such as Erastin, Sulfasalazine, and Sorafenib, inhibit the system Xc^-, leading to cystine depletion, impaired glutathione synthesis, and accumulation of reactive oxygen species (ROS). However, the efficacy of Class I inducers is highly cell type–specific, limiting their universal applicability across different tumour types (Zheng et al., 2021, Lachaier et al., 2014, Zhao et al., 2020, Yu et al., 2019). Class II agents, including RSL3, ML162, and ML210, directly inhibit glutathione peroxidase 4 (GPX4), preventing the detoxification of lipid peroxides. Class III inducers, like FIN56 and statins (fluvastatin, simvastatin, lovastatin acid), deplete coenzyme Q10, crucial for lipid antioxidant defence. Class IV inducers, such as Artesunate and $FeCl_2$, increase intracellular Fe2+ and ROS, promoting lipid peroxidation (Du and Guo, 2022, Ma et al., 2024). Class III agents promote ferroptosis by depleting CoQ10, weakening lipid antioxidant defences (e.g., FIN56, statins: fluvastatin, simvastatin, lovastatin acid) (Zhang et al., 2021b, Pearson et al., 2021). Class IV inducers increase intracellular Fe^{2+} and ROS, promoting lipid peroxidation (e.g., artesunate, hemin, haemoglobin, $FeCl_2$, salinomycin, neratinib, withaferin A) (Jin et al., 2023, Li et al., 2021b).

Additionally, nanoparticles (e.g., ZVI NPs, FeGd-HN@Pt@LF/RGD2) enhance ferroptosis by increasing iron and ROS levels within tumour cells (Adzavon et al., 2024). Other compounds, like Auranofin and Methotrexate, inhibit thioredoxin and dihydrofolate reductase (DHFR), respectively, disrupting cellular redox balance (Johnson et al., 2024) . These diverse mechanisms target cancer cells' metabolic weaknesses, offering promising therapeutic strategies (see Table. 1.5)

TABLE 1.5 FERROPTOSIS INDUCERS - CATEGORIZATION, MECHANISM, SUITABILITY FOR IN *VITRO* AND IN *VIVO* USE, AND AVAILABILITY IN CANCER THERAPY

Mechanism	**Compounds**	**Tumour variant**	***In vivo***	**Clinical Use**	**Radiotherapy**	**Reference**
Class I						
Inhibits SLC7A11/System x_c^-	Erastin	Glioma, lung cancer, fibrosarcoma, melanoma, breast cancer, cervical cancer, RCC	√		√	(Dixon et al., 2012, Yoshioka et al., 2019, Shadad et al., 2013, Zhao et al., 2021a)
	Piperazine Erastin (PE)	Fibrosarcoma	√			(Hassannia et al., 2019, Jin et al., 2024)
	Imidazole ketone Erastin (IKE)	DLBCL	√		√	(Zhang et al., 2019, Lei et al., 2021)
	Salfasalazine	Breast cancer, glioblastoma, fibrosarcoma, NSCLC, prostate cancer	√	√		(Li et al., 2020c, Lei et al., 2021)
	Sorafenib	AML, HCC, neuroblastoma, NSCLC, RCC	√	√		(Lachaier et al., 2014, Dixon et al., 2014, Louandre et al., 2015)
	Glutamate	NSCLC	√			(Kang et al., 2021)
GSH depletion	Cyst(e)inase	Prostate cancer, chronic lymphocytic leukemia and pancreatic cancer	√	√		(Saha et al., 2023, Badgley et al., 2020, Kerimoglu et al., 2022)
	Buthionine sulfoximine (BSO)	Melanoma, neuroblastoma	√			(Talty and Bosenberg, 2022, Sun et al., 2023b)
	Diphenyleneiodonium 2 (DPI2)	Fibrosarcoma cell				(Wang et al., 2022a)
	Cisplastin	Ovarian cancer, pancreatic cancer, NSCLC, urothelial cancer	√	√		(Du et al., 2023, Guo et al., 2018, Chen et al., 2023)
Class II						

Inhibits GPX4	1S,3R-RSL3	Glioblastoma, Fibrosarcoma, NSCLC, pancreatic cancer, leukemia	√		√	(Zhang et al., 2020, Li et al., 2020a, Lu et al., 2023)
	ML162	TNBC				(Beatty et al., 2021)
	ML210	CCC				(Zhou et al., 2019)
	Altretamine	Lymphoma, sarcoma, ovarian cancer	√	√		(Wang et al., 2022b, Nie et al., 2022)
Class III						
Degrade GPX4, activate SQS and deplete CoQ_{10}	FIN56	Fibrosarcoma, glioblastoma	√		√	(Zhang et al., 2021b, Pearson et al., 2021)
Inhibits CoQ_{10} synthesis, reduce GPX4 expression	Statins (fluvastatin, simvas-tatin, lovastatin acid)	Breast cancer, AML, HCC, MM, Fibrosarcoma, NSCLC	√	√	√	(Liu et al., 2022, Yao et al., 2021, Jiang et al., 2021a)
Class IV						
Increases intracellular Fe^{2+}	Artesunate	Pancreatic cancer	√	√	√	(Yu et al., 2023, Li et al., 2021b)
	Hemin,	Lung cancer, Breast cancer	√	√		(Wang et al., 2017, Gao et al., 2022, NaveenKumar et al., 2019, Almahi et al., 2022)
	Haemoglobin	Glioblastoma, leukemia	√	√	√	(Tang et al., 2021)
	$FeCl_2$	Colon cancer	√			(Hassannia et al., 2019)
	Lapatinib + siramesine	Breast cancer	√	√		(Ma et al., 2016, Tang et al., 2021)

	Salinomycin	Brain cancer	√	√		(Ou et al., 2022)
	Neratinib	Breast cancer	√	√		(Nagpal et al., 2019)
	Withaferin	CRC	√	√		(Hassannia et al., 2018)
	BAY 11–7085	CRC, cervical cancer				(Zhang et al., 2022a)
Nanoparticles						
Increases intracellular Fe^{2+} and ROS	ZVI NPs	Lung cancer	√			(Hsieh et al., 2021)
	FeGd-HN@Pt@LF/ RGD2	MEFs, Melanoma	√			(Yan et al., 2021, Liang et al., 2019)
	DGU:Fe/Dox	4T1	√			(Lei et al., 2021, Shi et al., 2022)
Other FINs						
Inhibits mitochondrial complexI	BAY 87–2243	NSCLC			√	(Ellinghaus et al., 2013, Helbig et al., 2014)
Inhibits thioredoxin	Auranofin/ Ferroptocide	Breast, lung cancer, NSCLC	√	√	√	(Kato et al., 2020, Hsieh et al., 2024)
Inhibits FSP1	iFSP1	Fibrosarcoma, NSCLC, AML	√		√	(Xavier da Silva et al., 2023, Nakamura et al., 2023)
	Trigonelline, brusatol	HCC, NSCLC, lymphoma, breast cancer	√		√	(Koeberle et al., 2023, Shin et al., 2018, Tian et al., 2022)
Inhibits DHFR	Methotrexate	neuroblastoma (NBL), Bladder cancer	√	√		(Sternberg et al., 1986, Thornton et al., 2016)
CoQ10 depletion	4-CBA	Lung cancer	√			(Koppula et al., 2022)
Inhibits GCH1	DAHP	Colorectal cancer				(Hu et al., 2022)
Promotes ferritinophagy	JQ-1	Pancreatic cancer, Astrocytoma, Glioblastoma	√	√	√	(Miller et al., 2021, Garcia et al., 2022, Wang et al., 2023c)

Erastin

Erastin is a small molecule, discovered in 2003 via high-throughput screening, induces ferroptosis by targeting mitochondrial voltage-dependent anion channels (VDACs) and inhibiting the cystine/glutamate antiporter system Xc− (SLC7A11/xCT). This inhibition results in cysteine deprivation, reducing glutathione (GSH) levels, and leading to the accumulation of lipid reactive oxygen species (L-ROS), culminating in ferroptotic cell death (Dixon et al., 2012).

Further studies revealed Erastin interacts with key molecular targets such as VDAC, p53, and SLC7A11, supporting its potential as a targeted anticancer agent. It disrupts cellular redox homeostasis by decreasing intracellular GSH, increasing oxidative stress, and impairing the antioxidant function of GPX4 (Zhao et al., 2020). This inhibition promotes ferroptosis through L-ROS accumulation and polyunsaturated fatty acids (PUFAs) consumption. Despite promising *in vitro* and *in vivo* results, clinical application of Erastin is limited due to its poor solubility and metabolic instability. To overcome these limitations, analogues such as piperazine-Erastin (PE) and imidazole ketone Erastin (IKE) have been developed. These compounds exhibit improved tumour growth inhibition and reduced toxicity. Combining these analogues with other treatments, including radiotherapy or chemotherapy, may further enhance therapeutic efficacy and minimize side effects (Shibata et al., 2019)(Xie et al., 2016).

1S,3R-RSL3 (RSL3)

RSL3 (Ras-selective lethal 3) is extensively used in ferroptosis studies due to its specific inhibition of glutathione peroxidase 4 (GPX4). Under normal conditions, GPX4 uses reduced glutathione (GSH) to reduce lipid hydroperoxides to alcohols, preventing lipid peroxidation (Sui et al., 2018). However, RSL3 inhibits GPX4, depleting GSH and causing lipid peroxides to accumulate, ultimately triggering ferroptotic cell death through membrane lipid peroxidation and mitochondrial dysfunction (Oh et al., 2022). Preclinical studies have demonstrated the

efficacy of RSL3 in inducing ferroptosis in various cancer models. In head and neck cancer cell lines, RSL3 treatment inhibits GPX4 activity, leading to lipid peroxide accumulation and ferroptotic cell death (Shin et al., 2018). Recent mechanistic studies have further elucidated RSL3's role in ferroptosis. For instance, RSL3 treatment upregulates p62 and nuclear factor erythroid 2-related factor 2 (Nrf2), key regulators of cellular antioxidant responses. RSL3 also inactivates Kelch-like ECH-associated protein 1 (Keap1), a negative regulator of Nrf2, thereby enhancing cellular antioxidant defences. (Yang et al., 2021a). This suggests that RSL3-induced ferroptosis involves a complex interplay between oxidative stress, antioxidant responses, and cell death pathways.

Despite its promise, the potential toxicity of RSL3 and its analogues in normal tissues necessitates careful evaluation in preclinical and clinical studies (Shintoku et al., 2017). Understanding the precise molecular mechanisms underlying RSL3-induced ferroptosis could identify novel therapeutic targets and optimize treatment strategies.

1.3.5 Ferroptosis inhibitors

Ferroptosis inhibitors counteract the oxidative processes leading to ferroptosis, protecting cells from death through various mechanisms, both *in vitro* and *in vivo*. Key types include endogenous radical trapping antioxidants (RTAs) like Vitamin E (inhibits LOX), Coenzyme Q10 (scavenges lipid peroxidation intermediates), BH4 (inhibits GPX4), Vitamin K1 (depletes glutathione), and hydropersulfides (inhibit lipid-peroxide free radicals)(Scarpellini et al., 2023, Jiang et al., 2021b) (see Table 1.6). Synthetic RTAs such as Ferrostatins, particularly Ferrostatin-1 (Fer-1), suppress 15-LOX/PEBP1 and reduce the labile iron pool, showing substantial protection against ferroptosis. Liproxstatins convert reduced glutathione to oxidized forms and increase GPX4 protein expression (Zilka et al., 2017). Tricyclic RTAs like Phenothiazine trap lipid radicals directly. Other RTAs, including CuATSM and SKI II, function similarly (Fiorentino et al., 2023). Synthetic ferroptosis inhibitors like Zileuton and baicalein inhibit LOX, while deferiprone and DFO act as iron chelators (Tian et al., 2024).

Fer-1 is particularly crucial for studying ferroptosis due to its high specificity and potency in inhibiting lipid peroxidation, making it an essential tool for understanding the molecular mechanisms of ferroptosis. Its effectiveness in preventing ferroptosis-related cell death also suggests significant therapeutic potential for diseases such as neurodegenerative disorders, ischemia-reperfusion injury, and certain cancers, which will be discussed in this section

TABLE 1.6 COMPREHENSIVE OVERVIEW OF DIFFERENT TYPES OF FERROPTOSIS INHIBITORS, MECHANISMS OF ACTION, AND THEIR USE IN VITRO AND IN VIVO

Type	Compound	Mechanism	In Vitro	In Vivo Use	References
Endogenous RTAs	Vitamin E (α-TOH)	LOX inhibition	Pfa1 cells	√	(Kagan et al., 2017, Kajarabille and Latunde-Dada, 2019)
	Coenzyme Q10 (Ubiquinone 10)	Scavenges lipid peroxidation intermediates, oxidizes, and regenerates via NADPH	Human cancer cell lines		(Bersuker et al., 2019, Shimada et al., 2016)
	BH4 (Tetrahydrobiopterin)	GPX4 inhibition	CRC		(Hu et al., 2022)
	Vitamin K1 (Phyllohydroquinone)	Glutathione depletion	NIH3T3, HT-1080	√	(Kolbrink et al., 2022)
	Hydropersulfides (GSSHs)	Directly inhibit Lipid-peroxide free radical	MEF	√	(Barayeu et al., 2023, Wu et al., 2022)
Synthetic RTAs	Ferrostatins (Ferrostatin-1 (Fer-1), UAMC-3203, SRS11-92, SRS9-11, SRS16-86, UAMC-2418, CFI-4061, CFI-4082	suppression of 15-LOX/PEBP1, reduces the labile iron pool	BeWo, PHKCs	√	(Anthonymuthu et al., 2021, Miotto et al., 2020, Zhao et al., 2023b)
	Liproxstatins (Liproxstatin-1 (Lip-1), Liproxstatin-2 (Lip-2))	Converts reduced GSH to oxidized GSSH, increases GPX4 protein expression	HK2	√	(Feng et al., 2019, Zhang et al., 2021a)
Tricyclic RTAs	Phenothiazine, morpholine, 3-CF3-8-tBu-PNX, CuATSM, CuATSP, SKI II, serdemetan, AZD3463, bazedoxifene	Directly traps lipid radicals and halts the chain reactions of lipid peroxidation			(Yang et al., 2021b, Scarpellini et al., 2023)
Other RTAs	CuATSM, CuATSP, SKI II, serdemetan, AZD3463, bazedoxifene	Directly traps lipid radicals			(Zilka et al., 2021, Scarpellini et al., 2023)
Synthetic RTA Ferroptosis Inhibitors	Zileuton, baicalein, PD-146176, docebenone, MK-886, BWA4C	Synthetic LOX Inhibitors			
	PKUMDL-LC-101, PKUMDL-LC-101-D04	Synthetic GPX4 Activators			

	Deferiprone, DFO, deferasirox, CPX, 2,2-BP, 1,10-phenanthroline, AKI-02	Iron Chelators			

However, the activity of these RTAs can vary depending on the assay conditions, such as the type of cell lines used (e.g., HT-1080 vs. Pfa-1 MEF) and the specific ferroptosis inducers (e.g., Erastin vs. RSL3) (Scarpellini et al., 2023).

Ferrostatins 1 (Fer-1)

The first ferroptosis inhibitor, Ferrostatin-1 (Fer-1), was discovered in 2012 through high-throughput screening of a diverse small molecule library. Initially identified as an arylalkylamine, Fer-1 prevents lipid hydroperoxide accumulation in an erastin-induced ferroptosis model in HT-1080 cells (Kwon et al., 2015). While it was initially considered solely a reductant, subsequent research in 2017 revealed its mechanism as a Radical-Trapping Antioxidant (RTA). Various studies have tried to modify the structure of Fer-1 to improve potency and develop new inhibitor, but it did not improve activity as expected. Hence, more studies needed for developing novel ferroptosis inhibitors with enhanced pharmacokinetic profiles while maintaining efficacy.

1.3.6 Ferroptosis sensitivity in cancer

Although the mechanisms underlying ferroptosis sensitivity in cancer cells are not yet fully understood, cells originating from different tissues exhibit varying degrees of susceptibility due to differences in their metabolic states. The next section has discussed how various ferroptosis inducers act and the potential initiation mechanisms involved. The following section of this thesis will focus on the specific pathways of ferroptosis induction in selected cancer types.

Breast Cancer

Research indicates that breast cancer cells demonstrate varied sensitivity to ferroptosis-inducing agents. Studies revealed that siramesine and lapatinib induce ferroptosis by increasing iron-dependent reactive oxygen species (ROS) production. Overexpression of cysteine dioxygenase type 1 (CDO1) exacerbates ferroptotic cell death by further accumulating high-level ROS due to decreased glutathione (GSH) levels. Conversely, MUC1-C can enhance GSH expression by forming a complex with CD44v, thereby inhibiting ferroptosis in breast cancer cells (Ma et al., 2017a).

Breast cancer cells show lower sensitivity to ferroptotic agents such as Erastin, RSL3, ML210, and ML162. However, siramesine, a lysosome-disrupting agent, and lapatinib, a tyrosine kinase inhibitor, have been found to induce ferroptosis by increasing cellular iron levels through upregulating transferrin and downregulating ferroportin-1. This cell death can be prevented by ferroptosis inhibitors like Fer-1 (Lachaier et al., 2014). Recent studies have further elucidated the role of ferroptosis in breast cancer treatment. For example, (Park et al., 2023) demonstrated that the combination of lapatinib with a ferroptosis inducer significantly increased cancer cell death compared to single-agent treatment. This synergistic effect was attributed to the enhanced production of lipid peroxides and depletion of cellular antioxidants. Moreover, (Song et al., 2020b) identified that targeting GPX4, a key regulator of ferroptosis,

sensitizes breast cancer cells to ferroptotic cell death, suggesting potential therapeutic strategies for overcoming resistance in breast cancer treatment.

Another important development is the identification of ferroptosis-related biomarkers in breast cancer. Research by (Xu et al., 2021) highlighted that ferroptosis-related gene signatures could predict prognosis and guide treatment strategies in breast cancer patients. This study emphasized the importance of personalized medicine and the potential of ferroptosis modulation as a therapeutic avenue. Additionally, emerging evidence suggests that the tumour microenvironment (TME) plays a crucial role in modulating ferroptosis sensitivity. Studies have shown that components of the TME, such as tumour-associated macrophages (TAMs) and cancer-associated fibroblasts (CAFs), can influence the redox balance and iron metabolism in breast cancer cells, thereby affecting their susceptibility to ferroptosis (Timperi and Romano, 2023).

Ovarian Cancer

Ovarian cancer cells exhibit high susceptibility to ferroptosis due to iron overload by tumor-initiating cells (TICs), characterized by overexpressed transferrin receptor 1 (TFR1) and reduced ferroportin (FPN) levels. Artesunate (ART) has been shown to induce ferroptosis in a ROS-dependent manner, and this effect can be reversed by ferrostatin-1. However, pretreatment with transferrin enhances ART-induced ferroptosis by increasing cellular iron levels (Rockfield et al., 2017).

Recent studies have further expanded our understanding of ferroptosis in ovarian cancer. (Battaglia et al., 2022) found that ferroptosis is crucial for overcoming chemoresistance in ovarian cancer cells. By inducing ferroptosis with ART and other ferroptosis inducers, researchers observed significant reduction in tumour growth and chemoresistance in ovarian cancer models. This highlights the potential of ferroptosis as a therapeutic strategy to treat refractory ovarian cancer.

Moreover, ferroptosis inducers enhance the sensitivity of tumour cells to ionizing radiation in ovarian cancer by increasing ROS and upregulating ACSL4. This can overcome radiation resistance, particularly when combined with radiotherapy in ovarian and cervical cancers (Zhang et al., 2022b).. Additionally, ferroptosis enhances T cell-mediated antitumor immunity by promoting lipid peroxidation (Wang et al., 2021, Wei et al., 2022). Nanoparticles and gene technology further improve therapeutic outcomes by targeting key gene loci and combining multiple treatment modalities (Guan et al., 2020, Shen et al., 2018).

Prostate Cancer

In prostate cancer, Erastin induces ferroptosis in Ras-mutated human prostate adenocarcinoma cells. The phosphorylation of HSF1-dependent HSPB1 confers resistance to Erastin-induced ferroptosis by inhibiting lipid ROS accumulation and iron uptake. Inhibition of

HSPB1 increases ferroptosis by promoting iron accumulation through upregulation of TFR1 and slight reduction of ferritin heavy chain 1 (FTH1) expression (Sun et al., 2015).

Recent research has provided additional insights into the mechanisms and therapeutic potential of inducing ferroptosis in prostate cancer. For instance, (Maccarinelli et al., 2023) discovered that the combination of ferroptosis inducers with androgen deprivation therapy (ADT) can enhance treatment efficacy. They demonstrated that ADT sensitizes prostate cancer cells to ferroptosis by downregulating GPX4, a crucial enzyme that protects cells from lipid peroxidation, thereby increasing the vulnerability of these cells to ferroptosis.

Combining ferroptosis inducers with radiotherapy increases sensitivity by promoting oxidative stress and lipid peroxidation (Feng et al., 2022). Immunotherapy efficacy is improved as CD8+ T cells induce ferroptosis, boosting antitumor immunity (Wang et al., 2019). Moreover, Liposome-coated nanoparticle in combination with chemodynamic-gas therapy triggers ferroptosis in prostate cancer by enhancing ROS production (Hong et al., 2024). These integrated ferroptosis strategies offer promising advancements for overcoming resistance in prostate cancer treatment.

Pancreatic Cancer

Pancreatic ductal adenocarcinoma (PDAC) cells, transformed by KRAS mutations, show resistance to apoptosis but are susceptible to ferroptosis. Artesunate induces ferroptosis in PDAC cells in an iron- and ROS-dependent manner. The ferroptosis inhibitor Fer-1, but not apoptosis or necrosis inhibitors, can block ART-induced lipid peroxidation and cell death, suggesting a specific mechanism of ferroptosis induction via modulation of iron-related genes (Eling et al., 2015).

Recent advancements have deepened our understanding of the role of ferroptosis in treating pancreatic ductal adenocarcinoma (PDAC). Combining RSL3, a GPx4 inhibitor, with

pharmacologic ascorbate (P-AscH−) showed significant promise as an adjunct to radiotherapy for PDAC. This combination enhanced the radiosensitivity of cancer cells while safeguarding normal tissues from radiation-induced damage. The increased effectiveness against cancer cells, attributed to the inhibition of GPX4 and the resultant rise in lipid peroxidation, underscores the potential of P-AscH− to improve the therapeutic index of radiotherapy, making it a more targeted and less harmful treatment approach (Chen et al., 2024).

Additionally, the small molecule MMRi62 has been shown to trigger ferroptosis by degrading ferritin heavy chain (FTH1) and mutant p53, inducing iron-dependent cell death and inhibiting metastasis in pancreatic cancer cells (Li et al., 2022b)

Stomach Cancer

In stomach cancer, Erastin induces ferroptosis in gastric cancer (GC) cells. This effect is reversible by ferrostatin-1 and liproxstatin-1. C-Myc enhances the expression of cysteine dioxygenase type 1 (CDO1), facilitating ferroptosis. Suppression of CDO1 leads to resistance against Erastin-induced ferroptosis by restoring cellular GPX4 expression and GSH levels and reducing ROS generation. Additionally, the CD44 variant (CD44v) stabilizes xCT at the plasma membrane, increasing cystine uptake for GSH synthesis and blocking ROS-induced stress signalling, thereby conferring resistance to ferroptosis (Hao et al., 2017).

Recent studies have added to the understanding of ferroptosis in gastric cancer. For instance, (Zhou et al., 2023) found that the transcription factor NRF2 plays a significant role in ferroptosis resistance in GC cells. NRF2 upregulation increases the expression of antioxidant genes, thereby reducing ROS levels and conferring resistance to ferroptosis. Targeting the NRF2 pathway could therefore enhance the susceptibility of GC cells to ferroptosis inducers.

Moreover, (Sun et al., 2024) reported that combining ferroptosis inducers with traditional chemotherapy drugs can improve therapeutic efficacy in GC. They demonstrated that using Erastin in combination with cisplatin resulted in synergistic effects, significantly increasing cancer cell death compared to either agent alone. This combination approach could help overcome resistance and enhance treatment outcomes in gastric cancer.

Liver Cancer

In liver cancer, ferroptosis is a key mechanism in sorafenib treatment for hepatocellular carcinoma (HCC). HCC cells deficient in retinoblastoma (RB) protein are more susceptible to ferroptosis due to increased oxidative stress. Metallothionein-1G (MT-1G) is a negative regulator of ferroptosis; its knockdown enhances sorafenib-induced ferroptosis by increasing lipid peroxidation and depleting GSH. The p62-Keap1-Nrf2 pathway and the Ras/Raf/MEK pathway play vital roles in protecting HCC cells from ferroptosis (Lachaier et al., 2014, Sun et al., 2016a)

Recent research has further elucidated the role of ferroptosis in HCC and identified additional therapeutic strategies. For example, Liang et al. (2022) discovered that the inhibition of SLC7A11, a cystine/glutamate antiporter, significantly increases the susceptibility of HCC cells to sorafenib-induced ferroptosis. This suggests that combining sorafenib with SLC7A11 inhibitors could potentiate ferroptosis and enhance therapeutic efficacy in HCC.

Additionally, researchers observed that deletion of GPX4 in mouse liver cells did not directly inhibit tumour growth but induced a robust tumour-suppressive immune response, characterized by cytotoxic CD8+ T cell infiltration driven by CXCL10. However, this response was counteracted by PD-L1 upregulation and MDSC infiltration. Blocking PD-1 or HMGB1 pathways enhanced T cell activation, improving survival. Hence, combining ferroptosis

induction with immune modulation offers promising therapeutic strategies for liver cancer (Conche et al., 2023).

Bladder cancer

Ferroptosis presents a promising therapeutic target in bladder cancer (BCa). A study demonstrated that simultaneously targeting both apoptosis and ferroptosis inhibits BCa cell progression by increasing Fe2+ and reactive oxygen species (ROS) levels, while reducing mitochondrial membrane potential and glutathione (GSH)/GPX4 levels. Additionally, this approach blocks signalling proteins such as PI3K, Akt, and mTOR, which further inhibits tumour growth and signalling pathways in xenografted tumours (Hao et al., 2022).

Another significant finding is the role of Arachidonate Lipoxygenase 5 (ALOX5) in ferroptosis resistance. Research shows that ALOX5 deficiency allows BCa cells to evade ferroptosis, contributing to disease progression. High pathological stage BCa cells with low ALOX5 expression exhibit resistance to ferroptosis, correlating with poorer survival outcomes. Therefore, targeting ALOX5 to induce ferroptosis could open new therapeutic avenues, particularly for cases resistant to traditional therapies (Liu et al., 2023b).

Moreover, advanced therapeutic strategies involving nanoparticles, such as superparamagnetic iron oxide nanoparticles (SPIONs), show promise in inducing ferroptosis. SPIONs can be guided by a magnetic field to deliver chemotherapeutic agents directly to tumour sites, improving targeting and reducing systemic toxicity. They also convert light to heat, enabling photothermal therapy that generates mild hyperthermia, controls drug release, and supplies iron, thus activating ferroptosis. Multifunctional magnetic nanoparticles like rPAE@SPIONs enhance tumour therapy by promoting both chemotherapy and ferroptosis through the controlled release of DOX and iron ions and inducing iron overload-triggered macrophage polarization (Cai et al., 2024). This comprehensive approach boosts the chemotherapeutic effect by inducing

ferroptosis in tumour cells, making these nanoparticles a promising tool in bladder cancer treatment.

Colorectal Cancer

Modulating the ferroptotic cell death pathway has emerged as a promising strategy to enhance the antitumor effects of drugs in colorectal cancer (CRC) treatment. Numerous studies indicate that pharmacological agents such as Erastin and RSL3, which induce ferroptosis, show significant potential in both in vitro and in vivo CRC models.

CRC treatment presents significant challenges, with radiation therapy (RT) being a common but inconsistently effective option. Targeting ferroptosis in CRC has demonstrated the ability to eliminate cancer cells resistant to other forms of cell death, thereby enhancing the efficacy of RT (Aguiar Junior et al., 2020). For instance, buthionine sulfoximine (BSO) enhances RT sensitivity by depleting glutathione (GSH) and inducing ferroptosis in CRC cells. Similarly, the anticancer drug RRx-001 acts as a radiosensitizer by inducing ferroptosis through the activation of Nrf2 (Li et al., 2021a, Lippmann et al., 2020).

These findings suggest that combining ferroptosis inducers with conventional therapies could improve treatment outcomes in CRC. By leveraging the unique mechanisms of ferroptosis, such as increased lipid peroxidation and disruption of cellular antioxidant defenses, these combined strategies hold potential for more effective CRC therapies.

Brain Tumours

Ferroptosis has emerged as a significant factor in the treatment of brain tumours such as gliomas, neuroblastoma, and meningiomas. Gliomas exhibit a high capacity for lipid synthesis with an abundance of polyunsaturated fatty acids (PUFAs), contributing to ferroptosis through increased expression of lipoxygenase and ACSL4 (Cheng et al., 2020, Han and Jiang, 2021).

These cells also manipulate iron metabolism, accumulating iron to support growth and metastasis (Dong et al., 2019). Glutathione peroxidase 4 (GPX4) is overexpressed in glioma tissues to prevent ferroptosis by reducing lipid peroxidation. Targeting GPX4 with inhibitors like RSL3 or by depleting glutathione (GSH) increases lipid peroxidation, leading to ferroptosis (Zhao et al., 2017). The system Xc- transporter, essential for amino acid homeostasis and GSH formation, is critical for glioma cell survival. Inhibiting system Xc-, especially under low glucose conditions, can induce ferroptosis (Hu et al., 2020).

Drugs such as sulfasalazine, which inhibits system Xc-, and artemisinin derivatives, which enhance haem-oxygenase-1 expression and increase intracellular iron, have been used to induce ferroptosis in glioma cells. Combining temozolomide, a standard glioma treatment, with radiotherapy, immunotherapy, and chemotherapy can improve efficacy and reduce resistance. Nanoparticle delivery systems further enhance the solubility, biocompatibility, and targeting of these compounds, providing a novel approach to glioblastoma treatment through ferroptosis (Wong et al., 2022).

Neuroblastoma (NB), a common extracranial tumour in children, evades ferroptosis via dopamine production, which drives ferritin overexpression and redistributes iron into mitochondria, reducing lipid ROS production. The MYCN oncogenic transcription factor also promotes system Xc- expression, allowing NB cells to escape ferroptosis (Floros et al., 2021). MYCN-amplified neuroblastoma is particularly sensitive to ferroptosis induced by cysteine deprivation, suggesting a therapeutic strategy by restricting cysteine to inhibit terminal neuroblastoma (Alborzinia et al., 2022). Furthermore, NF2 gene mutations predispose meningiomas to ferroptosis, regulated by the transcription factor MEF2C. MEF2C promotes the expression of NF2 and E-cadherin, inducing ferroptosis in tumour cells. Targeting MEF2C may offer a therapeutic approach for treating meningiomas by inducing ferroptosis (Bao et al., 2021).

Collectively, these insights into the role of ferroptosis in brain tumours highlight the potential for developing targeted therapies that induce ferroptosis, offering promising avenues for treatment, especially in cases resistant to conventional therapies.

1.4 Hypothesis

The central hypothesis of this thesis is that *TSC2* deficiency alters sensitivity to ferroptosis cell death.

1.5 Aims

To explore this hypothesis, analysis involving a combination of cytotoxic assays, biochemical assays, immunocytochemistry, western blot analysis and gene expression, will be applied to TSC2 cell line models.

1. To determine cytotoxic sensitivity in *TSC2* mutant and wild type cell line models upon exposure to ferroptosis inducers
2. To determine the exclusivity of cell death mode induced by ferroptosis inducers.
3. To develop assays to explore the biomarkers of ferroptosis e.g. lipid peroxidation, ROS and labile iron pool levels; and establish the modulated ferroptosis mechanism associated with *TSC2* loss and mTORC1 activity, and whether TSC patient tumours possess a ferroptosis gene expression signature.
4. To determine the role of antioxidant pathways linked to ferroptosis resistance.

1.6 Objectives

Aim 1 objectives:

a. This work sought to determine the sensitivity of ferroptosis induced cytotoxicity by employing the MTT assay in conjunction with Erastin and RSL3 exposure of two

candidate TSC model cell line models: ELT3 *TSC2(+/+)* and ELT3 *TSC2(−/−)*, and MEF *TSC2(+/+)* and MEF *TSC2(−/−)*.

b. Flow cytometric assessment of DRAQ7 membrane integrity would be used to confirm MTT cytotoxicity data.
c. Establish IC50 values for each ferroptosis inducer for each individual cell line.

Aim 2 objectives:

a. The exclusivity of cell death mode to be determined by MTT cell death rescue assays using apoptosis, necroptosis, iron chelator and ferroptosis inhibitors.

Aim 3 objectives:

a. A combination of Western Blotting, qPCR and fluorescent probes in conjunction with flow cytometry will be applied to quantify and cross validate molecular signatures of ferroptosis, such as level of lipid peroxidation, ROS, GSH, GPX4 and labile iron pool (LIP).
b. To determine the vulnerabilities of TSC-diseased cells that could lead to better therapies we will utilise the established methodologies from (a) in conjunction with RNA sequencing to identify differential mechanism(s) of drug action in the *Tsc2* edited cell lines that cause modulated ferroptosis induction.

Aim 4 objectives:

a. To established if other antioxidant pathway inhibitors modulate ferroptosis sensitivity in the candidate TSC2 *(+/+)* and TSC2 *(−/−)* ELT3 and MEF cell line models, NRF2 and FSP1 inhibitors will be employed in cytotoxicity assays. Immunocytochemistry will also be applied to determine NRF2 activation and translocation differences in the cell lines.

Chapter 2: Materials and methods

In general, experimental procedures were performed following standard protocols of Maelor Academic Unit of Medical and Surgical Sciences Lab, Wrexham. When procedures and kits were individualised, changes are indicated.

2.1 Materials

Materials, Reagents, kits, and equipment used for the research within this thesis are listed in the tables below. Reagents, kits and equipment and their supplier used for the outsourced mRNA sequencing are mentioned in the main text instead.

TABLE 2.1 CELL CULTURE REAGENTS

Name	**Supplier**
Acetic acid	Sigma-Aldrich
Dimethylsulfoxide (DMSO)	Fisher Scientific
Hydrochloric Acid (~37%)	Fisher Scientific
Immobilon-P PVDF Transfer Membrane	Millipore
MTT	Merck Life Science UK Limited
Sodium deoxycholate	Sigma-Aldrich
Sodium dodecyl sulfate	Sigma-Aldrich
Sodium Hydroxide	Sigma-Aldrich
Sodium orthovanadate	Sigma-Aldrich
Sucrose	Sigma-Aldrich
Triton X-100	Sigma-Aldrich
TWEEN 20	Sigma-Aldrich

Whatman Paper	Sigma-Aldrich

TABLE 2.2 GENERAL CELL CULTURE

Name	**Supplier**
Dulbecco's Modified Eagle's Medium - high glucose	Thermofisher Ltd
Fetal Bovine Serum	Thermofisher Ltd
Iso-propyl alcohol	Thermofisher Ltd
Penicillin-Streptomycin	Thermofisher Ltd
Phosphate Buffer Saline (PBS)	Thermofisher Ltd
Recovery Cell Culture Freezing Medium	Thermofisher Ltd
24-well Tissue Culture Plate	Thermofisher Ltd
75cm2 Tissue Culture Flask	Thermofisher Ltd
300cm2 Tissue Culture Flask	Thermofisher Ltd
96-well Flat Clear Bottom tissue culture plate	Thermofisher Ltd

TABLE 2.3 DRUGS AND PROBES

Name	**Supplier**	**Catalogue number**	**Stock Conc.**	**Working Conc.**
BODIPY C11	Life Technologies	B3932	10mM	10uM
Calcein AM	Invitrogen	C3100MP	100uM	250nM
Compound C	Merck	171261	10mM	5µM
CM-H2DCFDA C6827	Abcam (Cambridge, U.K.)		1mM	1uM

Deferiprone	Merck	30652-11-0	10mM	100uM
DRAQ7	Biostatus	DR71000	0.3mM	3uM
DAPI	Life technologies	C6827	1ug	
Erastin	Biotechne/Tocris	5449/10 10MG	10mM	15uM, 5uM
Ferrostatin-1	Merck	SM1-0583 5MG	10mM	10uM
Necrostatin-1	Biotechne/Tocris	2324/10 10MG	10mM	10uM
iFSP1	Biotechne/Tocris		10mM	10uM
Rapamycin	Sigma Aldrich	553210	100uM	20nM
RSL3	Biotechne/Tocris	6118/10 10 MG	10mM	1.2uM
Trigonelline	Sigma Aldrich	T5509	5mM	500uM
Z-VAD-FMK	Biotechne/Tocris	2163/1 1MG	10mM	10uM

2.2 Methodology

2.2.1 Cell Lines

***Tsc2* MEFs**: The murine TSC model cell lines used within this work were the *Tsc2*−/− (Tp53−/−) mouse embryonic fibroblasts (MEFs) and the *Tsc2*+/+ (wildtype) (Tp53−/−) MEFs, which were a kind gift from Prof. D. Kwaitowski (Harvard University). Both MEF cell lines were established by Zhang et al. (2003) by littermate pair crossings. Both MEF cell lines were null for Tp53 as authors found MEF cells null for Tsc2 alone showed early senescence. Therefore, Zhang et al. (2003) interbred *Tsc2*+/− mice with Tp53−/− mice to generate *Tsc2*+/− Tp53−/− mice, which in turn were interbred to generate *Tsc2*−/− Tp53−/− embryonic fibroblasts. Tp53 loss was found to rescue *Tsc2* loss induced senescence. *Tsc2*+/+ Tp53−/− embryonic fibroblasts were generated in the same manner. In this thesis, these cell lines will be referred to as *Tsc2*+/+ and *Tsc2*−/− MEF cells, respectively.

ELT3 cells: *Tsc2*(−/−) ELT3 (Eker rat leiomyoma-derived cells) and ELT3-*Tsc2* cells with *Tsc2* re-expression (to use as control cells) were kindly provided by Cheryl Walker (M.D. Anderson Cancer Centre, Houston, USA). Described here (Walker 2003). To clonal stable cell lines were generated, called ELT3-V3 that expressed empty vector, while human TSC2 was re-expressed in ELT3-T3. In this thesis, these cell lines will be referred to as ELT3 (−/−) and ELT3 (+/+) respectively.

These cell lines were provided by co-supervisor Prof. Andrew Tee (Cardiff University).

2.2.2 General Cell Culture

All the cell lines were cultured and maintained in Dulbecco's Modified Eagle Medium (DMEM) supplemented with 10% (v/v) foetal bovine serum (FBS), 1% v/v penicillin and streptomycin in a humidified incubator at 37 ^{O}C, 5% (v/v) CO_2. Cells were passaged once every 48 h using 3

x 1 mL washes with trypsin/EDTA (0.25 %) followed by incubation at 37 °C over 5 min. Cells were then resuspended in culture medium and re-seeded into a T75 cm^2 flask for continued culture. Surplus cells were used to setup experimentation at a set seeding density, as appropriate.

Cells were dissociated from tissue culture plastic through two sequential washes with trypsin-EDTA, which was aspirated off before incubation for 3 – 5 minutes at 37 °C . For long-term cell storage, cells were first trypsinised as previously described before resuspension in DMEM. Cells were then spun down at 5 min at 2000 rpm. Pelleted cells were then resuspended in 1 mL of recovery cell culture medium before being transferred to cryogenic vials that were initially frozen in a cell freezing container. Cryogenic vials were then transferred and kept in liquid nitrogen storage.

2.2.3 Drugs Concentrations for experimental design

In this study, the maximum dose of each drug was determined before cytotoxicity was observed. Concentrations of the ferroptosis inducers, Erastin and RSL3, were based on the initial characterization by the founders of the ferroptosis cell death mechanism (Dixon et al., 2012, Yang et al., 2014). The different cell death inhibitors used, including Z-VAD-FMK, Necrostatin-1, and Ferrostatin-1, were selected according to Yamaguchi et al. (2018). Concentrations of mTOR inhibitors for drug treatments were informed by extensive research within the TSC model cell lines by the Tee lab and the wider TSC research community. Specifically, 50nM rapamycin was used, a concentration demonstrated to inhibit phosphorylation of downstream mTORC1 substrates effectively (Dodd and Tee, 2015, Tee et al., 2002, Land and Tee, 2007). AMPK inhibition with Compound C (CC) at a dose of 5μM was selected based on its use in HCT116 cells, where AMPK inhibition by CC was shown to inhibit ferroptosis (Guo et al., 2019).

The iron chelator Deferiprone (DFP) was chosen over Deferoxamine (DFO) due to DFO's high hydrophilicity, which limits its intracellular penetration and necessitates high doses or continuous subcutaneous pumps for efficacy. In contrast, DFP's greater lipophilicity ensures better intracellular access (Cen et al., 2024, Park et al., 2023) . A dose response ranging from [6.5 to 100 μM] was employed to assess the effect on *Tsc2* +/+ and −/− MEF and ELT3 cells.

The initial concentration range of the NRF2 inhibitor Trigonelline (0.1-0.8 mM) was selected based on a study that characterized its efficacy in inhibiting NRF2 activity in HNC cell lines with elevated NRF2 activity due to a loss of function mutation in KEAP1, a negative regulator of NRF2 (Shin et al., 2018). The study found that concentrations between 0.4 and 0.8 mM were effective at reducing NRF2 activity, decreasing the intracellular glutathione pool, and reducing total antioxidant capacity in A549 cells. Consequently, 0.5 mM Trigonelline was selected for treating TSC2-deficient *Tsc2* −/− MEF cells, as little decrease in cell viability was observed at the upper limit of the initial concentration range tested for cytotoxicity.

A combination dose response of Erastin and RSL3 was conducted with 0.5 mM Trigonelline in both *Tsc2+/+* and *Tsc2* −/− MEF and ELT3 cells. Additionally, a dose response of the FSP1 inhibitor (iFSP1) was employed to elucidate the additional resistance mechanism linked to *Tsc2* loss. The dose for iFSP1 was selected based on its use in combination with RSL3 on PANC-1 pancreatic cancer cell lines, where the combined treatment increased cytotoxicity, indicating that inhibition of FSP1 sensitizes cancer cells to ferroptosis (Park et al., 2023).

The primary purpose of treating MEF and ELT3 cell lines with the ferroptosis-inducing drugs Erastin and RSL3 was to induce cell death and observe if there was selective cell death or resistance between *Tsc2*-deficient and competent cells in response to ferroptotic induction. Trigonelline and iFSP1 were employed to understand the resistance mechanism in *Tsc2* cell lines during ferroptosis.

2.2.4 Cytotoxicity Assay

2.2.4.1 DRAQ7 VIABILITY ASSAY BY FLOW-CYTOMETRY

Cells were seeded in 24 well plates ($5x10^4$) cells/well and incubated for 24 h. Cell were then treated with ferroptosis inducers (Erastin: 5, 2.5, 1.2, 0.6 and 0.3 μM) and (RSL3: 1.2, 0.06, 0.3, 0.15, 0.07 μM) alone or in combination with an NRF2 inhibitor (Trigonelline 0.05 mM) and incubated for another 24 h. Cells were then washed with 0.2 mL PBS and trypsinised (0.2 mL). Cells were collected and centrifuged at 400G for 5 min. Supernatant was discarded and 80 uL of DRAQ7 were added to each Eppendorf tube, vortexed and run on the flow-cytometer at FL4: Ex 633 nm, Em 695 nm. All cells were gated and only DRAQ7 negative large cells were considered viable. DRAQ7 negative small cells were considered as being apoptotic cells, therefore, they were not included in the gating for collecting viable cells.

Cell Preparation

Cells were placed into 96-well plates and incubated at 37 ºC overnight; cells were then treated with alkaloids in various concentrations. Each concentration was repeated in triplicate manner. Medium with or without compounds was replaced every 24 hours with fresh medium containing the same concentrations of compounds. Cells were then grown in the continuous

2.2.4.2 MTT COLOURIMETRY CELL VIABILITY ASSAY

In this study (supplementary data), the 3-(4,5-dimethylthiazol-2-yl)-2,5-diphenyl-2H-tetrazolium bromide (MTT) assay was used to measure cellular metabolic activity as an indicator of cell viability, proliferation and cytotoxicity. The method is based on the ability of a mitochondrial dehydrogenase from viable cells to cleave the tetrazolium rings of the pale yellow MTT and form purple formazan crystals which are impermeable to cell membranes.

Cell Preparation

Cells were placed into 96-well plates and incubated at 37 ºC overnight. Cells were then treated with ferroptosis inducers Erastin[5-0.3µM] and RSL3 [1.2-0.07µM] for MEFs and Erastin[15-0.9µM] and RSL3 [2-0.12µM] for ELT3 Tsc2 cell line models and

incubated for further 24 h. After the drug treatment, the cell culture medium was removed gently, each well was washed with 100µl PBS and 100µl MTT stock solution was then added to a final concentration of 0.5 µg/mL and incubated at 37 ºC for about 2 to 4 h until the purple formazan crystals had formed clearly. The number of living cells is directly proportional to the level of the formed formazan, which can be quantified photometrically (See Appendix Fig 1).

Absorbance measurement

The supernatant was discarded and 100µl acid isopropanol (4 mM HCl, 0.1% NP-40 in isopropanol) was added to each well to stop colour development and solubilize cells. The MTT solution was discarded carefully, formazan crystal was dissolved in 400 µL acidified isopropyl alcohol (0.04 N HCl) was added into each well. The plates were mounted on top of a shaker and were shaken for 10 min. Duplicate samples of 100 µL aliquots were transferred to 96 well plates and the absorbance was recorded at 570nm using a microplate reader (Bio-Rad, Hercules, CA). Cell viability (%) was calculated Cell viability (%) was calculated using control cells as positive control (100% cell viability). Whereas acidified isopropyl alcohol (0.04 N HCl) was as blank control (0% cell viability). The experiments were repeated three times independently.

2.2.4.3 CELL DEATH RESCUE ASSAYS

Previous MTT method was followed to evaluate different cell death modes in the observed death in the treated cells, excluding the determination of iron chelation.

MEF *(+/+)* were treated with Z-VAD [10µM], FS-1[10µM] or NS[10µM] alone ; or in combination with RSL3 IC50[0.15 µM]. Similarly, MEF *(−/−)* cells were subjected to the same inhibitors at the same doses, with the exception of RSL3 IC_{50}, which was adjusted to 0.28 µM for tsc2-

deficient cells, all for a duration of 24 hours. After the drug treatment, cells were treated with MTT and followed the same method (refer to section 2.2.4.2 for details)

Additionally, to examine the roles of mTORC1 and AMPK in cytotoxicity, Rapamycin [50nM], an mTORC1 inhibitor, and Compound C (CC) [10 μM], an AMPK inhibitor, were administered alone or in combination with RSL3 IC50 [0.15 μM]. The treatment regimen for MEF *(–/–)* cells mirrored that of MEF *(+/+)* cells, except for the concentration of RSL3 IC50, which was adjusted to 0.28 μM for Tsc2-deficient cells, all for a duration of 24 hours. After the drug treatment, cells were treated with MTT and followed the same method (refer to section 2.2.4.2 for details)

To investigate the impact of iron, varying doses [100-6.5μM] of the iron chelator Deferiprone were administered to both *Tsc2(+/+)* and *Tsc2(–/–)* MEF and ELT3 cell lines, either alone or in combination with RSL3 IC_{50} [0.14 μM] for *Tsc2(+/+)* cells and [0.28 μM] for Tsc2*(–/–)* cells, respectively, over a 24-hour period. Subsequently, a rescue assay was performed using the DRAQ7 viability method, as previously outlined (refer to section 2.2.4.1 for details).

2.2.5 Lipid-peroxidation and cellular ROS assay by flow cytometry

In this project, a dual parameter analysis of lipid peroxidation and ROS production was conducted using two commercially available probes specific for these biomarkers. Lipid peroxidation can be detected with the lipophilic probe, BODIPY® 665/676 dye. This probe exhibits a change in fluorescence after interaction with peroxyl radicals.

ROS production analysis ROS Production was analysed using the DCFDA/H2DCFDA - Cellular Reactive Oxygen Species Detection Assay Kit from Abcam (Cambridge, U.K.)

Lipid-peroxidation detection Probe: Bodipy 665/676 [Stock 10mM] Use at 10µM [1:1000 dilution]

ROS detection Probe: CM-H2DCFDA C6827 [stock 1mM] use at 1µM [1:1000 dilution]

Staining Solution preparation

1. 12µL of 1mM ROS dye and 12µL of 10mM Bodipy to 12000µL of warm PBS
2. Mix well and protect from light until needed.

Method

i. Cells were seeded in 24 well plates ($5x10^4$) cells/well and incubated for 24 h.

ii. Cells were treated with ferroptosis inducers (Erastin: 5, 2.5, 1.2, 0.6 and 0.3 µM) and (RSL3: 1.2, 0.06, 0.3, 0.15, 0.07 µM) alone or in combination with an NRF2 inhibitor (trigonelline 500 µM) and incubated for another 24 h.

iii. 1.5mL eppendorf centrifuge tubes were labelled according to the treated cells in the wells. Supernatant from each well was collected in labelled 1.5mL eppendorfs.

iv. 200uL warm PBS was added to each well to wash the cells and then aspirated PBS into the labelled eppendorfs.

v. Similarly, 200uL warm Trypsin was added to each washed well and incubate at 37°C/5% CO2/humidified air for 5mins. Cell monolayer of each well was checked for detachment before processing further.

vi. Trypsin was then gently triturate around well before collection in the labelled eppendorf tubes.

vii. Cells were given a final wash by 200µL PBS to each well, and carefully aspirated into the labelled eppendorf tubes.

viii. All the tubes containing cells were centrifuged at 300g for 4min.

ix. Supernatant of the centrifuged cells was carefully removed and discarded.

x. 80µL of staining solution being careful to record the volume used. For consistency keep the same volume and record any extra volumes remaining in tubes after aspiration of supernatant post centrifugation (Concentration differences of dye between samples will results in variation in staining.

xi. Cells were then resuspended by agitation/vortexing and incubate for 30min at 37°C/5% CO2/humidified air.

xii. Samples were run on Flow cytometer according to the setting mentioned below.

Cytometer Settings:

FL1: Ex 488nm Em 533/30nm [ROS]

FL4: Ex 640nm Em 670LP* [Lipid Peroxidation]

*Standard Configuration on BD Accuri C6 is FL4 filter [Em 675/25] and FL3 [Em 670LP] so filters need to be swapped around before and after experiment.

Data was first analysed in 'Front scatter' (FSC) versus 'Side scatter' (SSC), where data was gated to eliminate cell debris and fragments from final analysis. Revised data was then analysed in FSC (x axis) versus FL4 (sensor with a 675 nm long pass filter which is used to detect far red

fluorescent dyes) (Y axis). Data was gated in viable and non-viable populations using 101 on the Y axis as an approximate cut off point between the populations.

2.2.6. Labile Iron pool determination

As a key component of ferroptosis, determination of the labile iron pool (LIP) is an important parameter to measure in cancer cell types. To quantify LIP the established Calcein AM method was used.

ELT3 (+/+) and (-/-) cells were seeded in 24 well plates ($5x10^4$) cells/well and incubated for 24 h. Treated with ferroptosis inducer RSL3 over a dose range and incubated for another 24 h.

Staining solution preparation:

250nM of Calcein AM in PBS. (CAM/PBS; 400µL per well)

Method

i. Cells were seeded in 24 well plates ($5x10^4$) cells/well and incubated for 24 h.
ii. ELT3 Cells were treated with ferroptosis inducers RSL3: 0.1, 0.2, 0.51µM and incubated for another 24 h.
iii. Cells were stained with CalceinAM [250 nM] for 10 min before washing with PBS. Supernatant and washes from each well were collected into 1.5mL eppendorfs and centrifuged at 300G for 5min.
iv. Cell pellets were resuspended in 300 µL fresh media alone or with fresh media containing the iron chelator, Deferiprone, at a concentration of 100 µM.

v. Cells were incubated for a further 60 min at 37^{o}C/5% CO_2/humidified air. Following incubation cells were trypsinised and run on the BD Accuri C6 flow cytometer and Calcein fluorescence measured on FL1-A [λ_{Ex} 488 nm; λ_{Em} 533/30 nm].

vi. LIP was determined by subtraction of the median fluorescent intensity (MFI) of CalceinAM dyed cells (MFI_{CAM}) from the higher values of the chelator treated cells ($MFI_{CAM+Chelator}$).

$MFI_{CAM+Chelator} - MFI_{CAM} = LIP$

2.2.7 Western Blotting

TABLE 2.4 LIST OF INHIBITORS AND INDUCERS

Drug	**Conc**
Rapamycin	50nM
Compound C	5 μM
RSL3	1 μM
Erastin	2 μM

Rapamycin and Compound C treatments were performed overnight (~18h), followed by 4h RSL3 and Erastin

This experiment was repeated by Darius McPhail (2023McPhailD PhD.pdf (cardiff.ac.uk))

Cell lysate preparation

Tsc2(−/−) and wild-type MEFs were seeded within 75 cm^2 cell culture flask (Nunc™ Sterile Flask, Thermofisher scientific, UK) at a seeding density of $1.5x10^6$ and $1.8\ x10^6$ cells/mL, respectively. Cells were incubated until 80-90% confluency in15 ml culture media. After incubation, media was removed and replaced with either only media or various treatment as specified in relevant sections. Plates were then incubated for a desired time period (3, 6, 16), depending on whether target protein expression is being analysed for a specific time point or being analysed over several time points. After desired incubation period, media was removed. Cells were washed in ice-cold phosphate buffered saline (PBS) and cells were obtained by scraping off the plates into ependorfs (2.5ml) and labelled accordingly. Cells were then lysed in CytoBuster protein extraction reagent made up with protease and phosphatase inhibitor (1:100, 1:50 respectively). Pellet the cells by low speed centrifugation (e.g. 5 min at 2500 x g), drain the cell pellet well. Resuspend the cells in CytoBuster Protein Extraction Reagent using 150 μL per 10^6 cells. Samples were then transfered to a suitable tube and spin for 5 min at 16,000 x g at 4°C. Total protein was quantified at OD660 using PierceTM 660 nm reagent plus ionic detergent compatibility reagent (Thermofisher, 22663), before normalisation of each

sample to the lowest sample protein concentration per sample set, using sample buffer containing bromophenol blue. Samples were then stored at −20˚ C until needed.

SDS-PAGE

Electrophoresis was carried out using NuPAGETM Bis-Tris 4-12% (Thermo Fisher, NP0326BOX) and NuPAGETM Tris-acetate 3-8% (Thermo Fisher, EA0375BOX) gels, using NuPAGETM MES SDS running buffer (Thermo Fisher, NP0002) and NuPAGETM Tris-acetate SDS running buffer (Thermo Fisher, LA0041), respectively.as per manufacturer's protocol. Lysates previously standardised for protein concentration were loaded first heated to 90 oC for 10 mins before being centrifuged for 1 min at 13,000 rpm. Lysates were then loaded into the wells of pre-cast NuPAGE gels (Thermo Fisher NP0322BOX), with the first well being loaded with pre-stained protein ladder. Gels were initially run at 200 V for 10 min and then at 120 V until appropriate separation of the protein ladder was achieved.

Antibodies used in western blotting are listed in Table 2

TABLE 2.5: LIST OF ANTIBODIES, MOLECULAR WEIGHT AND SUPPLIERS. ALL PRIMARY ANTIBODIES HAVE A STOCK CONCENTRATION OF 1 MG/ML. ANTIBODY

Target Protein	**Predicted Band Size (kDa)**	**Dilution**	**Supplier**	**Product Code**
TSC2	200	1:2000	CST	4308
Ribosomal protein S6 (rpS6)	32	1:2000	CST	2317
Phospho-rpS6 (Ser235/236)	32	1:2000	CST	2211
Acetyl-CoA Carboxylase (ACC)	280	1:2000	CST	3662
Phospho-ACC (Ser79)	280	1:2000	CST	3661
SQSTM1/p62	47	1:2000	abcam	ab91526
GPX4	22	1:2000	abcam	52455S
HMOX1	33	1:2000	abcam	Ab68477
TFR1	84	1:2000	abcam	ab84036
Horse Radish Peroxidase (HRP)		1:10,000	CST	7074
β-actin	45	1:5000	CST	4970

Electrophoretic Transfer and Western Blot Analysis

After electrophoresis, separated proteins on gels were transferred to Immobilon®-P polyvinylidene difluoride membranes (Merck Life Science, IPVH00010) using wet transfer. Membranes were then blocked in 5% (w/v) dry powder milk in Tris-buffered saline (50 mM Tris-Cl pH 7.5, 150 mM NaCl) with 0.1% Tween 20 (TBS-T). Membranes were then probed with primary antibodies overnight at 4˚ C on an orbital shaker. Primary antibodies were diluted in TBS-T with 2% (w/v) bovine serum albumin (BSA) (Merck, A7908). Primary antibody sourcing and dilutions used can be found in Table 2.5. Membranes were washed in TBS-T prior to secondary staining with either anti-rabbit, anti-mouse, or anti-sheep HRP-conjugated secondary antibodies (1:10,000) (Merck) in TBS-T with 2% (w/v) dry powder milk. Membranes were incubated for 1 h at room temperature on an orbital shaker. Membranes were then washed in TBS-T prior to addition of enhanced chemiluminescence (ECL) reagent. Membranes were incubated for 1 min and then detected using Cytiva Amersham™ ECL Select™ western blotting detection reagent (Cytiva, RPN2235). Image analysis of the western blots was performed in ImageJ. (version 1.52i).

2.2.8 NRF2 nuclear translocation by Immunocytochemistry

Cells were treated as previously described in 2.2.1 but with slight modifications. Briefly, ethanol sterilised glass coverslips were placed in 24 well plates prior to seeding of cells. Treatments were administered but to facilitate capture of early nuclear translocation the time course for analysis of NRF2 relocation was 6h and 24h instead of just 24h. Cells were processed according to our 4% paraformaldehyde (PFA)/Glycine quenching method. Glycine will bind free aldehyde groups that would otherwise bind the primary and secondary antibodies, leading to high background. Background staining due to free aldehyde groups is likelier to occur when the fixative is glutaraldehyde or paraformaldehyde.

Supernatants were removed from 24 well plate wells and cells washed by the addition of 300uL of PBS for 5min. PBS was then removed, and cells fixed for 15min with 4% PFA at room temp. Subsequently cells were washed again in PBS (3 x 5min) before addition of 0.1M glycine quench buffer and incubation for 15min at room temperature (RT). After quenching cells were washed and permeabilized with 0.2 % Triton X–100 in PBS (permeabilization buffer) for 20min at RT. Following permeabilization, buffer was removed, and cells exposed to Bovine Serum Albumin (BSA) Blocking buffer (2% BSA in PBS) for 20min at RT. Primary rabbit anti-human/mouse/rat nrf2 polyclonal antibody (Invitrogen; PA5-27882), diluted 1:500 in blocking buffer, was then added to cell monolayers and incubated for 24h at 4^{o}C. Following 3x 5min washes in PBS, the secondary donkey anti-rabbit AlexaFluor 647 polyclonal antibody (Invitrogen; A31573), diluted 1:1000 in blocking buffer, was applied to the monolayers for 30min at RT. Monolayers were then washed 3 times in PBS for 5 min before incubating with DAPI [1μg/mL in PBS] for 15min at RT. Monolayers were washed 2x 5min with PBS and coverslips removed from 24 well plates onto tissue papers with monolayers facing up. 5 μL Fluoromount G was placed onto microscope slides and coverslips transferred onto the mountant. Cells were examined on a Leica DMII6000b microscope (Leica Biosystems, Wetzlar, Germany).

2.2.9 GSH determination using flow cytometry

MEF and ELT3 cells were kept in culture at 37^{o}C/5% CO_2/humidified air and were trypsinised at 70-90% confluence, counted using trypan blue and a haemocytometer, and seeded at 0.1 x10^{6}/mL into 96 well plates at a final volume of 100μL. After 24h monolayers were assessed for seeding efficiency and media changed. At <90% confluence cells had their supernatants removed and replaced with fresh media containing the fluorescent probe GSHTracer (Tocris Ltd) at a final concentration of 5μM. Cells were incubated for 30 min at 37^{o}C/5% CO_2/humidified air. After 30 min media was removed from wells, monolayers washed with warm PBS and monolayers trypsinised with 70uL trypsin to create single cell suspensions. Cells

were then placed in 1.5mL Eppendorfs and run on a BD Accuri C6 flow cytometer. Viable cells were selected for analysis based on forward and side scatter and fluorescence was measured on the FL-1 A channel [λ_{Ex} 488nm; λ_{Em} 533/30nm]. GSHTracer, also sold commercially as FreSHTracer), is ideally used as a ratiometric probe with separate excitations maxima for the unbound (500nm) and bound (430nm) probe. The probe has been used to yield relatively accurate measurements of intracellular Glutathione levels (Jeong et al., 2018). In the current application we used the probe in conjunction with blue laser excitation (488nm) which is minimal in its excitation of the GSH bound green version of the probe but near optimal for the unbound orange version. Crucially the emission spectra of the bound and unbound version are distinct and the 533/30nm filter for FL-1A is exclusive to the green GSH bound probe fluorescence spectrum with little, if any, spectral overlap from the emission spectrum of the unbound probe. Efficiently excited with a 488nm laser, the fluorescence of the unbound probe would be detectable in the FL-2A channel [λ_{Ex} 488nm; λ_{Em} 585/25nm]. High levels of GSH would manifest low orange fluorescence while low levels of GSH would result in a high signal in the FL-2A channel.

2.2.10 Polymerase Chain Reaction (PCR)

NRF2 and *FSP1*gene expression data was generated by Dr Jesse Champion (Cardiff University).

mRNA purification

Cells previously stored in RNA Protect Cell Reagent were thawed and then centrifuged for 5 min at 5,000 rpm. Supernatant was discarded and mRNA was purified from cell pellets using RNeasy Plus Mini Kit according to manufacturer's instructions. 10 µL of β-mercaptoethanol was added per 1 mL of RLT lysis buffer used. Cell lysates were homogenized using QIAshredders. Purified RNA was stored at −80 °C until use.

Complementary DNA (cDNA) Synthesis

Previously purified RNA was quantified using Qubit RNA Broad Range Assay Kit according to manufacturer's instructions on a Qubit 2.0 fluorometer. cDNA was synthesised from purified RNA using the Reverse Transcriptase Core kit according to manufacturer's instructions on a 65 G-Storm Thermal Cycler. Random nonamers, part of the kit, were used as reverse transcription primers. 200 ng per reaction volume (10 µL) for each sample, generating cDNA at 20 ng/µL (assuming 1:1 conversion of RNA to cDNA). cDNA was stored at −80 °C until use.

cDNA synthesis cycling conditions		
Step	Time (min)	Temperature (oC)
Initial Step	10	25
Reverse Transcription Step	30	48
Inactivation of RT Enzyme	5	95

2.2.11 mRNA sequencing

In this study, differentially expressed gene (DEG) analyses of four distinct RNA sequencing datasets were utilized. The datasets included comparisons between patient-derived TSC AML tumours and normal tissue, and MEF cells with *Tsc2* deficiency (*Tsc2 –/–)* versus wild-type *(Tsc2 +/+)*. Additionally, patient-derived samples of TSC-associated lesions, specifically subependymal nodules/subependymal giant cell astrocytomas (SEN/SEGA) and cortical tubers (TUB), were compared to non-TSC brain tissue (NB). Another dataset involved RNA sequencing of patient-derived renal TSC-associated angiomyolipoma (RA) samples compared to non-TSC kidney tissue (NK). The final dataset comprised patient-derived kidney tumours with a loss of

function in TSC2 (AML 621-101), which were subjected to RNA sequencing and compared to their normal TSC2 re-expressed counterparts.

Table

Contributors to mRNA Sequencing Data Sets			
Sample	**Sample preparation**	**RNA library preparation and sequencing**	**Transcriptomic analysis and gene ontology analysis**
TSC AML tumour versus normal	Dr. Jesse Champion (Cardiff University) [1]	Wales Gene Park (Cardiff University)	Wales Gene Park (Cardiff University)
MEF *Tsc2* (−/−) versus *Tsc2* (+/+)	Dr. Jesse Champion (Cardiff University) [1]	Wales Gene Park (Cardiff University)	Wales Gene Park (Cardiff University)
TSC Brain lesion versus non-TSC brain tissue	Prof. J. MacKeigan	(Martin et al., 2017)	GeneAnalytics (LifeMap Sciences, Inc., Covina, CA, USA).
Patient derived kidney tumour cells *TSC2* (−/−) versus *TSC2* (+/+) and AML *TSC2* (−/−) versus *TSC2* (+/+)	Mohammad Alzahrani and Dr Brian Calver (Cardiff University) [2].	Mohammad Alzahrani and Dr Brian Calver (Cardiff University).	Wales Gene Park (Cardiff University, UK)

1. https://orca.cardiff.ac.uk/id/eprint/161226/

2. https://orca.cardiff.ac.uk/id/eprint/167560/

Patient derived TSC AML tumour versus normal

Samples for RNA-sequencing were generated by Dr. Jesse Champion (Cardiff University). This RNA sequencing data set compared TSC2 deficient or TSC2 re-expressed AML cells cultured under either normoxia or hypoxia. Six biological repeats per cell line per condition (normoxia or hypoxia) were included within the analysis. Sequencing data was generated during the research contained within this thesis and is currently unpublished. Cell culture and sample preparation was undertaken within the Tee lab, the library preparation, RNA sequencing itself and subsequent DEG analyses was outsourced to Wales Gene Park (Cardiff University) (Johnson et al., 2018).

MEF *Tsc2* (–/–) versus *Tsc2* (+/+)

This RNA sequencing data set compared *Tsc2 +/+* MEF and *Tsc2 –/–* MEF cell lines. Samples for RNA-sequencing were generated by Dr. Jesse Champion (Cardiff University). Three biological repeats per cell line were included within the final analysis. Sequencing data was generated prior to the research contained within this thesis by the Tee lab and published in Johnson et al. (2018). Cell culture and sample preparation was undertaken within the Tee lab, the library preparation, RNA sequencing itself and subsequent DEG analyses was outsourced to Wales Gene Park (Cardiff University) (Johnson et al., 2018).

Patient-derived TSC Brain lesion versus non-TSC brain tissue

Samples of TSC patient-derived brain tumours (n=15) were collected by Prof. J. MacKeigan (Michigan State University, Grand Rapids, MI, USA). Transcriptomic analysis and gene ontology analysis of the patient-derived TSC samples were conducted by the author (Martin et al., 2017). Cells were washed in PBS and lysed in RNAprotect® Cell Reagent (Qiagen, 76104). RNA was extracted from six biological repeats using QIAshredder® (Qiagen, 79654) and RNAeasy® Mini kits (Qiagen, 74104) and then stored at −80 °C. RNA library preparation and sequencing were conducted using GeneAnalytics (LifeMap Sciences, Inc., Covina, CA, USA). Datasets were imported into Microsoft Excel to generate volcano plots. Heatmaps were generated using Prism

Patient derived kidney tumour cells *TSC2* (–/–) versus *TSC2* (+/+)

TSC patient-derived kidney tumour cells (AML 621-101) with loss of function of TSC2 and these cells with TSC2 re-expressed (AML 621-103) were subjected to RNA sequencing (n=6). This involved comparing AML 621-101 cells grown in 15% FBS to their normal TSC2 re-expressed counterparts (AML 621-103). Samples for RNA-sequencing were generated by Dr Mohammad Alzahrani and Dr Brian Calver (Cardiff University). TSC patient derived kidney tumour cells (AML 621-101) with loss of function of TSC2 and these cells with TSC2 re-expressed (AML 621-

103) were subjected to RNA sequencing (n=6, comparing 621-101 to 621-103 cells grown in 15% FBS). Bioinformatic work was carried out in collaboration with Wales Gene Park (Cardiff University, UK), except the Illumina® TruSeq® RNA sample preparation v2 kit (Illumina, Inc., Great Abington, Cambridgeshire, UK), which was used for library preparation according to the manufacturer's instructions. Following validation, the libraries were normalised to 8 nM and the pool was sequenced on the MiSeq with a 150 cycle, version 3, cartridge (both Illumina Inc) according to the manufacturer's instructions. Differentially expressed transcripts were identified using the DeSeq2 package in R (Love et al., 2014). All pairwise comparisons in the dataset were analysed. P values were corrected for multiple testing using the Benjamini–Hochberg false discovery rate (FDR) method. Gene expression analysis was performed as described in the previous section (Martin et al., 2017). Bioinformatic work was initially carried out by Wales Gene Park (Cardiff University) (Johnson et al., 2018). The datasets were then obtained and imported into Microsoft Excel, which contained the normalized data of the samples. This data was used to generate volcano plots of differentially expressed genes on normalized RNA sequence reads for genes linked to ferroptosis. Ferroptosis gene list was compiled based on literature review on genes associated with ferroptosis. When generating volcano plots, thresholds were set for genes that were differentially expressed at a fold change of >2.5 or <2.5, and a p-value < 0.01. Blue represents genes with reduced expression, while red represents genes with higher expression. Prism was used to generate HeatMaps. Similar to the RNA sequencing experiment described above, datasets were imported into Microsoft Excel to generate volcano plots. Heatmaps were generated using Prism.

2.3 Optimisation

In this dissertation, a primary focus was on conducting a cytotoxicity study using ferroptosis inducers to assess the susceptibility of *Tsc2* model MEF and ELT3 cells by utilizing Erastin and RSL3, with or without Trigonelline. The experiment was optimized using the MTT colorimetric assay and then repeated using the DRAQ7 flow cytometry technique.

Results from MTT assay revealed that optimized combinations of these treatments induced cell death resistance in *Tsc2*–/– MEFs and ELT3s mTOR-hyperactive sporadic cancer cells compared to their counterparts. Loss of *TSC1* or *TSC2* causes mTORC1 overactivation and other dysregulations in cellular metabolism. Targeting ferroptosis considering the contributions of TSC2-mediated dysregulation can lead to better therapeutic intervenes.

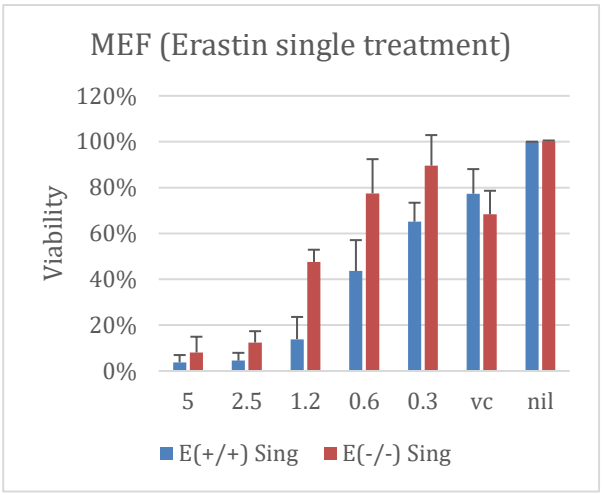

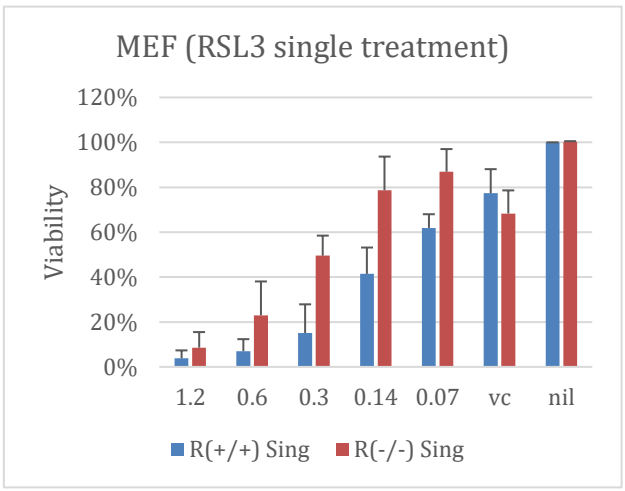

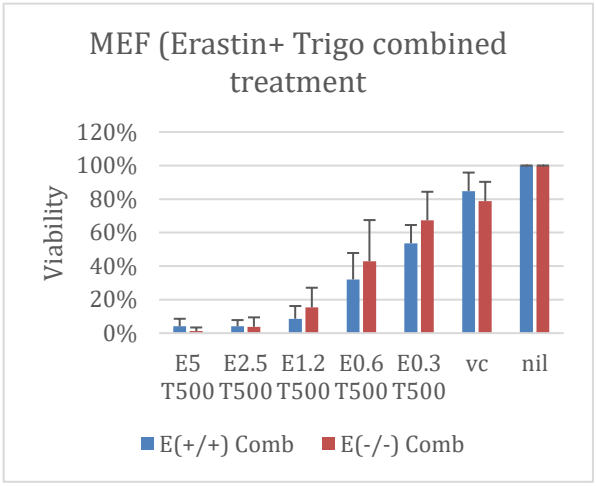

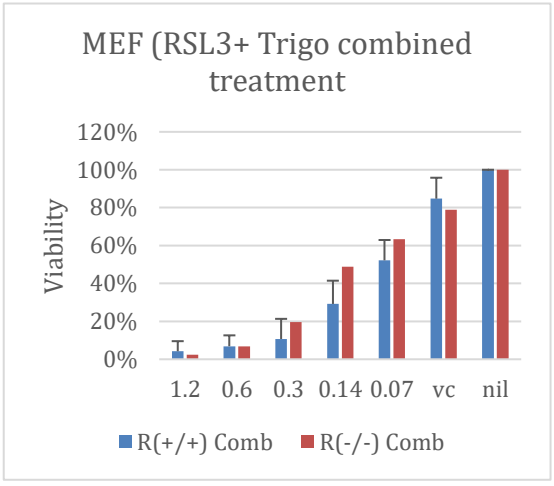

Fig. 1 MTT cell viability analysis of the effect Erastin and RSL3 on MEF *(+/+)* and MEF *(−/−)* cells with or without NRF2 inhibition by Trigonelline.

Western Blot:

Western blot analysis was used to see the expression of interests of proteins related to the Tsc2-cell line models and ferroptosis as a part of training in Cardiff University under supervision of Prof. Andrew Tee. The assay was then repeated by Dr. Darius McPhail (Cardiff University, which generated the final (See Fig. 3.8)

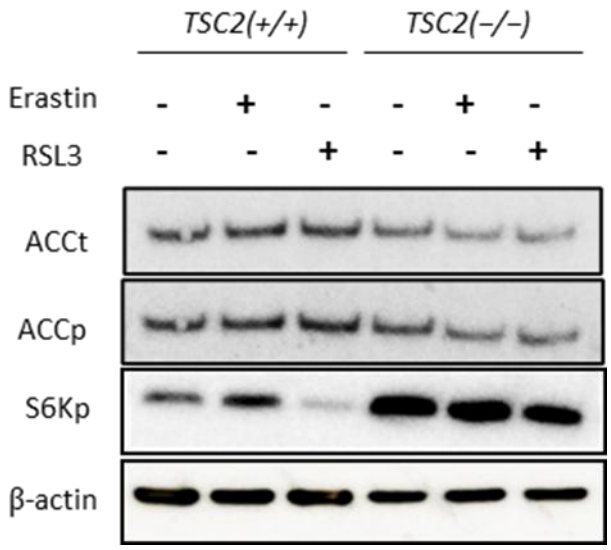

Fig.2 Western Blot Analysis of Ferroptosis Induction in *Tsc2*+/+ and *Tsc2*−/− MEF Cells

2.4 Statistical Analysis

Data analysis was carried out using Graphpad Prism version 8 and statistical testing was carried out as appropriate to the data captured and detailed in the relevant results section. Tests used included unpaired t-test, Mann Whitney U test, ordinary One-way ANOVA followed by post-hoc tests, Two way ANOVA followed by post hoc such as Holm-Sidak or Tukey's, or an independent samples Kruskal-Wallis test and post hoc Dunn's analysis (identified in individual figure legend). N= number of biological repeats and is identified on figure legends.

Chapter 3: Determination the role of *Tsc2* deficiency on the viability of ELT3 and MEF *Tsc2* model cell lines through ferroptosis induction.

3.1 Introduction

Molecular pathways and genetic mutations significantly affect cancer, particularly in the context of ferroptosis. *TSC2*, a tumour suppressor and negative regulator of mTORC1, is frequently mutated in various cancers. Loss of TSC2 leads to sustained mTORC1 activation, which promotes antioxidant defences (e.g., SLC7A11, GPX4), lipid biosynthesis via SREBP1-SCD1, and iron metabolism dysregulation, all of which influence ferroptosis sensitivity (Zhang et al., 2021c, Porstmann et al., 2008, Yi et al., 2020, Baba et al., 2018). Dual inhibition using mTORC1 inhibitors (e.g., Torin1, Rapamycin) alongside ferroptosis inducers (e.g., Salinomycin) has shown synergistic effects in various cancer models (Cosialls et al., 2023). Indeed, ferroptosis sensitivity in *TSC2*-deficient cells is also modulated by extrinsic and intrinsic stress responses, including hypoxia, ER stress, and AMPK signalling (Song et al., 2018, Li et al., 2022c, Brugarolas et al., 2003)

These findings point to a fundamental link between *TSC2* loss and ferroptosis, involving both mTORC1-dependent and -independent pathways. Targeting SLC7A11, GSH/GPX4, and mTOR concurrently may represent a promising strategy to induce ferroptotic cell death in TSC2-deficient cancers.

In this chapter, we investigate how *Tsc2* deficiency modulates ferroptosis sensitivity using *Tsc2+/+* and *Tsc2−/−* MEF and ELT3 cell lines. We employed two well-characterised ferroptosis inducers, Erastin and RSL3, and applied selective inhibitors of apoptosis (Z-VAD-FMK), necroptosis (Necrostatin-1), and ferroptosis (Ferrostatin-1) to confirm the mode of cell death after 24 hours of treatment.

To explore the role of iron in this process, we used the iron chelator Deferiprone (DFP), which exhibits superior lipophilicity and redox activity compared to Deferoxamine (DFO), and selectively chelates labile iron pools (LIP), contributing to increased ferroptosis sensitivity (Gallego-Murillo et al., 2023). Hence, to confirm the role of iron and its association with mTORC1 in our observed cell death, we utilised DFP to assess whether iron chelation could rescue cells from RSL3-induced death in *Tsc2*-deficient and the wild type MEF and ELT3 cells.

Additionally, we investigated the impact of mTORC1 inhibition using Rapamycin, which reduces cellular iron levels by downregulating transferrin receptor 1 (TfR1) and ferroportin expression, thus inhibiting ferroptosis (Bayeva et al., 2013, Baba et al., 2018). mTORC1 inhibition can lead to the activation of AMPK, a key energy sensor that regulates autophagy through downstream targets such as ULK1 and P70S6K. One autophagic process, ferritinophagy, selectively degrades ferritin to increase intracellular iron availability, thereby promoting ferroptosis (Zhong et al., 2020). In parallel, AMPK activation has been shown to suppress System Xc^- activity and downregulate GPX4 expression, both of which enhance ferroptotic sensitivity (Li et al., 2022c). To investigate the contribution of these interconnected pathways, we assessed the effects of the mTORC1 inhibitor Rapamycin and the AMPK inhibitor Compound C, both individually and in combination with RSL3

Despite these insights, the precise mechanisms by which *TSC2* loss enhances or protects against ferroptosis remain unclear. It is not yet fully understood whether ferroptosis susceptibility is driven solely by mTORC1 overactivation or by additional pathways dysregulated due to *TSC2* deficiency. Therefore, in this study, we aim to systematically examine how TSC2 loss influences ferroptosis and define the upstream and downstream signalling pathways involved.

3.1.5 Hypothesis

We hypothesise that *Tsc2* deficiency alters ferroptosis sensitivity.

3.2.6 Aims

To establish this, we aimed to:

1. Determine cytotoxic sensitivity in *Tsc2* mutant and wild type cell line models upon exposure to ferroptosis inducers and establish their IC50 concentrations.
2. Determine the exclusivity of cell death mode induced by ferroptosis inducers using specific cell death inhibitors.

3.2 Results

3.2.1 Optimised doses of ferroptosis inducers both Erastin and RSL3 showed *Tsc2 (+/+)* cells are susceptible and *Tsc2 (−/−)* cells are resistant to ferroptosis induction

Tsc2+/+ and *Tsc2−/−* MEF (referred to as MEF (*+/+*) and MEF (*−/−*), respectively) cells exhibited differential responses to different doses response of ferroptosis inducers Erastin and RSL3. Statistically significant differential responses between the cell lines with Erastin exposure were identified at doses of 0.6μM ($p<0.001$) and 1.2μM ($p<0.001$) (Fig 3.1A). Beyond these doses the majority of cells were ferroptotic and, thus, differences between cell lines responses were not discernible. With RSL3 statistically significant differences in viability between the cell lines were observed at 0.1μM ($p<0.001$) and 0.3μM ($p<0.05$) (Fig 3.1B). Again, higher doses resulted in the majority of cells in both cell types, (+/+) and (-/-), having near maximum cytotoxicity, and consequently, no discernible difference was observable at these doses. As detailed in the method section viable cells were determined based on size (large) and DRAQ7 negativity (See Fig 3.1C&D). This was based on the observations that treated cells exhibited DRAQ7 negative, morphologically small cells. These small cells are not viable, thus, selection of DRAQ7 positive cells only for determination of viability would have been misleading.

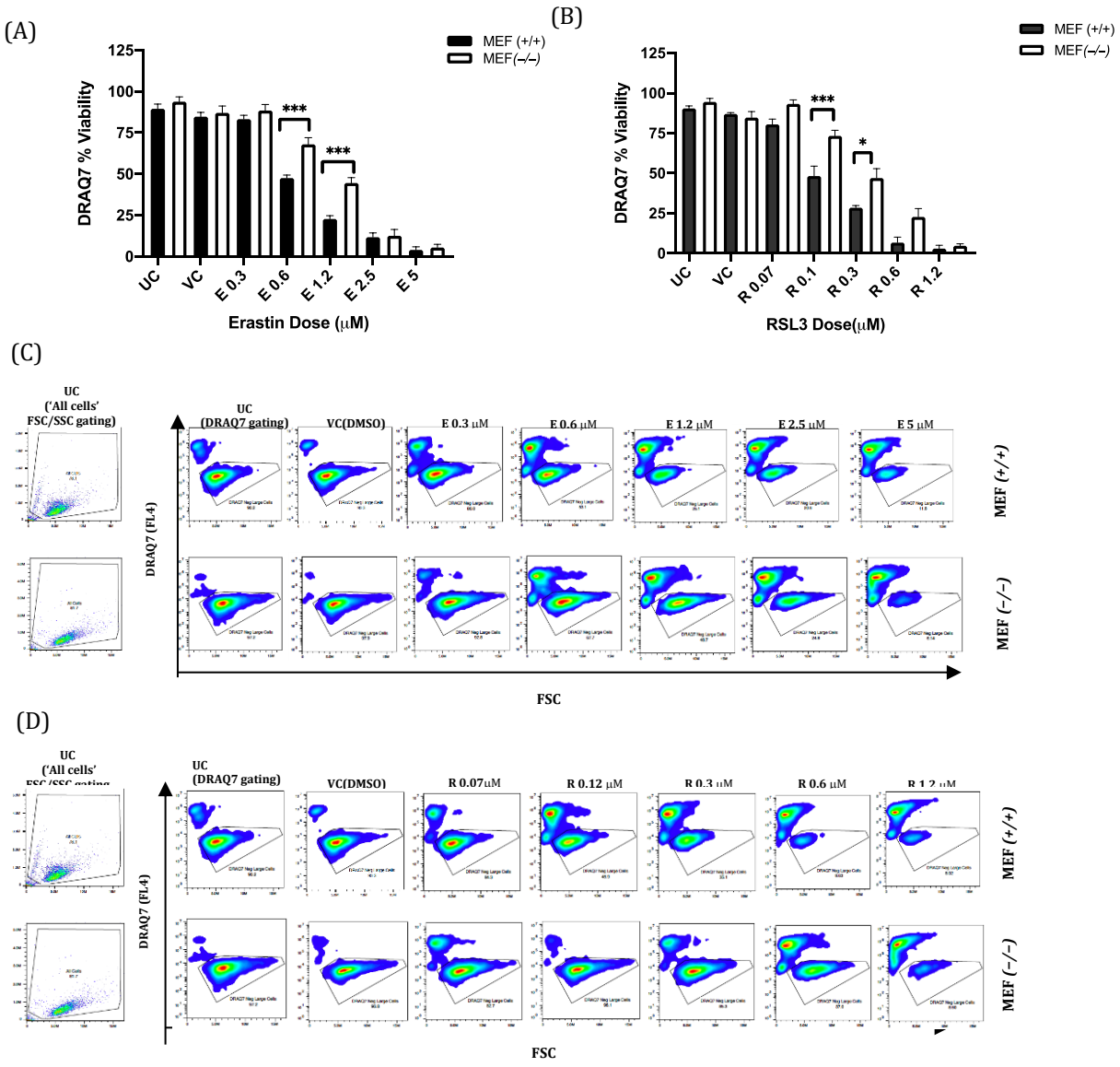

Figure 3.1 Effect of Ferroptosis inducers Erastin and RSL3 on MEF *(+/+)* and MEF *(–/–)* viability
MEF *(+/+)* and *(–/–)* cells were seeded at 1x10^5/mL cells in 24 well plates (500 μL/well). Cells were incubated overnight and then treated with (A) Erastin [5-0.3μM] or (B) RSL3 [1.2-0.07μM] for a further 24h at 37^{o}C/5% CO2/humidified air. DMSO was used as the vehicle control. DRAQ7 flow cytometry assay was used to determine cell viability after 24 h treatment with ferroptosis inducers. (C) and (D) are the representative data of (A) and (B), showing the gating for 'All cells' (FSC vs SSC) and DRAQ7 negative large cells (FSC vs FL4) as representative of viable cells. Statistical significance is shown between *Tsc2+/+* MEFs and *Tsc2-/-* MEFs for Erastin or RSL3 treatment (n=3; mean +/- SD; *p<0.05; ***p<0.001)

ELT3 (*+/+)* and ELT3 *(−/−)* subjected to Erastin and RSL3 dose responses showed a similar cell death pattern to the observations seen in MEFs. Between the ELT3 variants statistically significant differences were identified at 3.7μM ($p<0.05$) and 7.5μM ($p<0.05$) for Erastin, and 0.5μM ($p<0.05$) and 1μM ($p<0.05$) for RSL3 (Fig 3.2 A&B). As described in MEFs higher doses yielded no statistically significant differences between the (+/+) and (-/-) since the cytotoxicity plateaus at maximal cell loss. It is also salient to mention that ELT3 cell lines required higher doses of either Erastin or RSL3 (Fig 3.2 A&B) for comparable cell death levels seen in MEFs (Fig 3.1 A&B). This represents a five-to-six-fold higher concentration of the respective drugs to achieve an equivalent approximate 50% loss of viability in the ELT3 *(+/+)* cells relative to the MEF *(+/+)* cells. IC50 values for each cell line and for each drug were, thus, calculated (see 3.2.2).

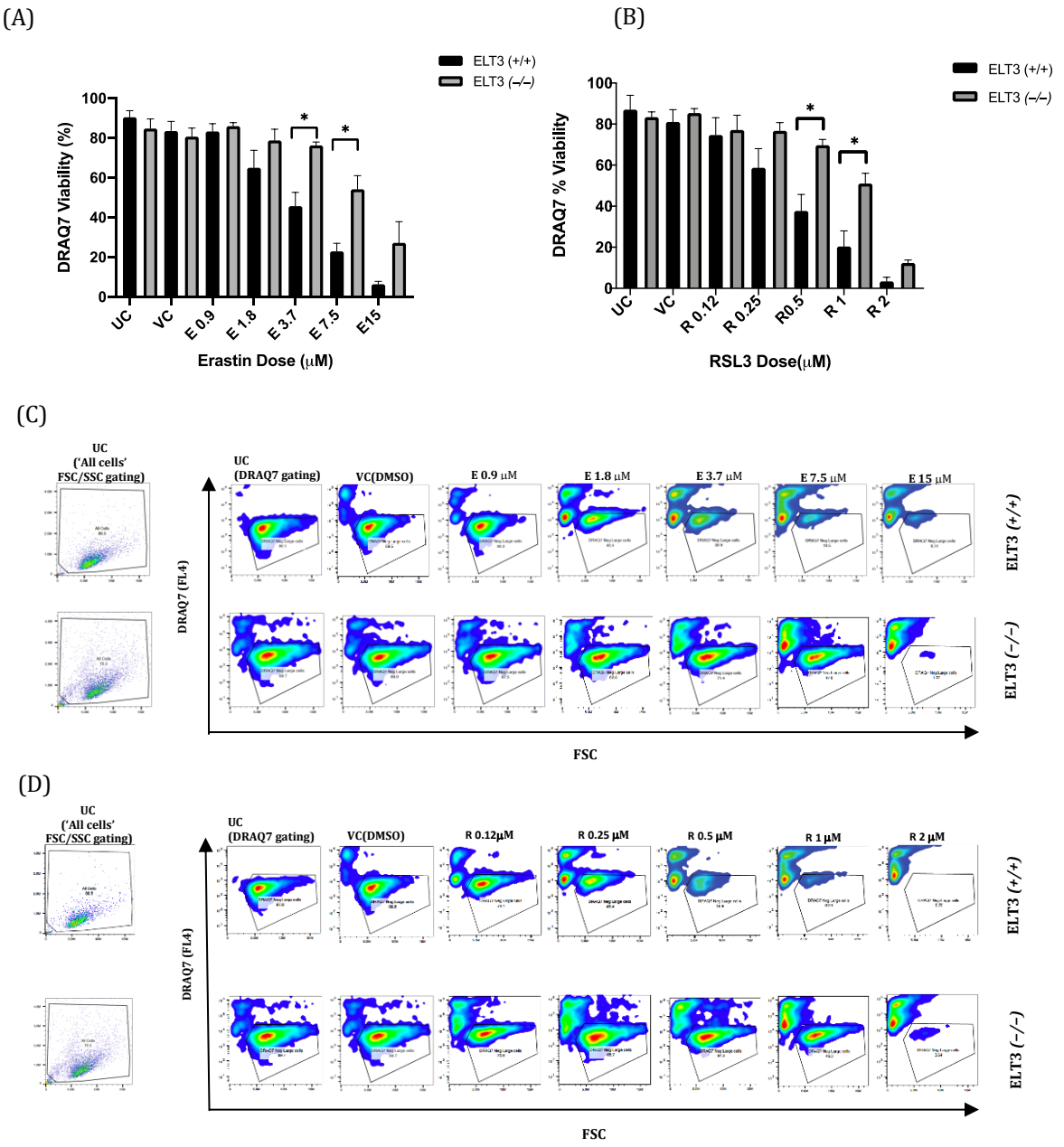

Figure 3.2 Effect of Ferroptosis inducers Erastin and RSL3 on ELT3 *(+/+)* and ELT3*(–/–)* DRAQ7 viability

ELT3*(+/+)* and *(–/–)* cells were seeded at 1x10^5/mL cells in 24 well plates (500 µL /well). Cells were incubated overnight and then treated with (A) Erastin [15-0.9µM] or (B) RSL3 [2-0.12µM] for a further 24h at 37^{o}C/5% CO2/humidified air. DMSO was used as a vehicle control. DRAQ7 flow cytometry assay was used to determine cell viability after 24 h treatment with ferroptosis inducers. (C) and (D) are the representative data of (A) and (B), showing the gating for 'All cells' (FSC vs SSC) and DRAQ7 negative cells (FSC vs FL4). Statistical significance is shown between *Tsc2(+/+)* ELT3s and *Tsc2(-/-)* ELT3s for Erastin or RSL3 treatment (n=3; mean +/- SD). *p<0.05. UC= Untreated Control, VC= Vehicle Control.

3.2.2 IC_{50} determination for Erastin and RSL3 revealed significantly lower values in *Tsc2 (+/+)* cells compared to *Tsc2 (–/–)* cells

Table 3.1 summarises the half-maximal inhibitory concentration (IC_{50}) values attained for both MEF and ELT3 *Tsc2* cell line variants with Fig 3.3 depicting the cumulative data for the respective dose responses in all the cell lines. For both drugs, and in each of MEF and ELT3, it is the Tsc2 deficient *(–/–)* variant that exhibits a higher IC_{50} value i.e. it is resistant to ferroptosis-mediated cell death induction.

TABLE 3.1. IC_{50} VALUES FOR ERASTIN AND RSL3 IN MEF AND ETL3 *TSC2* VARIANTS

Treatment	IC_{50} [μM]	Treatment	IC_{50} [μM]
MEF *(+/+)* E sing	0.595	ELT3 *(+/+)* E sing	3.207
MEF *(–/–)* E sing	0.988	ELT3 *(–/–)* E sing	8.444
MEF *(+/+)* R sing	0.142	ELT3 *(+/+)* R sing	0.424
MEF *(–/–)* R sing	0.281	ELT3 *(–/–)* R sing	0.855

Sing= single dose/ the treatment alone

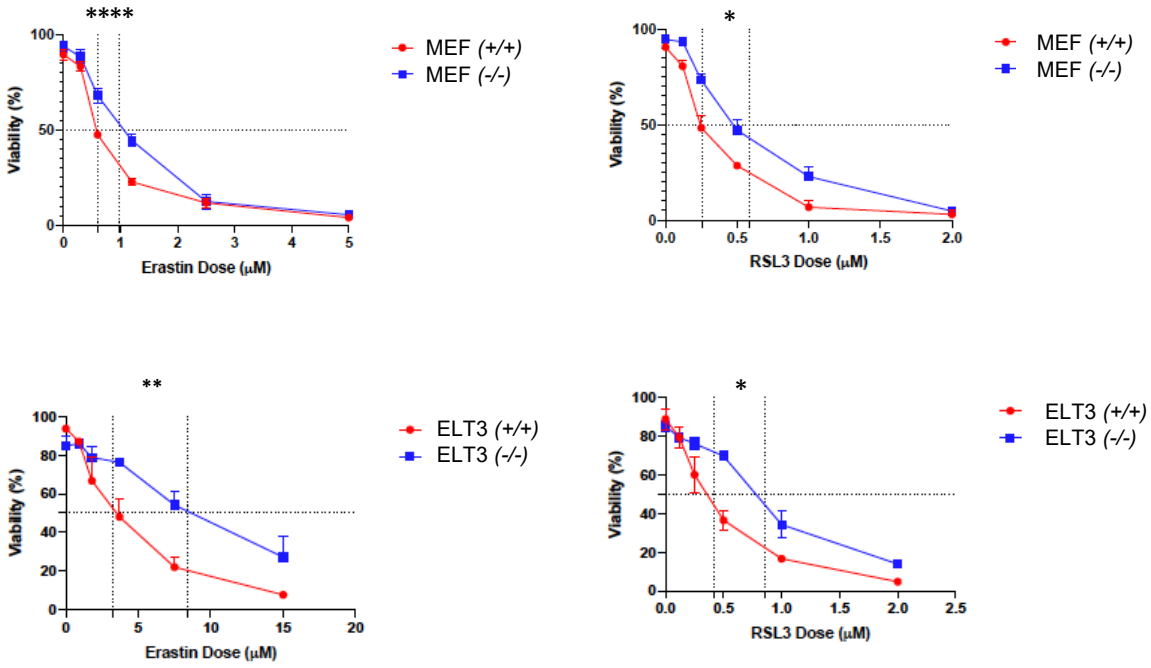

Fig. 3.3 IC_{50} Value determination for Erastin and RSL3 in ELT3 (*+/+*) and (*–/–*)

MEF and ELT3 *Tsc2* cell line variants were seeded at $1x10^5$/mL cells in 24 well plates (500 µL /well). Cells were incubated overnight and then treated with (A) Erastin [15-0.9µM] or (B) RSL3 [2-0.12µM] for a further 24h at 37°C/5% CO2/humidified air. Viability was assessed using DRAQ7 and laser scatter-based morphology assessment of cells by flow cytometric analysis. Viability was defined as DRAQ7 negative large cells (see Figs 3.1 & 3.2 for representative data). Graphs were plotted and IC_{50}s determined using GraphPad Prism Version 8. Unpaired two-tailed T tests were performed on IC_{50} values. (n=4; * p<0.05; ** p<0.01; *** p<0.001; **** p<0.0001)

3.2.3 Cell death inhibitors with the exception of FS-1 failed to rescue Erastin and RSL3 induced cell death in MEF*(+/+)* and *(−/−)* cell lines.

To establish the specific mode of cell death inhibitors of apoptosis (ZVAD-FMK), necroptosis (Necrostatin-1) and ferroptosis (Ferrostatin-1) were first given to untreated *Tsc2 (+/+)* and *Tsc2(−/−)* MEF cell lines at established maximal doses to demonstrate the lack of toxicity of the inhibitors themselves (Fig4 A and B). Subsequently, cells were treated concomitantly with RSL3 IC_{50} [0.14μM] and [0.28 μM] with or without inhibitors. Of the three inhibitors used only the ferroptosis inhibitor (FS-1) significantly rescued cell viability ($p=0.002$). This suggested that ferroptosis was the only mode of cell death induced in the RSL3-treated cell lines.

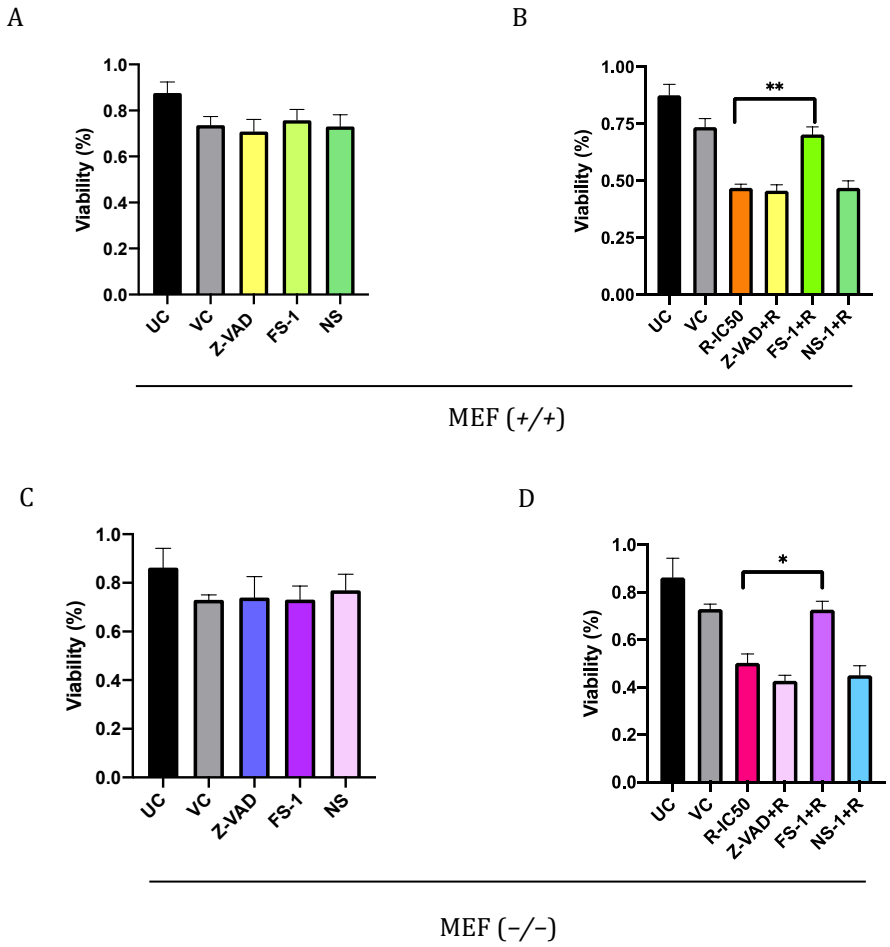

Fig. 3.4 Pharmacological Inhibition of cell death induction

(A) MEF *(+/+)* were treated with the cell death inhibitors Z-VAD-FMK (Z-VAD) [10μM], Ferrostatin-1 (FS-1)[10μM] or Necrostatin-1 (NS) [10μM] alone; or (B) in combination with RSL3 at the previously observed IC50 [0.5 μM] for this cell line. Similarly, MEF *(−/−)* were treated with the inhibitors alone (C); or in combination with RSL3 at the observed IC50 [0.9 μM] for this *Tsc2* deficient variant (D). There was no observable effect of cell death inhibitor exposure alone to either cell line. Concomitant exposure to the inhibitors and the ferroptosis inducer RSL3, however, revealed that only FS-1 significantly rescued the cell death induced. (Data was analysed by ordinary one-way ANOVA and Holm Sidak Post hoc analysis. n=3; *p=0.027; p**=0.002. UC= Untreated Control, VC= Vehicle Control.)

3.2.4 Iron chelation was effective to rescue RSL3 treated cell death in both Tsc2 re-expressed and Tsc2 deficient MEF and ELT3 cell lines.

Iron dependence for cell death, which is definitive of ferroptosis, was investigated using iron chelation. Deferiprone (DFP), a well characterised iron chelator, was initially exposed to cells over a dose range to assess its direct effects on cell viability across all cell lines. Thereafter, IC50 doses of the ferroptosis inducer, RSL3, were given to the cells and a dose range of DFP treatments given to assess their impact in prevention of ferroptosis induction. Direct exposure to DFP doses alone had no impact on cell viability in either MEF or ELT3 (Figs 3.5 and 3.6 (A) and (C)). With RSL3 exposure, however, a dose-dependent retardation of ferroptosis cytotoxicity was observable (Figs 3.5 & 3.6 B & D) and, notably, a difference between the *Tsc2* variant cell lines, *(+/+)* versus *(−/−)*, was evident with *(−/−)* cells more profoundly rescued by chelation; a significant rescue from cytotoxicity was achieved at 12.5μM DFP for MEF *(−/−)* cells versus 25μM DFP for MEF *(+/+)* (Fig 3.5 B & D).

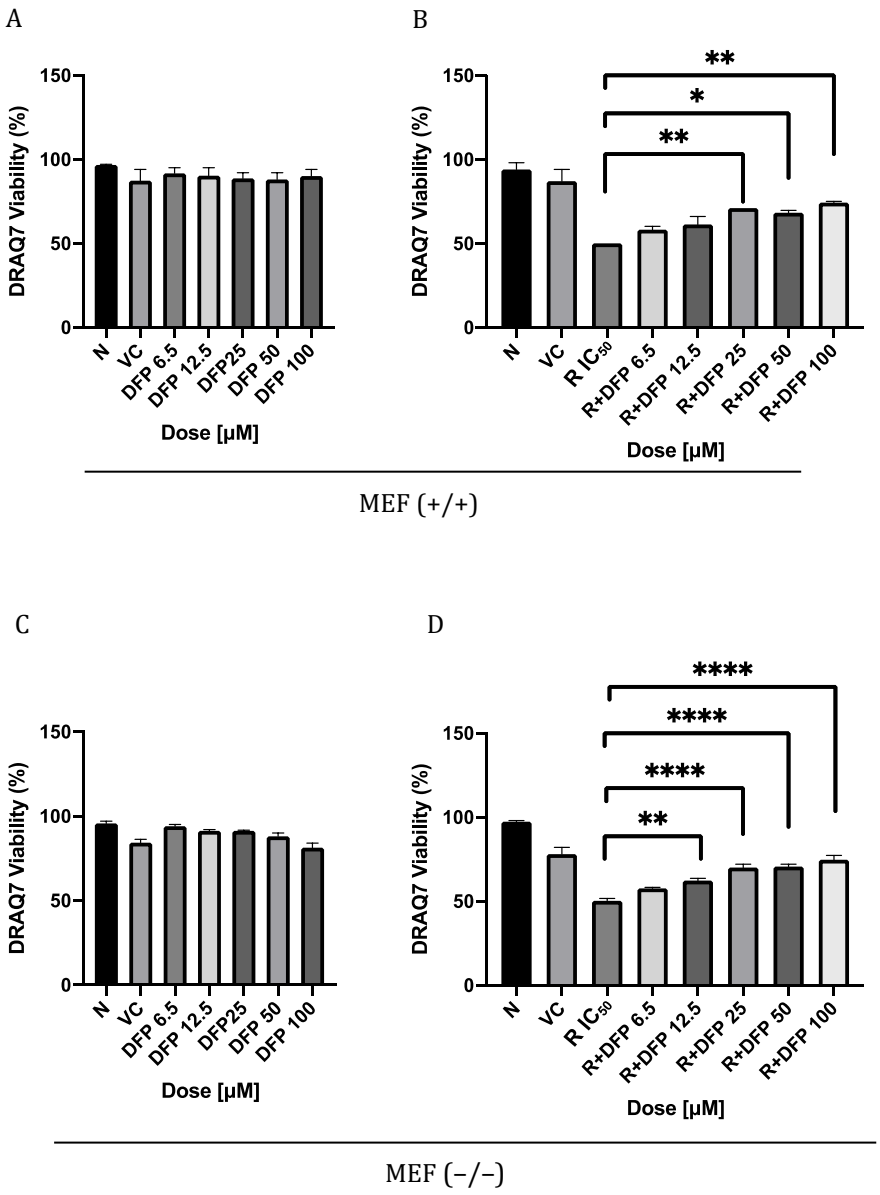

Fig. 3.5 Iron chelation rescues RSL3-induced cell death in MEF *Tsc2* cell lines

MEF *Tsc2* cell line variants were seeded at 1x10^5/mL cells in 24 well plates (500 µL /well). Cells were incubated overnight and then treated with a dose response of the the iron chelator, Deferiprone, alone (A & C) or in combination with, the estabished IC_{50} of RSL3 (B & D) for a further 24h at 37^{o}C/5% CO2/humidified air. Viability was assessed using DRAQ7 and laser scatter-based morphology assessment of cells by flow cytometric analysis. Viability was defined as DRAQ7 negative large cells. (Data was analysed by ordinary one way ANOVA and Tukey's post hoc analysis. n=4; *p<0.05; **p<0.01; ***p<0.001; ****p<0.0001). UC= Untreated Control, VC= Vehicle Control.

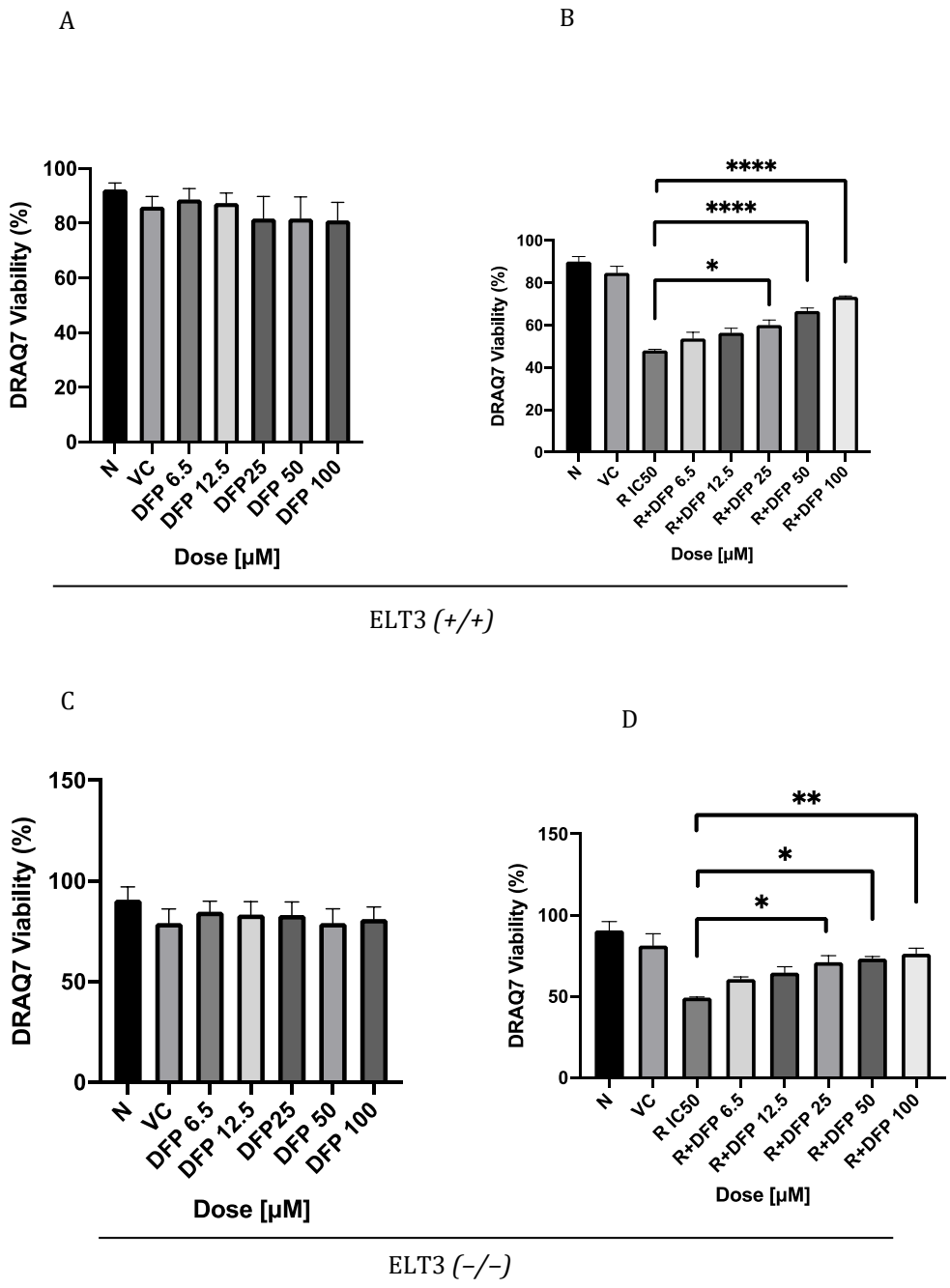

Fig. 3.6 Iron chelation rescues RSL3 induced cell death in ELT3 *Tsc2* cell lines

ELT3 *Tsc2* cell line variants were seeded at 1x10^5/mL cells in 24 well plates (500 µL /well). Cells were incubated overnight and then treated with a dose response of the the iron chelator, Deferiprone, alone (A & C) or in combination with, the estabished IC_{50} of RSL3 (B & D) for a further 24h at 37^{o}C/5% CO2/humidified air. Viability was assessed using DRAQ7 and laser scatter-based morphology assessment of cells by flow cytometric analysis. Viability was defined as DRAQ7 negative large cells. (Data was analysed by ordinary one way ANOVA and Tukey's post hoc analysis. n=4; *p<0.05; **p<0.01; ***p<0.001; ****p<0.0001). UC= Untreated Control, VC= Vehicle Control.

3.2.5 RSL3-induced cytotoxicity in *Tsc2 (+/+)* and *(−/−)* cells is mTOR independent but AMPK dependant.

To determine the role of mTORC1 and AMPK in RSL3-induced cell death, we first treated untreated *Tsc2+/+* and *Tsc2−/−* MEF and ELT3 cell lines with Rapamycin and Compound C at established maximal doses. This was done to confirm that these inhibitors were non-toxic when administered alone (Figs. 3.7). Cells were subsequently co-treated with RSL3 at IC_{50} doses, with or without the respective inhibitors.

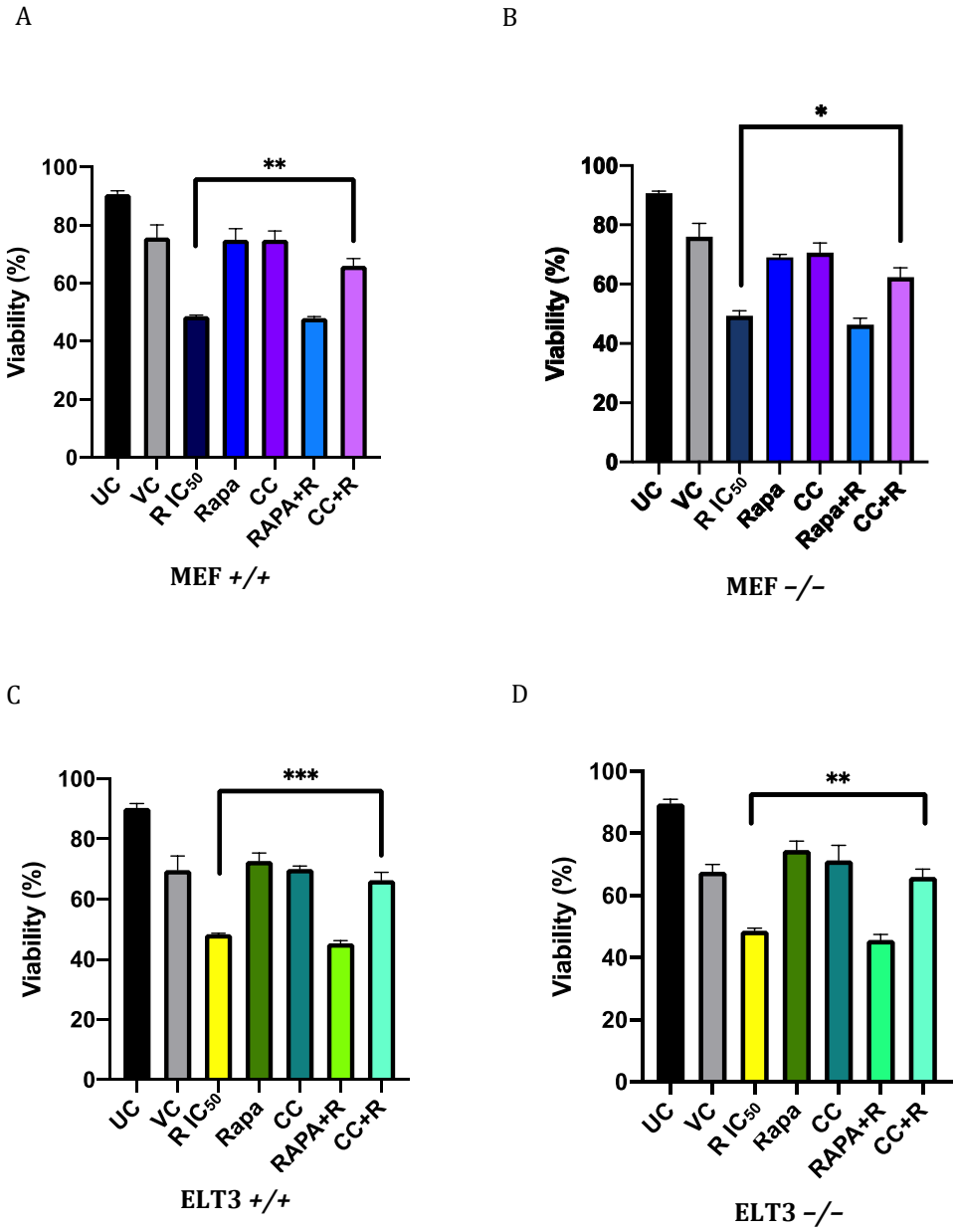

Fig. 3.7 Inhibition of mTOR and AMPK in MEF and ELT3 *Tsc2* cell lines

A) MEF and (B) ELT3 (+/+) and (−/−) cell lines were seeded at 1x10^5/mL cells in 24 well plates (500 µL /well). Cells were incubated overnight and then treated with the inhibitors of AMPK and mTOR, Compound C (CC) [5µM] and Rapamycin (Rapa) [50nM], respectively, for a further 24h at 37^{o}C/5% CO2/humidified air. Inhibitors were also used concomitantly with ferroptosis induction using the IC50 of RSL3 for the respective *Tsc2* variants. RSL3 alone and vehicle control were also employed. No effect on viability was observable via inhibitors alone in either cell line. RSL3 cytotoxicity was ameliorated by AMPK inhibition, via compound C, but not by mTOR inhibition via rapamycin. (Data was analysed by ordinary one way ANOVA and Tukey's post hoc analysis. n=4; *p<0.05; **p<0.01; ***p<0.001) UC= Untreated Control, VC= Vehicle Control.

Next, Western blotting was used to evaluate the activity of mTORC1 and AMPK in response to these treatments (Fig. 3.8). Phosphorylated ribosomal protein S6 (p-rpS6), a downstream target of mTORC1, was used to assess mTORC1 activity. Tsc2+/+ MEF cells exhibited low levels of p-rpS6, consistent with low mTORC1 activity. In contrast, Tsc2−/− MEF cells showed consistently high levels of p-rpS6, regardless of RSL3 treatment, indicating elevated mTORC1 signalling in the absence of Tsc2. Treatment with Rapamycin reduced p-rpS6 levels in Tsc2−/− cells, both in the presence and absence of RSL3, confirming effective inhibition of mTORC1 signalling.

AMPK activity was assessed by measuring phosphorylated acetyl-CoA carboxylase at serine 79 (p-ACC(S79)). In *Tsc2−/−* MEFs, p-ACC levels were reduced following Compound C treatment, indicating suppression of AMPK activity. Notably, RSL3 treatment increased p-ACC levels in both *Tsc2+/+* and *Tsc2−/−* cells, suggesting an increase in AMPK activity during ferroptosis induction.

Autophagy regulation was monitored via p62 protein levels. *Tsc2−/−* MEFs exhibited higher baseline levels of p62 compared to *Tsc2+/+* cells. Upon RSL3 treatment, p62 levels decreased in *Tsc2−/−* cells. In cells treated with Rapamycin, either alone or in combination with RSL3, p62 was undetectable, indicating that mTORC1 is involved in autophagy regulation and its consequent impact on ferroptosis.

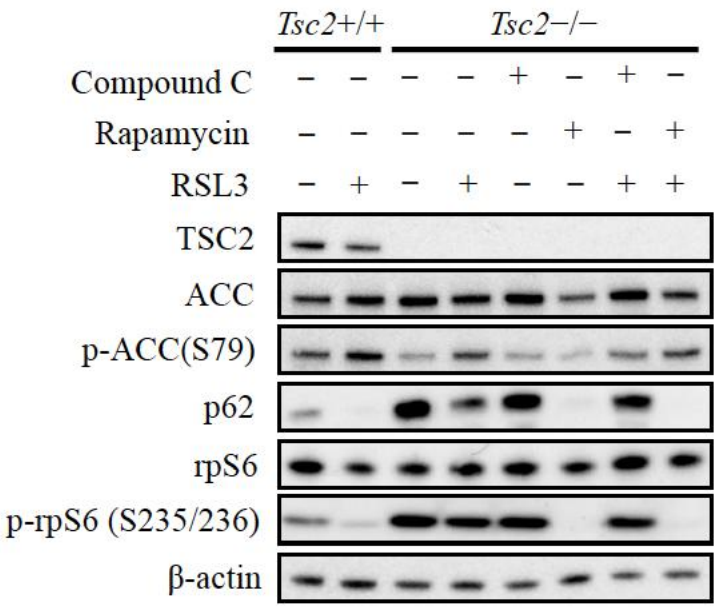

Fig. 3.8 Western Blot Analysis of Ferroptosis Induction in *Tsc2*+/+ and *Tsc2*−/− MEF Cells

Expression of TSC2 in MEF (*+/+*) cells and absent in MEF (−/−) cells, confirms the genotypic distinction between the cell lines. In *Tsc2*−/− cells, p-ACC(S79) levels are reduced, particularly under Compound C treatment, showing effective inhibition of AMPK activity. Increased levels in *Tsc2*−/− cells compared to *Tsc2 +/+* cells, suggesting altered autophagy regulation in the absence of *Tsc2*.The presence of Rapamycin affects p62 levels, highlighting the involvement of mTORC1 in autophagy regulation. *Tsc2*+/+ cells show reduced p-rpS6 levels upon Rapamycin treatment, indicating effective inhibition of mTORC1. *Tsc2*−/− cells have consistently high p-rpS6 levels, suggesting dysregulated mTORC1 activity in the absence of *Tsc2*. Used as a loading control to ensure equal protein loading across the lanes.

3.3 Discussion

This study represents the first comparative analysis of the effects of ferroptosis inducers Erastin and RSL3 in *Tsc2−/−* mTORC1 hyperactive cell lines vs their *Tsc2 +/+*counterparts. In this chapter, we have uncovered new findings on ferroptosis sensitivity in relation to *Tsc2* loss in MEF and ELT3 cell lines. Our goal was to establish differential ferroptotic sensitivity, develop IC_{50} values for the treatments, and investigate the mode of cell death induced in these cell lines.

Previous research has shown that loss of *Tsc2* promotes ferroptosis resistance in Tsc2−/− MEF cells by upregulating SLC7A11 through its downstream target endoplasmic reticulum oxidoreductase 1 alpha (ERO1α) (Wang et al., 2024b). Similarly, the loss of Tsc2 in the pituitary enhanced mTOR signalling and increased SLC7A11/System XC− expression in ELT3−/− cells, resulting in reduced sensitivity to ferroptosis (Li et al., 2019a). Aligned with these findings, our data showed that Tsc2−/− cells exhibited greater resistance to Erastin-induced cell death compared to Tsc2*+/+* cells, with respective IC_{50} values of 2.5 μM and 5 μM. Similarly, ELT3 cell lines showed differential sensitivity with IC_{50} values of 5μM +/+ and 10μM *(−/−)*. This consistency of higher sensitivity to Erastin in Tsc2*+/+* cell lines demonstrates that *Tsc2* plays an important role in ferroptosis induction in different cell line types. While there is consistency in response to the presence of *Tsc2*, the greater tolerance of ELT3 cell lines to Erastin may reflect their differentially upregulated ferroptosis genes compared to the respective MEF cell lines (Li et al., 2019a).

Another ferroptosis inducer, RSL3, which inhibits GPX4 and causes the accumulation of lipid peroxides (Yang et al., 2014), also induced greater ferroptosis in Tsc2*+/+* cells. IC_{50} values for RSL3 were 0.3 μM for Tsc2+/+ MEFs and 0.6 μM for Tsc2−/− MEFs, and 0.5 μM for Tsc2+/+ ELT3 cells and 0.8 μM for Tsc2−/− ELT3 cells. This suggests a higher tolerance to ferroptosis induction in ELT3 cells. The exact nature of these differences was not analysed in this thesis,

but research has shown that genotype/phenotype differences in the cell lines can influence their sensitivity to ferroptosis.

We then examined whether other forms of cell death contributed to the cytotoxic effects induced by Erastin and whether inhibition of one death pathway could activate compensatory mechanisms. MTT colorimetric assay of cellular metabolic activity as an indirect measure of viability revealed that treatment with 5 μM Fer-1 successfully rescued cell death in both Tsc2 (*+/+)* and Tsc2 *(−/−)* MEFs and ELT3 cells aligning with previous observations by (Dixon et al., 2012). However, inhibition of other cell death pathways did not significantly impact cell death, indicating that ferroptosis was the primary mode of cell death.

Furthermore, our DRAQ7 flow cytometry analysis demonstrated that the iron chelator deferiprone (DFP) rescued cells from RSL3-induced ferroptosis in a dose-dependent manner. Tsc2 *(−/−)* MEF cells displayed greater sensitivity to DFP, potentially due to upregulated antioxidant regulators associated with mTORC1 activation or stress response mediated upregulation of VEGF independent of mTORC1(Fraser et al., 2011). This heightened sensitivity to DFP in MEF *(−/−)* cells could potentially be linked to the upregulation of antioxidant regulators associated with mTORC1 activation. (Fraser et al., 2011). This suggests that *Tsc2*-deficient cells might have less iron available for chelation, making them more sensitive to iron chelators. Additionally, studies have shown that Tsc2 deficiency blocks iron accumulation within the cell by modulating the stability of Transferrin Receptor 1 (TfR1) and altering cellular iron flux (Bayeva et al., 2012). This observation aligns with our iron chelation rescue experiment data described in section 3.2.4 (Fig. 3.5). The role of iron in regulating ferroptosis in Tsc2-deficient cells will be discussed in detail in Chapter 4.

To confirm the activity mTORC1 during ferroptosis induction by RSL3, we aimed to utilize Rapamycin to assess the impact of mTORC1 inhibition in our cell lines. Interestingly, mTORC1

inhibition by 50nM Rapamycin for 24 hours did not affect the cytotoxicity detected in MEF or ELT3 Tsc2 variants when exposed to RSL3 (Fig 3.7). The Western blot data presented in Fig. 3.8, however, revealed that, while higher levels of phosphorylated rpS6 (p-rpS6), a downstream target protein of mTORC1 were observed in Tsc2 *(–/–)* cells, relative to Tsc2 *(+/+)* cells, RSL3 treatment did result in a small but detectible diminishing of p-rpS6 levels in both cell lines. More salient, was the observation that rapamycin inhibition of mTORC1, with and without RSL3 treatment, profoundly affected the levels of p-rpS6, such that bands were not detectable in Tsc2 *(–/–)*. The unphosphorylated protein (rpS6) was still present in the cells, and thus, mTORC1 activity was the key factor in phosphorylation of the protein. Taken together, the successful inhibition of rpS6 phosphorylation by Rapamycin and the lack of impact on ferroptosis induction by RSL3 (Fig. 3.7) suggest that mTORC1 hyperactivity is not a dominant factor in the ferroptosis resistance observed in Tsc2 *(–/–)* cells, and that other pathways may play a role.

Interestingly, other studies demonstrated that mTORC1 inhibitors like Torin and AZD8055, rather than rapamycin, sensitize cells to ferroptosis-induced cell death (Yangyun et al., 2022). (Zhang et al., 2021c). Additionally, research has suggested that prolonged exposure to high doses of Rapamycin [5 μM] can rescue cells from ferroptosis-induced death, contrasting with our use of a 50 nM dose (Liu et al., 2023a).

Consistent with our findings, Yangyun et al. (2022) reported that Everolimus exhibits synergistic effects with ferroptosis inducers in renal cell carcinoma models by promoting ferroptotic cell death. However, its clinical efficacy in brain tumours such as ependymomas and vestibular schwannomas has been limited, with studies showing incomplete mTORC1 inhibition and minimal therapeutic benefit (Karajannis et al., 2021, Bowers et al., 2023). These observations suggest that TSC2-deficient brain tumours may engage additional, mTOR-independent mechanisms that contribute to treatment resistance.

Next, we explored the role of AMPK, a regulator upstream of mTORC1, in RSL3-induced ferroptosis. Recent findings suggest that AMPK activation triggers ferroptosis independently of mTORC1 through BECN1 activation, GPX4 reduction, and p38-MAPK-mediated iron upregulation (Song et al., 2018). Aligning with these findings, our data (Fig. 3.7) showed that inhibiting AMPK activation with Compound C (CC) restored cell viability in all cell lines treated with their IC50 doses of RSL3, indicating that AMPK activation promotes ferroptosis sensitivity. Protein expression related to AMPK, monitored through phosphorylated ACC (p-ACC(S79)) levels, confirmed the viability data. p-ACC levels were decreased in Tsc2 *(−/−)* cells, particularly under Compound C treatment, indicating effective inhibition of AMPK. However, p-ACC levels were elevated during RSL3-induced ferroptosis in both Tsc2 *(+/+)* and Tsc2 (*−/−)* cells, suggesting that AMPK activation may promote ferroptosis under specific conditions.

However, the role of AMPK in the regulation of ferroptosis is controversial. For example, Lee et al. (2020) demonstrated that AMPK activation reduces ferroptosis sensitivity ferroptosis by inhibiting lipid biosynthesis through phosphorylation of acetyl-CoA carboxylase ACC, thereby reducing the pool of polyunsaturated fatty acids available for lipid peroxidation. Similarly, Li et al. (2020b) reported that AMPK activation inhibits ferroptosis in hepatocellular carcinoma cells by reducing fatty acid synthesis and promoting antioxidant responses These findings contradict our observations; hence, we hypothesise that the role of energy stress and AMPK on ferroptosis in cancer may be dependent on the context. Energy stress-mediated AMPK activation could either resist ferroptosis and promote tumour survival through the inhibition of unsaturated fatty acid synthesis or enhance ferroptosis and suppress tumour survival through the inhibition of protein biosynthesis or regulation of ferroptosis-related enzymes.

Despite the association between autophagy and ferroptosis through the degradation of iron into its toxic form, the current study didn't include autophagy inhibition due to time constraint. However, in this study, we observed an increased level of Sequestosome 1 (p62/SQSTM1) expression, which indicates altered autophagy regulation in Tsc2−/− cells compared to their counterparts (Fig 3.8). Elevated p62 levels are associated with the regulation of ferroptosis, primarily through the activation of antioxidant pathways. These pathways help mitigate lipid peroxidation, thereby contributing to ferroptosis resistance (Zhao et al., 2021b). RSL3 treatment completely reduced the overexpression of p62 in Tsc2 *(+/+)* cells but not in Tsc2 (−/−) cells, suggesting a differential response to ferroptosis induction. Rapamycin treatment reduced p62 levels, implicating mTORC1's involvement in autophagy regulation. This interaction highlights the role of mTORC1 in modulating autophagy processes and its impact on ferroptosis. Overall, the interplay between mTORC1, AMPK, and autophagy is crucial for regulating ferroptosis associated with *Tsc2* loss, with mTORC1 and AMPK significantly influencing ferroptosis sensitivity and induction, while autophagy contributes to the regulatory mechanisms involved.

In conclusion, our findings offer valuable insights into the mechanisms of ferroptosis resistance linked to *Tsc2* loss. Understanding these interactions can provide new insights into potential therapeutic strategies for overcoming ferroptosis resistance associated with Tsc2 deficiency.

Chapter 4 Confirmation and quantitation of ferroptotic regulators; and mechanistic insights in Tsc2 cell line models

4.2 Introduction

In the previous chapter, data from cell death inhibition assays established that the mode of observed cell death in *Tsc2* edited cell line model was ferroptosis. Therefore, in this chapter, we aim to investigate the biomarkers of ferroptosis to elucidate the mechanism of action of cell death in *Tsc2*-cell line model. Others have described ferroptosis as a lipid-peroxidation process in the cell membrane facilitated by intracellular iron-driven ROS (Dixon and Stockwell, 2014). Hence, we first employed specific assays to quantify lipid-peroxidation and ROS as the biomarkers of ferroptosis.

Ferroptosis is characterised by iron-driven oxidative stress causing lipid-peroxidation in the cell membrane (Dixon et al., 2012). Endogenous antioxidant systems, such as System X_C^-, facilitate the uptake of cystine, a precursor for glutathione (GSH). GSH in turn serves as a crucial cofactor for GPX4 activity, an enzyme that utilizes GSH as a reducing agent to detoxify lipid peroxides and protects cells from oxidative stress-induced ferroptosis. Therefore, lipid peroxidation, ROS and Labile Iron pool (LIP) are considered the primary biomarkers of ferroptosis (Bertrand, 2017).

Studies have elucidated the role of mTORC1 as a positive regulator of key factors in ferroptosis, including System X_C^-, and GPX4, while concurrently suppressing GPX4 expression. This suggests that combining agents targeting glutathione (GSH)/GPX4 and mTORC1 may potentiate ferroptosis induction by disrupting cellular antioxidant defences and amplifying lipid peroxidation and ROS accumulation (Zhang et al., 2021c). Additionally, cellular iron is pivotal in ROS generation via the Fenton reaction, with several iron-containing enzymes, such as

ALOXs, NOXs, and CYP, contributing to lipid peroxidation (Dixon et al., 2012, Yang and Stockwell, 2008, Kagan et al., 2017). Notably, mTOR has been implicated in the regulation of cellular iron homeostasis, as mTORC1 overexpression has been shown to decrease iron-induced ROS production, potentially protecting cells from iron-induced cell death by supressing ROS generation (Baba et al., 2018). This finding aligns with our observations from the previous chapter, where we noted that RSL3-mediated cytotoxicity was rescued by co-treatment with an iron chelator. While iron chelation and specific cell death inhibitors supported the specific mode of cell death as being ferroptosis in the previous chapter, our objective in this chapter is to characterise the primary biomarkers of ferroptosis. This includes assessing levels of lipid peroxidation, ROS, and Labile Iron Pool (LIP) using the same ferroptosis treatments employed in the previous chapter used to explore cytotoxicity in *Tsc2*-deficient cells and their counterparts. We further wish to investigate the involvement of proteins and genes regulating oxidative stress and iron metabolism in Tsc2 model cells.

Once an optimised combination was determined, the focus of this chapter was to identify the biomarkers of ferroptosis cell death and the mechanism of drug action.

Hypothesis

We hypothesise that ferroptosis regulators and biomarkers levels are altered in *Tsc2* deficient cells relative to their counterparts.

We hypothesize that the observed cell death is ferroptosis, and that this process is dysregulated in Tsc2-deficient cells compared to their wild-type counterparts.

Aims

To establish hypotheses we aimed to:

1. Characterise the biomarkers and regulators of ferroptosis..
2. Determine the role of additional pathways contributing to ferroptosis resistance in *Tsc2*-deficient cells..

4.2 Results

Having determined that ferroptosis was the mode of cell death induced by our treatments, we further confirmed and quantified ferroptosis using the lipid peroxidation biomarker probe C11 BODIPY in conjunction with the ROS probe CM-H_2DCFDA. Gating strategies and representative data for this dual parameter analysis are depicted in Figs 4.1 for Erastin and Fig 4.2 for RSL3. Morphological cell death was observable using forward and side scatter parameters and clearly indicate the expected cytotoxicity observed with dose responses of Erastin and RSL3. Fig 4.1 and Fig 4.2 also indicate the gating strategy for the selection of cells and the exclusion of debris which was basis of the data in the dual parameter plots of ROS levels versus C11 Bodipy peroxidation. These revealed the relative change in the biomarkers upon treatments with ferroptosis inducers. While presented together both ROS and Lipid peroxidation median fluorescence data were analysed separately and referred to below in individual sections.

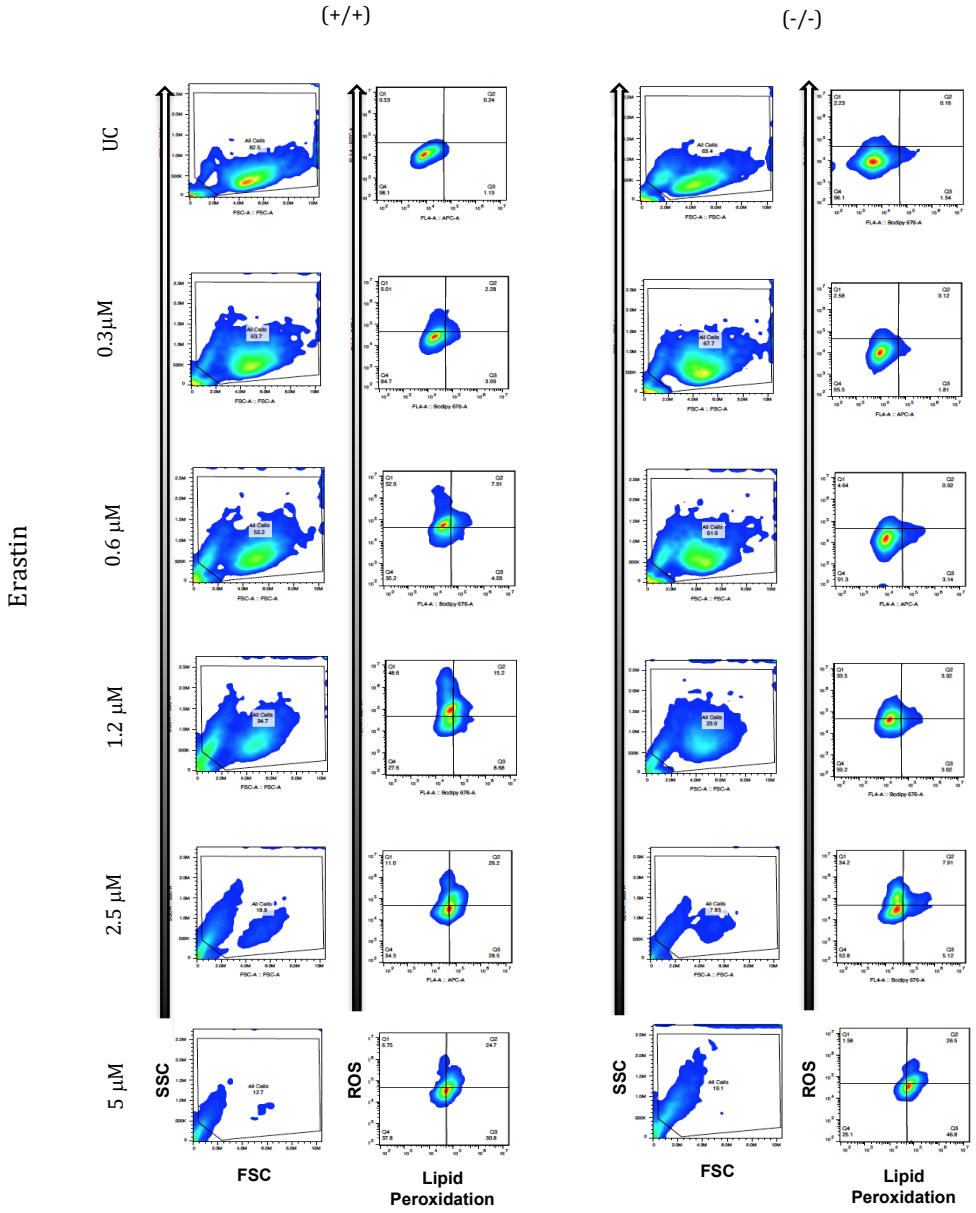

Fig. 4.1 Representative Flow Cytometric Analysis of Erastin-induced Lipid peroxidation and ROS

Representative data of one experiment are depicted for MEF cell lines, (+/+) and (-/-), treated with doses of Erastin for 24h. Forward and side scatter plots are presented in tandem with dual parameter plots of Lipid peroxidation (x-axis; C11 Bodipy 665/676; FL4A; λ_{EX} 633nm & λ_{EM} 675/25nm) versus ROS (y axis; CM-H_2DCFDA; FL1A; λ_{EX} 488nm & λ_{EM} 533/30nm)). The gating strategy involved selecting live and dead cells and excluding cellular debris based on forward and side scatter properties. Untreated controls (NIL) were then used to gate for Lipid peroxidation and ROS baselines.

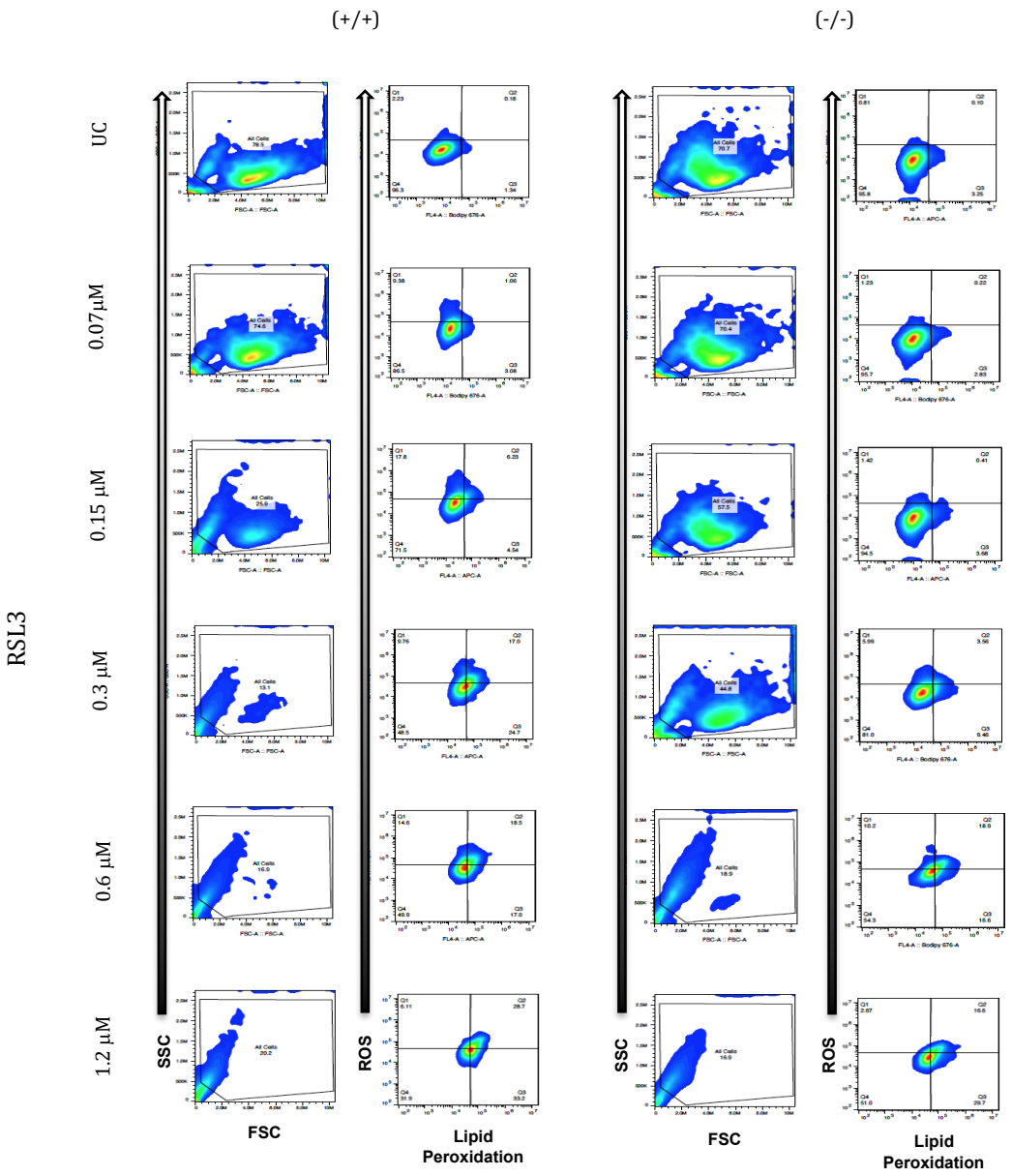

Fig. 4.2 Representative Flow Cytometric Analysis of RSL3-induced Lipid peroxidation and ROS

Representative data of one experiment are depicted for MEF cell lines,(+/+) and (-/-), treated with doses of RSL3 for 24h. Forward and side scatter plots are presented in tandem with dual parameter plots of Lipid peroxidation (x-axis; C11 Bodipy 665/676; FL4A; λ_{EX} 633nm & λ_{EM} 675/25nm) versus ROS (y axis; CM-H_2DCFDA; FL1A; λ_{EX} 488nm & λ_{EM} 533/30nm)). The gating strategy involved selecting live and dead cells and excluding cellular debris based on forward and side scatter properties. Untreated controls (UC) were then used to gate for Lipid peroxidation and ROS baselines.

4.2.1 Differential Induction of Lipid Peroxidation by Erastin and RSL3 in *Tsc2* Cell Line models

Erastin and RSL3 treatments differentially induced dose-dependent lipid peroxidation production over 24 hours in both *Tsc2 (+/+)* and *(−/−)* MEFs (Fig 4.3). Lipid peroxidation levels, measured using C11-BODIPY oxidation, closely paralleled cytotoxicity trends observed using DRAQ7 staining, with *Tsc2+/+* cells exhibiting higher lipid peroxidation compared to *Tsc2−/−* cells across multiple doses of both inducers. These findings indicate that *Tsc2+/+* cells undergo greater oxidative lipid damage in response to Erastin and RSL3.

MEF *(+/+)* cells exhibited significantly higher lipid-peroxidation levels at lower doses of Erastin [1.25 μM ($p<0.05$) and 2.5 μM ($p<0.001$)] compared to MEF *(−/−)* cells which had no significant increase at 1.25 μM but did exhibit a significant difference at 2.5 μM ($p<0.01$); this indicates a greater susceptibility to lipid peroxidation and ferroptosis. Similarly, RSL3 treatment resulted in a dose-dependent increase in lipid-peroxidation levels for *Tsc2* variant MEFs. MEF *(+/+)* cells showed significantly higher lipid-peroxidation levels at lower doses of RSL3 [0.3 μM and 0.6 μM ($p<0.0001$)] compared to MEF *(−/−)* cells which only exhibited significantly increased lipid-peroxidation levels at 0.6 μM ($p<0.0001$) and above.

The differential response to Erastin and RSL3 treatments highlights the distinct sensitivities of *Tsc2 (+/+)* and *Tsc2 (−/−)* cell lines to ferroptosis induction. *Tsc2 (+/+)* cells displayed higher lipid peroxidation levels at lower doses of both Erastin and RSL3, indicating a greater propensity for ferroptosis and cytotoxicity compared to *Tsc2 (−/−)* cells. These findings suggest that *Tsc2* status influences the cellular response to ferroptosis inducers, with Tsc2-deficient cells showing relative resistance, potentially due to an altered redox state.

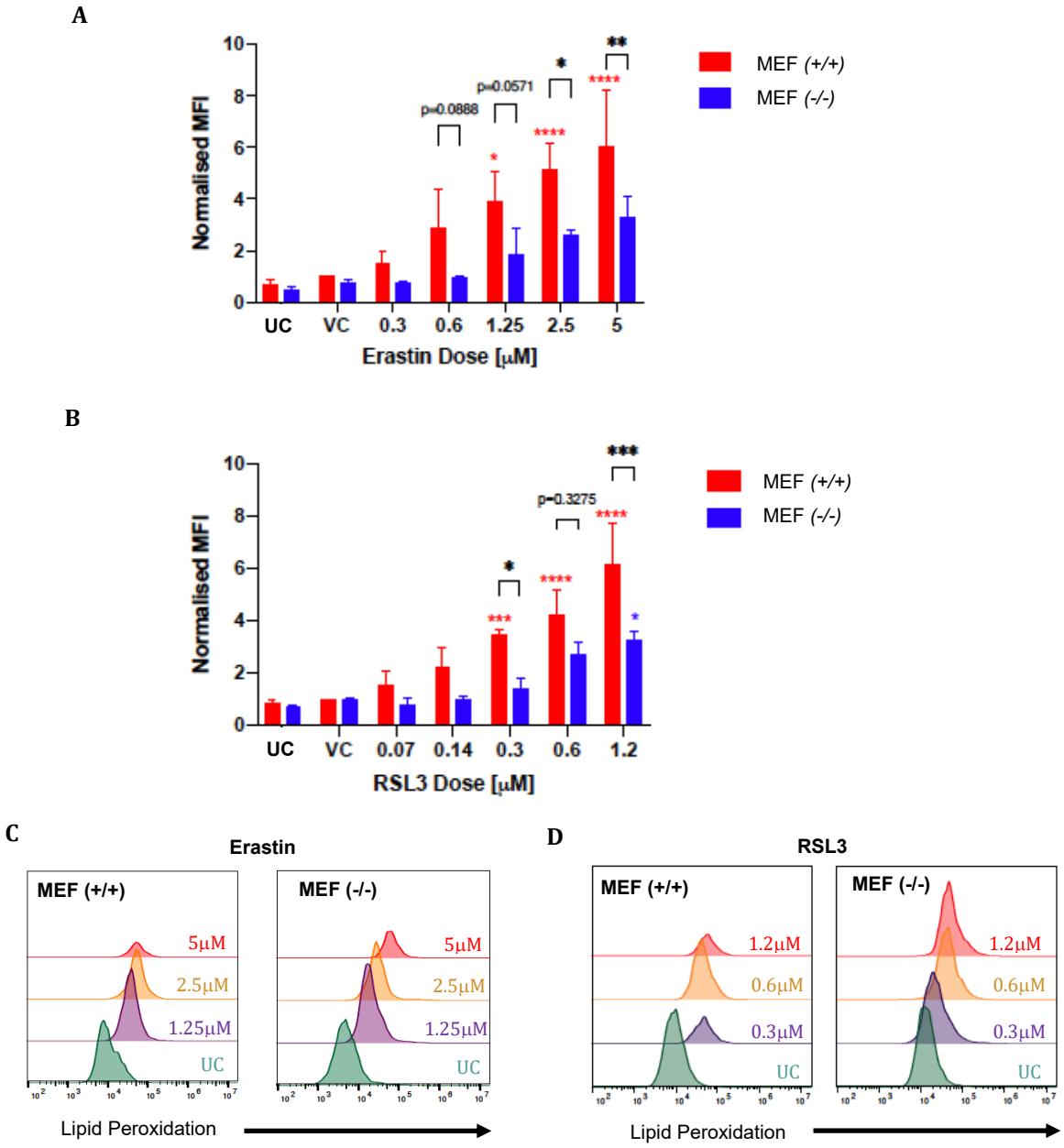

Fig. 4.3 Effect of Ferroptosis inducers Erastin and RSL3 on MEF (+/+) and MEF *(–/–)* levels of lipid peroxidation.

Both *Tsc2+/+* and *Tsc2–/–* MEFs (MEF*+/+ and* MEF *–/–,* respectively*)* seeded at 1x10^5/mL cells in 24 well plates and grown overnight before treatment with the ferroptosis inducers (A) Erastin [5-1.25μM] or (B) RSL-3 [1.2-0.3μM]. Cells were treated for 24h and then stained for ROS (CM-H_2DCFDA; [1μM] and Lipid peroxidation (Bodipy C11 [10μM]) concurrently. Samples were run on a BD Accuri C6 Flow cytometer. (FL1: λ_{Ex} 488nm λ_{Em} 533/30nm [ROS]; FL4: λ_{Ex} 640nm λ_{Em} 670LP* [Lipid Peroxidation (LPX)]). Representative histogram overlays of Lipid peroxidation levels in cells treated with Erastin (C) and RSL-3 (D) are provided. (Data was normalised against vehicle control of MEF (+/+) cells and was analysed by two way ANOVA. Holm-Sidak post hoc analysis was performed to compare cell lines and Tukey's post hoc analysis for dose response differences within a cell line. n=4; *p<0.05; **p<0.01; ***p<0.001; ****p<0.0001). UC= Untreated Control, VC= Vehicle Control.

4.2.2 Differential Induction of Reactive Oxygen Species (ROS) by Erastin and RSL3 in *Tsc2* Cell Line models

While lipid peroxidation accumulation determination using C11 Bodipy yielded straight forward data, concomitant determination of ROS levels using CM-H_2DCFDA in the cell lines at the 24h time point required more insight as the probe did not capture all ROS generated over 24h but instead measured the ROS activity at the 24h timepoint only. After 24 hours of treatment, however, we did observe notable differences in ROS levels across all cell lines (Fig 4.4).

In MEF *(−/−)* cell lines, there was a dose-dependent increase in ROS activity at the 24h time point with Erastin treatment. Significant differences were observed at a dose of 1.2μM and above (Fig 4.4 B). In contrast, MEF (*+/+*) cells exhibited a ROS activity profile that had dose-dependent higher activity up to 1.2μM followed by decreased activity for the remaining two higher doses (Fig 4.4 A). Taken together with the cytotoxicity and lipid peroxidation data this suggests that the kinetics of ferroptosis related ROS activity had already peaked in the ferroptosis sensitive MEF (*+/+*) and that the remaining dying cells were past peak ROS activity.

With RSL3 treatment there was a consistent dose-dependent increase in ROS activity at the 24h time point, however, a significant difference was only attainable for the MEF *(+/+)* cell line at the highest dose of 1.2 μM ($p<0.05$). This reflects a lack of power in the current study with the current number of repeats (n=4). Consistent with ferroptosis resistance the MEF *(−/−)* cells showed little perturbation of ROS activity at 24h with the lower doses of RSL3 compared to the *(+/+)* cell responses.

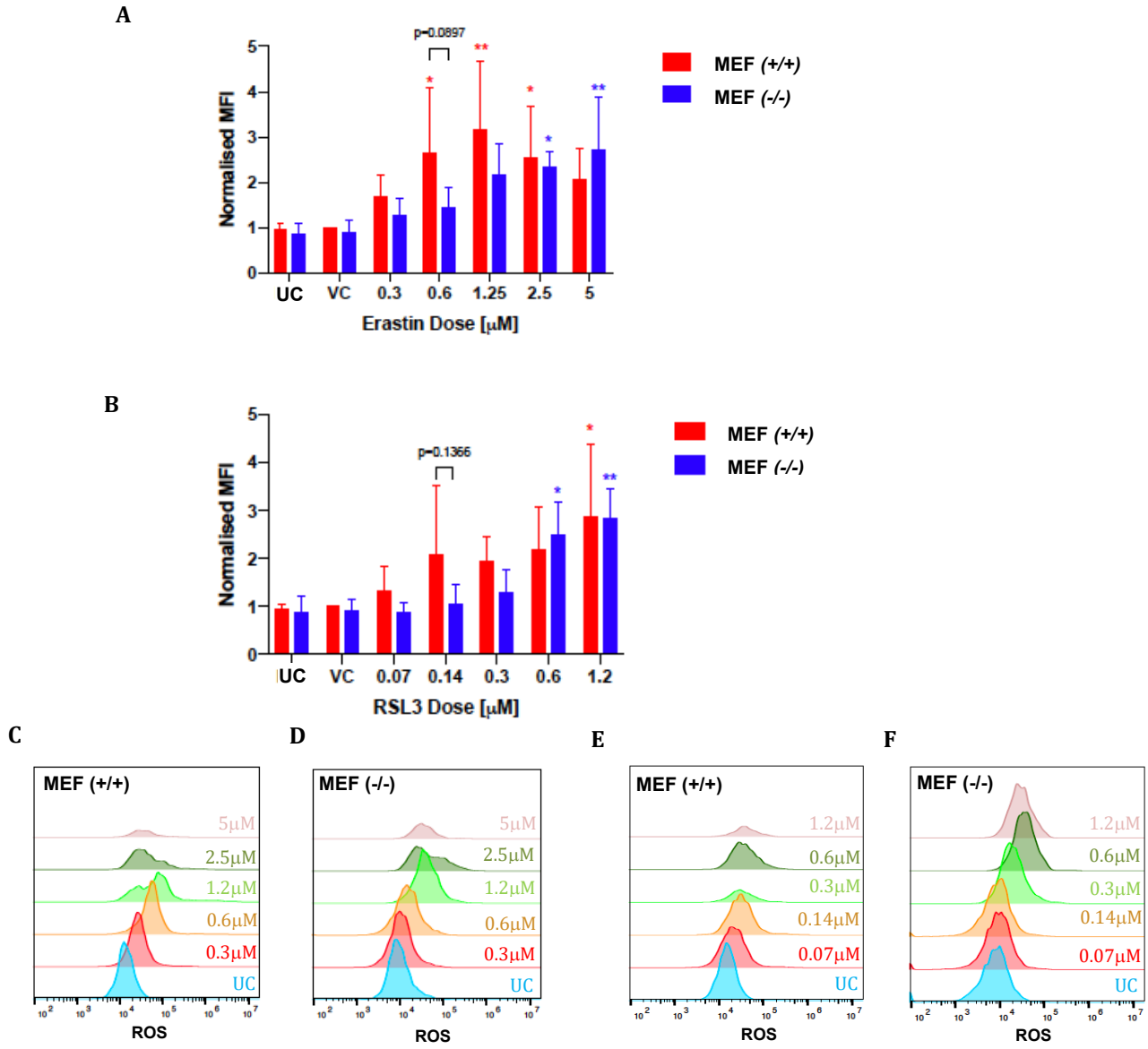

Fig. 4.4 Effect of Erastin and RSL3 treatment on ROS activity in MEF (+/+) and (-/-) cell lines

MEF (+/+) and *(−/−)* cells were treated for 24h with either Erastin or RSL3 dose ranges and then assessed for ROS activity using the probe CM-H_2DCFDA. (A) MEF (+/+) cells depict a dose dependent increase in ROS up to doses of 1.2 μM and thereafter a decrease for the final higher doses. (B) MEF *(−/−)* in contrast show a straightforward increase in ROS activity over the entire dose range. Similarly, for RSL3 both cell lines exhibited a dose-dependent increase in ROS activity at the 24h timepoint but only (+/+) cells (E) reached a statistically significant difference for the highest dose used. Lower doses of RSL3 appear to be less able to induce ROS activity in *(−/−)* cells (F) at 24h relative to the activity observed in (+/+). Representative histogram overlays of ROS fluorescence data for the dose responses are depicted in (C-D) for MEF (+/+) and (G-H) for MEF *(−/−)* cell lines. (Data was analysed by two way ANOVA. Holm-Sidak post hoc analysis was performed to compare cell lines and Tukey's post hoc analysis for dose response differences within a cell line. n=4; *p<0.05; **p<0.01; ***p<0.001; ****p<0.0001). UC= Untreated Control, VC= Vehicle Control.

4.2.3 *Tsc2 (−/−)* cells have elevated levels of GSH

Having established that *Tsc2*-deficient cells are less prone to ROS activation and lipid peroxidation associated with ferroptosis induction, a salient next step was to examine differences in the redox control systems between the two *Tsc2* cell line phenotypes. Specifically, we aimed to determine the differential levels of glutathione (GSH) between the *Tsc2* cell line variants. Glutathione levels were investigated using the GSH Tracer probe (Tocris Ltd), which exhibits increased green fluorescence with higher levels of GSH. Both MEF and ELT3 cells were analysed for GSH content using this probe in conjunction with flow cytometry.

The *(−/−)* ELT3 cells had significantly higher ($p<0.01$) GSH levels compared to the *(+/+)* cells. In contrast, the MEF cell lines exhibited the opposite trend between the *Tsc2* variants, with a significantly higher ($p<0.01$) GSH level in the *Tsc2*(*+/+*) cells. Moreover, the basal levels of GSH of the MEF (+/+) were significantly higher ($p<0.01$) compared to the ELT3(+/+) cell line.

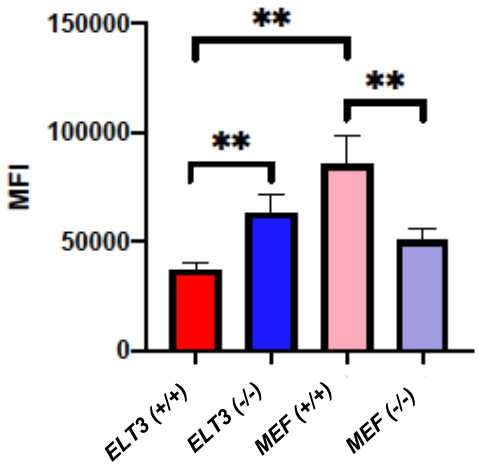

Fig. 4.5 Glutathione levels in *Tsc2* variant cell lines

Basal levels of Glutathione (GSH) in ELT3 *(+/+)* and ELT3 *(−/−)*, and MEF *(+/+)* and MEF *(−/−)* cells were assessed using the fluorescent probe, GSHTracer. Cells were analysed on a BD Accuri C6 flow cytometer and Median Fluorescence Intensity (MFI; FL1: Ex 488nm Em 533/30nm) measured for morphologically viable cells only (based on FSC and SSC). Data was subjected to ordinary one way ANOVA and Holm-Sidak post hoc analysis (ELT3 n=6; MEF n=10; ** $p < 0.01$).

4.2.4 RSL3 treatment showed significantly higher Labile iron pool in ELT3 (+/+) compared to the ELT3 (−/−) cells

The cellular labile iron pool (LIP) is a crucial reservoir of chelatable and redox-active iron, acting as a key intersection in cellular iron metabolism. Hence, we investigated the role of LIP in promoting ferroptosis and elucidated its contribution to ferroptosis susceptibilities between Tsc2 variants. To determine if the availability of cytoplasmic iron (Fe^{2+}) was contributing to ferroptosis susceptibility, we measured the LIP in ELT3 (+/+) and ELT3 *(−/−)* cells using the Calcein AM method in conjunction with an iron chelator. This approach allows for the quantification of the chelatable iron pool within cells. Additionally, cells were treated with RSL3, a known ferroptosis inducer, to assess changes in the iron pool during the ferroptotic process.

The results revealed at baseline (without RSL3 treatment), the LIP levels are relatively low in both ELT3 (+/+) and ELT3 (−/−) cells. However, there was a dose-dependent elevation in the LIP in both ELT3 *(+/+)* and ELT3 *(−/−)* cells following RSL3 treatment. Notably, the LIP was significantly higher at a lower dose in ELT3 *(+/+)* cells compared to ELT3 *(−/−)* cells. This differential increase in the LIP suggests that ELT3 *(+/+)* cells have a higher propensity to accumulate redox-active iron, which may enhance their susceptibility to ferroptosis induced by RSL3.

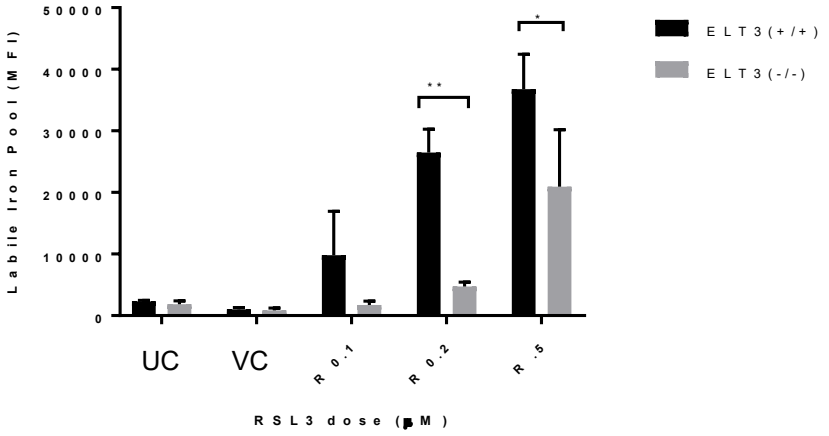

Fig. 4.6 Determination the Labile iron pool (LIP) in *Tsc2(+/+)* and *Tsc2(−/−)* cell lines

The elevated LIP in ELT3 *(+/+)* cells upon RSL3 treatment indicates that these cells are more prone to iron-catalysed lipid peroxidation, a hallmark of ferroptosis. In contrast, the lower LIP in ELT3 *(−/−)* cells may contribute to their relative resistance to ferroptosis under the same conditions. (Data was analysed by ordinary one way ANOVA and Holm-Sidak post hoc analysis was performed to compare cell lines. (n=3); *p<0.05; **p<0.01) UC= Untreated Control, VC= Vehicle Control.

4.2.5 Iron and lipid peroxidation-related antioxidant regulatory proteins expression were elevated on Tsc2 restored cells compared to the wild type

As previously discussed, ferroptosis is a distinct form of regulated cell death characterized by iron-dependent lipid peroxidation. Our earlier data confirmed that treatment with RSL3, a known ferroptosis inducer, resulted in a significantly higher labile iron pool (LIP) in ELT3 (*+/+*) cells compared to ELT3 *(−/−)* cells. This observation suggested a potential link between iron metabolism and the susceptibility to ferroptosis. To further explore the role of iron in the observed differences in cell death between the (*+/+*) and (−/−) MEF cells, we measured the expression levels of key molecules involved in iron and lipid metabolism in ferroptosis regulation, including HMOX1, TfR1 and GPX4.

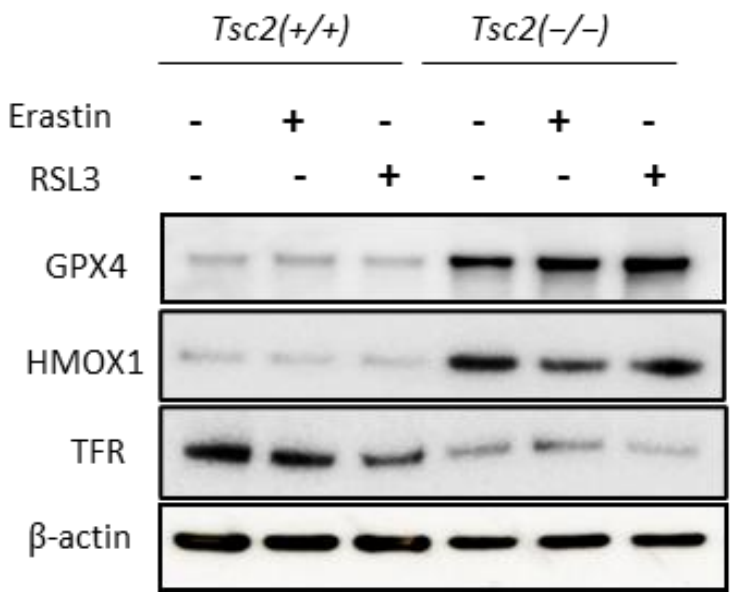

Fig. 4.7 Loss of *Tsc2* in MEF cell lines leads to elevated expression of antioxidant proteins and reduced expression of iron-related proteins

MEF cells lacking *Tsc2 (−/−)* or with re-expressed wild type *Tsc2 (+/+)*, were cultured overnight and treated with respective IC50 doses of Erastin (*Tsc2 (−/−)* = 0.595μM; *Tsc2 (+/+)* = 0.988μM) or RSL3 (*Tsc2 (−/−)* = 0.142μM; *Tsc2 (+/+)* = 0.281μM)) for 24 hours. Western blot analysis of lysates shows distinct differences between the cell lines with GPX4 and HMOX1 elevated but transferrin receptor decreased in *(−/−)* cells. β-actin was used as a loading control. Through western blotting lysates were assayed for target protein expression (n=1)

Western blot analysis was performed to assess the expression levels of TfR1, HMOX1, and GPX4 in MEF (+/+) and MEF (−/−) cell lines (Fig. 4.7).

HMOX1 protein levels appeared elevated in MEF (−/−) cells compared to MEF (+/+) cells. In contrast, TfR1 expression was higher in MEF (+/+) cells relative to MEF (−/−) cells. TfR1 is involved in the import of transferrin-bound iron, while HMOX1 contributes to the degradation of haem and release of iron. Although statistical analysis was not possible due to the single biological replicate, these observations suggest differences in iron-related protein expression between the genotypes.

GPX4 expression, a key regulator of lipid peroxidation, was also assessed and found to be elevated in MEF (−/−) cells compared to MEF (+/+) cells. This may reflect enhanced antioxidant capacity in the Tsc2-deficient background.

4.3 Discussion

In the previous chapter, data from cell death inhibition assays established that the mode of observed cell death in the Tsc2 edited cell line model was ferroptosis. Therefore, in this chapter, we investigated the biomarkers of ferroptosis to elucidate the mechanism of action of the cell death in *Tsc2*-cell line model. Ferroptosis is described as a lipid-peroxidation process in the cell membrane facilitated by intracellular iron-driven ROS (Dixon and Stockwell, 2014). Hence, we first employed specific assays to quantify lipid-peroxidation and ROS as the biomarkers of ferroptosis.

Lipid-Peroxidation studies using C11 BODIPY (Fig 4.3) exhibited the same trend of dose response that we observed in cytotoxicity studies. In the MEF cell lines, the *Tsc2(+/+)* had greater levels of C11 BODIPY peroxidation relative to the *Tsc2(−/−)* cells. Despite a low power of n=4, statistical comparison of the cell lines at the same erastin doses revealed significant differences at 5 and 2.5μM ($p<0.01$ and $p<0.05$, respectively). At 0.6 and 1.25μM the p values were 0.0888 and 0.0571, respectively, suggesting that improved power would also yield significant differences over these doses. RSL3 exhibited a similar trend with significant differences between cell line levels of lipid peroxidation observed at 0.3 and 1.2μM doses ($p<0.05$ and $p<0.001$, respectively).

For both RSL3 and erastin the ferroptosis sensitive MEF *(+/+)* exhibited significant differences from control for lipid peroxidation levels. The lowest dose attaining significant difference was 1,25μM for Erastin ($p<0.05$) and 0.3μM for RSL3 ($p<0.001$). MEF *(−/−)*, though a trend of rising levels of lipid peroxidation was visible in the data, had no statistically different levels of response over the dose range of erastin treatment and only the highest 1.2μM dose of RSL3 yield a difference relative to vehicle control ($p<0.05$). With respect to these data we have to consider both the low power of the study at n=4 as well as the fact that the lower level of lipid

peroxidation are consistent with a ferroptosis resistant cell line and that smaller levels of difference would be expected between doses in these studies and, thus, require increased power to detect those smaller differences, if they exist.

Lipid peroxidation analyses were concomitant with ROS studies using the probe, CM-H_2DCFDA. It is important to note that the data provided in this thesis were a snapshot of ROS levels at the 24h time point. Unlike lipid peroxidation, which is a relatively stable alteration dependent on ROS activity and can accumulate over the 24h period, ROS levels provide a current activity snapshot. This is crucial for data interpretation since ROS kinetics can vary over the 24h period between different doses of ferroptosis inducers and potentially between different cell lines. For MEF *(−/−)* cells both RSL3 and erastin treatment showed a visually identifiable dose-dependent increase in ROS levels at the 24h time point, indicating a straightforward increase in ROS with treatment. Significant differences were attained at 2.5 and 5 μM erastin ($p<0.05$ and $p<0.01$, respectively) and 0.6 and 1.2μM RSL3. MEF *(+/+)*, however, showed higher levels of ROS at mid range doses of 0.6-2.5 μM erastin ($p<0.05$ - $p<0.01$, over the range) possibly reflecting the kinetics of ROS levels at the 24h time point. Given the transient nature of ROS, earlier sampling may be required to capture peak ROS levels accurately. For RSL3 only the highest 1.2 μM dose yielded a significant different level of ROS ($p<0.05$). Again, both the nature of ROS kinetics and the power of the study need to be enhanced to better interpret this data. Direct cell line comparison for responses to different doses of the ferroptosis inducers did identify near significant differences. Erastin at 0.6 μM showed a $p=0.0897$ and RSL3 at 0.14 μM a $p=0.1366$. These p values and the associated mid-range doses suggest that more indepth analysis of ROS kinetics over the dose range with an increased power of the study ($n>4$) would better identify differences between the cell lines.

Iron plays a central role in ferroptosis through the generation of ROS via Fenton reactions. Elevated levels of LIP can enhance ROS production through Fenton reactions, promoting lipid peroxidation and ferroptotic cell death. These reactions produce highly reactive hydroxyl radicals (·OH) from hydrogen peroxide (H_2O_2), contributing to oxidative stress and lipid peroxidation (Chen et al., 2020b, Nishizawa et al., 2020). Labile iron pool (LIP) analysis revealed higher iron levels in ELT3(*+/+*) cells than in ELT3(−/−) cells following RSL3 treatment, suggesting that Tsc2 expression may enhance susceptibility to ferroptosis by promoting iron accumulation. The dose-dependent increase in LIP observed in ELT3(*+/+*) cells further supports the link between intracellular iron and ferroptotic activity. Previous results using the iron chelator DFP (Fig. 3.5) also confirmed the role of iron in ferroptosis across both MEF and ELT3 *Tsc2* model cell lines.

Western blot analysis in MEF cells revealed elevated TfR1 levels in Tsc2(*+/+*) cells and higher GPX4 and HMOX1 expression in Tsc2(−/−) cells. TfR1 mediates iron uptake and contributes to intracellular iron accumulation. Elevated TfR1 in Tsc2(+/+) cells is consistent with increased LIP in ELT3(*+/+*) cells and may explain their greater susceptibility to ferroptosis. Conversely, the higher levels of GPX4 and HMOX1 in Tsc2(−/−) cells suggest enhanced antioxidant and iron-recycling mechanisms, possibly contributing to ferroptosis resistance. Interestingly, Tsc2-deficient cells appeared more sensitive to DFP despite their lower LIP. This could be due to upregulation of antioxidant regulators downstream of mTORC1(Fraser et al., 2011), making the available iron more functionally significant despite being less abundant overall. Crucially, for this thesis the data ratifies our hypothesis that Tsc2 deletion manifests drug resistance through ferroptosis insensitivity and that this arises through manipulations of the labile iron pool, which are lower than their Tsc2 (*+/+*) equivalent cell lines. This suggests, cell death observed in Tsc2 expressing MEFs and ELT3s in chapter 3 (Fig. 3.1 and 3.2) distinctly demonstrate characteristics of ferroptosis cell death.

Glutathione (GSH), a key antioxidant composed of glutamine, cysteine, and glycine, plays a central role in maintaining redox homeostasis and regulating ROS levels. Because ROS are tightly controlled due to their role in both cellular signalling and oxidative damage, GSH is critical in limiting ROS accumulation and, by extension, ferroptosis (Ashraf et al., 2020)

Our data revealed differences in GSH levels between cell lines: Tsc2*(–/–)* ELT3 cells exhibited higher GSH levels relative to *(+/+)*($p < 0.01$), consistent with ferroptosis resistance, while MEF*(–/–)* cells showed lower GSH relative to *(+/+)* cells ($p < 0.01$), despite their reduced susceptibility to ferroptosis. It is also noteworthy that MEF *(+/+)* had almost double the levels of GSH relative to ELT3 *(+/+)* cells ($p < 0.01$). This suggests that GSH alone may not determine ferroptosis sensitivity and highlights the need to consider additional redox-regulatory mechanisms.

Understanding the differential GSH pattern between the MEF and ELT3 cell lines for the single *Tsc*2 variation could again be explained by the background expression variation between the cell lines and how these patterns are perturbed by the *Tsc*2 expression or absence. Differences in how GSH varies between (+/+) and *(–/–)* cells in the individual cell lines would similarly be explained by this genotype/phenotype background.

GPX4 is one of the key enzymes capable of reducing lipid hydroperoxides within cellular membranes, and its activity is strictly dependent on GSH. The GSH-GPX4 axis is thus central to preventing ferroptosis. When GSH levels are sufficient, GPX4 can effectively reduce lipid hydroperoxides, preventing the accumulation of toxic lipid ROS. However, when GSH is depleted, GPX4 activity declines, leading to the build-up of lipid peroxides and the onset of ferroptosis (Zou et al., 2019, Liu et al., 2020).

GPX4 is dependent on GSH to reduce lipid hydroperoxides and prevent ferroptosis. Our data showed increased GPX4 expression in both *Tsc2* deficient MEF and ELT3 cell lines. This pattern

was confirmed at both the protein level (Western blot) and mRNA level (hypoxia studies). Notably, hypoxia alone did not upregulate GPX4, reinforcing the role of Tsc2 loss in its regulation. These results support the hypothesis that elevated GPX4 contributes to ferroptosis resistance in *Tsc2*-deficient cell.

Moreover, HMOX1 is an enzyme that catalyses the degradation of haem to biliverdin, free iron, and carbon monoxide, which suggests an adaptive response to manage haem levels and possibly mitigate oxidative stress. The elevated HMOX1 levels in the *(−/−)* cells indicate an increased utilization of haeme-derived iron, which might be a compensatory mechanism for the reduced labile iron pool observed in these cells. Although mTOR activation has been linked to HMOX1, this relationship appears to be indirect. In a TSC mouse model, only a subset of cells with activated mTOR also exhibited elevated HMOX1 (Wang et al., 2023a), suggesting additional regulatory mechanisms—possibly involving miR155 and NRF2 activation.

In summary, this study characterised key ferroptosis biomarkers, including lipid peroxidation, ROS, iron levels, GSH, GPX4, and HMOX1; and revealed their modulation by Tsc2 status. These findings support the hypothesis that *Tsc2* loss confers resistance to ferroptosis through reduced labile iron and enhanced antioxidant defences. While results remain preliminary, they provide mechanistic insight into genotype-dependent ferroptosis susceptibility. Notably, the combination of increased TfR1, LIP, and ROS in *Tsc2(+/+)* cells, alongside upregulated GPX4 and HMOX1 in *Tsc2(−/−)* cells, underscores the complex interplay between iron metabolism and redox regulation in ferroptosis. Multiple replicates, additional validation techniques and compensatory pathways investigations are warranted to confirm these observations and the role of TSC2 deficiency in-ferroptosis regulation.

Chapter 5 Determination of the role of antioxidant pathways in ferroptosis

5.1 Introduction

In cancer cells, metabolic reprogramming and dysregulated signalling pathways can lead to increased ROS production and concomitant upregulation of cellular antioxidants to counteract excessive ROS and maintain redox homeostasis in the malignant cells (Zhao et al., 2023c). Consistent with this observation, multiple studies have indicated that the loss of either TSC1 or TSC2 results in heightened oxidative stress. For instance, (Chen et al., 2008) demonstrated that the deletion of *TSC1* in hematopoietic stem cells led to elevated levels of reactive oxygen species (ROS) and mitochondrial biogenesis. Similarly, heightened oxidative stress has been documented in cells lacking *Tsc2*, accompanied by an increase in the levels of glutathione; a pivotal endogenous antioxidant (Inoki et al., 2005).

Initially, we hypothesised that ferroptosis resistance in TSC2-deficient cells was primarily driven by hyperactivation of the mTORC1 pathway, a known downstream target of TSC2. However, our cytotoxicity data (Fig. 3.7) showed that treatment with Rapamycin, an mTORC1 inhibitor, did not significantly alter the ferroptosis sensitivity of Tsc2−/− cells. This suggested that other mechanisms, independent of mTORC1 activity, may contribute to the observed resistance to ferroptosis.

Cancer cells frequently exploit alternative antioxidant pathways to counteract oxidative stress, evade ferroptosis, and resist therapy. One such pathway is the system Xc^-–GSH–GPX4 axis, which we identified in the previous chapter as the central defence mechanism against ferroptosis in our TSC2 cell line models. However, several additional antioxidant systems, such

as, NRF2, FSP1–CoQ10, and GCH1–BH4 pathways have also been shown to modulate ferroptosis sensitivity and may be activated in a context-dependent manner.

Recent studies have highlighted that loss of Tsc2 can dysregulate antioxidant signalling networks beyond mTORC1, particularly by promoting ROS accumulation and engaging compensatory antioxidant defences. Among these, the NRF2 pathway plays a crucial role in regulating redox balance and cellular stress responses. NRF2 is a transcription factor that induces the expression of a range of cytoprotective genes, many of which are involved in antioxidant defence and iron metabolism. Its activation has been reported in Tsc2-deficient cells and may contribute to ferroptosis resistance through enhanced ROS detoxification and suppression of lipid peroxidation (Chio et al., 2016).

Given these observations, in this chapter we sought to investigate the role of NRF2 activation in promoting ferroptosis resistance in Tsc2-deficient cell lines. We assess the impact of pharmacological NRF2 inhibition using Trigonelline, both alone and in combination with ferroptosis inducers, to determine whether targeting this pathway can restore ferroptotic sensitivity Additionally, we aim to evaluate the expression of relevant proteins and genes, as well as the localization of NRF2 in the Tsc2 cell line models.

Finally, studies suggest that FSP1 functions independently of the GSH–GPX4 axis and acts in parallel with NRF2 to suppress lipid peroxidation (Gao et al., 2021a, Li et al., 2023). To investigate its potential role in ferroptosis sensitivity in Tsc2-deficient cells, we asses FSP1 expression and examined the effects of its pharmacological inhibition using iFSP1. While not exhaustive, these studies aim to establish a foundation for understanding how NRF2 and related antioxidant pathways contribute to ferroptosis resistance in Tsc2-deficient cancers.

5.1.3 Hypothesis

We hypothesise that the activation of NRF2 antioxidant pathway within *Tsc2* deficient cells has an impact on ferroptosis resistance.

5.2 Results

5.2.1 NRF2 inhibition through Trigonelline prevented Erastin and RSL3 mediated cell death resistance in Tsc2 deficient cells

To determine the effect of NRF2 inhibition in Tsc2 deficient cells we employed trigonelline, the pharmacological inhibitor of NRF2, in conjunction with exposure to IC_{50} values of ferroptosis inducers established in *Tsc2* re-expressing cells (+/+). In MEF cells the direct effect of NRF2 inhibition alone on viability was determined and found to be negligible (Fig 5.1 A). Subsequently, we employed a combined treatment of the IC50 dose of ferroptosis inducer, Erastin, established in MEF (+/+) cells together with the trigonelline dose range (Fig 5.1 B). As expected, the IC50 dose for (+/+) cells only managed approximately 30% loss of viability in the (-/-) cells when used alone. Studies have previously used trigonelline at concentrations ranging from 100 μM to 300 μM (Shin et al., 2018, Wang et al., 2024a) In our study, exposure to 800 μM trigonelline noticeably reduced cell viability, bringing it down to approximately 50%, which is comparable to the viability of Tsc2+/+ cells at their IC50 dose. Although 400 μM trigonelline also showed a reduction in viability, the effect was less pronounced. Based on these observations, we selected 500 μM as the working concentration for subsequent experiments.

(A) (B)

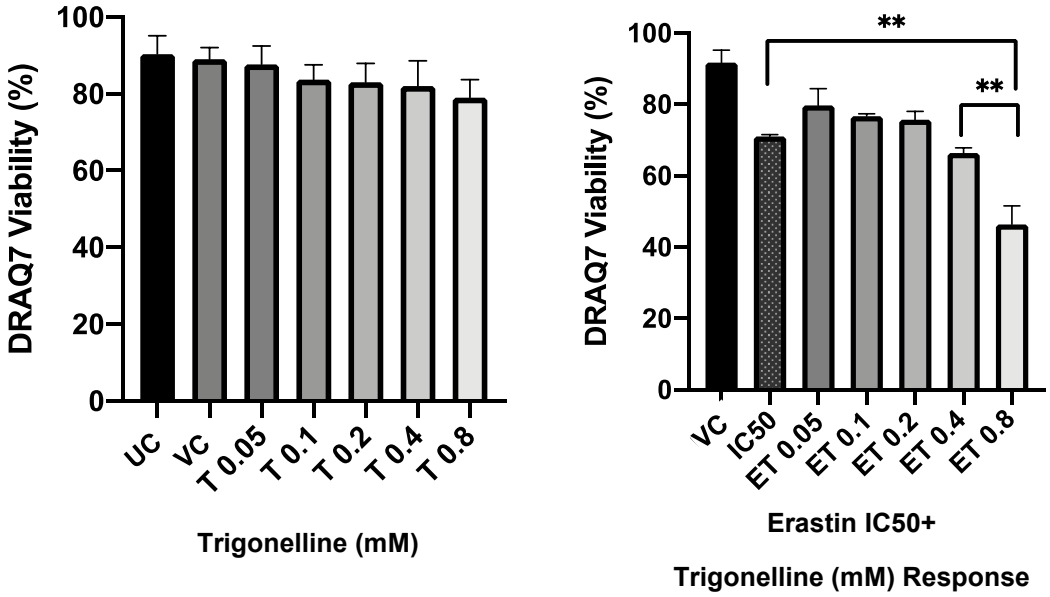

Fig. 5.1 Effect of NRF2 inhibition on Erastin sensitivity in MEF (-/-)

A dose range of the NRF2 inhibitor Trigonelline was applied to MEF (-/-) cells to ascertain the cytotoxic effects of the pharmacological inhibitor alone (A). In the absence of a detectable effect trigonelline was then applied in conjunction with the IC_{50} of Erastin previously established in MEF (+/+) [0.595μM] to ascertain if inhibition affected sensitivity to ferroptosis induction. Increased ferroptosis was observed beyond the 400μM dose of Trigonelline with the IC_{50} of Erastin. (Data was analysed by ordinary one way ANOVA and Tukey's post hoc analysis. n=4; *p<0.05; **p<0.01; ***p<0.001; ****p<0.0001). T denotes trigonelline & ET denotes Erastin IC_{50} + trigonelline. UC= Untreated Control, VC= Vehicle Control.

ELT3 cells were assessed for the impact of NRF inhibition using exposure to dose ranges of the ferroptosis inducers Erastin and RSL3 with or without concomitant treatment with trigonelline at 500μM (Fig 5.2). In both cases the NRF2 inhibitor resulted in increased sensitivity to ferroptosis induction with significant differences observed at the 3.7μM Erastin dose and

(A) (B)

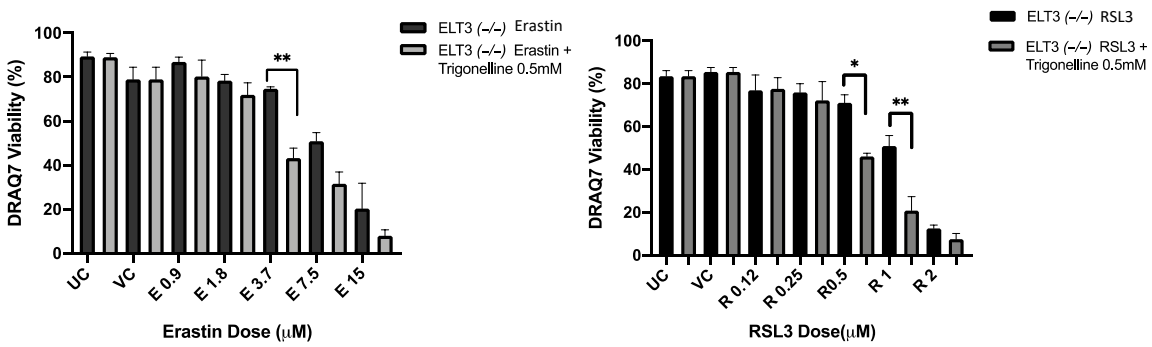

Fig. 5.2 Effect of combined Ferroptosis induction and NRF2 inhibition on ELT3 (+/+) and ELT3(−/−) viability

DRAQ7 flow cytometry assay determined the effects of (A) Erastin [15-0.5μM] or (B) RSL3 [2-0.12μM] on cell viability after 24 h treatment in combination with Trigonelline [500μM]. ELT3(+/+) and *(−/−)* cells were seeded at $1x10^5$/mL in 24 well plates (500 μL /well). Cells were incubated overnight and then treated with ferroptosis inducers, with and without Trigonelline, for a further 24h at 37°C/5% CO_2/humidified air. Statistically significant differences in viability between treatments with and without Trigonelline were identified for both Erastin and RSL3 treatments (Data was analysed by ordinary one way ANOVA and Tukey's post hoc analysis. n=3; *p<0.05; **p<0.01; ***p<0.001; ****p<0.0001). UC= Untreated Control, VC= Vehicle Control.

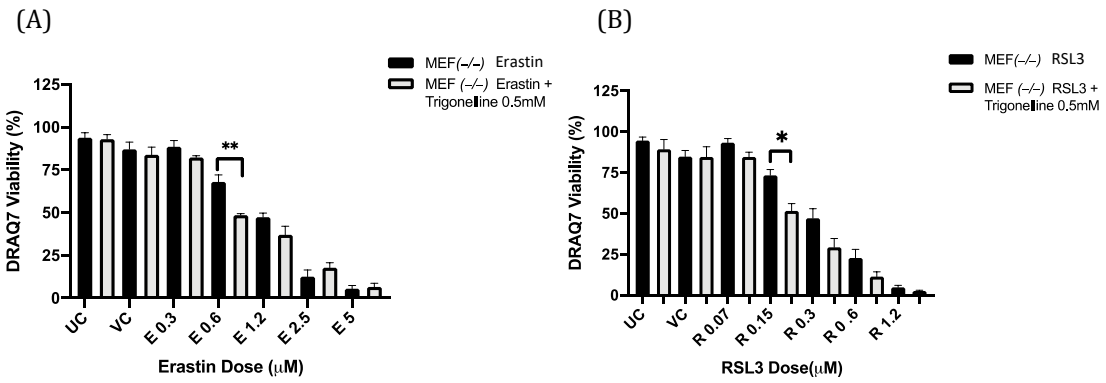

Fig. 5.3 Effect of combined Ferroptosis induction and NRF2 inhibition on MEF (+/+) and MEF(−/−) viability

DRAQ7 flow cytometry assay determined the effects of (A) Erastin [15-0.9μM] or (B) RSL3 [2-0.12μM] on cell viability after 24 h treatment in combination with Trigonelline [500μM]. MEF (+/+) and (−/−) cells were seeded at $1x10^5$/mL in 24 well plates (500 μL/well). Cells were incubated overnight and then treated with ferroptosis inducers, with and without Trigonelline, for a further 24h at 37°C/5% CO_2/humidified air. Statistically significant differences in viability between treatments with and without Trigonelline were identified for both Erastin and RSL3 treatments. (Data was analysed by ordinary one way ANOVA and Tukey's post hoc analysis. n=3; *p<0.05; **p<0.01; ***p<0.001; ****p<0.0001). UC= Untreated Control, VC= Vehicle Control.

TABLE 5.1 IC50 DETERMINATION FOR ERASTIN AND RSL3 IN COMBINATION WITH TRIGONELLINE REVEALED SIGNIFICANTLY LOWER VALUES IN TSC2 (−/−) CELLS COMPARED TO THE SINGLE TREATMENT

Treatment	IC50 [μM]	Treatment	IC50 [μM]
MEF *(−/−)* E sing	0.988	ELT3 *(−/−)* E sing	8.444
MEF *(−/−)* E+T comb	0.720	ELT3 *(−/−)* E+T comb	4.566
MEF *(−/−)* R sing	0.281	ELT3 *(−/−)* R sing	0.855
MEF *(−/−)* R+T comb	0.165	ELT3 *(−/−)* R+T comb	0.463

5.2.2 Trigonelline Combined with Erastin or RSL3 Increases Lipid Peroxidation in Tsc2-Deficient Cells

Having established that Nrf2 inhibition with trigonelline sensitized both ELT3 and MEF Tsc2-deficient cell lines to ferroptosis induction, we next sought to determine the direct impact on ROS-associated lipid peroxidation levels during ferroptosis induction. Tsc2-deficient MEFs were exposed to Erastin and RSL3, either alone or in combination with trigonelline (Fig. 5.4). Elevated levels of lipid peroxidation were observed in the Erastin and trigonelline combination-treated cells, indicating that Nrf2 inhibition altered the lipid peroxidation sensitivity of the Tsc2-deficient cells. Specifically, lower doses of both drugs achieved a significant difference from uninhibited controls.

Tsc2-deficient MEF cells exhibited significantly higher lipid peroxidation levels at lower doses of Erastin [1.25 μM ($p<0.05$) and 2.5 μM ($p<0.001$)] when treated with trigonelline compared to cells treated with Erastin alone. This indicates a greater susceptibility to ferroptosis through increased lipid peroxidation levels. Similarly, RSL3 treatment in MEF (−/−) cells only exhibited significantly increased lipid peroxidation levels at 0.6 μM ($p<0.0001$) and above. RSL3 treatment in combination with trigonelline showed a similar increase at a lower dose in the same cells.

These findings suggest that the ferroptosis resistance observed in Tsc2-deficient cells is linked to Nrf2 activation. Trigonelline-mediated inhibition of Nrf2 sensitizes these cells to ferroptosis by enhancing lipid peroxidation at lower doses of ferroptosis inducers.

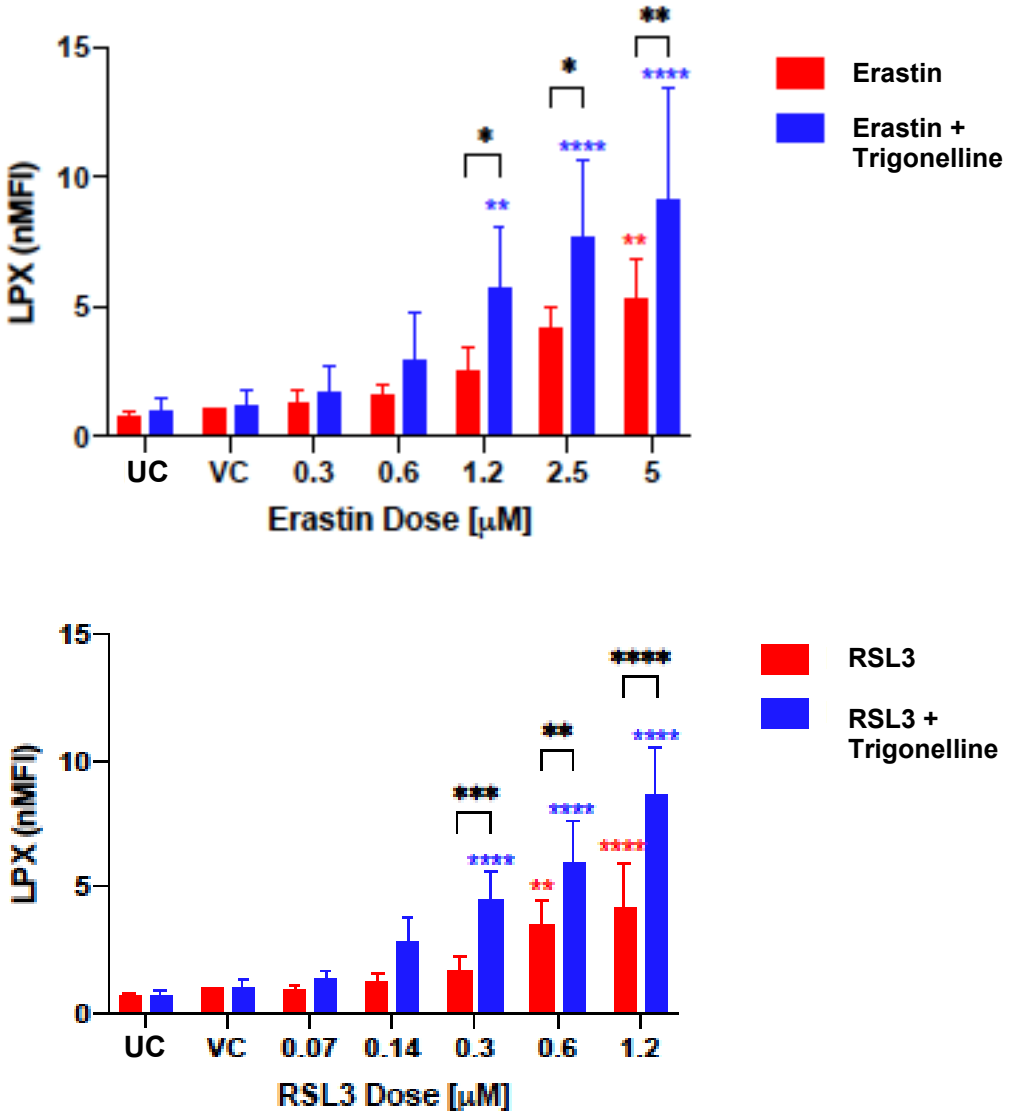

Fig. 5.4 Effect of NRF2 inhibitors on the levels of lipid peroxidation in MEF *Tsc2* deficient cells

Tsc2 deficient MEF (−/−) cells were seeded at 1x10^5/mL in 24 well plates and grown overnight before treatment with the ferroptosis inducers (A) Erastin (E) [5-0.3μM] or (B) RSL-3 (R) [1.2-0.07μM]; both single or in combination with in the NRF2 inhibitor, Trigonelline [0.5mM]. Cells were treated for 24h and then stained for Lipid peroxidation (Bodipy C11 [10μM]). Samples were run on a BD Accuri C6 Flow cytometer. (FL4: Ex 640nm Em 670LP* [Lipid Peroxidation]; (Data was analysed by two way ANOVA. Holm-Sidak post hoc analysis was performed to compare cell lines and Tukey's post hoc analysis for dose response differences within a cell line. n=4; *p<0.05; **p<0.01; ***p<0.001; ****p<0.0001). UC= Untreated Control, VC= Vehicle Control.

5.2.3 Differential Nuclear Translocation of NRF2 in Tsc2 model lines

Since our cytotoxicity and Lipid peroxidation data suggested NRF2 antioxidant pathway could be a factor conferring resistance to ferroptosis through diminishing available ROS within the cells, we employed immunocytochemistry to determine nrf2 nuclear translocation at 6h post treatment with IC50 values of ferroptosis inducer, RSL3. Untreated ELT3 *(–/–)* cells exhibited greater NRF2 expression relative to the (+/+) cells suggesting that this could represent a relatively increased antioxidant protective level in the *(–/–)* phenotype (Fig 5.5). This expression was predominantly cytoplasmic for both cell lines. Treatment with RSL3 resulted in a distinct nuclear translocation of NRF2 in the (-/-) cells with clear overlap between DAPI stained nuclei and NRF2 fluorescence and only some cytoplasmic staining remaining. ELT3 (+/+) cells retained their cytoplasmic staining at 6h post RSL3 treatment exhibiting little nuclear translocation.

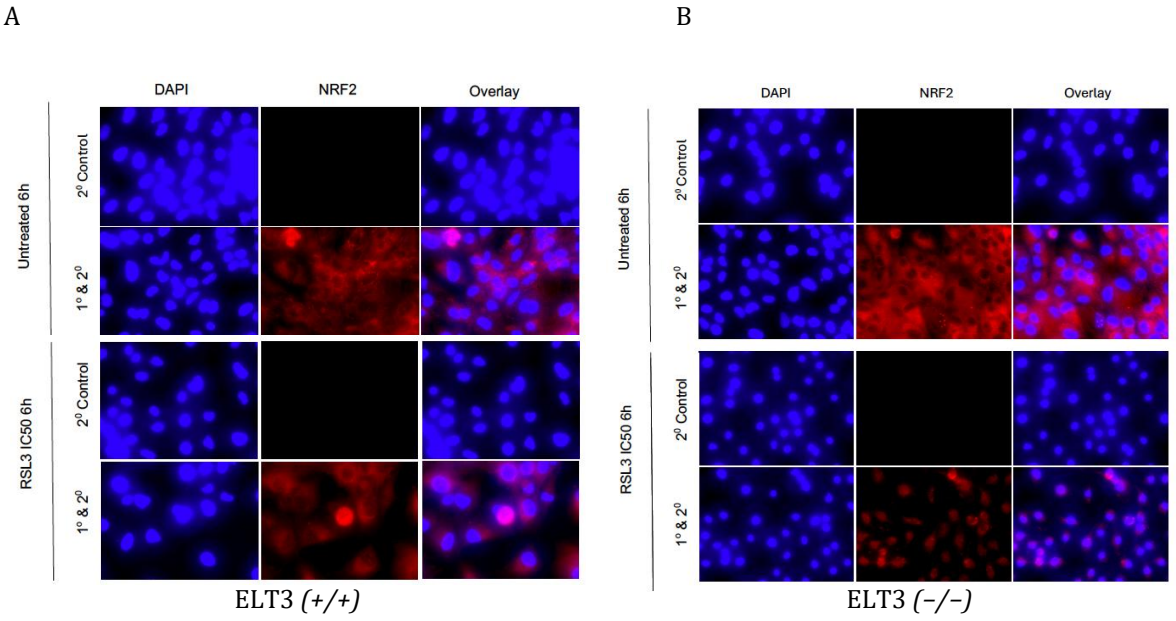

Fig. 5.5 NRF2 nuclear translocation post-ferroptosis induction.

ELT3 *(+/+)* and *(−/−)* cells were grown in 24 well plates containing sterile glass coverslips. Cells were left untreated or exposed to respective IC_{50} doses of RSL3 for each cell line and at 6h glass coverslips were removed and processed for immunocytochemistry to detect NRF2 using a 4% paraformaldehyde fixation and glycine quenching method. DAPI stained nuclei appear blue and in red you can observe the NRF2 staining which was achieved with a polyclonal anti-rat NRF2 antibody and a donkey anti-rat secondary conjugated to Alexafluor 647. Images were captured on a Leica DMII6000b Microscope and show separate capture of DAPI and NRF2 as well as overlays. All images were captured at the same settings ensuring that direct comparisons could be made and secondary antibody staining in the absence of the primary NRF2 antibody showed no non-specific binding. Untreated cells exhibit diffuse cytoplasmic staining of NRF2 in both cell lines with nuclei distinct by the absence of staining. *(−/−)* cells were brighter than (*+/+*) cells, indicating more NRF2 expression. At 6h post treatment with RSL3 *(−/−)* cells manifest nuclear translocation of NRF2 with staining coincident with DAPI staining. *(+/+)* exhibited some cells with nuclear translocation but most cells retained diffuse cytoplasmic staining. Image inspection and processing was conducted using Leica Application Suite for Windows 7, (Leica Biosystems; Wetzlar, Germany) and Image J 1.53a (National Institutes of Health; Maryland, USA).

5.2.4 Loss of Tsc2, but not hypoxia, elevates NRF2 mRNA expression

Hypoxia has been shown to elevate NRF2 target gene expression in various cancer cell lines, including lung and breast cancer (Kim et al., 2007; Syu et al., 2016). In both colon and breast cancer cells, silencing NRF2 suppressed the accumulation of HIF-1α, even under hypoxic conditions (Kim et al., 2011c; Lee et al., 2019). Recent findings reveal that NRF2 (NFE2L2) mRNA expression is significantly elevated upon the loss of Tsc2, regardless of oxygen availability, with a notable fold change (FC) in Tsc2-deficient cells. Specifically, in acute myeloid leukaemia (AML) Tsc2 deficient (−/−) cells, NFE2L2 mRNA expression shows a substantial increase compared to Tsc2 re-expressed (+/+) cells, reaching a maximum fold change (FC=3.22, p=0.0002) under hypoxic conditions (Figure 5.6). Interestingly, hypoxia itself did not significantly alter NFE2L2 expression in either Tsc2-deficient or Tsc2 RE AML cells, suggesting that the loss of Tsc2 is a more critical factor in modulating NRF2 expression than hypoxic conditions alone.

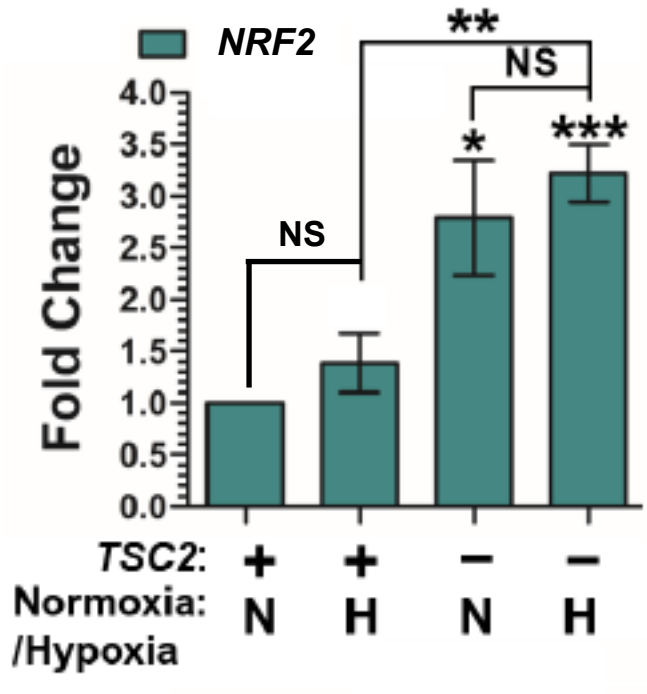

Fig. 5.6 Effect of hypoxia on NRF2 expression in TSC expressing and non-expression angiomyolipoma (AML)

AML cells lacking *TSC2* (−) or with Tsc2 expression re-established (+) were exposed to normoxic (N; 21% O2) and hypoxic (H; 1% O2) culture overnight. Cells were then harvested, lysed, mRNA purified and converted to cDNA before qPCR of target NRF2 gene (NFE2L2). Fold change is relative to expression in *TSC2* expressing cells under normoxia and normalised against the constitutively expressed gene Hydroxymethylbilane synthase (HMBS). Data was analysed by Kruskal-Wallis ANOVA and Dunn's post hoc analysis. Data represents mean ± s.e.m. ($n \geq 3$; * $p<0.05$; p** < 0.05, p*** <0.001; NS not significant.)

5.2.5 Nrf2 target genes are upregulated in TSC associated lesions and Tsc2 deficient AML and MEF cells

Further to our observations of NRF2's role in Tsc2-related ferroptosis resistance our cancer patient data revealed that in SEN/SEGA and AML differential gene expression of nrf2 related genes was modulated significantly versus normal tissue. This lends weight to the assertion that nrf2 and its related genes may be salient targets for future therapeutic targeting. Moreover, the differences between differential gene expression between the diseases serves to highlight that any specific cancer type must be assessed for its relevant changes in NRF2 and associated gene expression changes as this would be relevant to the proposed efficacy of a therapeutic targeting of nrf2. Indeed, future research may wish to assess which of the differentially expressed nrf2 targets is the key effector for the oncological phenotype in a given tumour or, more precisely, the cancer's chemoresistant/ferroptosis-resistance phenotype.

The presence or absence *TSC2* in any given tumour must always be considered against the genotype/phenotype background of the specific tumour in question as the *TSC2* gene product will act in that unique gene expression environment to exercise its effects on a given cell. This consideration also helps to explain the variety in differential gene expression observed in the data from the SEN/SEGA and AML samples, as well as variations in MEF and ELT3 observations presented earlier in this thesis.

In an age of single cell transcriptomics and with an understanding of the heterogeneity of cancer cells that leads to immune evasion, metastatic change and selection for resistant cells that can lead to relapse in treated patients one could suggest that personalised medicine may require a thorough assessment of a patients gene expression inclusive of ferroptosis and antioxidant genes that are salient to resistant phenotypes and ensure that appropriate

therapeutics regimens are applied to ensure that chemosensitivity is established for all cancer cells.

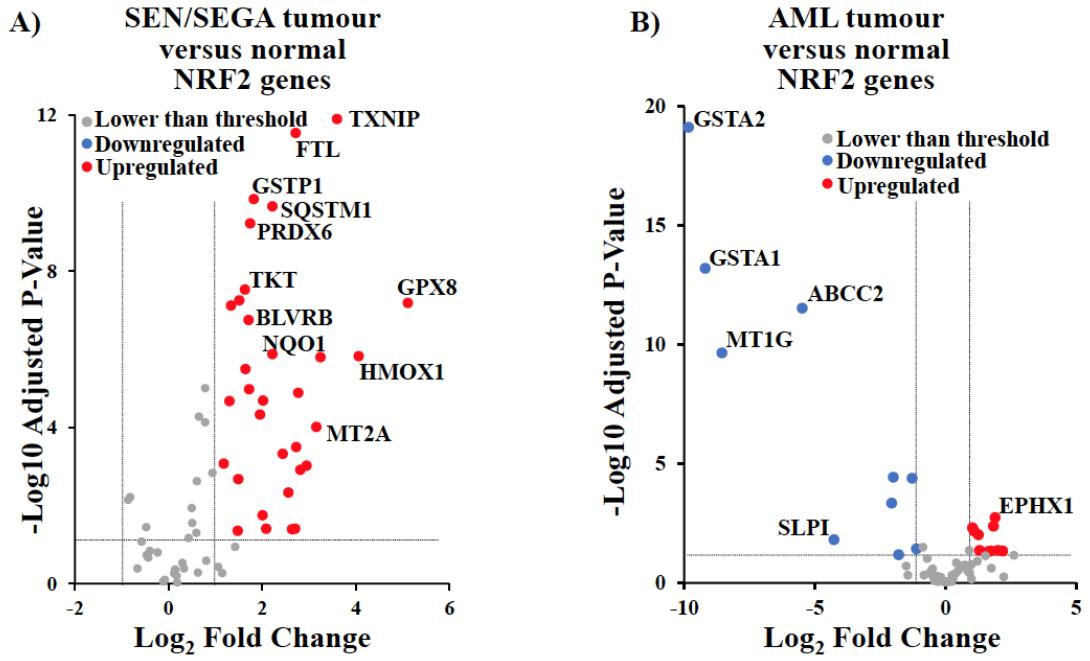

Fig. 5.7 Expression of NRF2 target genes is dysregulated in SEN/SEGA TSC lesions and AML cells associated with TSC2 loss

64 known NRF2 target genes were assessed for differential gene expression using methods described in section 2.2.10 and originally described by (Martin et al., 2017). Volcano plots were generated from previously published RNA sequencing data (Access to data granted by Prof Jeffrey MacKeigan). This data set compares genes expression of donated TSC patient tumours samples versus non-TSC healthy tissue samples. (A) 2 SEN (Subependymal nodules) and 18 SEGA (Subependymal giant cell astrocytomas) tumours versus normal unaffected brain tissue and (B) 11 AML tumours versus normal unaffected kidney tissue were compared. Differential gene expression (DEG) comparison is annotated above each plot. Grey lines at x-axis represent increase or decrease in fold change of 2 or -2, respectively. Grey line at y-axis represents significance threshold of 0.05. Genes annotated had a log2 fold change in expression greater or lower than 2 or -2 i.e. four-fold higher or lower in expression, respectively, and a -log10 adjusted p-value greater than 3 i.e. below 0.001 significance threshold. Upregulated genes are highlighted in red, downregulated genes highlighted in blue. Data shows upregulation of NRF2 gene target expression in SEN/SEGA, showing 32 upregulated genes. When comparing NRF2 gene target expression in AML tumours, only 10 genes were upregulated, while 10 genes were downregulated.

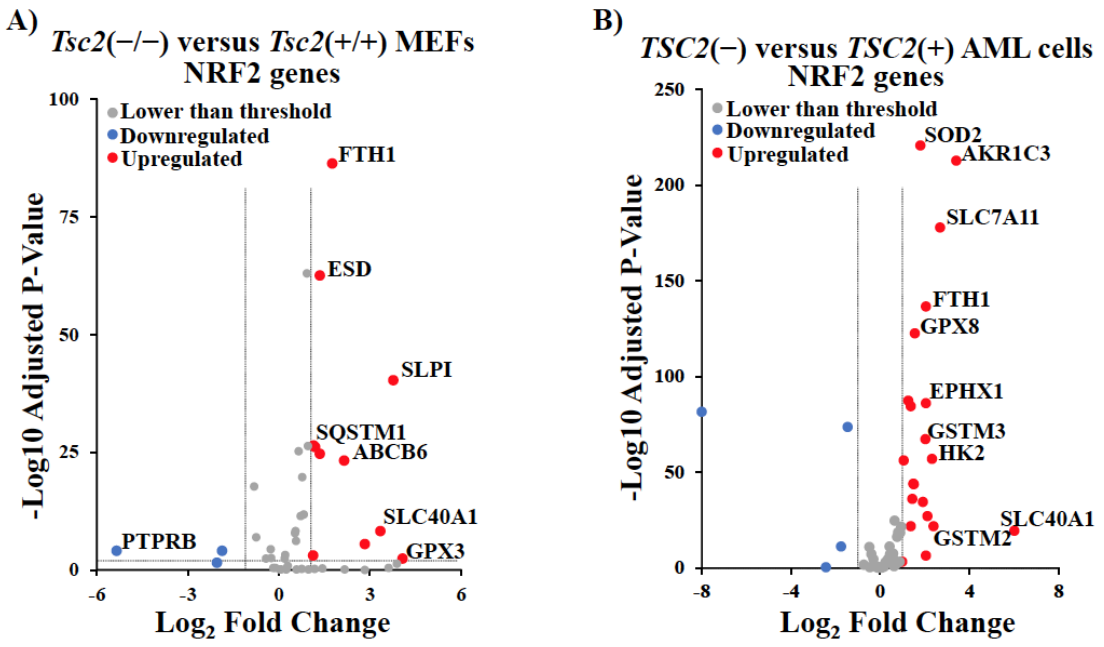

Fig. 5.8 Expression of NRF2 target genes are dysregulated in MEF and AML cells associated with TSC2 loss

64 known NRF2 target genes were assessed for differential gene expression using methods described in section 2.2.10 and originally described by Mohammad, A. (2023). (A) *Tsc2*(−/−) versus *Tsc2*(+/+) MEFs (n=3 for each cell line) and (B) *TSC2*(−) versus *TSC2*(+) AML cells (n=6). Thresholds were set, for greater than 1 Log_2 fold change and 1.3 –log10 adjusted P-value. Upregulated genes are highlighted in red, downregulated genes highlighted in blue. Data shows upregulation of NRF2 gene target expression in both samples with Tsc2 loss. Grey lines at x-axis represent increase or decrease in fold change of 2 or -2, respectively. Grey line at y-axis represents significance threshold of 0.05. Genes annotated had a log_2 fold change in expression greater or lower than 2 or -2 i.e. four-fold higher or lower in expression, respectively, and a -log10 adjusted p-value greater than 3 i.e. below 0.001 significance threshold.

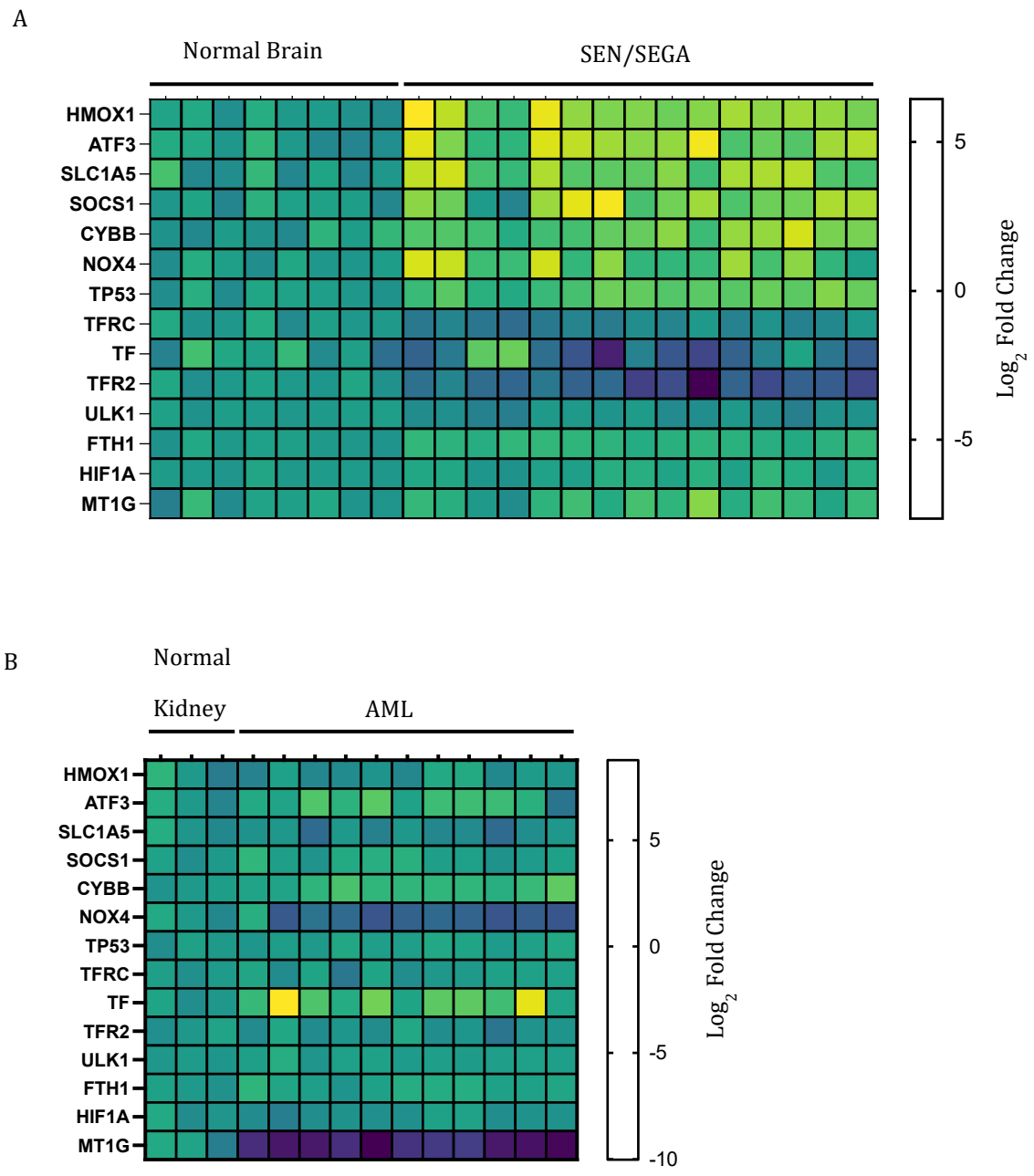

Fig. 5.9 Heat Maps of Ferroptosis-linked genes in SEG/SENA and normal kidney cells relative to AML

Gene expression data was used to create heat maps of the top hits for ferroptosis-related genes, and this was utilized to contrast the expression levels within individual patient tumours based on $\log_2$ fold change. Larger differences in gene expression of ferroptosis linked genes were observed in SEN/SEGA tumours when compared to AML tumours.

5.2.6 Inhibition of FSP1 sensitises cells to ferroptosis cell death

The newly identified regulator of ferroptosis, FSP1, was investigated to establish its role in the Tsc2 variant cell lines. ELT3 cell lines were first exposed to a dose range of FSP1 inhibitor to observe any direct cytotoxicity in the cells (Fig 5.11). No cytotoxicity was observed and, so, respective IC50 doses of RSL3 for the (+/+) and *(–/–)* cell lines were applied with the dose range of FSP1 inhibitor, and this exhibited a profound sensitisation to ferroptosis induction in both cell lines. Since respective RSL3 IC50s were being applied to the cell lines no differential sensitivity to FSP1 inhibition could be inferred from the current experiment.

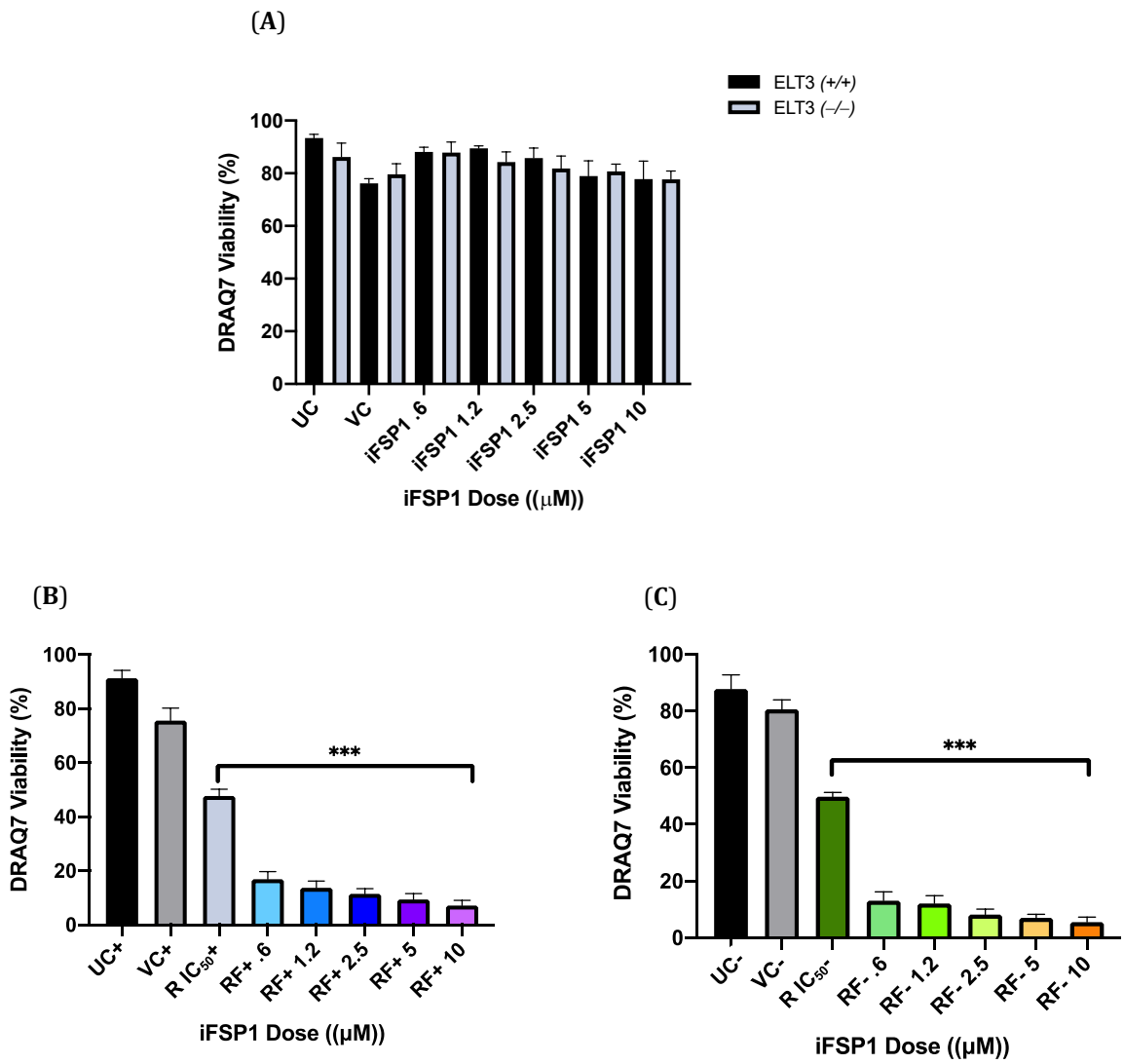

Fig. 5.10 Inhibition of FSP1 sensitizes cells to ferroptosis induction in *Tsc2* null and expressing cells.

Both *Tsc2* deficient and expressing ELT3 cells (ELT3 -/- and +/+, respectively) were seeded at $1x10^5$/mL in 24 well plates and grown overnight. (A) Cells were treated with a dose range of the FSP1 inhibitor, iFSP1, to establish cytotoxicity specific to the inhibitor alone. ELT3 (+/+) and (-/-) cells, (B) and (C) respectively, were treated with their respective IC_{50} doses of RSL3 (R) alone or in combination with the dose range of iFSP1. Cells were treated for 24h and then stained for DRAQ7. Samples were run on a BD Accuri C6 Flow cytometer and viable cells gated as large non-DRAQ7 positive cells. (FL4: Ex 640nm Em 670LP* [DRAQ7]). Data was analysed by one way ANOVA. Holm-Sidak post hoc analysis was performed to compare cell lines and Tukey's post hoc analysis for dose response differences within a cell line. n=4; *p<0.05; **p<0.01; ***p<0.001; ****p<0.0001). UC is untreated control and VC is vehicle control. RF refers to treatment with both RSL3 and iFSP1.

5.2.7 FSP1 mRNA is differentially expressed in Tsc2 cell line variants

Oxidative stress, mediated through NRF2, upregulates genes linked to iron metabolism and storage, thereby protecting against ferroptosis (Duarte et al., 2021). Key genes involved include FTH1, HMOX1, SLC7A11, and GPX4. FTH1 encodes a ferritin subunit, the primary iron storage protein (Theil et al., 2013), while HMOX1 encodes heme oxygenase 1, which breaks down heme (Chau et al., 2015). Expression levels of FTH1 and HMOX1 are significantly higher in Tsc2-deficient cells under hypoxia compared to Tsc2 rescue (RE) AML cells (FTH1: FC=4.78, p=1.57x10^-5; HMOX1: FC=92.58, p=0.0024). This elevated expression is consistent under both normoxic and hypoxic conditions, indicating that *Tsc2* loss significantly impacts iron metabolism genes.

FSP1 previously known as AIFM2, which cooperates with GPX4 to inhibit ferroptosis by repressing lipid peroxidation (Doll et al., 2019), and SLC7A11, which encodes the cysteine/glutamate antiporter essential for glutathione biosynthesis (Koppula et al., 2021), also show elevated expression in *Tsc2*-deficient cells. Specifically, under normoxia, *Tsc2*-deficient cells exhibit significantly higher levels of AIFM2 (FC=4.08, p=5.81x10^-7) and SLC7A11 (FC=11.09, p=0.0100) compared to Tsc2 RE cells. These findings suggest that Tsc2 loss enhances cysteine synthesis and import, leading to increased glutathione levels (Torrence et al., 2021; Champion et al., 2022). Additionally, AIFM2 and SLC7A11 expressions remain high in *Tsc2*-deficient cells under hypoxia, further underscoring the role of *Tsc2* in regulating oxidative stress responses and ferroptosis resistance.

Overall, these results highlight the significant impact of Tsc2 deficiency on ferroptosis resistance mechanisms through the upregulation of critical antioxidant and iron metabolism genes, independent of oxygen availability.

Further to its role in sensitivity towards ferroptosis we sought to determine if differentially transcribed or translated FSP1 could be observed between the cell lines. We clearly identified increased mRNA and protein expression of FSP1 in the Tsc2 *(–/–)* cell lines which correlated with their ferroptosis insensitivity (Fig 5.12). FSP1s role in mediating the observed variation in sensitivity between the variant cell lines was not investigated during the current study but is subject to ongoing investigation.

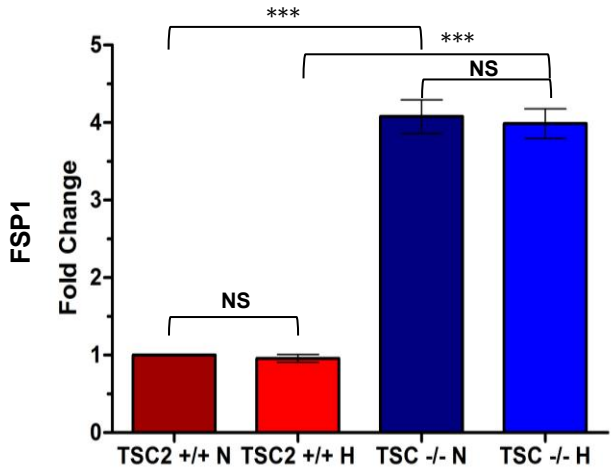

Fig. 5.11 Expression FSP1 mRNA in AML Cells

TSC2 deficient (***TSC2* −/−**) or *TSC2* re-expressed (***TSC2* +/+**) AML cells were cultured overnight before being lysed. mRNA was purified from lysates, converted to cDNA, and expression of target genes quantified via qPCR (n=3 minimum). Fold change in gene expression was calculated relative to the reference sample *TSC2* re-expressed under normoxia. Fold changes of FSP1 gene in samples were normalised to the housekeeping gene Hydroxymethylbilane synthase (*HMBS)*. Significance annotations above each bar on graph indicates significance of difference in fold change between each condition and the reference sample (*TSC2* RE cells under normoxia). Pairwise statistical comparisons between *TSC2* deficient cells under normoxia or hypoxia and between *TSC2 −/−* and *TSC2 +/+* cells under hypoxia are also annotated. Statistical analysis of differences in fold change (n=3 minimum) was by Student's t test. Significance denoted by: * = p <0.05, ** = p <0.01, *** = p< 0.001, NS = not significant. Bars represent standard error of the mean. **N**= Normoxia (21% O_2) or **H** = hypoxia (1% O_2).

5.3 Discussion

The data presented within this chapter reveal several novel findings on how TSC model cells respond to oxidative stress and highlights the role that NRF2 activity plays in these responses.

In our study, we initially screened the effect of the NRF2 inhibitor Trigonelline over a range of doses for any potential cytotoxicity on MEF *(–/–)* cells (Fig 5.1) and found no impact on cell viability. We, also, established that Trigonelline doses in combination with the IC_{50} dose of Erastin that was determined in MEF *(+/+)* cells had little effect until doses above 0.4mM were used. The doses above 0.4mM of Trigonelline significantly sensitised cells to ferroptosis, suggesting a link between NRF2 pathways and ferroptosis resistance. From these observations, and from equivalent literature findings on the applications of Trigonelline, we proceeded to assess both ELT3 and MEF cell lines with Erastin or RSL3, alone or in combination with Trigonelline at 0.5mM (Fig 5.2.and 5.3). We observed that using the Erastin and RSL3 IC_{50}s determined in *Tsc2 (+/+)* cells on *Tsc2 (–/–)* ELT3 and MEF cells showed little effect on viability until the NRF2 inhibitor was applied. IC_{50} values for Erastin and RSL3 with and without NRF2 inhibition (Table 5.1) clearly show the lower doses required in *Tsc2 (–/–)* cells when NRF2 inhibition was achieved. These finding indicate that NRF2 plays a crucial role in the ferroptosis resistance observed in Tsc2-deficient cells and its manipulation can re-sensitise cells to ferroptosis induction.

As an antioxidant pathway modulating ROS we next sought to determine if Lipid Peroxidation levels were perturbed in the NRF2 inhibited *Tsc2 (–/–)* cells (Fig 5.4). MEF *(–/–)* cells treated with dose ranges of Erastin or RSL3 exhibited higher levels of lipid peroxidation in the presence of the NRF2 inhibitor Trigonelline. A significant difference in Lipid Peroxidation levels was observed at lower doses of ferroptosis inducer. This was very suggestive of a mechanism of action for regulation of ferroptosis resistance in *Tsc2 (–/–)* cells. We, therefore, decided to

employ immunocytochemistry to assess the relative presence of NRF2 in both ELT3 *(−/−)* and *(+/+)* cells and to determine NRF2 activation, through nuclear translocation, in both cell lines during ferroptosis induction (Fig 5.5). Observations showed lower levels of cytoplasmic NRF2 protein in ELT3 *(+/+)* cells relative to *(−/−)* cells, which, alone, could be an important factor for resistance to ROS-induced lipid peroxidation and ferroptosis. Moreover, the nuclear translocation data, assessed at 6h post activation of ferroptosis using RSL3, revealed that *(−/−)* cells had predominantly nuclear NRF2 and little cytoplasmic NRF2, whereas the *(+/+)* cells still retained cytoplasmic NRF2. This translocation to the nucleus is crucial as it indicated that the higher NRF2 is also activatable in the (−/−) cells and during exposure to ferroptosis inducers is activated, thus, moderating the ROS that would otherwise be produced to facilitate Lipid Peroxidation and ferroptosis. It also suggests that significant differences in NRF2 associated gene transcription should be observed between the cells lines and that these gene products could also be involved in ferroptosis resistance.

The observed increase in NRF2 protein expression and activity in *Tsc2* deficient ELT3 was extended to observations of the impact of *Tsc2* loss on NRF2 mRNA expression in AML cells (Fig 5.6). *Tsc2* loss in these cells was associated with an over 2.5-fold increase in mRNA expression suggesting that *Tsc2* is a putative regulator of NRF2 gene transcription in many cell types. Furthermore, the association of *Tsc2* loss with NRF2 expression and ferroptosis resistance makes this gene's loss a key facet of the cancer phenotype while also providing an insight into a putative therapeutic intervention which would target inhibition of NRF2 in conjunction with chemotherapeutic or radiological interventions that rely on ROS production to manifest cancer cell death.

The NRF2 data presented here is consistent with Western blotting data previously presented in chapter 3 (Fig 3.8) which shows that p62 is upregulated in *Tsc2* deficient cells. NRF2 activation within *Tsc2* deficient cells has been proposed to be mediated by elevated expression

of the autophagic substrate p62 (Parkhitko et al. 2017). p62 sequesters NRF2 from its negative regulator Keap1 to stabilise NRF2 (Komatsu et al. 261 2010). In hepatocellular carcinoma, p62 regulation of NRF2 is a known driving mechanism of tumorigenesis (Umemura et al. 2016 and Inami et al. 2011). Surprisingly, however, Lam et al. (2017) found that p62 knockdown with siRNA within *Tsc2* −/− MEFs had no effect on the protein levels of NRF2. Instead, p62 knockdown decreased the intracellular pools of glutathione and expression of genes related to glutathione synthesis. Our own data showed that inhibition of P62 activity in Tsc2 deficient cells using Rapamycin had no impact on ferroptosis induction using RSL3 (Fig 3.7) despite the link between p62, NRF2 and ferroptosis resistance. The known effect of rapamycin treatment to reduce p62 levels in *Tsc2* deficient cells is probably due to enhanced autophagy through inhibition of mTORC1, which is known to cause autophagic degradation of p62 (Jung et al. 2009). Evidently, p62 is not the main driver of NRF2 activity within Tsc2-deficient cells. Alternatively, increased NRF2 expression is likely mediated by oxidative stress, a known disease facet of TSC (Chen et al. 2008, Suzuki et al. 2008 and Di Nardo et al. 2009). Increased oxidative stress inactivates Keap1, a negative regulator of Nrf2 (Tonelli et al. 2018). Our own assessment of the effect of hypoxia on NRF2 gene expression in MEF (*+/+*) and (−/−) cells revealed that an increase in mRNA was observed in both (+/+) and (−/−) cells but that the elevation did not reach a statistical difference within the power of the study. Supporting this hypothesis is the finding that elevating oxidative stress increased the expression of NRF2 targets within AML cells in which *Tsc2* was re-expressed (Fig 5.6).

Analyses of gene expression of NRF2 target genes in SEN/SEGA TSC lesions versus normal tissue, and in MEF cells with and without Tsc2 expression, revealed that Tsc2 loss was responsible for up and down regulation of many NRF2 targets (Figs. 5.7A and 5.8). The aforementioned p62 gene (SQSTM1) was upregulated in both when Tsc2 was lost which is consistent with our protein expression data for p62 but also ratifies our immunocytochemistry

observations of a modulated NRF2 pathway in *Tsc2* deficient cells. The data also provides putative therapeutic targets that are downstream of NRF2 and modulated in *Tsc2* deficient cells.

Table 5.2 below provides a summary of key genes identified in the analyses across the various samples and the functions associated with those gene products. It is clear that these genes are crucial in cellular metabolism and have impacts on redox control/oxidative stress management, detoxification, iron metabolism and protection of lipids. Those upregulated in Tsc2 loss would confer an advantageous protection on cells and would, thus, explain the resistance to ferroptosis and chemotherapeutics observed in this study and elsewhere. It should be noted that reference to individual genes in this study may not be appropriate when referring to gene expression changes, since the outcome phenotype will be based on the collective and interactive nature of the changes that manifest. This is a salient point when one considers that some of the down-regulated genes observed with *Tsc2* loss include those that are known to confer multi-drug resistance (*ABCC2*) or help detoxify therapeutic drugs, environmental toxins, and products of oxidative stress which can cause lipid peroxidation (GSTA1 and GSTA2). On balance, it is the myriad upregulated genes that outweigh the down-regulated genes, in this study, and confer advantage to cells that have accrued Tsc2 loss. Thus, for any given cancer its phenotype, and the heterogeneity of that phenotype within the tumour mass, would need to be ascertained to determine resistance to clinical intervention centred around NRF2, ferroptosis and oxidative stress.

TABLE 5.2 KEY NRF2 TARGET GENES MODULATED BY TSC2 LOSS

Gene	Gene Name	Functions
Upregulated upon Tsc2 Loss		
ABC6	Putative ABC transporter	putative ABC transporter
AKR1C3	Aldo-keto reductase family 1 member C3	catalyses the reduction of prostaglandin (PG) D2, PGH2 and phenanthrenequinone (PQ), and the oxidation of 9alpha,11beta-PGF2 to PGD2
BLVRB	Biliverdin reductase	Enables biliverdin reductase (NAD(P)+) activity and riboflavin reductase (NADPH) activity. Involved in heme catabolic process.

EPHX1	Epoxide hydrolase 1	functions in both the activation and detoxification of epoxides
ESD	Esterase D	enzyme is active toward numerous substrates including O-acetylated sialic acids, and it may be involved in the recycling of sialic acids.
FTH1	Ferritin heavy chain 1	major intracellular iron storage protein in prokaryotes and eukaryotes
FTL	Ferritin Light chain	major intracellular iron storage protein in prokaryotes and eukaryotes
GPX3	Glutathione peroxidase 3	protect cells against oxidative damage
GPX8	Glutathione Peroxidase 8	Enables peroxidase activity and predicted to be involved in cellular response to oxidative stress
GSTM2	Glutathione S-transferase mu 2	functions in the detoxification of electrophilic compounds, including carcinogens, therapeutic drugs, environmental toxins and products of oxidative stress, by conjugation with glutathione
GSTM3	Glutathione S-transferase mu 3	functions in the detoxification of electrophilic compounds, including carcinogens, therapeutic drugs, environmental toxins and products of oxidative stress, by conjugation with glutathione.
GSTP1	Glutathione S-Transferase pi 1	xenobiotic metabolism and play a role in susceptibility to cancer
HK2	Hexokinase 2	phosphorylates glucose to produce glucose-6-phosphate, the first step in most glucose metabolism pathways
HMOX1	Haem oxygenase 1	essential enzyme in heme catabolism, cleaves heme to form biliverdin, which is subsequently converted to bilirubin by biliverdin reductase, and carbon monoxide, a putative neurotransmitter.
MT2A	Metallothionein 2A	anti-oxidants, protect against hydroxyl free radicals, are important in homeostatic control of metal in the cell, and play a role in detoxification of heavy metals
NQO1	NAD(P)H quinone dehydrogenase 1	reduces quinones to hydroquinones. Prevents the one electron reduction of quinones that results in the production of radical species.
PRDX6	Peroxiredoxin 6	regulation of phospholipid turnover as well as in protection against oxidative injury
SLC40A1	Solute carrier family 40 member 1	involved in iron export from duodenal epithelial cells.
SLC7A11	Solute carrier family 7 member 11	member of a heteromeric, sodium-independent, anionic amino acid transport system that is highly specific for cysteine and glutamate.
SLPI	Secretory leukocyte peptidase inhibitor	secreted inhibitor which protects epithelial tissues from serine proteases. has antibacterial, antifungal and antiviral activity
SOD2	Superoxide Dismutase 2	binds to the superoxide by-products of oxidative phosphorylation and converts them to hydrogen peroxide and diatomic oxygen
SQSTM1	Sequestosome 1; p62	binds ubiquitin and regulates activation of the nuclear factor kappa-B (NF-kB) signalling pathway
TKT	Transketolase	channelling of excess sugar phosphates to glycolysis in the pentose phosphate pathway.
TXNIP	Thioredoxin interacting protein	major regulator of cellular redox signalling which protects cells from oxidative stress

Down-regulated upon Tsc2 Loss		
ABCC2	ATP binding cassette subfamily C member 2	transport various molecules across extra- and intra-cellular membranes; involved in multi-drug resistance
GSTA1	Glutathione S-transferase alpha 1	function to add glutathione to target electrophilic compounds, including carcinogens, therapeutic drugs, environmental toxins, and products of oxidative stress; has a particular role in protecting cells from reactive oxygen species and the products of peroxidation
GSTA2	Glutathione S-transferase alpha 2	function to add glutathione to target electrophilic compounds, including carcinogens, therapeutic drugs, environmental toxins, and products of oxidative stress; exhibit glutathione peroxidase activity thereby protecting the cells from reactive oxygen species and the products of peroxidation.
MT1G	Metallothionein 1G	Zinc ion binding activity; Involved in cellular response to metal ion; cellular response to vascular endothelial growth factor stimulus; and negative regulation of growth
PTPRB	Protein tyrosine phosphatase receptor type B	signalling molecules that regulate a variety of cellular processes including cell growth, differentiation, mitotic cycle, and oncogenic transformation. May regulate sodium channels; may play role in cell adhesion, neurite growth, and neuronal differentiation

The significant effect of Tsc2 loss on nrf2-related gene expression that can impact on ferroptotic sensitivity necessitated an assessment of ferroptosis-related gene expression changes in the same samples. The heat maps provided in Fig 5.9 provide an interesting observation of inconsistency in the significance of the impact on ferroptosis related genes in different tissues and their associated cancer phenotype when Tsc2 loss occurs. Normal brain versus SEN/SEGA had considerable ferroptosis-linked gene expression changes with multiple genes exhibiting up to and above 5-Fold changes (Log_2) in expression. Normal kidney versus AML, however, showed little similarity in these gene changes but did exhibit considerable changes in alternative genes, most notably MTG1, which was downregulated 10-fold relative to normal tissue. This observation reasserts the importance of outcome biology over individual genes comparisons. In a multi-gene system different perturbations or combinations of perturbations in gene expression could manifest the same overall outcome; in this case ferroptosis resistance. One must again consider the overall gene expression background for these perturbations since

they are occurring in different tissue types with tissue specific genes potential factors to consider in the final phenotype observed.

The identification of FSP1 as a negative regulator of ferroptosis led us to investigate its impact in our Tsc2 cell lines. Initially, we ensured that the inhibitor of FSP1 (iFSP1) had no cytotoxic effects on our ELT3 cell lines (Fig 5.11 (A)). Having established no loss of viability upon a range of dose exposures, we subsequently treated both ELT3 cells expressing Tsc2 and those that were Tsc2 deficient with their respective IC50 doses of RSL3 and the dose range of FSP1 inhibitor (Fig 5.11 (B) and (C)). There was a profound and significant ($p<0.001$) increase in ferroptosis related cytotoxicity across all doses used in both cell lines. This robustly demonstrated that FSP1 was active and important in both cell lines. The data did not reveal a distinct difference between the cell lines in their sensitivity to FSP1 inhibition with the doses used. This could have provided some insight into relative expression levels of the protein, which may have accounted for the resistance to ferroptosis associated with Tsc2 loss. While we did not get to investigate FSP1 levels in our ELT3 cells during this study we did assess relative expression of FSP mRNA in AML cells which were either Tsc2 deficient or expressing and under normoxic and hypoxic conditions (Fig 5.12); Hypoxia was investigated as it is well established as a factor in chemotherapeutic and radiotherapy resistance. Though hypoxia was not found to significantly alter expression of FSP1 in either cell line (thus, ruling it out as a mechanism of hypoxia-associated resistance) the difference in expression level of FSP1 between the cells lines was approximately 4-fold. The higher level of FSP1 expression in the TSC deficient cells could, thus, constitute a significant ferroptosis resistance mechanism in these cells. Increases in this ferroptosis inhibitor may be universal in Tsc2 driven cancers and make it a viable target for therapeutic intervention.

In conclusion, cells with *Tsc2* deficiency exhibited upregulation of NRF2 gene and protein expression as well as ferroptosis activation (nuclear translocation). *Tsc2* loss also altered NRF2-related gene expression and ferroptosis-related gene expression inclusive of increased ferroptosis inhibitor, FSP1, expression. This provides key new putative therapeutic targets for *Tsc2* driven tumours to overcome their associated therapeutic resistance.

6 General Discussion

6.1 Tsc2 Deficiency Confers Ferroptosis Resistance

Our findings demonstrate that *Tsc2*-deficient (*Tsc2*−/−) cells exhibit greater resistance to ferroptosis compared to their *Tsc2*+/+ counterparts. This conclusion is supported by the observed IC_{50} values for the ferroptosis inducers Erastin and RSL3. Specifically, *Tsc2*+/+ MEFs had lower IC_{50} values for Erastin and RSL3 compared to *Tsc2*−/− MEFs, indicating greater sensitivity to ferroptosis. Similarly, in ELT3 cell lines, *Tsc2+/+* cells had lower IC_{50} values compared to *Tsc2*−/− cells, further confirming the increased tolerance of *Tsc2*−/− cells to ferroptosis. These results clearly indicate that Tsc2*+/+* cells are more sensitive to ferroptosis, highlighting the crucial role of *Tsc2* in this cell death process. MTT cell viability rescue assays further supported these findings, where treatment with the ferroptosis inhibitor Fer-1 successfully rescued cell death in both *Tsc2*+/+ and *Tsc2*−/− MEF and ELT3 cells.

Iron chelation experiments using deferiprone (DFP) confirmed the critical role of iron in ferroptosis sensitivity across *Tsc2* variants. *Tsc2*-deficient cells, exhibiting overexpression of TFR, showed altered iron flux and accumulation, influencing their ferroptosis susceptibility. This iron chelation sensitivity is likely due to upregulated antioxidant pathways to mitigate iron-driven ROS, as suggested by Fraser et al. (2011). The implication is that *Tsc2*-deficient cells might have reduced iron availability for chelation, heightening their sensitivity to iron chelators.

6.2 mTORC1 Overactivation Alone Does Not Dictate Ferroptosis Sensitivity in *Tsc2*-Deficient Cells

Although mTORC1 hyperactivation is a hallmark of *Tsc2*-deficient cells, studies have shown that inhibiting mTORC1 alone does not completely restore ferroptosis sensitivity suggesting the involvement of additional pathways in ferroptosis resistance. Our results revealed that the cell death resulting from combined treatment with ferroptosis inducers and the mTORC1 inhibitor rapamycin [50nM] did not impact on ferroptosis sensitivity, indicating that mTORC1 overactivation alone is not the sole determinant of ferroptosis resistance in *Tsc2*-deficient cells. Previous studies have suggested that, unlike rapamycin, combining other mTORC1 inhibitors, such as Torin and Everolimus, with ferroptosis inducers can increase ferroptosis induction (Yangyun et al., 2022). This indicates that these alternative inhibitors may target additional pathways or mechanisms that contribute to ferroptosis resistance, thereby enhancing the effectiveness of the treatment. Understanding additional pathways and regulators involved in ferroptosis regulation upon *Tsc2* loss is crucial for overcoming ferroptosis resistance.

Role of AMPK

Recent research has identified AMP-activated protein kinase (AMPK), a key component of the PI3K pathway, as a crucial regulator of ferroptosis. Studies indicate that activated AMPK increases resistance to ferroptosis, while inactivated AMPK makes cells more susceptible. LKB1, an upstream kinase of AMPK inhibits biosynthesis of polyunsaturated fatty acids (PUFAs), particularly arachidonic and adrenic acids, essential for ferroptosis. Inhibition of ACC, through specific treatments or mutations, mimics AMPK's protective role. Consequently, this process protects cells from the accumulation of lipid hydroperoxides and ferroptosis (Li et al., 2020b).

However, there is an ongoing debate about AMPK's role in ferroptosis regulation. Cells under energy stress typically show increased reactive oxygen species (ROS) production, which promotes ferroptosis (Hay, 2020). A recent study found that AMPK activation is necessary for BECN1-induced ferroptosis, contradicting findings by Lee et al. (2019). BECN1, a critical regulator of autophagy, is phosphorylated by AMPK at Ser90/93/96, promoting the formation of the BECN1–SLC7A11 complex independent of mTORC1. This complex disrupts system Xc−-mediated glutathione homeostasis, inducing ferroptosis (Song et al., 2018, Zhong et al., 2020). Additionally, AMPK activation can reduce GPX4 expression at the transcription level by upregulating p53, independent of mTORC1 activity. This promotes ferroptosis in renal cancer via the JAK2/STAT3/p53 signalling axis (Li et al., 2022c). This further reinforces the important role of AMPK in MAPK signalling pathway activity on TFR1 regulation. In conclusion, the activation of the MAPK signalling pathway stimulates the expression of TFR1, leading to increased intracellular iron ions, ultimately causing ferroptosis (Wang et al., 2023b). Aligning with these findings, our data (Fig. 3.7) indicated that AMPK inhibition restored viability in all cell lines treated with their IC50 doses of a GPX4 inhibitor, RSL3, suggesting that AMPK promotes ferroptosis in both *Tsc2* functioning and deficient MEF and ELT3 cell lines. Our protein expression by western blot analysis (Fig. 3.8) revealed elevated level of phosphorylated ACC upon RSL3 treatment in *Tsc2* deficient cells.

Interestingly, dysregulation of the AMPK pathway can contribute to NRF2 activation through mechanisms that do not directly involve mTORC1. Conversely, Zhao et al. (2019) reported that AMPK inactivation promotes the expression of SREBP1/SCD1, leading to the production of monounsaturated fatty acids (MUFAs). Additionally, AMPK-mediated inhibition of ACC decreases NADPH consumption, enhancing cellular antioxidant defences and resistance to ferroptosis. LKB1, a serine/threonine kinase, enhances downstream AMPK and ACC phosphorylation, inhibiting PUFA production and limiting cellular vulnerability to ferroptosis

(Lee et al., 2020; Li et al., 2020b). These findings contradict our results; therefore, we propose that AMPK in ferroptosis regulation has a dual role and is dependent on the specific cellular context and regulatory pathways involved. Thus, the role of AMPK in ferroptosis regulation appears to be cell type- or disease-dependent, influenced by specific cellular environments and regulatory pathways.

Emerging evidence indicates that targeting ferroptosis holds significant potential as a therapeutic strategy for inhibiting tumour progression. However, while it is well-established that tumour cells frequently encounter energy stress, the impact of energy stress on ferroptosis in a *Tsc2*-deficient cell line model has not yet been thoroughly investigated. In this study, we demonstrated that energy stress-mediated AMPK activation effectively promotes ferroptosis in *Tsc2*-deficient cells. We anticipate that pharmacological activation of AMPK could have a synergistic effect with chemotherapy that induces ferroptosis, potentially enhancing the therapeutic effect or reducing chemoresistance. Further research is essential to unravel the interaction between AMPK and ferroptosis in the context of TSC deficiency and tumour development.

Role of autophagy

Ferroptosis is distinct from autophagic cell death, as evidenced by the fact that inhibiting autophagy does not effectively suppress ferroptotic cell death (Baba et al., 2018, Dixon et al., 2012). However, autophagy can still play a regulatory role at the molecular level in the process of ferroptosis, influencing pathways and mechanisms that affect cell susceptibility to ferroptotic triggers. Ferritinophagy, the autophagic degradation of ferritin, releases stored iron into the cellular labile iron pool, making it reactive and capable of participating in Fenton reactions that generate reactive oxygen species (ROS). The resulting increase in ROS levels promotes oxidative stress and lipid peroxidation, ultimately triggering ferroptosis (Hou et al.,

2016). In our Tsc2 re-expressing cells, where autophagy is functionally active and the iron-importing receptor TfR1 is overexpressed (Fig. 4.7), we observed increased sensitivity to Erastin- and RSL3-induced ferroptosis. While this association does not confirm a causal role for autophagy, it suggests that autophagy-related regulation of iron metabolism may contribute to ferroptosis susceptibility in TSC2-expressing cells

However, recent studies have also shown that autophagy protects cells from ferroptosis by stabilizing lysosomes, indicating a connection between autophagy and ferroptosis resistance. Intralysosomal ferritin stabilizes lysosomes by chelating iron, maintaining their integrity and function, and preventing the accumulation of toxic reactive oxygen species (ROS) and iron. This prevention of ROS and iron accumulation helps avert ferroptosis. Additionally, lysosome inhibitors have been demonstrated to reduce Erastin- and RSL3-induced ferroptotic cell death by inhibiting ROS production and preventing iron overload.

This mechanism helps explain why *Tsc2*-deficient cells exhibit greater sensitivity to the iron chelator deferiprone (DFP) compared to their wild-type counterparts (Fig. 3.5). This increased sensitivity is likely due to the altered regulation of iron homeostasis and autophagy pathways in *Tsc2*-deficient cells, resulting in less iron available for chelation. Consequently, iron chelation with DFP restores cell viability during RSL3-induced ferroptosis, suggesting that *Tsc2* deficiency disrupts iron homeostasis, making these cells more dependent on iron chelation for survival. These findings underscore the critical role of iron regulation and autophagy in ferroptosis resistance in *Tsc2* deficient cells.

Additionally, the signalling molecule STAT3 has been found to promote ferroptosis through the overexpression of cathepsin B and the activation of lysosomal cell death. Inhibiting STAT3 effectively blocks ferroptosis, highlighting the protective role of autophagy in regulating ferroptosis via lysosomal pathways. Moreover, autophagy regulates the expression and

function of metallothioneins (MTs), which bind iron and mitigate oxidative stress, thereby protecting cells from ferroptosis. By controlling the levels and activity of MTs, autophagy enhances their inhibitory influence on ferroptosis (Gao et al., 2016).

These findings suggest that autophagy can both promote and inhibit ferroptosis depending on the context and specific cellular conditions (Zhao et al., 2021b). The dual role of autophagy in ferroptosis regulation is exemplified by the p62-Keap1-NRF2 pathway, where p62 accumulation activates NRF2, increasing antioxidant defences and reducing ferroptosis sensitivity (Sun et al., 2016b). p62 in *Tsc2 (−/−)* MEFs was found to protect the mitochondria from ROS production-associated damage by maintaining the levels of glutathione (an essential antioxidant) and possibly by promoting mitophagy (Lam et al. 2017b).

Despite the association between autophagy and ferroptosis through the degradation of iron into its toxic form, the current study didn't include autophagy inhibition due to time constraints. We do, however, note that our Western blot analysis (Fig. 3.8) revealed an upregulation of p62, a negative marker of autophagy, in *Tsc2 (−/−)* MEFs, indicating altered autophagy regulation in these cells compared to their *Tsc2 (+/+)* counterparts. Elevated p62 levels suggest disrupted autophagic flux, impacting cellular responses to stress and damage. When treated with RSL3, p62 levels were reduced in both cell lines but remained elevated in Tsc2 *(−/−)* cells relative to *Tsc2 (+/+),* indicating a differential response to ferroptosis induction likely due to impaired autophagic clearance. Rapamycin, an mTORC1 inhibitor, reduced p62 levels in both cell types, implicating mTORC1 in autophagy regulation and its influence on ferroptosis. Elevated p62 levels in *Tsc2 (−/−)* cells are associated with resistance to ferroptosis through the activation of the NRF2 antioxidant pathway, as p62 sequesters KEAP1, stabilizing and activating NRF2, which enhances cellular resistance to oxidative stress and ferroptosis (Yuan et al., 2022). These findings suggest that increased p62 levels in *Tsc2 (−/−)* cells promote ferroptosis resistance by enhancing antioxidant defences via the NRF2 pathway, highlighting the complex interplay

between autophagy, mTORC1 signalling, and oxidative stress responses in determining cellular sensitivity to ferroptosis.

Studies have shown that the WDR45/WIPI4 complex, which includes ATG2, AMPK, and ULK1 under nutrient-rich conditions, is crucial for autophagy regulation. Rapamycin, an autophagy inducer, did not prevent cell death caused by WIPI4 knockout (KO), suggesting an autophagy-independent mechanism in ferroptosis regulation (Zhu et al., 2024). This finding aligns with our cytotoxicity data following Rapamycin exposure (Fig. 3.7), indicating that mTORC1 and autophagy are not the sole determinants of ferroptosis regulation. WIPI4 depletion increases ATG2A localization at ER-mitochondria contact sites, disrupting lipid regulation and enhancing ferroptosis. Elevated mitochondrial phosphatidylethanolamine (PE) levels promote ferroptosis due to polyunsaturated PE's role in lipid peroxidation. The LKB1-AMPK network also influences WIPI proteins, with WIPI3 interacting with the TSC complex upon Tsc2 phosphorylation at serine 1,387. These findings underscore the crucial role of AMPK-WIPI-mediated mitochondrial PE generation in regulating ferroptosis, independent of autophagy and mTORC1. Our findings of AMPK inhibition interference in ferroptosis induction, thus, suggests that these proteins should be investigated in our models to determine their impact on the observed differences in cell lines with *Tsc2* expression.

The loss of *Tsc2* disrupts AMPK signalling, further contributing to oxidative stress and impairing the cell's ability to respond to metabolic stress (Gwinn et al., 2008). This disruption can lead to a decrease in the expression and activity of key antioxidant enzymes, exacerbating cellular damage caused by oxidative stress.

Moreover, *Tsc2* deficiency has been linked to alterations in the activity of the FOXO transcription factors, which are involved in the regulation of oxidative stress responses. FOXO transcription factors promote the expression of genes encoding antioxidant proteins such as

superoxide dismutase (SOD) and catalase. *Tsc2* loss can inhibit FOXO activity, reducing the cell's ability to manage reactive oxygen species (ROS) and contributing to increased oxidative damage (Chen et al., 2010).

In terms of hypoxia and HIF-1α signalling, *Tsc2* deficient cells have been characterised as 'psuedohypoxic'; a term describing the phenomena of hypoxic-like signalling even under conditions of plentiful oxygen (Hayashi et al. 2019). Data within this thesis (Fig 5.6 and 5.11) found that in the context of *Tsc2*, there were no significant changes in transcription of either NRF2 and FSP1 genes under hypoxic conditions for both Tsc2 expressing and non-expressing cells.

6.3 Mechanisms Underlying Ferroptosis Resistance in Tsc2-Deficient Cells

***Tsc2* deficiency alters ROS-mediated Lipid Peroxidation:** Chapter 4 data confirmed that *Tsc2*-deficient cells exhibit decreased LPOX levels upon treatment with Erastin and RSL3, indicating resistance to ferroptosis. This decreased sensitivity aligns with cytotoxicity data from Chapter 3, where Tsc2-deficient cells showed increased survival. Conversely, higher LPOX levels in *Tsc2*+/+ MEF and ELT3 cells indicate greater sensitivity to ferroptosis, reinforcing the link between *Tsc2* expression and susceptibility to ferroptotic cell death. Elevated iron levels drive these processes, with LIP enhancements increasing ROS via Fenton reactions, thereby facilitating lipid peroxidation and ferroptotic cell death (Chen et al., 2020a, Borquez and Urrutia, 2024).

ROS: Although Erastin and RSL3 typically increase ROS production, low ROS levels were observed in Tsc2-deficient cells during ferroptosis induction. The low ROS levels in *Tsc2* deficient cells during ferroptosis induction is likely to be attributed to their activation of

antioxidant regulators and pathways to neutralise the ROS initially produced upon exposure to ferroptosis inducers (Chen et al., 2021b).

Our Western blot analysis showed p62 over expression in *Tsc2* deficient MEFs, which is associated with limiting oxidative stress by promoting glutamine uptake and GSH synthesis. Knockdown of p62 reduces mitochondrial membrane polarization, increases superoxide production, and decreases oxygen consumption. Exogenous GSH acts as an antioxidant, mitigating mitochondrial damage and supporting *T*sc2-null cell growth, thus, highlighting p62's role in tumorigenesis by regulating redox homeostasis. Others have also shown that *Tsc2* deficient ELT3 cells have p62 overexpression.

GSHTracer probe, revealed a significant increase ($p < 0.01$) in GSH levels in ELT3 *(−/−)* cells which is consistent with p62 overexpression but interestingly MEF *(−/−)* cells exhibited a significant decrease ($p < 0.01$) in GSH levels. This suggests that elevated GSH levels in *Tsc2*-deficient ELT3 cells might contribute to their ferroptosis resistance but in MEF cells other mechanisms are required to explain their resistance to ferroptosis induction. Further studies are planned to validate these findings with enhanced detection methods.

Since RSL3 directly targets and inhibits GPX4, the enzyme critical for reducing lipid hydroperoxides, it is plausible that higher concentrations of RSL3 are required to induce equivalent ferroptotic effects in Tsc2-deficient cells compared to Tsc2-expressing cells. Our Western blot data revealed elevated GPX4 protein levels in Tsc2 *(−/−)* cells, suggesting a stronger antioxidant defence that could reduce ROS accumulation and protect against ferroptosis. This interpretation is supported by GPX4 gene expression analysis under hypoxic and normoxic conditions, which showed that Tsc2 deletion, rather than hypoxia, drives GPX4 upregulation. These findings provide insight into a potential mechanism by which Tsc2 loss

confers ferroptosis resistance, although the differential GPX4 expression may also contribute to the altered dose-response to RSL3 observed between the two cell types.

***Tsc2* deficiency alters intracellular iron levels:**

The differential LIP responses between ELT3 *(+/+)* and ELT3 *(−/−)* cells to RSL3 treatment further highlight the role of Tsc2 in modulating ferroptosis sensitivity through iron metabolism. ELT3 *(+/+)* cells showed significantly higher LIP increases, suggesting that *Tsc2* enhances susceptibility to ferroptosis by promoting iron accumulation. This dose-dependent LIP elevation corroborates the role of RSL3 in ferroptosis induction by increasing intracellular iron levels, with ELT3 *(+/+)* cells exhibiting higher ferroptotic activity compared to ELT3 *(−/−)* cells.

Given the lower labile iron pools in *Tsc2*-deficient cells, their reduced capacity for ferroptosis execution is unsurprising. This lower LIP means that these cells require less iron chelator to significantly impact their iron reserves. While direct LIP supplementation was not explored, it remains a potential target for increasing ferroptosis susceptibility in *Tsc2*-deficient cells. Iron chelation, already used clinically for conditions like hemochromatosis, may represent a viable combinatorial treatment approach for ferroptosis-targeted cancer therapies. Our data support the hypothesis that *Tsc2* deletion contributes to chemoresistance via ferroptosis insensitivity by manipulating the labile iron pool, validating our observations of ferroptosis characteristics in *Tsc2* MEFs and ELT3 cell line models.

6.4 *Tsc2* Mutation Drives Additional Antioxidant Response in Ferroptosis resistance

6.3.1 Activation of NRF2

It is well established that overaction of mTORC1 due to *Tsc2* loss is associated with various antioxidant pathways, including NRF2 activation, GSH/GPX4 synthesis, and intracellular iron metabolism, and that these help cancer cells cope with the elevated oxidative stress associated with rapid growth and metabolism (Zarei et al., 2019, Liu et al., 2021, Han et al., 2020, Baba et al., 2018). Although inhibition of mTORC1 did not alter ferroptosis sensitivity, different antioxidant-related proteins, genes and their targets that are modulated by mTORC1, e.g. NRF2, FSP1, HMOX1, GPX4, were overexpressed in *Tsc2* deficient cells. We have discussed the role of Hypoxia (HIF1α) which also impacts ferroptosis through GSH depletion and the activation of antioxidants via antioxidant signalling pathway (Schneider et al., 2008). Our data showed it was the loss of *Tsc2*, but not hypoxia that elevates NRF2 mRNA expression AML cells. So, there must be additional pathways involved in neutralising oxidative stress during ferroptosis (Brugarolas et al., 2003).

NRF2 plays a central role in cancer progression, not only because of its antioxidant activity but also because it establishes crosstalk with several oncogenic pathways, including mammalian target of rapamycin (mTOR), Heat Shock Factor1 (HSF1), and mutant (mut) p53. At the molecular level, mTOR activation leads to the upregulation of key genes involved in cell proliferation, survival, and metabolism. By enhancing protein synthesis, mTOR enables cancer cells to overcome the cytotoxic effects of chemotherapy mTOR is also known in conferring resistance through activation of cancer pathway to different chemotherapy regimens.

The activity of NRF2 is tightly regulated at the post-translational level, and mTOR has been implicated in modulating NRF2 protein levels and activity through various mechanisms.

Studies have shown that mTOR signalling can influence NRF2 protein stability. Activation of mTORC1 has been reported to promote the degradation of NRF2 by enhancing its ubiquitination and subsequent proteasomal degradation. Conversely, inhibition of mTORC1 with rapamycin or other mTOR inhibitors can stabilize NRF2 protein levels, leading to increased NRF2 activity and transcriptional output. In addition to affecting NRF2 stability, mTOR signalling can also impact NRF2 nuclear translocation, which is essential for its transcriptional activity. Activation of mTORC1 has been associated with impaired NRF2 nuclear translocation, thereby reducing its ability to induce the expression of antioxidant and detoxification genes. Conversely, inhibition of mTORC1 can promote NRF2 nuclear translocation and enhance its transcriptional activity.

However, AMPK can act as an upstream mediator of NRF2 signalling. It seems that AMPK activation is vital for inducing NRF2 signalling (Song et al., 2020a). By stimulating NRF2 signalling, AMPK protects against oxidative stress and enhances expression of downstream targets such as HMOX1, GPX4 (Song et al., 2020a).

6.3.2 Activation of FSP1

Our study demonstrated that targeting FSP1 significantly sensitizes *Tsc2*-deficient cells to ferroptosis (Fig. 5.10). This finding aligns with recent research emphasizing the role of ferroptosis suppressor protein 1 (FSP1) in modulating ferroptosis resistance. Specifically, analyses of the Cancer Therapeutics Response Portal (CTRP) revealed that FSP1 (also known as AIFM2) exhibited the most striking positive correlation with resistance to multiple class 2 FINs that inactivate GPX4, including RSL3, ML162, and ML210, which is consistent with recent reports that FSP1 acts in parallel to GPX4 to inhibit ferroptosis(Sui et al., 2018)

Endogenous antioxidants related proteins linked to ferroptosis regulation and iron metabolism/storage were also overexpressed upon loss of *Tsc2*, as seen in Fig. 4.8.

Our study showed targeting FSP1 could sensitise *Tsc2* deficient cells to ferroptosis (Fig. 5.10). This finding aligns with recent research emphasizing the role of ferroptosis suppressor protein 1 (FSP1) in modulating ferroptosis resistance. Evidence in studies focussed on stress granule and FSP1 related drug resistance underscores the complexity of ferroptosis regulation *Tsc2* in tumour. *Tsc2* deficiency is known to increase stress granule formation in cells as well as increase the stress granule core component G3BP1. In *TSC2* expressing cells downregulation of HDLBP (high-density lipoprotein-binding protein), which recruits *Tsc2* to stress granules and co-localises with G3BP1, did not affect overall stress granule production but did result in fewer stress granules containing *Tsc2*. Furthermore, in an *in vivo* study G3BP1 was associated with a decrease in subcutaneous tumour size of 75% *in vivo* (Kosmas et al., 2021). Together, these suggest that HDLBP-mediated recruitment of *Tsc2* to stress granules is essential for tumour growth suppression i.e. it may be a tumour suppressor gene. In contrast to this anti-tumour activity HDLBP overexpression in hepatocellular carcinoma (HCC) limited the ferroptosis inducing capacity of pharmacological ferroptosis inducers, which suggests its role in ferroptosis drug resistance. The exact mechanisms of this resistance are not known currently, but HDLBP does stabilise the large non-coding RNA FAL (lncFAL), which leads to activation of Ferroptosis HDLBP overexpression in hepatocellular carcinoma (HCC) limits the effectiveness of ferroptosis-inducing drugs by stabilizing the large non-coding RNA lncFAL, which activates Ferroptosis suppressor protein (FSP1) and antioxidant pathways, thereby contributing to drug resistance (Feicht and Jansen, 2024). Which should be elucidated further in the context of *Tsc2* loss in ferroptosis regulation.

Further research is warranted to explore the mechanistic pathways linking Tsc2 loss, oxidative stress and NRF2 activation to develop targeted therapies that can effectively disrupt this axis and improve clinical outcomes for ferroptosis.

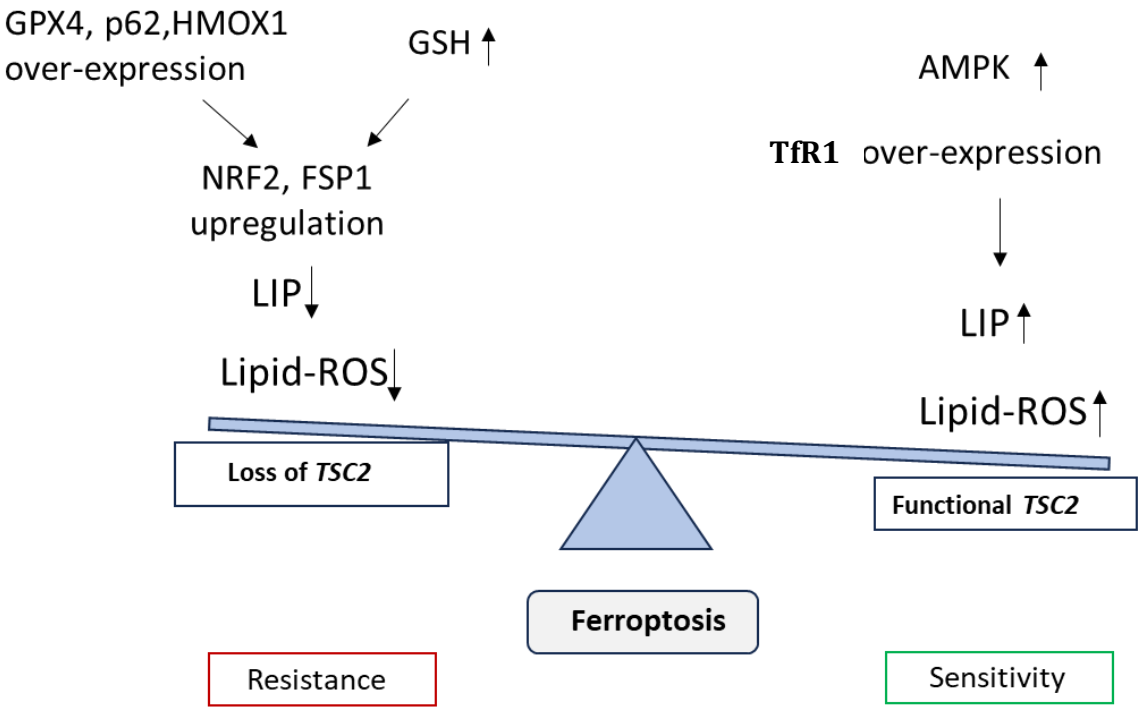

Fig 6.1 *Tsc2*-related Factors affecting Ferroptosis Sensitivity

LIP: Labile Iron Pool. TfR1: Transferrin Receptor. Lipid-ROS: ROS-mediated Lipid peroxidation

6.5 Pathways Beyond the Known: Additional Signalling in Ferroptosis

It is well demonstrated that drugs that reduce mTOR activity are only partially successful in the treatment of TSC, suggesting that mTOR-independent pathways play a role in disease development and drug resistance (Ali et al., 2022, Habib et al., 2016). Hence, other mechanistic insights into *Tsc2* loss-mediated Ferroptosis Sensitivity, independent of mTORC1, must be sought as they may play a crucial role in ferroptosis resistance. Below, we briefly discuss some of the other candidate pathways.

Role of MAPK

The mitogen-activated protein kinase (MAPK) pathway plays a pivotal role in regulating oxidative stress and ferroptosis, with AMPK acting as a cellular energy sensor that intersects with these processes. The classical RAS–RAF–MEK–ERK cascade is central to this regulation, where MEK activity has been identified as a key determinant of ferroptosis sensitivity, and ERK1/2 activation is often observed during ferroptotic responses (Wang et al., 2023b). This study showed RAS-mutated cancer cells tend to exhibit heightened sensitivity to Erastin-induced ferroptosis. For instance, HL-60 cells harbouring the NRAS Q61L mutation are more susceptible to Erastin-induced ferroptosis compared to their wild-type counterparts. Conversely, reduced KRAS or BRAF activity has been associated with decreased ferroptosis sensitivity in certain contexts. Interestingly, ferroptosis sensitivity is not exclusive to RAS-mutant cells; for example, diffuse large B-cell lymphoma and renal carcinoma cell lines lacking RAS pathway mutations also show vulnerability to ferroptotic death.

Recent studies have added further complexity to this regulatory network. Chemotherapy-activated MAPK signalling has been shown to induce ERK-mediated phosphorylation of RFNG at the Ser255 residue (Di et al., 2024). This phosphorylated RFNG translocates to the nucleus,

where it suppresses p53 activation, leading to the upregulation of SLC7A11 and enhancing resistance to both apoptosis and ferroptosis.

Role of Endoplasmic reticulum (ER) stress

The loss of *Tsc2* leads to the accumulation of disorganized and unfolded proteins within the endoplasmic reticulum (ER), triggering ER stress. When ER stress is triggered, the unfolded protein response (UPR) activates protein kinase RNA-like ER kinase (PERK), which phosphorylates eukaryotic initiation factor 2 alpha (eIF2α). This phosphorylation reduces global protein synthesis to help manage the load of unfolded proteins (McEneaney and Tee, 2019). As phosphorylated eIF2α levels increase, the expression of activating transcription factor 4 (ATF4) is upregulated. ATF4 plays a crucial role in enhancing the cell's stress response capacity by increasing the expression of genes involved in antioxidant responses and amino acid metabolism.

ER stress typically acts as a protective mechanism against ferroptosis by maintaining cellular survival through pathways like the PERK-eIF2α-ATF4 pathway and the activation of NRF2 (Huang et al., 2024). However, if ER stress is severe or prolonged, these protective mechanisms can fail, leading to ferroptosis through the activation of pro-ferroptotic pathways such as eIF2α-ATF4-CHOP. For instance, in pancreatic ductal adenocarcinoma (PDAC) cells, Erastin induces the phosphorylation of PERK and increases ATF4 expression, which upregulates system Xc– and HSPA5. HSPA5 forms a complex with GPX4, preventing its degradation and maintaining cellular antioxidant capacity (Zerbato et al., 2023).

Further research by (Kato et al., 2012) has indicated that partial knockdown of Tsc2 specifically activates the IRE1-JNK pathway without triggering the PERK and ATF6 pathways. This selective activation of the IRE1-JNK pathway without PERK and ATF6 can modulate the cell's fate towards death rather than survival, contributing to ferroptosis, especially under conditions

where the accumulation ROS and lipid peroxides are prevalent. Complete TSC deletion leads to strong, sustained mTORC1 activation, resulting in the activation of all UPR branches due to protein overproduction and reduced degradation. Conversely, partial TSC knockdown selectively activates the IRE1 pathway. This suggests that the extent of mTORC1 activation and the specific UPR pathways activated play crucial roles in determining whether ER stress will inhibit or promote ferroptosis.

Furthermore, endoplasmic reticulum zinc homeostasis, regulated by ZIP7, significantly influences ferroptosis sensitivity independent of mTORC1. Zinc chelation suppresses ferroptosis, while zinc addition promotes it. Inhibiting ZIP7 protects against ferroptosis and induces ER stress responses. (Chen et al., 2021a). These findings suggest ZIP7 as a potential therapeutic target for diseases involving ferroptosis and zinc dysregulation.

Other Signalling Pathways linked to TSC2 loss

There are other signalling pathways that are closely associated with AMPK or mTOR modulation upon *Tsc2* loss. SIRT3, a NAD-dependent mitochondrial protein deacetylase, regulates ROS production. Reduction of protein levels of SIRT3 inhibits the activation of the AMPK/mTOR signalling pathway and, thus, inhibits cells from undergoing autophagy-dependent ferroptosis (Han et al., 2020).

Epidermal growth factor receptor (EGFR), a receptor tyrosine kinase, is closely related to cellular autophagy. Studies showed that GALNT14 could downregulate glycosylation of EGFR to inhibit mTOR activity, causing autophagy and ferroptosis (Li et al., 2022a). It was also reported that EGFR inhibition could enhance cellular sensitivity to ferroptosis by upregulating LC3B-II to induce autophagy. Therefore, there is a correlation between EGFR and mTOR. Additionally, p62/SQSTM1, which accumulates in TSC2-deficient cells, is another regulator of ferroptosis acting outside canonical mTORC1 control. It promotes glutamine metabolism,

glutathione synthesis, and mitochondrial integrity. Through binding to KEAP1, p62 stabilises NRF2, leading to increased antioxidant gene expression(Lam et al., 2017) Importantly, this p62–KEAP1–NRF2 axis can be activated independently of mTORC1 and plays a significant role in mediating ferroptosis resistance (Ichimura et al., 2013).

6.6 The Clinical Application of Targeting NRF2 to Induce Ferroptosis in Tsc2-Driven Cancers

Ferroptosis has garnered significant interest for its potential to target cancer cells resistant to traditional therapies. Current strategies primarily focus on the system Xc− GPX4 axis, using drugs like Erastin and Sorafenib. GPX4 inhibitors such as RSL3 are commonly employed to induce ferroptosis. However, recent studies suggest that inhibiting additional antioxidant pathways like NRF2 and FSP1 alongside GPX4 can overcome ferroptosis resistance in cancer cells.

Our research reveals that, beyond regulating mTORC1, *Tsc2* deficiency increases glutathione synthesis and activates the NRF2 and FSP1 antioxidant pathways during ferroptosis. Specifically, NRF2 nuclear translocation occurs during RSL3-induced ferroptosis, and RNA sequencing data show that *Tsc2* loss correlates with the activation of NRF2 target genes. Elevated NRF2 levels enhance the expression of genes involved in glutathione biosynthesis, detoxification of

NRF2 plays a central role in regulating initial ROS levels and maintaining redox homeostasis, enabling cancer cells to survive under oxidative stress. Therefore, targeting NRF2 to disrupt this antioxidant defence and promote ferroptosis may represent a promising therapeutic strategy in TSC2-deficient cancers.

Although there are no clinically approved NRF2 inhibitors specifically for cancer treatment, several experimental compounds targeting the NRF2 pathway are currently under clinical

investigation. These inhibitors aim to disrupt the antioxidant defences that cancer cells utilize to survive under oxidative stress. Ferroptosis inducers such as Erastin analogue PRLX 93936 and artemisinin/artesunate have already entered clinical trials (See Table 1.5).

Evidence from Clinical Studies

Breast Cancer:

Inhibiting NRF2 can enhance the effectiveness of conventional therapies by making cancer cells more susceptible to treatments like chemotherapy and radiotherapy. For instance, TNBC cells, which rely on high NRF2 activity to survive oxidative stress, become more sensitive to ionizing radiation when treated with an NRF2 inhibitor ML385 (Qin et al., 2021). Additionally, Levistilide A (LA) induces ferroptosis in breast cancer cells by activating the NRF2-HMOX1 signalling pathway. This activation catalyses the cleavage of haem to form biliverdin, carbon monoxide, and ferrous iron (Fe2+), which increases iron-driven ROS levels to promote ferroptosis and impairs mitochondrial integrity (Yang et al., 2022). Conversely, research indicates that Erastin, a ferroptosis inducer, is more effective with reduced NRF2 activity, as overexpression of GSK-3β enhances Erastin-triggered ferroptosis by increasing ROS and promoting cell death. Additionally, the NRF2 inhibitor Brusatol significantly reduces tumour growth and boosts the efficacy of chemotherapeutic agents like trastuzumab in HER2-positive breast cancer models (Ghareghomi et al., 2022) .

Our data demonstrated that the loss of *Tsc2* activates the NRF2 antioxidant response, in parallel with pathways such as AMPK activation during ferroptosis induction. Furthermore, studies have shown that NRF2 activation leads to resistance to PI3K and mTORC1 inhibitors in breast cancer cell lines (Bertucci et al., 2023). Additionally, studies have shown that breast cancer patients with low *TSC2* levels have poorer clinical outcomes, linking *TSC2* deficiency to more aggressive tumour behaviour. Combination treatments, such as Metformin, which activates

AMPK, synergise with mTOR inhibitors and sulfasalazine to treat HER2-positive breast cancer, highlighting additional *TSC2*-mediated pathway activation (Zhou et al., 2001, Wang et al., 2014, Yang et al., 2022). Thus, integrating NRF2 inhibitors with ferroptosis inducers represents a compelling approach to enhance therapeutic efficacy in cancers harbouring Tsc2 mutations.

Kidney Cancer

TSC2 mutations contribute to renal cancer by activating mTORC1 and disrupting cellular antioxidant responses. Our study highlighted, NRF2 and its target genes are dysregulated in AML compared to normal kidney tissue and between MEF cells which were either Tsc2 expressing or deficient.

TSC2-deficient cells rely on CDK7-dependent transcription of NRF2 for survival. The CDK7 inhibitor THZ1 effectively inhibits the growth of *Tsc1* and *Tsc2*-deficient cells by increasing ROS levels significantly reducing tumour size in mice. With SY-1365, a derivative of THZ1, in clinical trials, targeting NRF2 presents a promising therapeutic strategy for cancers with *TSC1/TSC2* mutations, leveraging ferroptosis and enhanced oxidative stress to combat tumour growth (Zarei et al., 2019). NRF2 also upregulates the expression of GPX4, an essential enzyme that protects cells from lipid peroxidation and consequent ferroptosis (Pan et al., 2023).

Dipeptidyl peptidase 9 (DPP9) interferes with the KEAP1-NRF2 interaction by binding to KEAP1, thereby stabilizing NRF2. This stabilization reduces ROS levels, decreasing ferroptosis and increasing resistance to the drug sorafenib, primarily through the NRF2 target SLC7A11. These findings suggest that DPP9 overexpression drives NRF2 pathway hyperactivation, promoting tumorigenesis and drug resistance in clear cell renal cell carcinoma (ccRCC) (Chang et al., 2023).

Recent studies indicate that the combination of melatonin and zileuton effectively inhibits RSL3-induced ferroptosis in kidney injury models by activating the AKT/mTOR/NRF2

signalling pathway. This combination therapy synergistically reverses the downregulation of GPX4 and the upregulation of lipid peroxidation markers like 4-HNE and HMOX1. The treatment enhances NRF2 expression and its nuclear translocation, crucial for activating antioxidant defence mechanisms (Jung et al., 2023, Ma et al., 2020). These findings highlight the potential of targeting the AKT/mTOR/NRF2 axis to induce sensitivity to ferroptosis and improve therapeutic outcomes in renal cancer with Tsc2 mutations.

Brain cancer

TSC2 mutation leads to growth of benign and malignant tumours in the brain such as SEN/SEGAs and Glioblastomas (GBM). Our study clearly demonstrated that NRF2 and its target genes are dysregulated in SEN/SEGA compared to normal brain tissue and between MEF cells, which were either *Tsc2* expressing or deficient. Hence, targeting ferroptosis in brain cancer with *TSC2* mutations and NRF2 activation, offers a promising therapeutic strategy due to the unique metabolic and oxidative stress conditions in these cells. Other studies have shown TSC mutations and focal cortical dysplasia type IIb (FCD IIb) lead to chronic oxidative stress and persistent activation of NRF2 and its target genes, disrupting redox balance and iron metabolism, contributing to epileptogenesis. Dysmorphic cells overexpress system Xc− to manage increased intracellular iron from mTOR activity, indicating adaptation to oxidative conditions (Arena et al., 2019, Zimmer et al., 2020). Targeting NRF2 and using ferroptosis-inducing agents can circumvent the side effects of current mTOR inhibitors, making ferroptosis a viable treatment strategy.

Additionally, glioblastoma patients often have a poor prognosis due to temozolomide (TMZ) resistance mediated by NRF2 activation.(Almeida Lima et al., 2023, de Souza et al., 2022). Interestingly, high levels of NRF2 result in collateral sensitivity in glioblastoma via the expression of its pro-ferroptotic target ABCC1, which contributes to GSH depletion when the

system Xc− is blocked during ferroptosis induction by Erastin. Silencing ABCC1, an NRF2 target that reduces GSH levels, increased TMZ sensitivity and resistance to Erastin. These findings suggest that integrating NRF2 inhibition with ferroptosis induction could enhance therapeutic efficacy in *Tsc2*-driven cancers and overcome resistance in glioblastoma.

Colorectal cancer:

In colorectal carcinoma, alterations in the *Tsc2* gene occur in 4.78% of patients, with 4.15% specifically presenting Tsc2 mutations (Tapia-Valladares et al., 2024). This genetic alteration plays a significant role in the progression and treatment resistance of colorectal cancer. Recent research emphasizes the critical role of NRF2 in mediating chemoresistance and ferroptosis resistance in colorectal cancer.

Studies have shown that treatments with chemotherapeutic agents such as oxaliplatin and lobaplatin elevate NRF2 expression in colorectal cancer cells (Huang et al., 2023). This increased NRF2 activity counteracts the cytotoxic effects of these drugs, contributing to chemotherapy resistance. GPX4, a critical regulator of ferroptosis, is typically expressed at higher levels in colorectal cancer tissues than in normal tissues. Interestingly, both oxaliplatin and lobaplatin treatments have been found to reduce GPX4 expression, thereby promoting ferroptosis *in vitro*. NRF2, known for its role in scavenging reactive oxygen species (ROS), also promotes GPX4 expression and thereby reduces ferroptosis. Knockdown of NRF2 followed by chemotherapy significantly decreases GPX4 expression, indicating an increased sensitivity to ferroptosis. Moreover, inhibiting NRF2 signalling in HER2-overexpressing colon cancer patients is essential for overcoming oxaliplatin resistance, highlighting NRF2 as a crucial target for enhancing chemotherapy efficacy (Pirpour Tazehkand et al., 2018). Targeting NRF2 pathway in conjunction with Tsc2 could present a promising therapeutic strategy in colorectal

cancer, potentially overcoming resistance to conventional therapies and promoting cell death through ferroptosis sensitivity.

Liver cancer

Increased liver tumour formation is linked to abnormal p62 aggregates, defective autophagy, and excessive NRF2 activation, rather than fibrosis, cMYC, or mTOR activity (Kondylis et al., 2022). This is particularly relevant in cancers with *Tsc2* mutations where autophagy is already compromised (Di Nardo et al., 2014). Hepatocellular carcinoma (HCC) cells treated with NRF2 inhibitors camptothecin and brusatol (both are in clinical trials) sensitized to sorafenib treatment (Sun et al., 2023a, Sun et al., 2016a). This further supports the idea that NRF2 inhibition can enhance the efficacy of ferroptosis-inducing therapies and combination-targeting approach could lead to more effective treatment outcomes by overcoming resistance mechanisms in *Tsc2* driven cancers.

Other cancers

Targeting NRF2 in cancer therapy is gaining traction due to its role in chemoresistance and ferroptosis regulation. Agents like temozolomide-1 and homoharringtonine promote chemosensitivity in various tumours by disrupting the redox balance. (de Souza et al., 2022). Compounds such as apigenin, omipalisib, and entinostat block NRF2 mRNA translation, showing anticancer effects in hepatic, gastric, and sarcoma cancers (Gao et al., 2017).

Additionally, convallatoxin and trigonelline inhibit NRF2 by promoting its degradation and preventing its nuclear accumulation, enhancing sensitivity to anticancer agents in NSCLC and pancreatic cancer cells. Flavonoid luteolin suppresses NRF2 nuclear translocation, increasing chemosensitivity and inducing apoptosis in NSCLC and colorectal cancer cells, leading to clinical trials for tongue squamous cell carcinoma. ML385, a small molecule inhibitor, suppresses NRF2-MAF binding, enhancing chemosensitivity in NSCLC, while ATRA enhances

sensitivity in neuroblastoma and leukaemia cells by repressing NRF2 transcription. In other lung cancer studies, the natural compound convallatoxin has been identified as a potent inhibitor of NRF2 activity.

Flavonoid luteolin has been found to inhibit NRF2-dependent antioxidant gene induction, increasing the chemosensitivity of NSCLC cells by suppressing NRF2 nuclear translocation and reducing intracellular glutathione (GSH) content. Luteolin also induces reactive oxygen species (ROS) overproduction, activating the intrinsic apoptotic pathway in colorectal cancer cells. These promising preclinical results have led to a phase-1 clinical trial evaluating luteolin's efficacy in patients with tongue squamous cell carcinoma.

ML385, a small molecule inhibitor, suppresses NRF2-MAF binding and enhances chemosensitivity in NSCLC cells, particularly in the context of KEAP1 inactivation. The vitamin A derivative, all-trans retinoic acid (ATRA), has been used successfully to enhance the sensitivity of chemoresistant neuroblastoma cells to bortezomib and increase the cytotoxic effects of arsenic trioxide in leukaemia cells. ATRA represses NRF2 transcription and prevents its nuclear translocation by promoting its association with the nuclear receptor RARα.

These findings suggest that strategic targeting of NRF2 and the induction of ferroptosis represent a multifaceted approach to cancer therapy, particularly where Tsc2 mutations are prevalent. By disrupting NRF2's role in chemoresistance and leveraging ferroptosis mechanisms, it is possible to enhance the efficacy of existing treatments and develop novel therapeutic strategies. Continued research and clinical trials are essential to fully realize the potential of these approaches in combating various types of cancers.

6.7 Limitations

As with all studies findings inevitably beg further questions or further ratification of the observations made by using alternative methods, extended parameters or further statistical power. This study has made several important observations which are currently being built upon through extended studies but some of limitations of the data presented here are discussed here.

While studies have highlighted that mTORC2 is unlikely to be active within the TSC model cells utilised within this work, there are conflicting reports on whether mTORC2 activity is enhanced or repressed in TSC cells and lesions and this had not been addressed in the current thesis. Park et al. (2023) observed that HeLa cells in which *Tsc2* was knocked down, insulin stimulated increase in mTORC2 kinase activity was significantly blunted relative to that observed in control HeLa cells. These findings were substantiated in the *Tsc2 (−/−)* MEF cells. The authors confirmed these findings were unlikely the result of feedback inhibition of mTORC2 by mTORC1 through the use of siRNA targeting of RAPTOR in *Tsc2 (−/−)* MEF cells. RAPTOR knockdown did not restore the blunted kinase activity of mTORC2 in response to insulin stimulation within these cells. Further research by Huang et al. (2009) founds that several mTORC2 mediated phosphorylation events are disrupted in both *Tsc2* deficient cells and lesions. Therefore, within both the Tsc2 deficient MEF and Tsc2 *(−/−)* ELT3 cell lines utilised by the present work, loss of Tsc2 itself likely hampers growth factor signalling to mTORC2 outside of the inhibitory role of mTORC1 hyperactivity to mTORC2.

While NRF2 nuclear translocation at 6 hours did yield distinct differences between the Tsc2 deficient and expressing cells it would be salient to increase and extend the interrogation timepoints to establish the detailed kinetics of nrf2 activity in the differing cells upon

ferroptosis inducer exposure. Similarly, ROS contributions to ferroptosis between the cell lines would be better determined through increased timepoints over 24h.

Aside from the limitations already discussed, there are important limitations to this research that should be considered when interpreting the findings of this thesis. The use of MEF and ELT3 cell lines in which *Tsc2* has been re-expressed as a control presents with some disadvantages. Firstly, these cells are not a true 'healthy' control, nor are they heterozygous for functional *Tsc2*, as would typically be the case for cells from non-lesion tissue in TSC patients. Secondly, *Tsc2* was over-expressed within these MEF and ELT3 cells, and therefore expression of Tsc2 protein likely does not reflect what would be expected in *Tsc2* competent cells. Whilst the FBS concentrations used for cell culture in the growth assays described in chapter 3 were deemed necessary for proliferation and growth of those cells, there are issues with including FBS in the experimental design. General problems with FBS include that FBS concentrations for optimal cell growth do not necessarily reflect the normal function or signalling environment for a given cell line. Additionally, the constituent signalling factors present in FBS, represent a black box, in that for example which growth factor and cytokines are present in the FBS and ay what concentrations is unknown. And therefore, it is very likely many signalling pathways are activated in the TSC model cell lines by the presence of FBS. Compounding this issue, is that given the animal origin of FBS, it is highly likely there was batch variability between FBS lots used for cell culture over the course of research for this thesis. Another problem with using FBS in regard to studying mTOR signalling, is there will be enhanced growth factor signalling to both mTORC1 and mTORC2 complexes and inhibition of the Tsc1/Tsc2 complex in *Tsc2* positive cells. Activation of mTORC2 would likely enhance pro-survival and proliferation signalling pathways, which could have affected the findings throughout the research for this thesis. Another important limitation of the present work concerns the concentrations of drugs that were used. Drug titrations for the inhibitors used to target proteins in the specific cell lines

used within this thesis, under the specific culture conditions, were not performed. The concentrations of rapamycin and Ku-0063794 that are effective in inhibiting mTORC1 in TSC model cell lines are well documented. Within the present work mTORC2 and autophagy activity was not assayed within the TSC cell lines. Inclusion of FBS in cell culture media likely would promote enhanced growth factor signalling, which could activate mTORC2, especially through the PI3K signalling pathway. mTORC2 therefore could be affecting cell signalling readouts and phenotypes within the AML and MEF cell lines. As described previously within this chapter, mTORC2 activity is likely repressed, and growth factor signalling to mTORC2 impaired, within the *Tsc2* deficient MEF and Tsc2 *(−/−)* ELT3 cells. However, without upstream and downstream markers of mTORC2 activity, such as mTORC2 specific Akt1, AMPK and PKCα phosphorylation, the status of mTORC2 and therefore its impact on potential findings cannot be concluded with any degree of certainty. Without actually quantifying ROS, treatment of *Tsc2* deficient cells with the aforementioned compounds was assumed to modulate the redox environment of these cells but was not firmly proven.

6.8 Research Impact

Targeting ferroptosis in *Tsc2* mutation model cell lines represents a promising frontier in the quest for more effective treatments for Tuberous Sclerosis Complex (TSC). This approach leverages the unique vulnerabilities of *Tsc2*-deficient cells, which exhibit altered oxidative and iron metabolism. These cells' reliance on iron-dependent lipid peroxidation for survival presents an opportunity to induce ferroptosis, a form of regulated cell death distinct from apoptosis and necrosis. Researchers aim to exploit these metabolic disruptions to develop novel therapeutic strategies that go beyond the capabilities of current mTOR inhibitors. This could potentially improve patient outcomes and pave the way for new cancer therapy avenues,

as the mechanisms underlying ferroptosis resistance in *Tsc2*-deficient cells are likely to yield significant advancements in biomedical research and clinical practice.

Research into combinatorial treatments that employ ferroptosis inducers and antioxidant pathway inhibitors are justified based on the new data presented in this thesis and that originating elsewhere in the literature. With several components and interacting factors, investigating metabolic pathway perturbations and ferroptosis in *Tsc2*-deficient cells can uncover new biomarkers and druggable targets, such as components of the NRF2 pathway or iron metabolism regulators. These insights can guide the development of targeted therapies not only for TSC but also for other cancers with similar metabolic dysregulations.

To fully realize the potential of ferroptosis-targeted therapies in TSC, several research directions need to be pursued. Preclinical studies are crucial to assess the efficacy and safety of ferroptosis inducers in Tsc2-deficient models. This includes evaluating different ferroptosis inducers, such as Erastin and RSL3, in combination with NRF2, FSP1 inhibitors. Comprehensive *in vitro* and *in vivo* studies will help determine the best therapeutic combinations and dosages.

Mechanistic studies are also essential to further elucidate the molecular mechanisms by which *Tsc2* mutations influence ferroptosis sensitivity. Understanding the interplay between mTORC1/AMPK signalling, NRF2 and FSP1 antioxidant pathways activation, and iron metabolism is crucial. For instance, NRF2 and FSP1 activation can enhance the expression of antioxidant genes like SLC7A11 and GPX4 respectively, supporting glutathione synthesis and helping neutralize lipid peroxides. Targeting these pathways in *Tsc2*-deficient cells could disrupt this protective mechanism, sensitizing them to ferroptosis.

Clinical translation of these findings will require identifying suitable biomarkers for patient stratification and monitoring treatment response during clinical trials. Optimizing drug delivery methods to target ferroptosis in TSC lesions without affecting normal tissues is

essential for minimizing side effects. Additionally, understanding the context-specific effects of AMPK activation in ferroptosis regulation is vital, as AMPK plays a dual role in ferroptosis. Energy stress-mediated AMPK activation could either resist ferroptosis and promote tumour survival through the inhibition of unsaturated fatty acid synthesis or enhance ferroptosis and suppress tumour survival through the inhibition of protein biosynthesis or regulation of ferroptosis-related enzymes.

In conclusion, targeting ferroptosis in *Tsc2* mutation model cell lines opens new avenues for therapeutic intervention in TSC. By focusing on the vulnerabilities of *Tsc2*-deficient cells, such as their altered oxidative and iron metabolism, researchers can develop novel strategies to manage TSC more effectively and improve patient outcomes. This approach not only addresses the limitations of current mTOR inhibitors but also provides a framework for understanding and treating other cancers with similar metabolic dysregulations. As research in this area progresses, it is expected to yield significant advancements in biomedical research and clinical practice, ultimately benefiting TSC, TSC-related cancer patients and those suffering from related diseases.

6.9 Future work

Future research should focus on several critical areas to further elucidate the mechanisms of ferroptosis resistance and develop effective therapeutic strategies for *Tsc2*-deficient cancers. First, the exploration of alternative mTOR inhibitors beyond Rapamycin, such as Torin and Everolimus, should be prioritized to assess their potential in enhancing ferroptosis sensitivity. Investigating the role of autophagy in *Tsc2*-deficient cells will provide insights into additional pathways that might be targeted to overcome resistance. Additionally, extending studies to human cells and various other cell types will help validate these findings across different biological systems. Understanding the detailed mechanisms by which AMPK modulates ferroptosis, particularly through pathways such as SIRT3 and the cadherin-NE2-Hippo-YAP axis, is crucial. Measuring reactive oxygen species (ROS) at different time points will elucidate the dynamics of ferroptosis induction. Evaluating other NRF2 inhibitors at lower, safer doses and conducting dose-response studies for FSP1 inhibitors will refine therapeutic approaches. To confirm the role of NRF2 in ferroptosis regulation in *Tsc2*-deficient cells, future research should include silencing NRF2 using siRNA (small interfering RNA) techniques. This approach will allow us to specifically target and reduce NRF2 expression, providing direct evidence of its involvement in ferroptosis resistance. Moreover, inhibiting other signalling pathways that contribute to ferroptosis sensitivity independently of mTORC1 will broaden the scope of potential treatments. Optimizing the combination of NRF2 inhibitors with ferroptosis inducers, determining effective dosing regimens, and identifying biomarkers for patient response are essential. Conducting clinical trials to evaluate the safety and efficacy of these combination therapies in cancers with known *Tsc2* mutations and high NRF2 activity will be critical. These studies should also investigate the influence of different stress conditions and metabolic states on these pathways, ultimately identifying additional targets to enhance treatment outcomes.

6.10 Conclusion

The aim of this thesis was to identify the mechanisms behind ferroptosis drug resistance in the context of *Tsc2* loss and to discover novel drug combinations that can sensitize *Tsc2*-deficient cells to ferroptosis, thereby overcoming this resistance. This study revealed that Tsc2 deficiency in MEF and ELT3 manifest ferroptosis resistance relative to Tsc2 expressing counterparts. Interestingly, activation of AMPK, rather than inhibition of mTORC1 hyperactivity, was found to sensitize these cells to ferroptosis. The resistance mechanism in *Tsc2*-deficient cells also involved the activation of the NRF2 antioxidant pathway, with additional contributions from the FSP1 pathway. Combination treatment of the NRF2 inhibitor Trigonelline and FSP1 inhibitor, iFSP1, with ferroptosis inducers (Erastin and RSL3) effectively reduced resistance in *Tsc2* deficient cell lines. Gene expression data further highlighted altered NRF2 target gene expression in TSC tumours and cell lines. Ferroptosis related gene expression was also altered in TSC deficiency among different tumours but, intriguingly, the altered ferroptosis genes varied between sample types.

These findings highlight that antioxidant pathways and ferroptosis-related genes, and their products are candidate therapeutic targets that can be exploited in *Tsc2*-deficiency-driven ferroptosis resistance. Prior to this study, none of these combinations had been tested in a TSC-based environment, and thus, this study represents the first supporting evidence for their potential therapeutic exploitation to overcome ferroptosis drug resistance in *Tsc2*-deficient cancers.

References

ADEDOYIN, O., BODDU, R., TRAYLOR, A., LEVER, J. M., BOLISETTY, S., GEORGE, J. F. & AGARWAL, A. 2018. Heme oxygenase-1 mitigates ferroptosis in renal proximal tubule cells. *Am J Physiol Renal Physiol,* 314**,** F702-F714.

ADZAVON, K. P., ZHAO, W., HE, X. & SHENG, W. 2024. Ferroptosis resistance in cancer cells: nanoparticles for combination therapy as a solution. *Front Pharmacol,* 15**,** 1416382.

AGUIAR JUNIOR, S., OLIVEIRA, M. M., SILVA, D., MELLO, C. A. L., CALSAVARA, V. F. & CURADO, M. P. 2020. Survival of Patients with Colorectal Cancer in a Cancer Center. *Arq Gastroenterol,* 57**,** 172-177.

ALBORZINIA, H., FLOREZ, A. F., KRETH, S., BRUCKNER, L. M., YILDIZ, U., GARTLGRUBER, M., ODONI, D. I., POSCHET, G., GARBOWICZ, K., SHAO, C., KLEIN, C., MEIER, J., ZEISBERGER, P., NADLER-HOLLY, M., ZIEHM, M., PAUL, F., BURHENNE, J., BELL, E., SHAIKHKARAMI, M., WURTH, R., STAINCZYK, S. A., WECHT, E. M., KRETH, J., BUTTNER, M., ISHAQUE, N., SCHLESNER, M., NICKE, B., STRESEMANN, C., LLAMAZARES-PRADA, M., REILING, J. H., FISCHER, M., AMIT, I., SELBACH, M., HERRMANN, C., WOLFL, S., HENRICH, K. O., HOFER, T., TRUMPP, A. & WESTERMANN, F. 2022. MYCN mediates cysteine addiction and sensitizes neuroblastoma to ferroptosis. *Nat Cancer,* 3**,** 471-485.

ALEXANDER, A., CAI, S. L., KIM, J., NANEZ, A., SAHIN, M., MACLEAN, K. H., INOKI, K., GUAN, K. L., SHEN, J., PERSON, M. D., KUSEWITT, D., MILLS, G. B., KASTAN, M. B. & WALKER, C. L. 2010. ATM signals to TSC2 in the cytoplasm to regulate mTORC1 in response to ROS. *Proc Natl Acad Sci U S A,* 107**,** 4153-8.

ALI, E. S., MITRA, K., AKTER, S., RAMPROSHAD, S., MONDAL, B., KHAN, I. N., ISLAM, M. T., SHARIFI-RAD, J., CALINA, D. & CHO, W. C. 2022. Recent advances and limitations of mTOR inhibitors in the treatment of cancer. *Cancer Cell Int,* 22**,** 284.

ALMAHI, W. A., YU, K. N., MOHAMMED, F., KONG, P. & HAN, W. 2022. Hemin enhances radiosensitivity of lung cancer cells through ferroptosis. *Exp Cell Res,* 410**,** 112946.

ALMEIDA LIMA, K., OSAWA, I. Y. A., RAMALHO, M. C. C., DE SOUZA, I., GUEDES, C. B., SOUZA FILHO, C. H. D., MONTEIRO, L. K. S., LATANCIA, M. T. & ROCHA, C. R. R. 2023. Temozolomide Resistance in Glioblastoma by NRF2: Protecting the Evil. *Biomedicines,* 11.

ANANDHAN, A., DODSON, M., SHAKYA, A., CHEN, J., LIU, P., WEI, Y., TAN, H., WANG, Q., JIANG, Z., YANG, K., GARCIA, J. G., CHAMBERS, S. K., CHAPMAN, E., OOI, A., YANG-HARTWICH, Y., STOCKWELL, B. R. & ZHANG, D. D. 2023. NRF2 controls iron homeostasis and ferroptosis through HERC2 and VAMP8. *Sci Adv,* 9**,** eade9585.

ANTHONYMUTHU, T. S., TYURINA, Y. Y., SUN, W. Y., MIKULSKA-RUMINSKA, K., SHRIVASTAVA, I. H., TYURIN, V. A., CINEMRE, F. B., DAR, H. H., VANDEMARK, A. P., HOLMAN, T. R., SADOVSKY, Y., STOCKWELL, B. R.,

HE, R. R., BAHAR, I., BAYIR, H. & KAGAN, V. E. 2021. Resolving the paradox of ferroptotic cell death: Ferrostatin-1 binds to 15LOX/PEBP1 complex, suppresses generation of peroxidized ETE-PE, and protects against ferroptosis. *Redox Biol,* 38**,** 101744.

ARENA, A., ZIMMER, T. S., VAN SCHEPPINGEN, J., KOROTKOV, A., ANINK, J. J., MUHLEBNER, A., JANSEN, F. E., VAN HECKE, W., SPLIET, W. G., VAN RIJEN, P. C., VEZZANI, A., BAAYEN, J. C., IDEMA, S., IYER, A. M., PERLUIGI, M., MILLS, J. D., VAN VLIET, E. A. & ARONICA, E. 2019. Oxidative stress and inflammation in a spectrum of epileptogenic cortical malformations: molecular insights into their interdependence. *Brain Pathol,* 29**,** 351-365.

ASHRAF, A., JEANDRIENS, J., PARKES, H. G. & SO, P. W. 2020. Iron dyshomeostasis, lipid peroxidation and perturbed expression of cystine/glutamate antiporter in Alzheimer's disease: Evidence of ferroptosis. *Redox Biol,* 32**,** 101494.

ASRANI, K., MURALI, S., LAM, B., NA, C. H., PHATAK, P., SOOD, A., KAUR, H., KHAN, Z., NOE, M., ANCHOORI, R. K., TALBOT, C. C., JR., SMITH, B., SKARO, M. & LOTAN, T. L. 2019. mTORC1 feedback to AKT modulates lysosomal biogenesis through MiT/TFE regulation. *J Clin Invest,* 129**,** 5584-5599.

BABA, Y., HIGA, J. K., SHIMADA, B. K., HORIUCHI, K. M., SUHARA, T., KOBAYASHI, M., WOO, J. D., AOYAGI, H., MARH, K. S., KITAOKA, H. & MATSUI, T. 2018. Protective effects of the mechanistic target of rapamycin against excess iron and ferroptosis in cardiomyocytes. *Am J Physiol Heart Circ Physiol,* 314**,** H659-H668.

BACKER, J. M. 2008. The regulation and function of Class III PI3Ks: novel roles for Vps34. *Biochem J,* 410**,** 1-17.

BADGLEY, M. A., KREMER, D. M., MAURER, H. C., DELGIORNO, K. E., LEE, H. J., PUROHIT, V., SAGALOVSKIY, I. R., MA, A., KAPILIAN, J., FIRL, C. E. M., DECKER, A. R., SASTRA, S. A., PALERMO, C. F., ANDRADE, L. R., SAJJAKULNUKIT, P., ZHANG, L., TOLSTYKA, Z. P., HIRSCHHORN, T., LAMB, C., LIU, T., GU, W., SEELEY, E. S., STONE, E., GEORGIOU, G., MANOR, U., IUGA, A., WAHL, G. M., STOCKWELL, B. R., LYSSIOTIS, C. A. & OLIVE, K. P. 2020. Cysteine depletion induces pancreatic tumor ferroptosis in mice. *Science,* 368**,** 85-89.

BAO, Z., HUA, L., YE, Y., WANG, D., LI, C., XIE, Q., WAKIMOTO, H., GONG, Y. & JI, J. 2021. MEF2C silencing downregulates NF2 and E-cadherin and enhances Erastin-induced ferroptosis in meningioma. *Neuro Oncol,* 23**,** 2014-2027.

BARAYEU, U., SCHILLING, D., EID, M., XAVIER DA SILVA, T. N., SCHLICKER, L., MITRESKA, N., ZAPP, C., GRATER, F., MILLER, A. K., KAPPL, R., SCHULZE, A., FRIEDMANN ANGELI, J. P. & DICK, T. P. 2023. Hydropersulfides inhibit lipid peroxidation and ferroptosis by scavenging radicals. *Nat Chem Biol,* 19**,** 28-37.

BATTAGLIA, A. M., SACCO, A., PERROTTA, I. D., FANIELLO, M. C., SCALISE, M., TORELLA, D., LEVI, S., COSTANZO, F. & BIAMONTE, F. 2022. Iron Administration Overcomes Resistance to Erastin-Mediated Ferroptosis in Ovarian Cancer Cells. *Front Oncol,* 12**,** 868351.

BAYEVA, M., GHEORGHIADE, M. & ARDEHALI, H. 2013. Mitochondria as a therapeutic target in heart failure. *J Am Coll Cardiol,* 61**,** 599-610.

BAYEVA, M., KHECHADURI, A., PUIG, S., CHANG, H. C., PATIAL, S., BLACKSHEAR, P. J. & ARDEHALI, H. 2012. mTOR regulates cellular iron homeostasis through tristetraprolin. *Cell Metab,* 16**,** 645-57.

BEATTY, A., SINGH, T., TYURINA, Y. Y., TYURIN, V. A., SAMOVICH, S., NICOLAS, E., MASLAR, K., ZHOU, Y., CAI, K. Q., TAN, Y., DOLL, S., CONRAD, M., SUBRAMANIAN, A., BAYIR, H., KAGAN, V. E., RENNEFAHRT, U. & PETERSON, J. R. 2021. Ferroptotic cell death triggered by conjugated linolenic acids is mediated by ACSL1. *Nat Commun,* 12**,** 2244.

BEN-SAHRA, I. & MANNING, B. D. 2017. mTORC1 signaling and the metabolic control of cell growth. *Curr Opin Cell Biol,* 45**,** 72-82.

BERSUKER, K., HENDRICKS, J. M., LI, Z., MAGTANONG, L., FORD, B., TANG, P. H., ROBERTS, M. A., TONG, B., MAIMONE, T. J., ZONCU, R., BASSIK, M. C., NOMURA, D. K., DIXON, S. J. & OLZMANN, J. A. 2019. The CoQ oxidoreductase FSP1 acts parallel to GPX4 to inhibit ferroptosis. *Nature,* 575**,** 688-692.

BERTHELOOT, D., LATZ, E. & FRANKLIN, B. S. 2021. Necroptosis, pyroptosis and apoptosis: an intricate game of cell death. *Cell Mol Immunol,* 18**,** 1106-1121.

BERTRAND, R. L. 2017. Iron accumulation, glutathione depletion, and lipid peroxidation must occur simultaneously during ferroptosis and are mutually amplifying events. *Med Hypotheses,* 101**,** 69-74.

BERTUCCI, A., BERTUCCI, F. & GONCALVES, A. 2023. Phosphoinositide 3-Kinase (PI3K) Inhibitors and Breast Cancer: An Overview of Current Achievements. *Cancers (Basel),* 15.

BJORNSSON, J., SHORT, M. P., KWIATKOWSKI, D. J. & HENSKE, E. P. 1996. Tuberous sclerosis-associated renal cell carcinoma. Clinical, pathological, and genetic features. *Am J Pathol,* 149**,** 1201-8.

BORQUEZ, D. A. & URRUTIA, P. J. 2024. Iron regulatory protein 1: the deadly switch of ferroptosis. *Neural Regen Res,* 19**,** 477-478.

BOU ANTOUN, N. & CHIONI, A. M. 2023. Dysregulated Signalling Pathways Driving Anticancer Drug Resistance. *Int J Mol Sci,* 24.

BOULBES, D. R., SHAIKEN, T. & SARBASSOV DOS, D. 2011. Endoplasmic reticulum is a main localization site of mTORC2. *Biochem Biophys Res Commun,* 413**,** 46-52.

BOWERS, D. C., RAJARAM, V., KARAJANNIS, M. A., GARDNER, S. L., SU, J. M., BAXTER, P., PARTAP, S. & KLESSE, L. J. 2023. Phase II study of everolimus for recurrent or progressive pediatric ependymoma. *Neurooncol Adv,* 5**,** vdad011.

BROWN, E. J., ALBERS, M. W., SHIN, T. B., ICHIKAWA, K., KEITH, C. T., LANE, W. S. & SCHREIBER, S. L. 1994. A mammalian protein targeted by G1-arresting rapamycin-receptor complex. *Nature,* 369**,** 756-8.

BROWNE, G. J. & PROUD, C. G. 2004. A novel mTOR-regulated phosphorylation site in elongation factor 2 kinase modulates the activity of the kinase and its binding to calmodulin. *Mol Cell Biol,* 24**,** 2986-97.

BRUGAROLAS, J. B., VAZQUEZ, F., REDDY, A., SELLERS, W. R. & KAELIN, W. G., JR. 2003. TSC2 regulates VEGF through mTOR-dependent and -independent pathways. *Cancer Cell,* 4**,** 147-58.

CAI, X., RUAN, L., WANG, D., ZHANG, J., TANG, J., GUO, C., DOU, R., ZHOU, M., HU, Y. & CHEN, J. 2024. Boosting chemotherapy of bladder cancer cells by

ferroptosis using intelligent magnetic targeting nanoparticles. *Colloids Surf B Biointerfaces,* 234**,** 113664.
CAO, J. Y. & DIXON, S. J. 2016. Mechanisms of ferroptosis. *Cell Mol Life Sci,* 73**,** 2195-209.
CEN, J., ZHU, H., HONG, C., ZHANG, X., LIU, S., YANG, B., YU, Y., WEN, Y., CAO, J. & CHEN, W. 2024. Synthesis and structure-activity optimization of hydroxypyridinones against rhabdomyolysis-induced acute kidney injury. *Eur J Med Chem,* 263**,** 115933.
CHAN, J. Y. & KWONG, M. 2000. Impaired expression of glutathione synthetic enzyme genes in mice with targeted deletion of the Nrf2 basic-leucine zipper protein. *Biochim Biophys Acta,* 1517**,** 19-26.
CHANG, K., CHEN, Y., ZHANG, X., ZHANG, W., XU, N., ZENG, B., WANG, Y., FENG, T., DAI, B., XU, F., YE, D. & WANG, C. 2023. DPP9 Stabilizes NRF2 to Suppress Ferroptosis and Induce Sorafenib Resistance in Clear Cell Renal Cell Carcinoma. *Cancer Res,* 83**,** 3940-3955.
CHEN, C., LIU, Y., LIU, R., IKENOUE, T., GUAN, K. L., LIU, Y. & ZHENG, P. 2008. TSC-mTOR maintains quiescence and function of hematopoietic stem cells by repressing mitochondrial biogenesis and reactive oxygen species. *J Exp Med,* 205**,** 2397-408.
CHEN, G. Y., O'LEARY, B. R., DU, J., CARROLL, R. S., STEERS, G. J., BUETTNER, G. R. & CULLEN, J. J. 2024. Pharmacologic Ascorbate Radiosensitizes Pancreatic Cancer but Radioprotects Normal Tissue: The Role of Oxidative Stress-Induced Lipid Peroxidation. *Antioxidants (Basel),* 13.
CHEN, P. H., WU, J., XU, Y., DING, C. C., MESTRE, A. A., LIN, C. C., YANG, W. H. & CHI, J. T. 2021a. Zinc transporter ZIP7 is a novel determinant of ferroptosis. *Cell Death Dis,* 12**,** 198.
CHEN, S., CHEN, Y., ZHANG, Y., KUANG, X., LIU, Y., GUO, M., MA, L., ZHANG, D. & LI, Q. 2020a. Iron Metabolism and Ferroptosis in Epilepsy. *Front Neurosci,* 14**,** 601193.
CHEN, X., YU, C., KANG, R. & TANG, D. 2020b. Iron Metabolism in Ferroptosis. *Front Cell Dev Biol,* 8**,** 590226.
CHEN, Y., CHEN, H., RHOAD, A. E., WARNER, L., CAGGIANO, T. J., FAILLI, A., ZHANG, H., HSIAO, C. L., NAKANISHI, K. & MOLNAR-KIMBER, K. L. 1994. A putative sirolimus (rapamycin) effector protein. *Biochem Biophys Res Commun,* 203**,** 1-7.
CHEN, Y., LI, Y., HUANG, L., DU, Y., GAN, F., LI, Y. & YAO, Y. 2021b. Antioxidative Stress: Inhibiting Reactive Oxygen Species Production as a Cause of Radioresistance and Chemoresistance. *Oxid Med Cell Longev,* 2021**,** 6620306.
CHEN YUTING, H. L., XIA JUNJIE, QIU YU, YI KE, WANG JINCHENG 2023. Research progress on the role of transcription factor T-bet in the pathogenesis of chronic obstructive pulmonary disease. *Basic & Clinical Medicine,* 43**,** 1322-1325.
CHEN, Z., WANG, W., ABDUL RAZAK, S. R., HAN, T., AHMAD, N. H. & LI, X. 2023. Ferroptosis as a potential target for cancer therapy. *Cell Death Dis,* 14**,** 460.
CHENG, J., FAN, Y. Q., LIU, B. H., ZHOU, H., WANG, J. M. & CHEN, Q. X. 2020. ACSL4 suppresses glioma cells proliferation via activating ferroptosis. *Oncol Rep,* 43**,** 147-158.

CHEONG, H. & KLIONSKY, D. J. 2015. mTORC1 maintains metabolic balance. *Cell Res,* 25**,** 1085-6.
CHEU, J. W., LEE, D., LI, Q., GOH, C. C., BAO, M. H., YUEN, V. W., ZHANG, M. S., YANG, C., CHAN, C. Y., TSE, A. P., SIT, G. F., LIU, C. X., NG, I. O., WONG, C. M. & WONG, C. C. 2023. Ferroptosis Suppressor Protein 1 Inhibition Promotes Tumor Ferroptosis and Anti-tumor Immune Responses in Liver Cancer. *Cell Mol Gastroenterol Hepatol,* 16**,** 133-159.
CHIANG, S. K., CHEN, S. E. & CHANG, L. C. 2018. A Dual Role of Heme Oxygenase-1 in Cancer Cells. *Int J Mol Sci,* 20.
CHIARINI, F., EVANGELISTI, C., MCCUBREY, J. A. & MARTELLI, A. M. 2015. Current treatment strategies for inhibiting mTOR in cancer. *Trends Pharmacol Sci,* 36**,** 124-35.
CHO, H. Y., GLADWELL, W., WANG, X., CHORLEY, B., BELL, D., REDDY, S. P. & KLEEBERGER, S. R. 2010. Nrf2-regulated PPARgamma expression is critical to protection against acute lung injury in mice. *Am J Respir Crit Care Med,* 182**,** 170-82.
CHONG, Z. Z. 2015. mTOR: A Novel Therapeutic Target for Diseases of Multiple Systems. *Curr Drug Targets,* 16**,** 1107-32.
COFFEY, N. J. & SIMON, M. C. 2024. Metabolic alterations in hereditary and sporadic renal cell carcinoma. *Nat Rev Nephrol,* 20**,** 233-250.
CONCHE, C., FINKELMEIER, F., PESIC, M., NICOLAS, A. M., BOTTGER, T. W., KENNEL, K. B., DENK, D., CETECI, F., MOHS, K., ENGEL, E., CANLI, O., DABIRI, Y., PEIFFER, K. H., ZEUZEM, S., SALINAS, G., LONGERICH, T., YANG, H. & GRETEN, F. R. 2023. Combining ferroptosis induction with MDSC blockade renders primary tumours and metastases in liver sensitive to immune checkpoint blockade. *Gut,* 72**,** 1774-1782.
COSIALLS, E., PACREAU, E., DURUEL, C., CECCACCI, S., ELHAGE, R., DESTERKE, C., ROGER, K., GUERRERA, C., DUCLOUX, R., SOUQUERE, S., PIERRON, G., NEMAZANYY, I., KELLY, M., DALMAS, E., CHANG, Y., GOFFIN, V., MEHRPOUR, M. & HAMAI, A. 2023. mTOR inhibition suppresses salinomycin-induced ferroptosis in breast cancer stem cells by ironing out mitochondrial dysfunctions. *Cell Death Dis,* 14**,** 744.
CUADRADO, A., ROJO, A. I., WELLS, G., HAYES, J. D., COUSIN, S. P., RUMSEY, W. L., ATTUCKS, O. C., FRANKLIN, S., LEVONEN, A. L., KENSLER, T. W. & DINKOVA-KOSTOVA, A. T. 2019. Therapeutic targeting of the NRF2 and KEAP1 partnership in chronic diseases. *Nat Rev Drug Discov,* 18**,** 295-317.
CURATOLO, P., MOAVERO, R. & DE VRIES, P. J. 2015. Neurological and neuropsychiatric aspects of tuberous sclerosis complex. *Lancet Neurol,* 14**,** 733-45.
DAI, E., MENG, L., KANG, R., WANG, X. & TANG, D. 2020. ESCRT-III-dependent membrane repair blocks ferroptosis. *Biochem Biophys Res Commun,* 522**,** 415-421.
DAZERT, E. & HALL, M. N. 2011. mTOR signaling in disease. *Curr Opin Cell Biol,* 23**,** 744-55.
DE SOUZA, I., MONTEIRO, L. K. S., GUEDES, C. B., SILVA, M. M., ANDRADE-TOMAZ, M., CONTIERI, B., LATANCIA, M. T., MENDES, D., PORCHIA, B., LAZARINI, M., GOMES, L. R. & ROCHA, C. R. R. 2022. High levels of NRF2

sensitize temozolomide-resistant glioblastoma cells to ferroptosis via ABCC1/MRP1 upregulation. *Cell Death Dis,* 13**,** 591.

DEAVER, J. W., LOPEZ, S. M., RYAN, P. J., NGHIEM, P. P., RIECHMAN, S. E. & FLUCKEY, J. D. 2020. Regulation of cellular anabolism by mTOR: or how I learned to stop worrying and love translation. *Sports Med Health Sci,* 2**,** 195-201.

DEMETRIADES, C., PLESCHER, M. & TELEMAN, A. A. 2016. Lysosomal recruitment of TSC2 is a universal response to cellular stress. *Nat Commun,* 7**,** 10662.

DI NARDO, A., WERTZ, M. H., KWIATKOWSKI, E., TSAI, P. T., LEECH, J. D., GREENE-COLOZZI, E., GOTO, J., DILSIZ, P., TALOS, D. M., CLISH, C. B., KWIATKOWSKI, D. J. & SAHIN, M. 2014. Neuronal Tsc1/2 complex controls autophagy through AMPK-dependent regulation of ULK1. *Hum Mol Genet,* 23**,** 3865-74.

DI, Y., ZHANG, X., WEN, X., QIN, J., YE, L., WANG, Y., SONG, M., WANG, Z. & HE, W. 2024. MAPK Signaling-Mediated RFNG Phosphorylation and Nuclear Translocation Restrain Oxaliplatin-Induced Apoptosis and Ferroptosis. *Adv Sci (Weinh),* 11**,** e2402795.

DIBBLE, C. C., ELIS, W., MENON, S., QIN, W., KLEKOTA, J., ASARA, J. M., FINAN, P. M., KWIATKOWSKI, D. J., MURPHY, L. O. & MANNING, B. D. 2012. TBC1D7 is a third subunit of the TSC1-TSC2 complex upstream of mTORC1. *Mol Cell,* 47**,** 535-46.

DIXON, S. J., LEMBERG, K. M., LAMPRECHT, M. R., SKOUTA, R., ZAITSEV, E. M., GLEASON, C. E., PATEL, D. N., BAUER, A. J., CANTLEY, A. M., YANG, W. S., MORRISON, B., 3RD & STOCKWELL, B. R. 2012. Ferroptosis: an iron-dependent form of nonapoptotic cell death. *Cell,* 149**,** 1060-72.

DIXON, S. J., PATEL, D. N., WELSCH, M., SKOUTA, R., LEE, E. D., HAYANO, M., THOMAS, A. G., GLEASON, C. E., TATONETTI, N. P., SLUSHER, B. S. & STOCKWELL, B. R. 2014. Pharmacological inhibition of cystine-glutamate exchange induces endoplasmic reticulum stress and ferroptosis. *Elife,* 3**,** e02523.

DIXON, S. J. & STOCKWELL, B. R. 2014. The role of iron and reactive oxygen species in cell death. *Nat Chem Biol,* 10**,** 9-17.

DIXON, S. J., WINTER, G. E., MUSAVI, L. S., LEE, E. D., SNIJDER, B., REBSAMEN, M., SUPERTI-FURGA, G. & STOCKWELL, B. R. 2015. Human Haploid Cell Genetics Reveals Roles for Lipid Metabolism Genes in Nonapoptotic Cell Death. *ACS Chem Biol,* 10**,** 1604-9.

DODD, K. M. & DUNLOP, E. A. 2016. Tuberous sclerosis--A model for tumour growth. *Semin Cell Dev Biol,* 52**,** 3-11.

DODD, K. M. & TEE, A. R. 2015. STAT3 and mTOR: co-operating to drive HIF and angiogenesis. *Oncoscience,* 2**,** 913-4.

DOLL, S., FREITAS, F. P., SHAH, R., ALDROVANDI, M., DA SILVA, M. C., INGOLD, I., GOYA GROCIN, A., XAVIER DA SILVA, T. N., PANZILIUS, E., SCHEEL, C. H., MOURAO, A., BUDAY, K., SATO, M., WANNINGER, J., VIGNANE, T., MOHANA, V., REHBERG, M., FLATLEY, A., SCHEPERS, A., KURZ, A., WHITE, D., SAUER, M., SATTLER, M., TATE, E. W., SCHMITZ, W., SCHULZE, A., O'DONNELL, V., PRONETH, B., POPOWICZ, G. M., PRATT, D. A., ANGELI, J. P. F. & CONRAD, M. 2019. FSP1 is a glutathione-independent ferroptosis suppressor. *Nature,* 575**,** 693-698.

DOLL, S., PRONETH, B., TYURINA, Y. Y., PANZILIUS, E., KOBAYASHI, S., INGOLD, I., IRMLER, M., BECKERS, J., AICHLER, M., WALCH, A., PROKISCH, H., TRUMBACH, D., MAO, G., QU, F., BAYIR, H., FULLEKRUG, J., SCHEEL, C. H., WURST, W., SCHICK, J. A., KAGAN, V. E., ANGELI, J. P. & CONRAD, M. 2017. ACSL4 dictates ferroptosis sensitivity by shaping cellular lipid composition. *Nat Chem Biol,* 13**,** 91-98.

DOLMA, S., LESSNICK, S. L., HAHN, W. C. & STOCKWELL, B. R. 2003. Identification of genotype-selective antitumor agents using synthetic lethal chemical screening in engineered human tumor cells. *Cancer Cell,* 3**,** 285-96.

DONG, H., FAN, Y., ZHANG, W., GU, N. & ZHANG, Y. 2019. Catalytic Mechanisms of Nanozymes and Their Applications in Biomedicine. *Bioconjug Chem,* 30**,** 1273-1296.

DU, R., CHENG, X., JI, J., LU, Y., XIE, Y., WANG, W., XU, Y. & ZHANG, Y. 2023. Mechanism of ferroptosis in a rat model of premature ovarian insufficiency induced by cisplatin. *Sci Rep,* 13**,** 4463.

DU, Y. & GUO, Z. 2022. Recent progress in ferroptosis: inducers and inhibitors. *Cell Death Discov,* 8**,** 501.

DUNLOP, E. A. & TEE, A. R. 2014. mTOR and autophagy: a dynamic relationship governed by nutrients and energy. *Semin Cell Dev Biol,* 36**,** 121-9.

DUVEL, K., YECIES, J. L., MENON, S., RAMAN, P., LIPOVSKY, A. I., SOUZA, A. L., TRIANTAFELLOW, E., MA, Q., GORSKI, R., CLEAVER, S., VANDER HEIDEN, M. G., MACKEIGAN, J. P., FINAN, P. M., CLISH, C. B., MURPHY, L. O. & MANNING, B. D. 2010. Activation of a metabolic gene regulatory network downstream of mTOR complex 1. *Mol Cell,* 39**,** 171-83.

EBRAHIMI-FAKHARI, D., MEYER, S., VOGT, T., PFOHLER, C. & MULLER, C. S. L. 2017. Dermatological manifestations of tuberous sclerosis complex (TSC). *J Dtsch Dermatol Ges,* 15**,** 695-700.

EFEYAN, A. & SABATINI, D. M. 2010. mTOR and cancer: many loops in one pathway. *Curr Opin Cell Biol,* 22**,** 169-76.

EHNINGER, D., DE VRIES, P. J. & SILVA, A. J. 2009. From mTOR to cognition: molecular and cellular mechanisms of cognitive impairments in tuberous sclerosis. *J Intellect Disabil Res,* 53**,** 838-51.

EIJKEMANS, M. J., VAN DER WAL, W., REIJNDERS, L. J., ROES, K. C., VAN WAALWIJK VAN DOORN-KHOSROVANI, S. B., PELLETIER, C., MAGESTRO, M. & ZONNENBERG, B. 2015. Long-term Follow-up Assessing Renal Angiomyolipoma Treatment Patterns, Morbidity, and Mortality: An Observational Study in Tuberous Sclerosis Complex Patients in the Netherlands. *Am J Kidney Dis,* 66**,** 638-45.

ELING, N., REUTER, L., HAZIN, J., HAMACHER-BRADY, A. & BRADY, N. R. 2015. Identification of artesunate as a specific activator of ferroptosis in pancreatic cancer cells. *Oncoscience,* 2**,** 517-32.

ELLINGHAUS, P., HEISLER, I., UNTERSCHEMMANN, K., HAERTER, M., BECK, H., GRESCHAT, S., EHRMANN, A., SUMMER, H., FLAMME, I., OEHME, F., THIERAUCH, K., MICHELS, M., HESS-STUMPP, H. & ZIEGELBAUER, K. 2013. BAY 87-2243, a highly potent and selective inhibitor of hypoxia-induced gene activation has antitumor activities by inhibition of mitochondrial complex I. *Cancer Med,* 2**,** 611-24.

FEICHT, J. & JANSEN, R. P. 2024. The high-density lipoprotein binding protein HDLBP is an unusual RNA-binding protein with multiple roles in cancer and disease. *RNA Biol,* 21**,** 1-10.

FENG, D., SHI, X., XIONG, Q., ZHANG, F., LI, D., WEI, W. & YANG, L. 2022. A Ferroptosis-Related Gene Prognostic Index Associated With Biochemical Recurrence and Radiation Resistance for Patients With Prostate Cancer Undergoing Radical Radiotherapy. *Front Cell Dev Biol,* 10**,** 803766.

FENG, Y., MADUNGWE, N. B., IMAM ALIAGAN, A. D., TOMBO, N. & BOPASSA, J. C. 2019. Liproxstatin-1 protects the mouse myocardium against ischemia/reperfusion injury by decreasing VDAC1 levels and restoring GPX4 levels. *Biochem Biophys Res Commun,* 520**,** 606-611.

FERNANDEZ, Y., ANGLADE, F. & MITJAVILA, S. 2000. Paraquat and iron-dependent lipid peroxidation. NADPH versus NADPH-generating systems. *Biol Trace Elem Res,* 74**,** 191-201.

FIDALGO DA SILVA, E., FONG, J., ROYE-AZAR, A., NADI, A., DROUILLARD, C., PILLON, A. & PORTER, L. A. 2021. Beyond Protein Synthesis; The Multifaceted Roles of Tuberin in Cell Cycle Regulation. *Front Cell Dev Biol,* 9**,** 806521.

FINGAR, D. C. & BLENIS, J. 2004. Target of rapamycin (TOR): an integrator of nutrient and growth factor signals and coordinator of cell growth and cell cycle progression. *Oncogene,* 23**,** 3151-71.

FIORENTINO, F., NOCENTINI, A., ROTILI, D., SUPURAN, C. T. & MAI, A. 2023. Antihistamines, phenothiazine-based antipsychotics, and tricyclic antidepressants potently activate pharmacologically relevant human carbonic anhydrase isoforms II and VII. *J Enzyme Inhib Med Chem,* 38**,** 2188147.

FLOROS, K. V., CAI, J., JACOB, S., KURUPI, R., FAIRCHILD, C. K., SHENDE, M., COON, C. M., POWELL, K. M., BELVIN, B. R., HU, B., PUCHALAPALLI, M., RAMAMOORTHY, S., SWIFT, K., LEWIS, J. P., DOZMOROV, M. G., GLOD, J., KOBLINSKI, J. E., BOIKOS, S. A. & FABER, A. C. 2021. MYCN-Amplified Neuroblastoma Is Addicted to Iron and Vulnerable to Inhibition of the System Xc-/Glutathione Axis. *Cancer Res,* 81**,** 1896-1908.

FOUZDER, C., MUKHUTY, A., MUKHERJEE, S., MALICK, C. & KUNDU, R. 2021. Trigonelline inhibits Nrf2 via EGFR signalling pathway and augments efficacy of Cisplatin and Etoposide in NSCLC cells. *Toxicol In Vitro,* 70**,** 105038.

FRANZ, D. N., BELOUSOVA, E., SPARAGANA, S., BEBIN, E. M., FROST, M., KUPERMAN, R., WITT, O., KOHRMAN, M. H., FLAMINI, J. R., WU, J. Y., CURATOLO, P., DE VRIES, P. J., WHITTEMORE, V. H., THIELE, E. A., FORD, J. P., SHAH, G., CAUWEL, H., LEBWOHL, D., SAHMOUD, T. & JOZWIAK, S. 2013. Efficacy and safety of everolimus for subependymal giant cell astrocytomas associated with tuberous sclerosis complex (EXIST-1): a multicentre, randomised, placebo-controlled phase 3 trial. *Lancet,* 381**,** 125-32.

FRAPPAOLO, A. & GIANSANTI, M. G. 2023. Using Drosophila melanogaster to Dissect the Roles of the mTOR Signaling Pathway in Cell Growth. *Cells,* 12.

FRASER, S. T., MIDWINTER, R. G., BERGER, B. S. & STOCKER, R. 2011. Heme Oxygenase-1: A Critical Link between Iron Metabolism, Erythropoiesis, and Development. *Adv Hematol,* 2011**,** 473709.

FRIEDMANN ANGELI, J. P., SCHNEIDER, M., PRONETH, B., TYURINA, Y. Y., TYURIN, V. A., HAMMOND, V. J., HERBACH, N., AICHLER, M., WALCH, A., EGGENHOFER, E., BASAVARAJAPPA, D., RADMARK, O., KOBAYASHI, S., SEIBT, T., BECK, H., NEFF, F., ESPOSITO, I., WANKE, R., FORSTER, H., YEFREMOVA, O., HEINRICHMEYER, M., BORNKAMM, G. W., GEISSLER, E. K., THOMAS, S. B., STOCKWELL, B. R., O'DONNELL, V. B., KAGAN, V. E., SCHICK, J. A. & CONRAD, M. 2014. Inactivation of the ferroptosis regulator Gpx4 triggers acute renal failure in mice. *Nat Cell Biol,* 16**,** 1180-91.

FU, W. & HALL, M. N. 2020. Regulation of mTORC2 Signaling. *Genes (Basel),* 11.

FUHRMANN, D. C., MONDORF, A., BEIFUSS, J., JUNG, M. & BRUNE, B. 2020. Hypoxia inhibits ferritinophagy, increases mitochondrial ferritin, and protects from ferroptosis. *Redox Biol,* 36**,** 101670.

FUJIMOTO, Y., MORITA, T. Y., OHASHI, A., HAENO, H., HAKOZAKI, Y., FUJII, M., KASHIMA, Y., KOBAYASHI, S. S. & MUKOHARA, T. 2020. Combination treatment with a PI3K/Akt/mTOR pathway inhibitor overcomes resistance to anti-HER2 therapy in PIK3CA-mutant HER2-positive breast cancer cells. *Sci Rep,* 10**,** 21762.

GALLEGO-MURILLO, J. S., YAGCI, N., PINHO, E. M., WAHL, S. A., VAN DEN AKKER, E. & VON LINDERN, M. 2023. Iron-loaded deferiprone can support full hemoglobinization of cultured red blood cells. *Sci Rep,* 13**,** 6960.

GAO, A. M., ZHANG, X. Y. & KE, Z. P. 2017. Apigenin sensitizes BEL-7402/ADM cells to doxorubicin through inhibiting miR-101/Nrf2 pathway. *Oncotarget,* 8**,** 82085-82091.

GAO, G., XIE, Z., LI, E. W., YUAN, Y., FU, Y., WANG, P., ZHANG, X., QIAO, Y., XU, J., HOLSCHER, C., WANG, H. & ZHANG, Z. 2021a. Dehydroabietic acid improves nonalcoholic fatty liver disease through activating the Keap1/Nrf2-ARE signaling pathway to reduce ferroptosis. *J Nat Med,* 75**,** 540-552.

GAO, J., ZHOU, H., ZHAO, Y., LU, L., ZHANG, J., CHENG, W., SONG, X., ZHENG, Y., CHEN, C. & TANG, J. 2021b. Time-course effect of ultrasmall superparamagnetic iron oxide nanoparticles on intracellular iron metabolism and ferroptosis activation. *Nanotoxicology,* 15**,** 366-379.

GAO, M., MONIAN, P., PAN, Q., ZHANG, W., XIANG, J. & JIANG, X. 2016. Ferroptosis is an autophagic cell death process. *Cell Res,* 26**,** 1021-32.

GAO, R., WANG, J., HUANG, J., WANG, T., GUO, L., LIU, W., GUAN, J., LIANG, D., MENG, Q. & PAN, H. 2024. FSP1-mediated ferroptosis in cancer: from mechanisms to therapeutic applications. *Apoptosis*.

GAO, X., ZHANG, Y., ARRAZOLA, P., HINO, O., KOBAYASHI, T., YEUNG, R. S., RU, B. & PAN, D. 2002. Tsc tumour suppressor proteins antagonize amino-acid-TOR signalling. *Nat Cell Biol,* 4**,** 699-704.

GAO, Z., ZHANG, Z., GU, D., LI, Y., ZHANG, K., DONG, X., LIU, L., ZHANG, J., CHEN, J., WU, D. & ZENG, M. 2022. Hemin mitigates contrast-induced nephropathy by inhibiting ferroptosis via HO-1/Nrf2/GPX4 pathway. *Clin Exp Pharmacol Physiol,* 49**,** 858-870.

GARCIA, P. L., MILLER, A. L., ZENG, L., VAN WAARDENBURG, R., YANG, E. S. & YOON, K. J. 2022. The BET Inhibitor JQ1 Potentiates the Anticlonogenic Effect of Radiation in Pancreatic Cancer Cells. *Front Oncol,* 12**,** 925718.

GHAREGHOMI, S., HABIBI-REZAEI, M., ARESE, M., SASO, L. & MOOSAVI-MOVAHEDI, A. A. 2022. Nrf2 Modulation in Breast Cancer. *Biomedicines,* 10.

GOLLOB, M. H., GREEN, M. S., TANG, A. S., GOLLOB, T., KARIBE, A., ALI HASSAN, A. S., AHMAD, F., LOZADO, R., SHAH, G., FANANAPAZIR, L., BACHINSKI, L. L. & ROBERTS, R. 2001. Identification of a gene responsible for familial Wolff-Parkinson-White syndrome. *N Engl J Med,* 344**,** 1823-31.

GREEN, D. R. & LLAMBI, F. 2015. Cell Death Signaling. *Cold Spring Harb Perspect Biol,* 7.

GUAN, Q., GUO, R., HUANG, S., ZHANG, F., LIU, J., WANG, Z., YANG, X., SHUAI, X. & CAO, Z. 2020. Mesoporous polydopamine carrying sorafenib and SPIO nanoparticles for MRI-guided ferroptosis cancer therapy. *J Control Release,* 320**,** 392-403.

GUERTIN, D. A., STEVENS, D. M., THOREEN, C. C., BURDS, A. A., KALAANY, N. Y., MOFFAT, J., BROWN, M., FITZGERALD, K. J. & SABATINI, D. M. 2006. Ablation in mice of the mTORC components raptor, rictor, or mLST8 reveals that mTORC2 is required for signaling to Akt-FOXO and PKCalpha, but not S6K1. *Dev Cell,* 11**,** 859-71.

GUO, J., XU, B., HAN, Q., ZHOU, H., XIA, Y., GONG, C., DAI, X., LI, Z. & WU, G. 2018. Ferroptosis: A Novel Anti-tumor Action for Cisplatin. *Cancer Res Treat,* 50**,** 445-460.

GUO, Y., LIU, X., LIU, D., LI, K., WANG, C., LIU, Y., HE, B. & SHI, P. 2019. Inhibition of BECN1 Suppresses Lipid Peroxidation by Increasing System Xc(-) Activity in Early Brain Injury after Subarachnoid Hemorrhage. *J Mol Neurosci,* 67**,** 622-631.

GUPTA, N. & HENSKE, E. P. 2018. Pulmonary manifestations in tuberous sclerosis complex. *Am J Med Genet C Semin Med Genet,* 178**,** 326-337.

GYAMFI, J., KIM, J. & CHOI, J. 2022. Cancer as a Metabolic Disorder. *Int J Mol Sci,* 23.

HABIB, E., LINHER-MELVILLE, K., LIN, H. X. & SINGH, G. 2015. Expression of xCT and activity of system xc(-) are regulated by NRF2 in human breast cancer cells in response to oxidative stress. *Redox Biol,* 5**,** 33-42.

HABIB, S. L., AL-OBAIDI, N. Y., NOWACKI, M., PIETKUN, K., ZEGARSKA, B., KLOSKOWSKI, T., ZEGARSKI, W., DREWA, T., MEDINA, E. A., ZHAO, Z. & LIANG, S. 2016. Is mTOR Inhibitor Good Enough for Treatment All Tumors in TSC Patients? *J Cancer,* 7**,** 1621-1631.

HAN, D., JIANG, L., GU, X., HUANG, S., PANG, J., WU, Y., YIN, J. & WANG, J. 2020. SIRT3 deficiency is resistant to autophagy-dependent ferroptosis by inhibiting the AMPK/mTOR pathway and promoting GPX4 levels. *J Cell Physiol,* 235**,** 8839-8851.

HAN, L. & JIANG, C. 2021. Evolution of blood-brain barrier in brain diseases and related systemic nanoscale brain-targeting drug delivery strategies. *Acta Pharm Sin B,* 11**,** 2306-2325.

HANAHAN, D. & WEINBERG, R. A. 2011. Hallmarks of cancer: the next generation. *Cell,* 144**,** 646-74.

HAO, J., ZHANG, W. & HUANG, Z. 2022. Bupivacaine modulates the apoptosis and ferroptosis in bladder cancer via phosphatidylinositol 3-kinase (PI3K)/AKT pathway. *Bioengineered,* 13**,** 6794-6806.

HAO, S., LIANG, B., HUANG, Q., DONG, S., WU, Z., HE, W. & SHI, M. 2018. Metabolic networks in ferroptosis. *Oncol Lett,* 15**,** 5405-5411.

HAO, S., YU, J., HE, W., HUANG, Q., ZHAO, Y., LIANG, B., ZHANG, S., WEN, Z., DONG, S., RAO, J., LIAO, W. & SHI, M. 2017. Cysteine Dioxygenase 1 Mediates Erastin-Induced Ferroptosis in Human Gastric Cancer Cells. *Neoplasia,* 19**,** 1022-1032.

HARA, K., YONEZAWA, K., WENG, Q. P., KOZLOWSKI, M. T., BELHAM, C. & AVRUCH, J. 1998. Amino acid sufficiency and mTOR regulate p70 S6 kinase and eIF-4E BP1 through a common effector mechanism. *J Biol Chem,* 273**,** 14484-94.

HASSANNIA, B., VANDENABEELE, P. & VANDEN BERGHE, T. 2019. Targeting Ferroptosis to Iron Out Cancer. *Cancer Cell,* 35**,** 830-849.

HASSANNIA, B., WIERNICKI, B., INGOLD, I., QU, F., VAN HERCK, S., TYURINA, Y. Y., BAYIR, H., ABHARI, B. A., ANGELI, J. P. F., CHOI, S. M., MEUL, E., HEYNINCK, K., DECLERCK, K., CHIRUMAMILLA, C. S., LAHTELA-KAKKONEN, M., VAN CAMP, G., KRYSKO, D. V., EKERT, P. G., FULDA, S., DE GEEST, B. G., CONRAD, M., KAGAN, V. E., VANDEN BERGHE, W., VANDENABEELE, P. & VANDEN BERGHE, T. 2018. Nano-targeted induction of dual ferroptotic mechanisms eradicates high-risk neuroblastoma. *J Clin Invest,* 128**,** 3341-3355.

HAYANO, M., YANG, W. S., CORN, C. K., PAGANO, N. C. & STOCKWELL, B. R. 2016. Loss of cysteinyl-tRNA synthetase (CARS) induces the transsulfuration pathway and inhibits ferroptosis induced by cystine deprivation. *Cell Death Differ,* 23**,** 270-8.

HE, D., WU, H., XIANG, J., RUAN, X., PENG, P., RUAN, Y., CHEN, Y. G., WANG, Y., YU, Q., ZHANG, H., HABIB, S. L., DE PINHO, R. A., LIU, H. & LI, B. 2020. Gut stem cell aging is driven by mTORC1 via a p38 MAPK-p53 pathway. *Nat Commun,* 11**,** 37.

HELBIG, L., KOI, L., BRUCHNER, K., GURTNER, K., HESS-STUMPP, H., UNTERSCHEMMANN, K., BAUMANN, M., ZIPS, D. & YAROMINA, A. 2014. BAY 87-2243, a novel inhibitor of hypoxia-induced gene activation, improves local tumor control after fractionated irradiation in a schedule-dependent manner in head and neck human xenografts. *Radiat Oncol,* 9**,** 207.

HINNEBUSCH, A. G. 2012. Translational homeostasis via eIF4E and 4E-BP1. *Mol Cell,* 46**,** 717-9.

HOLZ, M. K., BALLIF, B. A., GYGI, S. P. & BLENIS, J. 2021. mTOR and S6K1 mediate assembly of the translation preinitiation complex through dynamic protein interchange and ordered phosphorylation events. *Cell,* 184**,** 2255.

HONG, Y., HOU, W., OU, D., LIN, M., LUO, M. & WEI, Q. 2024. Liposome-coated nanoparticle triggers prostate cancer ferroptosis through synergetic chemodynamic-gas therapy. *Nanoscale Adv,* 6**,** 524-533.

HOU, W., XIE, Y., SONG, X., SUN, X., LOTZE, M. T., ZEH, H. J., 3RD, KANG, R. & TANG, D. 2016. Autophagy promotes ferroptosis by degradation of ferritin. *Autophagy,* 12**,** 1425-8.

HOUSE, I. G., SAVAS, P., LAI, J., CHEN, A. X. Y., OLIVER, A. J., TEO, Z. L., TODD, K. L., HENDERSON, M. A., GIUFFRIDA, L., PETLEY, E. V., SEK, K., MARDIANA, S., GIDE, T. N., QUEK, C., SCOLYER, R. A., LONG, G. V., WILMOTT, J. S., LOI, S., DARCY, P. K. & BEAVIS, P. A. 2020. Macrophage-

Derived CXCL9 and CXCL10 Are Required for Antitumor Immune Responses Following Immune Checkpoint Blockade. *Clin Cancer Res,* 26**,** 487-504.

HSIEH, C. H., HSIEH, H. C., SHIH, F. S., WANG, P. W., YANG, L. X., SHIEH, D. B. & WANG, Y. C. 2021. An innovative NRF2 nano-modulator induces lung cancer ferroptosis and elicits an immunostimulatory tumor microenvironment. *Theranostics,* 11**,** 7072-7091.

HSIEH, M. S., LING, H. H., SETIAWAN, S. A., HARDIANTI, M. S., FONG, I. H., YEH, C. T. & CHEN, J. H. 2024. Therapeutic targeting of thioredoxin reductase 1 causes ferroptosis while potentiating anti-PD-1 efficacy in head and neck cancer. *Chem Biol Interact,* 395**,** 111004.

HU, Q., WEI, W., WU, D., HUANG, F., LI, M., LI, W., YIN, J., PENG, Y., LU, Y., ZHAO, Q. & LIU, L. 2022. Blockade of GCH1/BH4 Axis Activates Ferritinophagy to Mitigate the Resistance of Colorectal Cancer to Erastin-Induced Ferroptosis. *Front Cell Dev Biol,* 10**,** 810327.

HU, Z., MI, Y., QIAN, H., GUO, N., YAN, A., ZHANG, Y. & GAO, X. 2020. A Potential Mechanism of Temozolomide Resistance in Glioma-Ferroptosis. *Front Oncol,* 10**,** 897.

HUANG, M., WANG, Y., WU, X. & LI, W. 2024. Crosstalk between Endoplasmic Reticulum Stress and Ferroptosis in Liver Diseases. *Front Biosci (Landmark Ed),* 29**,** 221.

HUANG, Y., DAI, Z., BARBACIORU, C. & SADEE, W. 2005. Cystine-glutamate transporter SLC7A11 in cancer chemosensitivity and chemoresistance. *Cancer Res,* 65**,** 7446-54.

HUANG, Y., YANG, W., YANG, L., WANG, T., LI, C., YU, J., ZHANG, P., YIN, Y., LI, R. & TAO, K. 2023. Nrf2 inhibition increases sensitivity to chemotherapy of colorectal cancer by promoting ferroptosis and pyroptosis. *Sci Rep,* 13**,** 14359.

ICHIMURA, Y., WAGURI, S., SOU, Y. S., KAGEYAMA, S., HASEGAWA, J., ISHIMURA, R., SAITO, T., YANG, Y., KOUNO, T., FUKUTOMI, T., HOSHII, T., HIRAO, A., TAKAGI, K., MIZUSHIMA, T., MOTOHASHI, H., LEE, M. S., YOSHIMORI, T., TANAKA, K., YAMAMOTO, M. & KOMATSU, M. 2013. Phosphorylation of p62 activates the Keap1-Nrf2 pathway during selective autophagy. *Mol Cell,* 51**,** 618-31.

INOKI, K., CORRADETTI, M. N. & GUAN, K. L. 2005. Dysregulation of the TSC-mTOR pathway in human disease. *Nat Genet,* 37**,** 19-24.

INOKI, K., LI, Y., XU, T. & GUAN, K. L. 2003. Rheb GTPase is a direct target of TSC2 GAP activity and regulates mTOR signaling. *Genes Dev,* 17**,** 1829-34.

INOKI, K., LI, Y., ZHU, T., WU, J. & GUAN, K. L. 2002. TSC2 is phosphorylated and inhibited by Akt and suppresses mTOR signalling. *Nat Cell Biol,* 4**,** 648-57.

ITOH, K., CHIBA, T., TAKAHASHI, S., ISHII, T., IGARASHI, K., KATOH, Y., OYAKE, T., HAYASHI, N., SATOH, K., HATAYAMA, I., YAMAMOTO, M. & NABESHIMA, Y. 1997. An Nrf2/small Maf heterodimer mediates the induction of phase II detoxifying enzyme genes through antioxidant response elements. *Biochem Biophys Res Commun,* 236**,** 313-22.

JEONG, E. M., YOON, J. H., LIM, J., SHIN, J. W., CHO, A. Y., HEO, J., LEE, K. B., LEE, J. H., LEE, W. J., KIM, H. J., SON, Y. H., LEE, S. J., CHO, S. Y., SHIN, D. M., CHOI, K. & KIM, I. G. 2018. Real-Time Monitoring of Glutathione in Living Cells

Reveals that High Glutathione Levels Are Required to Maintain Stem Cell Function. *Stem Cell Reports,* 10**,** 600-614.
JIANG, W., HU, J. W., HE, X. R., JIN, W. L. & HE, X. Y. 2021a. Statins: a repurposed drug to fight cancer. *J Exp Clin Cancer Res,* 40**,** 241.
JIANG, X., STOCKWELL, B. R. & CONRAD, M. 2021b. Ferroptosis: mechanisms, biology and role in disease. *Nat Rev Mol Cell Biol,* 22**,** 266-282.
JIN, X., TANG, J., QIU, X., NIE, X., OU, S., WU, G., ZHANG, R. & ZHU, J. 2024. Ferroptosis: Emerging mechanisms, biological function, and therapeutic potential in cancer and inflammation. *Cell Death Discov,* 10**,** 45.
JIN, Y., WU, S., ZHANG, L., YAO, G., ZHAO, H., QIAO, P. & ZHANG, J. 2023. Artesunate inhibits osteoclast differentiation by inducing ferroptosis and prevents iron overload-induced bone loss. *Basic Clin Pharmacol Toxicol,* 132**,** 144-153.
JOHNSON, C. E., DUNLOP, E. A., SEIFAN, S., MCCANN, H. D., HAY, T., PARFITT, G. J., JONES, A. T., GILES, P. J., SHEN, M. H., SAMPSON, J. R., ERRINGTON, R. J., DAVIES, D. M. & TEE, A. R. 2018. Loss of tuberous sclerosis complex 2 sensitizes tumors to nelfinavir-bortezomib therapy to intensify endoplasmic reticulum stress-induced cell death. *Oncogene,* 37**,** 5913-5925.
JOHNSON, C. E. & TEE, A. R. 2017. Exploiting cancer vulnerabilities: mTOR, autophagy, and homeostatic imbalance. *Essays Biochem,* 61**,** 699-710.
JOHNSON, S. R. & TATTERSFIELD, A. E. 2002. Lymphangioleiomyomatosis. *Semin Respir Crit Care Med,* 23**,** 85-92.
JOHNSON, S. S., LIU, D., EWALD, J. T., ROBLES-PLANELLS, C., CHRISTENSEN, K. A., BAYANBOLD, K., WELS, B. R., SOLST, S. R., O'DORISIO, M. S., ALLEN, B. G., MENDA, Y., SPITZ, D. R. & FATH, M. A. 2024. Auranofin Inhibition of Thioredoxin Reductase Sensitizes Lung Neuroendocrine Tumor Cells (NETs) and Small Cell Lung Cancer (SCLC) Cells to Sorafenib as well as Inhibiting SCLC Xenograft Growth. *bioRxiv*.
JUNG, K. H., KIM, S. E., GO, H. G., LEE, Y. J., PARK, M. S., KO, S., HAN, B. S., YOON, Y. C., CHO, Y. J., LEE, P., LEE, S. H., KIM, K. & HONG, S. S. 2023. Synergistic Renoprotective Effect of Melatonin and Zileuton by Inhibition of Ferroptosis via the AKT/mTOR/NRF2 Signaling in Kidney Injury and Fibrosis. *Biomol Ther (Seoul),* 31**,** 599-610.
KAGAN, V. E., MAO, G., QU, F., ANGELI, J. P., DOLL, S., CROIX, C. S., DAR, H. H., LIU, B., TYURIN, V. A., RITOV, V. B., KAPRALOV, A. A., AMOSCATO, A. A., JIANG, J., ANTHONYMUTHU, T., MOHAMMADYANI, D., YANG, Q., PRONETH, B., KLEIN-SEETHARAMAN, J., WATKINS, S., BAHAR, I., GREENBERGER, J., MALLAMPALLI, R. K., STOCKWELL, B. R., TYURINA, Y. Y., CONRAD, M. & BAYIR, H. 2017. Oxidized arachidonic and adrenic PEs navigate cells to ferroptosis. *Nat Chem Biol,* 13**,** 81-90.
KAJARABILLE, N. & LATUNDE-DADA, G. O. 2019. Programmed Cell-Death by Ferroptosis: Antioxidants as Mitigators. *Int J Mol Sci,* 20.
KANG, Y. P., MOCKABEE-MACIAS, A., JIANG, C., FALZONE, A., PRIETO-FARIGUA, N., STONE, E., HARRIS, I. S. & DENICOLA, G. M. 2021. Non-canonical Glutamate-Cysteine Ligase Activity Protects against Ferroptosis. *Cell Metab,* 33**,** 174-189 e7.

KARAJANNIS, M. A., MAUGUEN, A., MALOKU, E., XU, Q., DUNBAR, E. M., PLOTKIN, S. R., YAFFEE, A., WANG, S., ROLAND, J. T., SEN, C., PLACANTONAKIS, D. G., GOLFINOS, J. G., ALLEN, J. C., VITANZA, N. A., CHIRIBOGA, L. A., SCHNEIDER, R. J., DENG, J., NEUBERT, T. A., GOLDBERG, J. D., ZAGZAG, D., GIANCOTTI, F. G. & BLAKELEY, J. O. 2021. Phase 0 Clinical Trial of Everolimus in Patients with Vestibular Schwannoma or Meningioma. *Mol Cancer Ther,* 20**,** 1584-1591.

KATO, H., NAKAJIMA, S., SAITO, Y., TAKAHASHI, S., KATOH, R. & KITAMURA, M. 2012. mTORC1 serves ER stress-triggered apoptosis via selective activation of the IRE1-JNK pathway. *Cell Death Differ,* 19**,** 310-20.

KATO, I., KASUKABE, T. & KUMAKURA, S. 2020. Menin-MLL inhibitors induce ferroptosis and enhance the anti-proliferative activity of auranofin in several types of cancer cells. *Int J Oncol,* 57**,** 1057-1071.

KENERSON, H. L., AICHER, L. D., TRUE, L. D. & YEUNG, R. S. 2002. Activated mammalian target of rapamycin pathway in the pathogenesis of tuberous sclerosis complex renal tumors. *Cancer Res,* 62**,** 5645-50.

KERIMOGLU, B., LAMB, C., MCPHERSON, R. D., ERGEN, E., STONE, E. M. & OOI, A. 2022. Cyst(e)inase-Rapamycin Combination Induces Ferroptosis in Both In Vitro and In Vivo Models of Hereditary Leiomyomatosis and Renal Cell Cancer. *Mol Cancer Ther,* 21**,** 419-426.

KERINS, M. J. & OOI, A. 2018. The Roles of NRF2 in Modulating Cellular Iron Homeostasis. *Antioxid Redox Signal,* 29**,** 1756-1773.

KIM, J. Y., KWON, Y. G. & KIM, Y. M. 2023. The stress-responsive protein REDD1 and its pathophysiological functions. *Exp Mol Med,* 55**,** 1933-1944.

KIM, T.-W., KIM, Y.-J., KIM, H.-T., PARK, S.-R., LEE, M.-Y., PARK, Y.-D., LEE, C.-H. & JUNG, J.-Y. 2016. NQO1 Deficiency Leads Enhanced Autophagy in Cisplatin-Induced Acute Kidney Injury Through the AMPK/TSC2/mTOR Signaling Pathway. *Antioxidants & Redox Signaling,* 24**,** 867-883.

KINGSWOOD, J. C., D'AUGERES, G. B., BELOUSOVA, E., FERREIRA, J. C., CARTER, T., CASTELLANA, R., COTTIN, V., CURATOLO, P., DAHLIN, M., DE VRIES, P. J., FEUCHT, M., FLADROWSKI, C., GISLIMBERTI, G., HERTZBERG, C., JOZWIAK, S., LAWSON, J. A., MACAYA, A., NABBOUT, R., O'CALLAGHAN, F., BENEDIK, M. P., QIN, J., MARQUES, R., SANDER, V., SAUTER, M., TAKAHASHI, Y., TOURAINE, R., YOUROUKOS, S., ZONNENBERG, B., JANSEN, A. C., CONSORTIUM, T. & INVESTIGATORS, T. 2017. TuberOus SClerosis registry to increase disease Awareness (TOSCA) - baseline data on 2093 patients. *Orphanet J Rare Dis,* 12**,** 2.

KOEBERLE, S. C., KIPP, A. P., STUPPNER, H. & KOEBERLE, A. 2023. Ferroptosis-modulating small molecules for targeting drug-resistant cancer: Challenges and opportunities in manipulating redox signaling. *Med Res Rev,* 43**,** 614-682.

KOLBRINK, B., VON SAMSON-HIMMELSTJERNA, F. A., MESSTORFF, M. L., RIEBELING, T., NISCHE, R., SCHMITZ, J., BRASEN, J. H., KUNZENDORF, U. & KRAUTWALD, S. 2022. Vitamin K1 inhibits ferroptosis and counteracts a detrimental effect of phenprocoumon in experimental acute kidney injury. *Cell Mol Life Sci,* 79**,** 387.

KONDYLIS, V., SCHNEIDER, F., SCHORN, F., OIKONOMOU, N., STRAUB, B. K., WERNER, S., ROSENSTIEL, P. & PASPARAKIS, M. 2022. p62 Promotes Survival and Hepatocarcinogenesis in Mice with Liver-Specific NEMO Ablation. *Cancers (Basel),* 14.

KOPPULA, P., LEI, G., ZHANG, Y., YAN, Y., MAO, C., KONDIPARTHI, L., SHI, J., LIU, X., HORBATH, A., DAS, M., LI, W., POYUROVSKY, M. V., OLSZEWSKI, K. & GAN, B. 2022. A targetable CoQ-FSP1 axis drives ferroptosis- and radiation-resistance in KEAP1 inactive lung cancers. *Nat Commun,* 13**,** 2206.

KOSMAS, K., FILIPPAKIS, H., KHABIBULLIN, D., TURKIEWICZ, M., LAM, H. C., YU, J., KEDERSHA, N. L., ANDERSON, P. J. & HENSKE, E. P. 2021. TSC2 Interacts with HDLBP/Vigilin and Regulates Stress Granule Formation. *Mol Cancer Res,* 19**,** 1389-1397.

KOTULSKA, K., BORKOWSKA, J., MANDERA, M., ROSZKOWSKI, M., JURKIEWICZ, E., GRAJKOWSKA, W., BILSKA, M. & JOZWIAK, S. 2014. Congenital subependymal giant cell astrocytomas in patients with tuberous sclerosis complex. *Childs Nerv Syst,* 30**,** 2037-42.

KOVTUNOVYCH, G., ECKHAUS, M. A., GHOSH, M. C., OLLIVIERRE-WILSON, H. & ROUAULT, T. A. 2010. Dysfunction of the heme recycling system in heme oxygenase 1-deficient mice: effects on macrophage viability and tissue iron distribution. *Blood,* 116**,** 6054-62.

KRAFT, V. A. N., BEZJIAN, C. T., PFEIFFER, S., RINGELSTETTER, L., MULLER, C., ZANDKARIMI, F., MERL-PHAM, J., BAO, X., ANASTASOV, N., KOSSL, J., BRANDNER, S., DANIELS, J. D., SCHMITT-KOPPLIN, P., HAUCK, S. M., STOCKWELL, B. R., HADIAN, K. & SCHICK, J. A. 2020. GTP Cyclohydrolase 1/Tetrahydrobiopterin Counteract Ferroptosis through Lipid Remodeling. *ACS Cent Sci,* 6**,** 41-53.

KUANG, F., LIU, J., TANG, D. & KANG, R. 2020. Oxidative Damage and Antioxidant Defense in Ferroptosis. *Front Cell Dev Biol,* 8**,** 586578.

KWIATKOWSKI, D. J. 2003. Tuberous sclerosis: from tubers to mTOR. *Ann Hum Genet,* 67**,** 87-96.

KWON, M. Y., PARK, E., LEE, S. J. & CHUNG, S. W. 2015. Heme oxygenase-1 accelerates erastin-induced ferroptotic cell death. *Oncotarget,* 6**,** 24393-403.

LACHAIER, E., LOUANDRE, C., GODIN, C., SAIDAK, Z., BAERT, M., DIOUF, M., CHAUFFERT, B. & GALMICHE, A. 2014. Sorafenib induces ferroptosis in human cancer cell lines originating from different solid tumors. *Anticancer Res,* 34**,** 6417-22.

LAM, H. C., BAGLINI, C. V., LOPE, A. L., PARKHITKO, A. A., LIU, H. J., ALESI, N., MALINOWSKA, I. A., EBRAHIMI-FAKHARI, D., SAFFARI, A., YU, J. J., PEREIRA, A., KHABIBULLIN, D., OGOREK, B., NIJMEH, J., KAVANAGH, T., HANDEN, A., CHAN, S. Y., ASARA, J. M., OLDHAM, W. M., DIAZ-MECO, M. T., MOSCAT, J., SAHIN, M., PRIOLO, C. & HENSKE, E. P. 2017. p62/SQSTM1 Cooperates with Hyperactive mTORC1 to Regulate Glutathione Production, Maintain Mitochondrial Integrity, and Promote Tumorigenesis. *Cancer Res,* 77**,** 3255-3267.

LAND, S. C. & TEE, A. R. 2007. Hypoxia-inducible factor 1alpha is regulated by the mammalian target of rapamycin (mTOR) via an mTOR signaling motif. *J Biol Chem,* 282**,** 20534-43.

LAPLANTE, M. & SABATINI, D. M. 2012. mTOR signaling in growth control and disease. *Cell,* 149**,** 274-93.

LEE, H., ZANDKARIMI, F., ZHANG, Y., MEENA, J. K., KIM, J., ZHUANG, L., TYAGI, S., MA, L., WESTBROOK, T. F., STEINBERG, G. R., NAKADA, D., STOCKWELL, B. R. & GAN, B. 2020. Energy-stress-mediated AMPK activation inhibits ferroptosis. *Nat Cell Biol,* 22**,** 225-234.

LEI, G., MAO, C., YAN, Y., ZHUANG, L. & GAN, B. 2021. Ferroptosis, radiotherapy, and combination therapeutic strategies. *Protein Cell,* 12**,** 836-857.

LI, B., YANG, L., PENG, X., FAN, Q., WEI, S., YANG, S., LI, X., JIN, H., WU, B., HUANG, M., TANG, S., LIU, J. & LI, H. 2020a. Emerging mechanisms and applications of ferroptosis in the treatment of resistant cancers. *Biomed Pharmacother,* 130**,** 110710.

LI, C., CHEN, H., LAN, Z., HE, S., CHEN, R., WANG, F., LIU, Z., LI, K., CHENG, L., LIU, Y., SUN, K., WAN, X., CHEN, X., PENG, H., LI, L., ZHANG, Y., JING, Y., HUANG, M., WANG, Y., WANG, Y., JIANG, J., ZHA, X., CHEN, L. & ZHANG, H. 2019a. mTOR-dependent upregulation of xCT blocks melanin synthesis and promotes tumorigenesis. *Cell Death Differ,* 26**,** 2015-2028.

LI, C., DONG, X., DU, W., SHI, X., CHEN, K., ZHANG, W. & GAO, M. 2020b. LKB1-AMPK axis negatively regulates ferroptosis by inhibiting fatty acid synthesis. *Signal Transduct Target Ther,* 5**,** 187.

LI, D. & LI, Y. 2020. The interaction between ferroptosis and lipid metabolism in cancer. *Signal Transduct Target Ther,* 5**,** 108.

LI, H. W., LIU, M. B., JIANG, X., SONG, T., FENG, S. X., WU, J. Y., DENG, P. F. & WANG, X. Y. 2022a. GALNT14 regulates ferroptosis and apoptosis of ovarian cancer through the EGFR/mTOR pathway. *Future Oncol,* 18**,** 149-161.

LI, J., CAO, F., YIN, H. L., HUANG, Z. J., LIN, Z. T., MAO, N., SUN, B. & WANG, G. 2020c. Ferroptosis: past, present and future. *Cell Death Dis,* 11**,** 88.

LI, J., LAMA, R., GALSTER, S. L., INIGO, J. R., WU, J., CHANDRA, D., CHEMLER, S. R. & WANG, X. 2022b. Small-Molecule MMRi62 Induces Ferroptosis and Inhibits Metastasis in Pancreatic Cancer via Degradation of Ferritin Heavy Chain and Mutant p53. *Mol Cancer Ther,* 21**,** 535-545.

LI, J., YEN, C., LIAW, D., PODSYPANINA, K., BOSE, S., WANG, S. I., PUC, J., MILIARESIS, C., RODGERS, L., MCCOMBIE, R., BIGNER, S. H., GIOVANELLA, B. C., ITTMANN, M., TYCKO, B., HIBSHOOSH, H., WIGLER, M. H. & PARSONS, R. 1997. PTEN, a putative protein tyrosine phosphatase gene mutated in human brain, breast, and prostate cancer. *Science,* 275**,** 1943-7.

LI, K., XU, K., HE, Y., LU, L., MAO, Y., GAO, P., LIU, G., WU, J., ZHANG, Y., XIANG, Y., LUO, Z. & CAI, K. 2021a. Functionalized Tumor-Targeting Nanosheets Exhibiting Fe(II) Overloading and GSH Consumption for Ferroptosis Activation in Liver Tumor. *Small,* 17**,** e2102046.

LI, M., ZHOU, Y., CHEN, C., YANG, T., ZHOU, S., CHEN, S., WU, Y. & CUI, Y. 2019b. Efficacy and safety of mTOR inhibitors (rapamycin and its analogues) for tuberous sclerosis complex: a meta-analysis. *Orphanet J Rare Dis,* 14**,** 39.

LI, M. H., CHA, Y. N. & SURH, Y. J. 2006. Peroxynitrite induces HO-1 expression via PI3K/Akt-dependent activation of NF-E2-related factor 2 in PC12 cells. *Free Radic Biol Med,* 41**,** 1079-91.

LI, W., LIANG, L., LIU, S., YI, H. & ZHOU, Y. 2023. FSP1: a key regulator of ferroptosis. *Trends Mol Med,* 29**,** 753-764.

LI, Y., JIN, C., SHEN, M., WANG, Z., TAN, S., CHEN, A., WANG, S., SHAO, J., ZHANG, F., ZHANG, Z. & ZHENG, S. 2020d. Iron regulatory protein 2 is required for artemether -mediated anti-hepatic fibrosis through ferroptosis pathway. *Free Radic Biol Med,* 160**,** 845-859.

LI, Y., ZHANG, Y., QIU, Q., WANG, L., MAO, H., HU, J., CHEN, Z., DU, Y. & LIU, X. 2022c. Energy-Stress-Mediated AMPK Activation Promotes GPX4-Dependent Ferroptosis through the JAK2/STAT3/P53 Axis in Renal Cancer. *Oxid Med Cell Longev,* 2022**,** 2353115.

LI, Z. J., DAI, H. Q., HUANG, X. W., FENG, J., DENG, J. H., WANG, Z. X., YANG, X. M., LIU, Y. J., WU, Y., CHEN, P. H., SHI, H., WANG, J. G., ZHOU, J. & LU, G. D. 2021b. Artesunate synergizes with sorafenib to induce ferroptosis in hepatocellular carcinoma. *Acta Pharmacol Sin,* 42**,** 301-310.

LIANG, C., ZHANG, X., YANG, M. & DONG, X. 2019. Recent Progress in Ferroptosis Inducers for Cancer Therapy. *Adv Mater,* 31**,** e1904197.

LIAO, J. C., LEE, K. T., YOU, B. J., LEE, C. L., CHANG, W. T., WU, Y. C. & LEE, H. Z. 2015. Raf/ERK/Nrf2 signaling pathway and MMP-7 expression involvement in the trigonelline-mediated inhibition of hepatocarcinoma cell migration. *Food Nutr Res,* 59**,** 29884.

LIM, H. K., CHOI, Y. A., PARK, W., LEE, T., RYU, S. H., KIM, S. Y., KIM, J. R., KIM, J. H. & BAEK, S. H. 2003. Phosphatidic acid regulates systemic inflammatory responses by modulating the Akt-mammalian target of rapamycin-p70 S6 kinase 1 pathway. *J Biol Chem,* 278**,** 45117-27.

LIM, J., LEE, J., BOO, Y. & KIM, W. J. 2024. A polymeric iron oxide nanocomplex loaded with sulfasalazine: an approach for inducing ferritinophagy-assisted ferroptosis for anti-cancer therapy. *Nanoscale,* 16**,** 742-751.

LIN, L. S., SONG, J., SONG, L., KE, K., LIU, Y., ZHOU, Z., SHEN, Z., LI, J., YANG, Z., TANG, W., NIU, G., YANG, H. H. & CHEN, X. 2018. Simultaneous Fenton-like Ion Delivery and Glutathione Depletion by MnO(2) -Based Nanoagent to Enhance Chemodynamic Therapy. *Angew Chem Int Ed Engl,* 57**,** 4902-4906.

LIPPMANN, J., PETRI, K., FULDA, S. & LIESE, J. 2020. Redox Modulation and Induction of Ferroptosis as a New Therapeutic Strategy in Hepatocellular Carcinoma. *Transl Oncol,* 13**,** 100785.

LIU, M., KONG, X. Y., YAO, Y., WANG, X. A., YANG, W., WU, H., LI, S., DING, J. W. & YANG, J. 2022. The critical role and molecular mechanisms of ferroptosis in antioxidant systems: a narrative review. *Ann Transl Med,* 10**,** 368.

LIU, Q. & WANG, K. 2019. The induction of ferroptosis by impairing STAT3/Nrf2/GPx4 signaling enhances the sensitivity of osteosarcoma cells to cisplatin. *Cell Biol Int,* 43**,** 1245-1256.

LIU, T., WANG, P., YIN, H., WANG, X., LV, J., YUAN, J., ZHU, J. & WANG, Y. 2023a. Rapamycin reverses ferroptosis by increasing autophagy in MPTP/MPP(+)-induced models of Parkinson's disease. *Neural Regen Res,* 18**,** 2514-2519.

LIU, T., XU, X., LI, J., BAI, M., ZHU, W., LIU, Y., LIU, S., ZHAO, Z., LI, T., JIANG, N., BAI, Y., JIN, Q., ZHANG, Y., ZHENG, Y., ZHOU, S., ZHAN, S., SUN, Y., LIANG, G., LUO, Y., CHEN, X., GUO, H. & YANG, R. 2023b. ALOX5 deficiency contributes to bladder cancer progression by mediating ferroptosis escape. *Cell Death Dis,* 14**,** 800.

LIU, Y. & GU, W. 2022. p53 in ferroptosis regulation: the new weapon for the old guardian. *Cell Death Differ,* 29**,** 895-910.

LIU, Y., WANG, Y., LIU, J., KANG, R. & TANG, D. 2020. Interplay between MTOR and GPX4 signaling modulates autophagy-dependent ferroptotic cancer cell death. *Cancer Gene Ther*.

LIU, Y., WANG, Y., LIU, J., KANG, R. & TANG, D. 2021. Interplay between MTOR and GPX4 signaling modulates autophagy-dependent ferroptotic cancer cell death. *Cancer Gene Ther,* 28**,** 55-63.

LOEWITH, R., JACINTO, E., WULLSCHLEGER, S., LORBERG, A., CRESPO, J. L., BONENFANT, D., OPPLIGER, W., JENOE, P. & HALL, M. N. 2002. Two TOR complexes, only one of which is rapamycin sensitive, have distinct roles in cell growth control. *Mol Cell,* 10**,** 457-68.

LOU, J., ZHOU, Y., FENG, Z., MA, M., YAO, Y., WANG, Y., DENG, Y. & WU, Y. 2020. Caspase-Independent Regulated Necrosis Pathways as Potential Targets in Cancer Management. *Front Oncol,* 10**,** 616952.

LOUANDRE, C., MARCQ, I., BOUHLAL, H., LACHAIER, E., GODIN, C., SAIDAK, Z., FRANCOIS, C., CHATELAIN, D., DEBUYSSCHER, V., BARBARE, J. C., CHAUFFERT, B. & GALMICHE, A. 2015. The retinoblastoma (Rb) protein regulates ferroptosis induced by sorafenib in human hepatocellular carcinoma cells. *Cancer Lett,* 356**,** 971-7.

LOVE, M. I., HUBER, W. & ANDERS, S. 2014. Moderated estimation of fold change and dispersion for RNA-seq data with DESeq2. *Genome Biol,* 15**,** 550.

LU, Z., XIAO, B., CHEN, W., TANG, T., ZHUO, Q. & CHEN, X. 2023. The potential of ferroptosis combined with radiotherapy in cancer treatment. *Front Oncol,* 13**,** 1085581.

MA, H., WANG, X., ZHANG, W., LI, H., ZHAO, W., SUN, J. & YANG, M. 2020. Melatonin Suppresses Ferroptosis Induced by High Glucose via Activation of the Nrf2/HO-1 Signaling Pathway in Type 2 Diabetic Osteoporosis. *Oxid Med Cell Longev,* 2020**,** 9067610.

MA, L., CHEN, Z., ERDJUMENT-BROMAGE, H., TEMPST, P. & PANDOLFI, P. P. 2005. Phosphorylation and functional inactivation of TSC2 by Erk implications for tuberous sclerosis and cancer pathogenesis. *Cell,* 121**,** 179-93.

MA, S., DIELSCHNEIDER, R. F., HENSON, E. S., XIAO, W., CHOQUETTE, T. R., BLANKSTEIN, A. R., CHEN, Y. & GIBSON, S. B. 2017a. Ferroptosis and autophagy induced cell death occur independently after siramesine and lapatinib treatment in breast cancer cells. *PLoS One,* 12**,** e0182921.

MA, S., HENSON, E. S., CHEN, Y. & GIBSON, S. B. 2016. Ferroptosis is induced following siramesine and lapatinib treatment of breast cancer cells. *Cell Death Dis,* 7**,** e2307.

MA, W., HU, N., XU, W., ZHAO, L., TIAN, C. & KAMEI, K. I. 2024. Ferroptosis inducers: A new frontier in cancer therapy. *Bioorg Chem,* 146**,** 107331.

MA, X., ZHANG, S., HE, L., RONG, Y., BRIER, L. W., SUN, Q., LIU, R., FAN, W., CHEN, S., YUE, Z., KIM, J., GUAN, K. L., LI, D. & ZHONG, Q. 2017b. MTORC1-mediated NRBF2 phosphorylation functions as a switch for the class III PtdIns3K and autophagy. *Autophagy,* 13**,** 592-607.

MACCARINELLI, F., COLTRINI, D., MUSSI, S., BUGATTI, M., TURATI, M., CHIODELLI, P., GIACOMINI, A., DE CILLIS, F., CATTANE, N., CATTANEO, A., LIGRESTI, A., ASPERTI, M., POLI, M., VERMI, W., PRESTA, M. & RONCA, R. 2023. Iron supplementation enhances RSL3-induced ferroptosis to treat naive and prevent castration-resistant prostate cancer. *Cell Death Discov,* 9**,** 81.

MAGTANONG, L., KO, P. J., TO, M., CAO, J. Y., FORCINA, G. C., TARANGELO, A., WARD, C. C., CHO, K., PATTI, G. J., NOMURA, D. K., OLZMANN, J. A. & DIXON, S. J. 2019. Exogenous Monounsaturated Fatty Acids Promote a Ferroptosis-Resistant Cell State. *Cell Chem Biol,* 26**,** 420-432 e9.

MANCIAS, J. D., WANG, X., GYGI, S. P., HARPER, J. W. & KIMMELMAN, A. C. 2014. Quantitative proteomics identifies NCOA4 as the cargo receptor mediating ferritinophagy. *Nature,* 509**,** 105-9.

MANNES, A. M., SEILER, A., BOSELLO, V., MAIORINO, M. & CONRAD, M. 2011. Cysteine mutant of mammalian GPx4 rescues cell death induced by disruption of the wild-type selenoenzyme. *FASEB J,* 25**,** 2135-44.

MANNING, B. D. & CANTLEY, L. C. 2003. Rheb fills a GAP between TSC and TOR. *Trends Biochem Sci,* 28**,** 573-6.

MANNING, B. D. & CANTLEY, L. C. 2007. AKT/PKB signaling: navigating downstream. *Cell,* 129**,** 1261-74.

MAO, Z. & ZHANG, W. 2018. Role of mTOR in Glucose and Lipid Metabolism. *Int J Mol Sci,* 19.

MARTIN, K. R., ZHOU, W., BOWMAN, M. J., SHIH, J., AU, K. S., DITTENHAFER-REED, K. E., SISSON, K. A., KOEMAN, J., WEISENBERGER, D. J., COTTINGHAM, S. L., DEROOS, S. T., DEVINSKY, O., WINN, M. E., CHERNIACK, A. D., SHEN, H., NORTHRUP, H., KRUEGER, D. A. & MACKEIGAN, J. P. 2017. The genomic landscape of tuberous sclerosis complex. *Nat Commun,* 8**,** 15816.

MAY, C. D., LANDERS, S. M., BOLSHAKOV, S., MA, X., INGRAM, D. R., KIVLIN, C. M., WATSON, K. L., SANNAA, G. A. A., BHALLA, A. D., WANG, W. L., LAZAR, A. J. & TORRES, K. E. 2017. Co-targeting PI3K, mTOR, and IGF1R with small molecule inhibitors for treating undifferentiated pleomorphic sarcoma. *Cancer Biol Ther,* 18**,** 816-826.

MAZHAB-JAFARI, M. T., MARSHALL, C. B., ISHIYAMA, N., HO, J., DI PALMA, V., STAMBOLIC, V. & IKURA, M. 2012. An autoinhibited noncanonical mechanism of GTP hydrolysis by Rheb maintains mTORC1 homeostasis. *Structure,* 20**,** 1528-39.

MCENEANEY, L. J. & TEE, A. R. 2019. Finding a cure for tuberous sclerosis complex: From genetics through to targeted drug therapies. *Adv Genet,* 103**,** 91-118.

MCKIE, A. T., BARROW, D., LATUNDE-DADA, G. O., ROLFS, A., SAGER, G., MUDALY, E., MUDALY, M., RICHARDSON, C., BARLOW, D., BOMFORD, A., PETERS, T. J., RAJA, K. B., SHIRALI, S., HEDIGER, M. A., FARZANEH, F. &

SIMPSON, R. J. 2001. An iron-regulated ferric reductase associated with the absorption of dietary iron. *Science,* 291**,** 1755-9.

MEDVETZ, D., PRIOLO, C. & HENSKE, E. P. 2015. Therapeutic targeting of cellular metabolism in cells with hyperactive mTORC1: a paradigm shift. *Mol Cancer Res,* 13**,** 3-8.

MENON, A. V., LIU, J., TSAI, H. P., ZENG, L., YANG, S., ASNANI, A. & KIM, J. 2022. Excess heme upregulates heme oxygenase 1 and promotes cardiac ferroptosis in mice with sickle cell disease. *Blood,* 139**,** 936-941.

MIEULET, V. & LAMB, R. F. 2010. Tuberous sclerosis complex: linking cancer to metabolism. *Trends Mol Med,* 16**,** 329-35.

MILLER, A. L., GARCIA, P. L., FEHLING, S. C., GAMBLIN, T. L., VANCE, R. B., COUNCIL, L. N., CHEN, D., YANG, E. S., VAN WAARDENBURG, R. & YOON, K. J. 2021. The BET Inhibitor JQ1 Augments the Antitumor Efficacy of Gemcitabine in Preclinical Models of Pancreatic Cancer. *Cancers (Basel),* 13.

MIOTTO, G., ROSSETTO, M., DI PAOLO, M. L., ORIAN, L., VENERANDO, R., ROVERI, A., VUCKOVIC, A. M., BOSELLO TRAVAIN, V., ZACCARIN, M., ZENNARO, L., MAIORINO, M., TOPPO, S., URSINI, F. & COZZA, G. 2020. Insight into the mechanism of ferroptosis inhibition by ferrostatin-1. *Redox Biol,* 28**,** 101328.

MISHIMA, E., ITO, J., WU, Z., NAKAMURA, T., WAHIDA, A., DOLL, S., TONNUS, W., NEPACHALOVICH, P., EGGENHOFER, E., ALDROVANDI, M., HENKELMANN, B., YAMADA, K. I., WANNINGER, J., ZILKA, O., SATO, E., FEEDERLE, R., HASS, D., MAIDA, A., MOURAO, A. S. D., LINKERMANN, A., GEISSLER, E. K., NAKAGAWA, K., ABE, T., FEDOROVA, M., PRONETH, B., PRATT, D. A. & CONRAD, M. 2022. A non-canonical vitamin K cycle is a potent ferroptosis suppressor. *Nature,* 608**,** 778-783.

MITSUISHI, Y., TAGUCHI, K., KAWATANI, Y., SHIBATA, T., NUKIWA, T., ABURATANI, H., YAMAMOTO, M. & MOTOHASHI, H. 2012. Nrf2 redirects glucose and glutamine into anabolic pathways in metabolic reprogramming. *Cancer Cell,* 22**,** 66-79.

MOU, Y., WANG, J., WU, J., HE, D., ZHANG, C., DUAN, C. & LI, B. 2019. Ferroptosis, a new form of cell death: opportunities and challenges in cancer. *J Hematol Oncol,* 12**,** 34.

NAGPAL, A., REDVERS, R. P., LING, X., AYTON, S., FUENTES, M., TAVANCHEH, E., DIALA, I., LALANI, A., LOI, S., DAVID, S., ANDERSON, R. L., SMITH, Y., MERINO, D., DENOYER, D. & POULIOT, N. 2019. Neoadjuvant neratinib promotes ferroptosis and inhibits brain metastasis in a novel syngeneic model of spontaneous HER2(+ve) breast cancer metastasis. *Breast Cancer Res,* 21**,** 94.

NAKAMURA, T., HIPP, C., SANTOS DIAS MOURAO, A., BORGGRAFE, J., ALDROVANDI, M., HENKELMANN, B., WANNINGER, J., MISHIMA, E., LYTTON, E., EMLER, D., PRONETH, B., SATTLER, M. & CONRAD, M. 2023. Phase separation of FSP1 promotes ferroptosis. *Nature,* 619**,** 371-377.

NAVEENKUMAR, S. K., HEMSHEKHAR, M., KEMPARAJU, K. & GIRISH, K. S. 2019. Hemin-induced platelet activation and ferroptosis is mediated through ROS-driven proteasomal activity and inflammasome activation: Protection by Melatonin. *Biochim Biophys Acta Mol Basis Dis,* 1865**,** 2303-2316.

NIE, Q., HU, Y., YU, X., LI, X. & FANG, X. 2022. Induction and application of ferroptosis in cancer therapy. *Cancer Cell Int,* 22**,** 12.

NISHIZAWA, H., MATSUMOTO, M., SHINDO, T., SAIGUSA, D., KATO, H., SUZUKI, K., SATO, M., ISHII, Y., SHIMOKAWA, H. & IGARASHI, K. 2020. Ferroptosis is controlled by the coordinated transcriptional regulation of glutathione and labile iron metabolism by the transcription factor BACH1. *J Biol Chem,* 295**,** 69-82.

NORTHRUP, H., ARONOW, M. E., BEBIN, E. M., BISSLER, J., DARLING, T. N., DE VRIES, P. J., FROST, M. D., FUCHS, Z., GOSNELL, E. S., GUPTA, N., JANSEN, A. C., JOZWIAK, S., KINGSWOOD, J. C., KNILANS, T. K., MCCORMACK, F. X., POUNDERS, A., ROBERDS, S. L., RODRIGUEZ-BURITICA, D. F., ROTH, J., SAMPSON, J. R., SPARAGANA, S., THIELE, E. A., WEINER, H. L., WHELESS, J. W., TOWBIN, A. J., KRUEGER, D. A. & INTERNATIONAL TUBEROUS SCLEROSIS COMPLEX CONSENSUS, G. 2021. Updated International Tuberous Sclerosis Complex Diagnostic Criteria and Surveillance and Management Recommendations. *Pediatr Neurol,* 123**,** 50-66.

OH, S. J., IKEDA, M., IDE, T., HUR, K. Y. & LEE, M. S. 2022. Mitochondrial event as an ultimate step in ferroptosis. *Cell Death Discov,* 8**,** 414.

OSHIRO, N., TAKAHASHI, R., YOSHINO, K., TANIMURA, K., NAKASHIMA, A., EGUCHI, S., MIYAMOTO, T., HARA, K., TAKEHANA, K., AVRUCH, J., KIKKAWA, U. & YONEZAWA, K. 2007. The proline-rich Akt substrate of 40 kDa (PRAS40) is a physiological substrate of mammalian target of rapamycin complex 1. *J Biol Chem,* 282**,** 20329-39.

OU, M., JIANG, Y., JI, Y., ZHOU, Q., DU, Z., ZHU, H. & ZHOU, Z. 2022. Role and mechanism of ferroptosis in neurological diseases. *Mol Metab,* 61**,** 101502.

OU, Y., WANG, S. J., LI, D., CHU, B. & GU, W. 2016. Activation of SAT1 engages polyamine metabolism with p53-mediated ferroptotic responses. *Proc Natl Acad Sci U S A,* 113**,** E6806-E6812.

OUYANG, L., SHI, Z., ZHAO, S., WANG, F. T., ZHOU, T. T., LIU, B. & BAO, J. K. 2012. Programmed cell death pathways in cancer: a review of apoptosis, autophagy and programmed necrosis. *Cell Prolif,* 45**,** 487-98.

OZGA, A. J., CHOW, M. T. & LUSTER, A. D. 2021. Chemokines and the immune response to cancer. *Immunity,* 54**,** 859-874.

PAN, M., WANG, Z., WANG, Y., JIANG, X., FAN, Y., GONG, F., SUN, Y. & WANG, D. 2023. Celastrol alleviated acute kidney injury by inhibition of ferroptosis through Nrf2/GPX4 pathway. *Biomed Pharmacother,* 166**,** 115333.

PARK, J. H., PYUN, W. Y. & PARK, H. W. 2020. Cancer Metabolism: Phenotype, Signaling and Therapeutic Targets. *Cells,* 9.

PARK, S. Y., JEONG, K. J., POIRE, A., ZHANG, D., TSANG, Y. H., BLUCHER, A. S. & MILLS, G. B. 2023. Irreversible HER2 inhibitors overcome resistance to the RSL3 ferroptosis inducer in non-HER2 amplified luminal breast cancer. *Cell Death Dis,* 14**,** 532.

PEARSON, A. N., CARMICHEAL, J., JIANG, L., LEI, Y. L. & GREEN, M. D. 2021. Contribution of Lipid Oxidation and Ferroptosis to Radiotherapy Efficacy. *Int J Mol Sci,* 22.

PENG, F., LIAO, M., QIN, R., ZHU, S., PENG, C., FU, L., CHEN, Y. & HAN, B. 2022a. Regulated cell death (RCD) in cancer: key pathways and targeted therapies. *Signal Transduct Target Ther,* 7**,** 286.

PENG, Y., WANG, Y., ZHOU, C., MEI, W. & ZENG, C. 2022b. PI3K/Akt/mTOR Pathway and Its Role in Cancer Therapeutics: Are We Making Headway? *Front Oncol,* 12**,** 819128.

PETERSON, T. R., SENGUPTA, S. S., HARRIS, T. E., CARMACK, A. E., KANG, S. A., BALDERAS, E., GUERTIN, D. A., MADDEN, K. L., CARPENTER, A. E., FINCK, B. N. & SABATINI, D. M. 2011. mTOR complex 1 regulates lipin 1 localization to control the SREBP pathway. *Cell,* 146**,** 408-20.

PIRPOUR TAZEHKAND, A., AKBARZADEH, M., VELAIE, K., SADEGHI, M. R. & SAMADI, N. 2018. The role of Her2-Nrf2 axis in induction of oxaliplatin resistance in colon cancer cells. *Biomed Pharmacother,* 103**,** 755-766.

POPE, L. E. & DIXON, S. J. 2023. Regulation of ferroptosis by lipid metabolism. *Trends Cell Biol,* 33**,** 1077-1087.

POPULO, H., LOPES, J. M. & SOARES, P. 2012. The mTOR signalling pathway in human cancer. *Int J Mol Sci,* 13**,** 1886-1918.

PORSTMANN, T., SANTOS, C. R., GRIFFITHS, B., CULLY, M., WU, M., LEEVERS, S., GRIFFITHS, J. R., CHUNG, Y. L. & SCHULZE, A. 2008. SREBP activity is regulated by mTORC1 and contributes to Akt-dependent cell growth. *Cell Metab,* 8**,** 224-36.

QIN, S., HE, X., LIN, H., SCHULTE, B. A., ZHAO, M., TEW, K. D. & WANG, G. Y. 2021. Nrf2 inhibition sensitizes breast cancer stem cells to ionizing radiation via suppressing DNA repair. *Free Radic Biol Med,* 169**,** 238-247.

RADHAKRISHNAN, R. & VERMA, S. 2011. Clinically relevant imaging in tuberous sclerosis. *J Clin Imaging Sci,* 1**,** 39.

RAMLAUL, K. & AYLETT, C. H. S. 2018. Signal integration in the (m)TORC1 growth pathway. *Front Biol (Beijing),* 13**,** 237-262.

RHEE, S. G. & BAE, S. H. 2015. The antioxidant function of sestrins is mediated by promotion of autophagic degradation of Keap1 and Nrf2 activation and by inhibition of mTORC1. *Free Radic Biol Med,* 88**,** 205-211.

ROBLEDINOS-ANTON, N., FERNANDEZ-GINES, R., MANDA, G. & CUADRADO, A. 2019. Activators and Inhibitors of NRF2: A Review of Their Potential for Clinical Development. *Oxid Med Cell Longev,* 2019**,** 9372182.

ROCKFIELD, S., RAFFEL, J., MEHTA, R., REHMAN, N. & NANJUNDAN, M. 2017. Iron overload and altered iron metabolism in ovarian cancer. *Biol Chem,* 398**,** 995-1007.

ROH, J. L., KIM, E. H., JANG, H. & SHIN, D. 2017. Nrf2 inhibition reverses the resistance of cisplatin-resistant head and neck cancer cells to artesunate-induced ferroptosis. *Redox Biol,* 11**,** 254-262.

ROMERO, R., SAYIN, V. I., DAVIDSON, S. M., BAUER, M. R., SINGH, S. X., LEBOEUF, S. E., KARAKOUSI, T. R., ELLIS, D. C., BHUTKAR, A., SANCHEZ-RIVERA, F. J., SUBBARAJ, L., MARTINEZ, B., BRONSON, R. T., PRIGGE, J. R., SCHMIDT, E. E., THOMAS, C. J., GOPARAJU, C., DAVIES, A., DOLGALEV, I., HEGUY, A., ALLAJ, V., POIRIER, J. T., MOREIRA, A. L., RUDIN, C. M., PASS, H. I., VANDER HEIDEN, M. G., JACKS, T. &

PAPAGIANNAKOPOULOS, T. 2017. Keap1 loss promotes Kras-driven lung cancer and results in dependence on glutaminolysis. *Nat Med,* 23**,** 1362-1368.
SAHA, A., ZHAO, S., KINDALL, A., WILDER, C., FRIEDMAN, C. A., CLARK, R., GEORGIOU, G., STONE, E., KIDANE, D. & DIGIOVANNI, J. 2023. Cysteine depletion sensitizes prostate cancer cells to agents that enhance DNA damage and to immune checkpoint inhibition. *J Exp Clin Cancer Res,* 42**,** 119.
SAHA, S., BUTTARI, B., PANIERI, E., PROFUMO, E. & SASO, L. 2020. An Overview of Nrf2 Signaling Pathway and Its Role in Inflammation. *Molecules,* 25.
SAMUELS, Y., WANG, Z., BARDELLI, A., SILLIMAN, N., PTAK, J., SZABO, S., YAN, H., GAZDAR, A., POWELL, S. M., RIGGINS, G. J., WILLSON, J. K., MARKOWITZ, S., KINZLER, K. W., VOGELSTEIN, B. & VELCULESCU, V. E. 2004. High frequency of mutations of the PIK3CA gene in human cancers. *Science,* 304**,** 554.
SANCAK, Y., THOREEN, C. C., PETERSON, T. R., LINDQUIST, R. A., KANG, S. A., SPOONER, E., CARR, S. A. & SABATINI, D. M. 2007. PRAS40 is an insulin-regulated inhibitor of the mTORC1 protein kinase. *Mol Cell,* 25**,** 903-15.
SARBASSOV, D. D., ALI, S. M., KIM, D. H., GUERTIN, D. A., LATEK, R. R., ERDJUMENT-BROMAGE, H., TEMPST, P. & SABATINI, D. M. 2004. Rictor, a novel binding partner of mTOR, defines a rapamycin-insensitive and raptor-independent pathway that regulates the cytoskeleton. *Curr Biol,* 14**,** 1296-302.
SARBASSOV, D. D., ALI, S. M. & SABATINI, D. M. 2005a. Growing roles for the mTOR pathway. *Curr Opin Cell Biol,* 17**,** 596-603.
SARBASSOV, D. D., ALI, S. M., SENGUPTA, S., SHEEN, J. H., HSU, P. P., BAGLEY, A. F., MARKHARD, A. L. & SABATINI, D. M. 2006. Prolonged rapamycin treatment inhibits mTORC2 assembly and Akt/PKB. *Mol Cell,* 22**,** 159-68.
SARBASSOV, D. D., GUERTIN, D. A., ALI, S. M. & SABATINI, D. M. 2005b. Phosphorylation and regulation of Akt/PKB by the rictor-mTOR complex. *Science,* 307**,** 1098-101.
SATO, T., NAKASHIMA, A., GUO, L., COFFMAN, K. & TAMANOI, F. 2010. Single amino-acid changes that confer constitutive activation of mTOR are discovered in human cancer. *Oncogene,* 29**,** 2746-52.
SAXTON, R. A. & SABATINI, D. M. 2017. mTOR Signaling in Growth, Metabolism, and Disease. *Cell,* 168**,** 960-976.
SCARPELLINI, C., KLEJBOROWSKA, G., LANTHIER, C., HASSANNIA, B., VANDEN BERGHE, T. & AUGUSTYNS, K. 2023. Beyond ferrostatin-1: a comprehensive review of ferroptosis inhibitors. *Trends Pharmacol Sci,* 44**,** 902-916.
SCHALM, S. S., FINGAR, D. C., SABATINI, D. M. & BLENIS, J. 2003. TOS motif-mediated raptor binding regulates 4E-BP1 multisite phosphorylation and function. *Curr Biol,* 13**,** 797-806.
SCHNEIDER, A., YOUNIS, R. H. & GUTKIND, J. S. 2008. Hypoxia-induced energy stress inhibits the mTOR pathway by activating an AMPK/REDD1 signaling axis in head and neck squamous cell carcinoma. *Neoplasia,* 10**,** 1295-302.
SCHOTT, C., GRAAB, U., CUVELIER, N., HAHN, H. & FULDA, S. 2015. Oncogenic RAS Mutants Confer Resistance of RMS13 Rhabdomyosarcoma Cells to Oxidative Stress-Induced Ferroptotic Cell Death. *Front Oncol,* 5**,** 131.

SETO, B. 2012. Rapamycin and mTOR: a serendipitous discovery and implications for breast cancer. *Clin Transl Med,* 1**,** 29.
SHACKELFORD, D. B. & SHAW, R. J. 2009. The LKB1-AMPK pathway: metabolism and growth control in tumour suppression. *Nat Rev Cancer,* 9**,** 563-75.
SHADAD, A. K., SULLIVAN, F. J., MARTIN, J. D. & EGAN, L. J. 2013. Gastrointestinal radiation injury: prevention and treatment. *World J Gastroenterol,* 19**,** 199-208.
SHAW, R. J. & CANTLEY, L. C. 2006. Ras, PI(3)K and mTOR signalling controls tumour cell growth. *Nature,* 441**,** 424-30.
SHEN, Z., SONG, J., YUNG, B. C., ZHOU, Z., WU, A. & CHEN, X. 2018. Emerging Strategies of Cancer Therapy Based on Ferroptosis. *Adv Mater,* 30**,** e1704007.
SHI, Z., ZHENG, J., TANG, W., BAI, Y., ZHANG, L., XUAN, Z., SUN, H. & SHAO, C. 2022. Multifunctional Nanomaterials for Ferroptotic Cancer Therapy. *Front Chem,* 10**,** 868630.
SHIBATA, Y., YASUI, H., HIGASHIKAWA, K., MIYAMOTO, N. & KUGE, Y. 2019. Erastin, a ferroptosis-inducing agent, sensitized cancer cells to X-ray irradiation via glutathione starvation in vitro and in vivo. *PLoS One,* 14**,** e0225931.
SHIMADA, K., HAYANO, M., PAGANO, N. C. & STOCKWELL, B. R. 2016. Cell-Line Selectivity Improves the Predictive Power of Pharmacogenomic Analyses and Helps Identify NADPH as Biomarker for Ferroptosis Sensitivity. *Cell Chem Biol,* 23**,** 225-235.
SHIMOBAYASHI, M. & HALL, M. N. 2014. Making new contacts: the mTOR network in metabolism and signalling crosstalk. *Nat Rev Mol Cell Biol,* 15**,** 155-62.
SHIN, D., KIM, E. H., LEE, J. & ROH, J. L. 2018. Nrf2 inhibition reverses resistance to GPX4 inhibitor-induced ferroptosis in head and neck cancer. *Free Radic Biol Med,* 129**,** 454-462.
SHINTOKU, R., TAKIGAWA, Y., YAMADA, K., KUBOTA, C., YOSHIMOTO, Y., TAKEUCHI, T., KOSHIISHI, I. & TORII, S. 2017. Lipoxygenase-mediated generation of lipid peroxides enhances ferroptosis induced by erastin and RSL3. *Cancer Sci,* 108**,** 2187-2194.
SHOWKAT, M., BEIGH, M. A. & ANDRABI, K. I. 2014. mTOR Signaling in Protein Translation Regulation: Implications in Cancer Genesis and Therapeutic Interventions. *Mol Biol Int,* 2014**,** 686984.
SONENBERG, N. & GINGRAS, A. C. 1998. The mRNA 5' cap-binding protein eIF4E and control of cell growth. *Curr Opin Cell Biol,* 10**,** 268-75.
SONG, C., HEPING, H., SHEN, Y., JIN, S., LI, D., ZHANG, A., REN, X., WANG, K., ZHANG, L., WANG, J. & SHI, D. 2020a. AMPK/p38/Nrf2 activation as a protective feedback to restrain oxidative stress and inflammation in microglia stimulated with sodium fluoride. *Chemosphere,* 244**,** 125495.
SONG, X., WANG, X., LIU, Z. & YU, Z. 2020b. Role of GPX4-Mediated Ferroptosis in the Sensitivity of Triple Negative Breast Cancer Cells to Gefitinib. *Front Oncol,* 10**,** 597434.
SONG, X., ZHU, S., CHEN, P., HOU, W., WEN, Q., LIU, J., XIE, Y., LIU, J., KLIONSKY, D. J., KROEMER, G., LOTZE, M. T., ZEH, H. J., KANG, R. & TANG, D. 2018. AMPK-Mediated BECN1 Phosphorylation Promotes Ferroptosis by Directly Blocking System X(c)(-) Activity. *Curr Biol,* 28**,** 2388-2399 e5.

SRIVASTAVA, R., FERNANDEZ-GINES, R., ENCINAR, J. A., CUADRADO, A. & WELLS, G. 2022. The current status and future prospects for therapeutic targeting of KEAP1-NRF2 and beta-TrCP-NRF2 interactions in cancer chemoresistance. *Free Radic Biol Med,* 192**,** 246-260.

STERNBERG, C. N., YAGODA, A., BANDER, N. H., WHITMORE, W. F., JR., HUFFMAN, J. L., FLEISHER, M., MELAMED, M., FANUCCHI, M. P., HOLLANDER, P. & VAUGHAN, E. D., JR. 1986. Phase I/II trial of intravesical methotrexate for superficial bladder tumors. *Cancer Chemother Pharmacol,* 18**,** 265-9.

STOCKWELL, B. R., FRIEDMANN ANGELI, J. P., BAYIR, H., BUSH, A. I., CONRAD, M., DIXON, S. J., FULDA, S., GASCON, S., HATZIOS, S. K., KAGAN, V. E., NOEL, K., JIANG, X., LINKERMANN, A., MURPHY, M. E., OVERHOLTZER, M., OYAGI, A., PAGNUSSAT, G. C., PARK, J., RAN, Q., ROSENFELD, C. S., SALNIKOW, K., TANG, D., TORTI, F. M., TORTI, S. V., TOYOKUNI, S., WOERPEL, K. A. & ZHANG, D. D. 2017. Ferroptosis: A Regulated Cell Death Nexus Linking Metabolism, Redox Biology, and Disease. *Cell,* 171**,** 273-285.

SUI, S., ZHANG, J., XU, S., WANG, Q., WANG, P. & PANG, D. 2019. Ferritinophagy is required for the induction of ferroptosis by the bromodomain protein BRD4 inhibitor (+)-JQ1 in cancer cells. *Cell Death Dis,* 10**,** 331.

SUI, X., ZHANG, R., LIU, S., DUAN, T., ZHAI, L., ZHANG, M., HAN, X., XIANG, Y., HUANG, X., LIN, H. & XIE, T. 2018. RSL3 Drives Ferroptosis Through GPX4 Inactivation and ROS Production in Colorectal Cancer. *Front Pharmacol,* 9**,** 1371.

SULAIMANOV, N., KLOSE, M., BUSCH, H. & BOERRIES, M. 2017. Understanding the mTOR signaling pathway via mathematical modeling. *Wiley Interdiscip Rev Syst Biol Med,* 9.

SUN, B., ZHENG, X., ZHANG, X., ZHANG, H. & JIANG, Y. 2024. Oxaliplatin-Loaded Mil-100(Fe) for Chemotherapy-Ferroptosis Combined Therapy for Gastric Cancer. *ACS Omega,* 9**,** 16676-16686.

SUN, L., WANG, H., LIU, Q., MENG, F., ZHANG, J., LI, X., CHANG, S., LI, G. & CHEN, F. 2023a. Camptothecin improves sorafenib sensitivity by inhibiting Nrf2-ARE pathway in hepatocellular carcinoma. *Oncol Rep,* 49.

SUN, S., SHEN, J., JIANG, J., WANG, F. & MIN, J. 2023b. Targeting ferroptosis opens new avenues for the development of novel therapeutics. *Signal Transduct Target Ther,* 8**,** 372.

SUN, X., NIU, X., CHEN, R., HE, W., CHEN, D., KANG, R. & TANG, D. 2016a. Metallothionein-1G facilitates sorafenib resistance through inhibition of ferroptosis. *Hepatology,* 64**,** 488-500.

SUN, X., OU, Z., CHEN, R., NIU, X., CHEN, D., KANG, R. & TANG, D. 2016b. Activation of the p62-Keap1-NRF2 pathway protects against ferroptosis in hepatocellular carcinoma cells. *Hepatology,* 63**,** 173-84.

SUN, X., OU, Z., XIE, M., KANG, R., FAN, Y., NIU, X., WANG, H., CAO, L. & TANG, D. 2015. HSPB1 as a novel regulator of ferroptotic cancer cell death. *Oncogene,* 34**,** 5617-25.

SUN, Y., ZHAO, D., WANG, G., WANG, Y., CAO, L., SUN, J., JIANG, Q. & HE, Z. 2020. Recent progress of hypoxia-modulated multifunctional nanomedicines to enhance

photodynamic therapy: opportunities, challenges, and future development. *Acta Pharm Sin B,* 10**,** 1382-1396.
TAGUCHI, K. & YAMAMOTO, M. 2017. The KEAP1-NRF2 System in Cancer. *Front Oncol,* 7**,** 85.
TALTY, R. & BOSENBERG, M. 2022. The role of ferroptosis in melanoma. *Pigment Cell Melanoma Res,* 35**,** 18-25.
TANG, D., CHEN, X., KANG, R. & KROEMER, G. 2021. Ferroptosis: molecular mechanisms and health implications. *Cell Res,* 31**,** 107-125.
TANG, D., KANG, R., BERGHE, T. V., VANDENABEELE, P. & KROEMER, G. 2019. The molecular machinery of regulated cell death. *Cell Res,* 29**,** 347-364.
TAPIA-VALLADARES, C., VALENZUELA, G., GONZALEZ, E., MAUREIRA, I., TORO, J., FREIRE, M., SEPULVEDA-HERMOSILLA, G., AMPUERO, D., BLANCO, A., GALLEGOS, I., MORALES, F., ERICES, J. I., BARAJAS, O., AHUMADA, M., CONTRERAS, H. R., GONZALEZ, J., ARMISEN, R. & MARCELAIN, K. 2024. Distinct Driver Pathway Enrichments and a High Prevalence of TSC2 Mutations in Right Colon Cancer in Chile: A Preliminary Comparative Analysis. *Int J Mol Sci,* 25.
TARANGELO, A. & DIXON, S. 2018. The p53-p21 pathway inhibits ferroptosis during metabolic stress. *Oncotarget,* 9**,** 24572-24573.
TEE, A. R., FINGAR, D. C., MANNING, B. D., KWIATKOWSKI, D. J., CANTLEY, L. C. & BLENIS, J. 2002. Tuberous sclerosis complex-1 and -2 gene products function together to inhibit mammalian target of rapamycin (mTOR)-mediated downstream signaling. *Proc Natl Acad Sci U S A,* 99**,** 13571-6.
TEE, A. R., SAMPSON, J. R., PAL, D. K. & BATEMAN, J. M. 2016. The role of mTOR signalling in neurogenesis, insights from tuberous sclerosis complex. *Semin Cell Dev Biol,* 52**,** 12-20.
THIELE, E. A., BEBIN, E. M., FILLOUX, F., KWAN, P., LOFTUS, R., SAHEBKAR, F., SPARAGANA, S. & WHELESS, J. 2022. Long-term cannabidiol treatment for seizures in patients with tuberous sclerosis complex: An open-label extension trial. *Epilepsia,* 63**,** 426-439.
THORNTON, C. C., AL-RASHED, F., CALAY, D., BIRDSEY, G. M., BAUER, A., MYLROIE, H., MORLEY, B. J., RANDI, A. M., HASKARD, D. O., BOYLE, J. J. & MASON, J. C. 2016. Methotrexate-mediated activation of an AMPK-CREB-dependent pathway: a novel mechanism for vascular protection in chronic systemic inflammation. *Ann Rheum Dis,* 75**,** 439-48.
TIAN, X., LI, X., PAN, M., YANG, L. Z., LI, Y. & FANG, W. 2024. Progress of Ferroptosis in Ischemic Stroke and Therapeutic Targets. *Cell Mol Neurobiol,* 44**,** 25.
TIAN, Z., YANG, Y., WU, H., CHEN, Y., JIA, H., ZHU, L., HE, R., JIN, Y., ZHOU, B., GE, C., SUN, Y. & YANG, Y. 2022. The Nrf2 inhibitor brusatol synergistically enhances the cytotoxic effect of lapatinib in HER2-positive cancers. *Heliyon,* 8**,** e10410.
TIMPERI, E. & ROMANO, E. 2023. Stromal circuits involving tumor-associated macrophages and cancer-associated fibroblasts. *Front Immunol,* 14**,** 1194642.
TORRENCE, M. E., MACARTHUR, M. R., HOSIOS, A. M., VALVEZAN, A. J., ASARA, J. M., MITCHELL, J. R. & MANNING, B. D. 2021. The mTORC1-mediated

activation of ATF4 promotes protein and glutathione synthesis downstream of growth signals. *Elife,* 10.

TUNGSUKRUTHAI, S., REAMTONG, O., ROYTRAKUL, S., SUKRONG, S., VINAYANWATTIKUN, C. & CHANVORACHOTE, P. 2021. Targeting AKT/mTOR and Bcl-2 for Autophagic and Apoptosis Cell Death in Lung Cancer: Novel Activity of a Polyphenol Compound. *Antioxidants (Basel),* 10.

UNNI, N. & ARTEAGA, C. L. 2019. Is Dual mTORC1 and mTORC2 Therapeutic Blockade Clinically Feasible in Cancer? *JAMA Oncol,* 5**,** 1564-1565.

VILLAR, V. H., NGUYEN, T. L., DELCROIX, V., TERES, S., BOUCHECAREILH, M., SALIN, B., BODINEAU, C., VACHER, P., PRIAULT, M., SOUBEYRAN, P. & DURAN, R. V. 2017. mTORC1 inhibition in cancer cells protects from glutaminolysis-mediated apoptosis during nutrient limitation. *Nat Commun,* 8**,** 14124.

VIVANCO, I. & SAWYERS, C. L. 2002. The phosphatidylinositol 3-Kinase AKT pathway in human cancer. *Nat Rev Cancer,* 2**,** 489-501.

WANG, H., AN, P., XIE, E., WU, Q., FANG, X., GAO, H., ZHANG, Z., LI, Y., WANG, X., ZHANG, J., LI, G., YANG, L., LIU, W., MIN, J. & WANG, F. 2017. Characterization of ferroptosis in murine models of hemochromatosis. *Hepatology,* 66**,** 449-465.

WANG, H., CHENG, Q., BAO, L., LI, M., CHANG, K. & YI, X. 2023a. Cytoprotective Role of Heme Oxygenase-1 in Cancer Chemoresistance: Focus on Antioxidant, Antiapoptotic, and Pro-Autophagy Properties. *Antioxidants (Basel),* 12.

WANG, H., PENG, S., CAI, J. & BAO, S. 2021. Silencing of PTPN18 Induced Ferroptosis in Endometrial Cancer Cells Through p-P38-Mediated GPX4/xCT Down-Regulation. *Cancer Manag Res,* 13**,** 1757-1765.

WANG, H., YU, X., LIU, D., QIAO, Y., HUO, J., PAN, S., ZHOU, L., WANG, R., FENG, Q. & LIU, Z. 2024a. VDR Activation Attenuates Renal Tubular Epithelial Cell Ferroptosis by Regulating Nrf2/HO-1 Signaling Pathway in Diabetic Nephropathy. *Adv Sci (Weinh),* 11**,** e2305563.

WANG, H. T., JU, J., WANG, S. C., ZHANG, Y. H., LIU, C. Y., WANG, T., YU, X., WANG, F., CHENG, X. R., WANG, K. & CHEN, Z. Y. 2022a. Insights Into Ferroptosis, a Novel Target for the Therapy of Cancer. *Front Oncol,* 12**,** 812534.

WANG, L., CHEN, X. & YAN, C. 2022b. Ferroptosis: An emerging therapeutic opportunity for cancer. *Genes Dis,* 9**,** 334-346.

WANG, L., WU, J., LU, J., MA, R., SUN, D. & TANG, J. 2015. Regulation of the cell cycle and PI3K/Akt/mTOR signaling pathway by tanshinone I in human breast cancer cell lines. *Mol Med Rep,* 11**,** 931-9.

WANG, W., GREEN, M., CHOI, J. E., GIJON, M., KENNEDY, P. D., JOHNSON, J. K., LIAO, P., LANG, X., KRYCZEK, I., SELL, A., XIA, H., ZHOU, J., LI, G., LI, J., LI, W., WEI, S., VATAN, L., ZHANG, H., SZELIGA, W., GU, W., LIU, R., LAWRENCE, T. S., LAMB, C., TANNO, Y., CIESLIK, M., STONE, E., GEORGIOU, G., CHAN, T. A., CHINNAIYAN, A. & ZOU, W. 2019. CD8(+) T cells regulate tumour ferroptosis during cancer immunotherapy. *Nature,* 569**,** 270-274.

WANG, X., TAN, X., ZHANG, J., WU, J. & SHI, H. 2023b. The emerging roles of MAPK-AMPK in ferroptosis regulatory network. *Cell Commun Signal,* 21**,** 200.

WANG, Y., WEI, J., LI, L., FAN, C. & SUN, Y. 2014. Combined Use of Metformin and Everolimus Is Synergistic in the Treatment of Breast Cancer Cells. *Oncol Res,* 22**,** 193-201.

WANG, Z., ZONG, H., LIU, W., LIN, W., SUN, A., DING, Z., CHEN, X., WAN, X., LIU, Y., HU, Z., ZHANG, H., LI, H., LIU, Y., LI, D., ZHANG, S. & ZHA, X. 2024b. Augmented ERO1alpha upon mTORC1 activation induces ferroptosis resistance and tumor progression via upregulation of SLC7A11. *J Exp Clin Cancer Res,* 43**,** 112.

WANG, Z. Q., ZHANG, Z. C., WU, Y. Y., PI, Y. N., LOU, S. H., LIU, T. B., LOU, G. & YANG, C. 2023c. Bromodomain and extraterminal (BET) proteins: biological functions, diseases, and targeted therapy. *Signal Transduct Target Ther,* 8**,** 420.

WATAYA-KANEDA, M. 2015. Mammalian target of rapamycin and tuberous sclerosis complex. *J Dermatol Sci,* 79**,** 93-100.

WEI, S., QIU, T., YAO, X., WANG, N., JIANG, L., JIA, X., TAO, Y., WANG, Z., PEI, P., ZHANG, J., ZHU, Y., YANG, G., LIU, X., LIU, S. & SUN, X. 2020. Arsenic induces pancreatic dysfunction and ferroptosis via mitochondrial ROS-autophagy-lysosomal pathway. *J Hazard Mater,* 384**,** 121390.

WEI, T. T., ZHANG, M. Y., ZHENG, X. H., XIE, T. H., WANG, W., ZOU, J., LI, Y., LI, H. Y., CAI, J., WANG, X., TAN, J., YANG, X., YAO, Y. & ZHU, L. 2022. Interferon-gamma induces retinal pigment epithelial cell Ferroptosis by a JAK1-2/STAT1/SLC7A11 signaling pathway in Age-related Macular Degeneration. *FEBS J,* 289**,** 1968-1983.

WENZEL, S. E., TYURINA, Y. Y., ZHAO, J., ST CROIX, C. M., DAR, H. H., MAO, G., TYURIN, V. A., ANTHONYMUTHU, T. S., KAPRALOV, A. A., AMOSCATO, A. A., MIKULSKA-RUMINSKA, K., SHRIVASTAVA, I. H., KENNY, E. M., YANG, Q., ROSENBAUM, J. C., SPARVERO, L. J., EMLET, D. R., WEN, X., MINAMI, Y., QU, F., WATKINS, S. C., HOLMAN, T. R., VANDEMARK, A. P., KELLUM, J. A., BAHAR, I., BAYIR, H. & KAGAN, V. E. 2017. PEBP1 Wardens Ferroptosis by Enabling Lipoxygenase Generation of Lipid Death Signals. *Cell,* 171**,** 628-641 e26.

WONG, K. H., YANG, D., CHEN, S., HE, C. & CHEN, M. 2022. Development of nanoscale drug delivery systems of dihydroartemisinin for cancer therapy: A review. *Asian J Pharm Sci,* 17**,** 475-490.

WU, Y. C., HUANG, C. S., HSIEH, M. S., HUANG, C. M., SETIAWAN, S. A., YEH, C. T., KUO, K. T. & LIU, S. C. 2024. Targeting of FSP1 regulates iron homeostasis in drug-tolerant persister head and neck cancer cells via lipid-metabolism-driven ferroptosis. *Aging (Albany NY),* 16**,** 627-647.

WU, Z., KHODADE, V. S., CHAUVIN, J. R., RODRIGUEZ, D., TOSCANO, J. P. & PRATT, D. A. 2022. Hydropersulfides Inhibit Lipid Peroxidation and Protect Cells from Ferroptosis. *J Am Chem Soc,* 144**,** 15825-15837.

XAVIER DA SILVA, T. N., SCHULTE, C., ALVES, A. N., MARIC, H. M. & FRIEDMANN ANGELI, J. P. 2023. Molecular characterization of AIFM2/FSP1 inhibition by iFSP1-like molecules. *Cell Death Dis,* 14**,** 281.

XU, Z., XIE, Y., MAO, Y., HUANG, J., MEI, X., SONG, J., SUN, Y., YAO, Z. & SHI, W. 2021. Ferroptosis-Related Gene Signature Predicts the Prognosis of Skin Cutaneous Melanoma and Response to Immunotherapy. *Front Genet,* 12**,** 758981.

YAMAGUCHI, Y., KASUKABE, T. & KUMAKURA, S. 2018. Piperlongumine rapidly induces the death of human pancreatic cancer cells mainly through the induction of ferroptosis. *Int J Oncol,* 52**,** 1011-1022.

YAMAKADO, K., TANAKA, N., NAKAGAWA, T., KOBAYASHI, S., YANAGAWA, M. & TAKEDA, K. 2002. Renal angiomyolipoma: relationships between tumor size, aneurysm formation, and rupture. *Radiology,* 225**,** 78-82.

YAMASAKI, M., MIYATA, H., FUJIWARA, Y., TAKIGUCHI, S., NAKAJIMA, K., NISHIDA, T., YASUDA, T., MATSUYAMA, J., MORI, M. & DOKI, Y. 2010. p53 genotype predicts response to chemotherapy in patients with squamous cell carcinoma of the esophagus. *Ann Surg Oncol,* 17**,** 634-42.

YAN, H. F., ZOU, T., TUO, Q. Z., XU, S., LI, H., BELAIDI, A. A. & LEI, P. 2021. Ferroptosis: mechanisms and links with diseases. *Signal Transduct Target Ther,* 6**,** 49.

YANG, J., MO, J., DAI, J., YE, C., CEN, W., ZHENG, X., JIANG, L. & YE, L. 2021a. Cetuximab promotes RSL3-induced ferroptosis by suppressing the Nrf2/HO-1 signalling pathway in KRAS mutant colorectal cancer. *Cell Death Dis,* 12**,** 1079.

YANG, W., LIU, X., SONG, C., JI, S., YANG, J., LIU, Y., YOU, J., ZHANG, J., HUANG, S., CHENG, W., SHAO, Z., LI, L. & YANG, S. 2021b. Structure-activity relationship studies of phenothiazine derivatives as a new class of ferroptosis inhibitors together with the therapeutic effect in an ischemic stroke model. *Eur J Med Chem,* 209**,** 112842.

YANG, W. S., KIM, K. J., GASCHLER, M. M., PATEL, M., SHCHEPINOV, M. S. & STOCKWELL, B. R. 2016. Peroxidation of polyunsaturated fatty acids by lipoxygenases drives ferroptosis. *Proc Natl Acad Sci U S A,* 113**,** E4966-75.

YANG, W. S., SRIRAMARATNAM, R., WELSCH, M. E., SHIMADA, K., SKOUTA, R., VISWANATHAN, V. S., CHEAH, J. H., CLEMONS, P. A., SHAMJI, A. F., CLISH, C. B., BROWN, L. M., GIROTTI, A. W., CORNISH, V. W., SCHREIBER, S. L. & STOCKWELL, B. R. 2014. Regulation of ferroptotic cancer cell death by GPX4. *Cell,* 156**,** 317-331.

YANG, W. S. & STOCKWELL, B. R. 2008. Synthetic lethal screening identifies compounds activating iron-dependent, nonapoptotic cell death in oncogenic-RAS-harboring cancer cells. *Chem Biol,* 15**,** 234-45.

YANG, W. S. & STOCKWELL, B. R. 2016. Ferroptosis: Death by Lipid Peroxidation. *Trends Cell Biol,* 26**,** 165-176.

YANG, Y., LU, Y., ZHANG, C., GUO, Q., ZHANG, W., WANG, T., XIA, Z., LIU, J., CHENG, X., XI, T., JIANG, F. & ZHENG, L. 2022. Phenazine derivatives attenuate the stemness of breast cancer cells through triggering ferroptosis. *Cell Mol Life Sci,* 79**,** 360.

YANGYUN, W., GUOWEI, S., SHUFEN, S., JIE, Y., RUI, Y. & YU, R. 2022. Everolimus accelerates Erastin and RSL3-induced ferroptosis in renal cell carcinoma. *Gene,* 809**,** 145992.

YAO, X., XIE, R., CAO, Y., TANG, J., MEN, Y., PENG, H. & YANG, W. 2021. Simvastatin induced ferroptosis for triple-negative breast cancer therapy. *J Nanobiotechnology,* 19**,** 311.

YE, L., VARAMINI, B., LAMMING, D. W., SABATINI, D. M. & BAUR, J. A. 2012. Rapamycin has a biphasic effect on insulin sensitivity in C2C12 myotubes due to sequential disruption of mTORC1 and mTORC2. *Front Genet,* 3**,** 177.

YI, J., ZHU, J., WU, J., THOMPSON, C. B. & JIANG, X. 2020. Oncogenic activation of PI3K-AKT-mTOR signaling suppresses ferroptosis via SREBP-mediated lipogenesis. *Proc Natl Acad Sci U S A,* 117**,** 31189-31197.

YOSHIOKA, R., FUJIEDA, Y., SUZUKI, Y., KANNO, O., NAGAHIRA, A., HONDA, T., MURAKAWA, M. & YUKIURA, H. 2019. Novel mouse model for evaluating in vivo efficacy of xCT inhibitor. *J Pharmacol Sci,* 140**,** 242-247.

YU, H., YAN, J., LI, Z., YANG, L., JU, F. & SUN, Y. 2023. Recent trends in emerging strategies for ferroptosis-based cancer therapy. *Nanoscale Adv,* 5**,** 1271-1290.

YU, H., YANG, C., JIAN, L., GUO, S., CHEN, R., LI, K., QU, F., TAO, K., FU, Y., LUO, F. & LIU, S. 2019. Sulfasalazine-induced ferroptosis in breast cancer cells is reduced by the inhibitory effect of estrogen receptor on the transferrin receptor. *Oncol Rep,* 42**,** 826-838.

YU, Z., CHEN, J., TAKAGI, E., WANG, F., SAHA, B., LIU, X., JOUBERT, L. M., GLEASON, C. E., JIN, M., LI, C., NOWOTNY, C., AGARD, D., CHENG, Y. & PEARCE, D. 2022. Interactions between mTORC2 core subunits Rictor and mSin1 dictate selective and context-dependent phosphorylation of substrate kinases SGK1 and Akt. *J Biol Chem,* 298**,** 102288.

YUAN, F., SUN, Q., ZHANG, S., YE, L., XU, Y., DENG, G., XU, Z., ZHANG, S., LIU, B. & CHEN, Q. 2022. The dual role of p62 in ferroptosis of glioblastoma according to p53 status. *Cell Biosci,* 12**,** 20.

YUAN, H., LI, X., ZHANG, X., KANG, R. & TANG, D. 2016. Identification of ACSL4 as a biomarker and contributor of ferroptosis. *Biochem Biophys Res Commun,* 478**,** 1338-43.

ZAREI, M., DU, H., NASSAR, A. H., YAN, R. E., GIANNIKOU, K., JOHNSON, S. H., LAM, H. C., HENSKE, E. P., WANG, Y., ZHANG, T., ASARA, J. & KWIATKOWSKI, D. J. 2019. Tumors with TSC mutations are sensitive to CDK7 inhibition through NRF2 and glutathione depletion. *J Exp Med,* 216**,** 2635-2652.

ZERBATO, B., GOBBI, M., LUDWIG, T., BRANCATO, V., PESSINA, A., BRAMBILLA, L., WEGNER, A. & CHIARADONNA, F. 2023. PGM3 inhibition shows cooperative effects with erastin inducing pancreatic cancer cell death via activation of the unfolded protein response. *Front Oncol,* 13**,** 1125855.

ZHANG, B., CHEN, X., RU, F., GAN, Y., LI, B., XIA, W., DAI, G., HE, Y. & CHEN, Z. 2021a. Liproxstatin-1 attenuates unilateral ureteral obstruction-induced renal fibrosis by inhibiting renal tubular epithelial cells ferroptosis. *Cell Death Dis,* 12**,** 843.

ZHANG, C., LIU, X., JIN, S., CHEN, Y. & GUO, R. 2022a. Ferroptosis in cancer therapy: a novel approach to reversing drug resistance. *Mol Cancer,* 21**,** 47.

ZHANG, J., GAO, Z., YIN, J., QUON, M. J. & YE, J. 2008. S6K directly phosphorylates IRS-1 on Ser-270 to promote insulin resistance in response to TNF-(alpha) signaling through IKK2. *J Biol Chem,* 283**,** 35375-82.

ZHANG, K., HU, W. H., ZHANG, C., MENG, F. G., CHEN, N. & ZHANG, J. G. 2013. Predictors of seizure freedom after surgical management of tuberous sclerosis complex: a systematic review and meta-analysis. *Epilepsy Res,* 105**,** 377-83.

ZHANG, X., GUO, Y., LI, H. & HAN, L. 2021b. FIN56, a novel ferroptosis inducer, triggers lysosomal membrane permeabilization in a TFEB-dependent manner in glioblastoma. *J Cancer,* 12**,** 6610-6619.

ZHANG, X., LI, X., ZHENG, C., YANG, C., ZHANG, R., WANG, A., FENG, J., HU, X., CHANG, S. & ZHANG, H. 2022b. Ferroptosis, a new form of cell death defined after radiation exposure. *Int J Radiat Biol,* 98**,** 1201-1209.

ZHANG, X., SUI, S., WANG, L., LI, H., ZHANG, L., XU, S. & ZHENG, X. 2020. Inhibition of tumor propellant glutathione peroxidase 4 induces ferroptosis in cancer cells and enhances anticancer effect of cisplatin. *J Cell Physiol,* 235**,** 3425-3437.

ZHANG, Y., SWANDA, R. V., NIE, L., LIU, X., WANG, C., LEE, H., LEI, G., MAO, C., KOPPULA, P., CHENG, W., ZHANG, J., XIAO, Z., ZHUANG, L., FANG, B., CHEN, J., QIAN, S. B. & GAN, B. 2021c. mTORC1 couples cyst(e)ine availability with GPX4 protein synthesis and ferroptosis regulation. *Nat Commun,* 12**,** 1589.

ZHANG, Y., TAN, H., DANIELS, J. D., ZANDKARIMI, F., LIU, H., BROWN, L. M., UCHIDA, K., O'CONNOR, O. A. & STOCKWELL, B. R. 2019. Imidazole Ketone Erastin Induces Ferroptosis and Slows Tumor Growth in a Mouse Lymphoma Model. *Cell Chem Biol,* 26**,** 623-633 e9.

ZHAO, H., JI, B., CHEN, J., HUANG, Q. & LU, X. 2017. Gpx 4 is involved in the proliferation, migration and apoptosis of glioma cells. *Pathol Res Pract,* 213**,** 626-633.

ZHAO, J., XU, B., XIONG, Q., FENG, Y. & DU, H. 2021a. Erastin-induced ferroptosis causes physiological and pathological changes in healthy tissues of mice. *Mol Med Rep,* 24.

ZHAO, S., GUO, Y. & YIN, X. 2023a. Lipid Peroxidation in Ferroptosis and Association with Nonalcoholic Fatty Liver Disease. *Front Biosci (Landmark Ed),* 28**,** 332.

ZHAO, Y., JIANG, B., HUANG, D., LOU, J., LI, G., LIU, J., DUAN, F., YUAN, Y. & SU, X. 2023b. Ferrostatin-1 post-treatment attenuates acute kidney injury in mice by inhibiting ferritin production and regulating iron uptake-related proteins. *PeerJ,* 11**,** e15786.

ZHAO, Y., LI, Y., ZHANG, R., WANG, F., WANG, T. & JIAO, Y. 2020. The Role of Erastin in Ferroptosis and Its Prospects in Cancer Therapy. *Onco Targets Ther,* 13**,** 5429-5441.

ZHAO, Y., LU, J., MAO, A., ZHANG, R. & GUAN, S. 2021b. Autophagy Inhibition Plays a Protective Role in Ferroptosis Induced by Alcohol via the p62-Keap1-Nrf2 Pathway. *J Agric Food Chem,* 69**,** 9671-9683.

ZHAO, Y., YE, X., XIONG, Z., IHSAN, A., ARES, I., MARTINEZ, M., LOPEZ-TORRES, B., MARTINEZ-LARRANAGA, M. R., ANADON, A., WANG, X. & MARTINEZ, M. A. 2023c. Cancer Metabolism: The Role of ROS in DNA Damage and Induction of Apoptosis in Cancer Cells. *Metabolites,* 13.

ZHENG, J., SATO, M., MISHIMA, E., SATO, H., PRONETH, B. & CONRAD, M. 2021. Sorafenib fails to trigger ferroptosis across a wide range of cancer cell lines. *Cell Death Dis,* 12**,** 698.

ZHONG, Y., TIAN, F., MA, H., WANG, H., YANG, W., LIU, Z. & LIAO, A. 2020. FTY720 induces ferroptosis and autophagy via PP2A/AMPK pathway in multiple myeloma cells. *Life Sci,* 260**,** 118077.

ZHOU, G., MYERS, R., LI, Y., CHEN, Y., SHEN, X., FENYK-MELODY, J., WU, M., VENTRE, J., DOEBBER, T., FUJII, N., MUSI, N., HIRSHMAN, M. F., GOODYEAR, L. J. & MOLLER, D. E. 2001. Role of AMP-activated protein kinase in mechanism of metformin action. *J Clin Invest,* 108**,** 1167-74.

ZHOU, H. & HUANG, S. 2010. The complexes of mammalian target of rapamycin. *Curr Protein Pept Sci,* 11**,** 409-24.

ZHOU, H., LIU, Q., ZHANG, J., YAO, J., WANG, C., ZHANG, Y., LI, Y., ZHANG, X. & ZHANG, L. 2020. Cytochrome P450-Mediated Bioactivation: Implication for the Liver Injury Induced by Fraxinellone, A Bioactive Constituent from Dictamni Cortex. *Chem Res Toxicol,* 33**,** 1960-1968.

ZHOU, Y., CHEN, Y., SHI, Y., WU, L., TAN, Y., LI, T., CHEN, Y., XIA, J. & HU, R. 2023. FAM117B promotes gastric cancer growth and drug resistance by targeting the KEAP1/NRF2 signaling pathway. *J Clin Invest,* 133.

ZHOU, Y., WANG, Y., ZHOU, W., CHEN, T., WU, Q., CHUTTURGHOON, V. K., LIN, B., GENG, L., YANG, Z., ZHOU, L. & ZHENG, S. 2019. YAP promotes multi-drug resistance and inhibits autophagy-related cell death in hepatocellular carcinoma via the RAC1-ROS-mTOR pathway. *Cancer Cell Int,* 19**,** 179.

ZHU, J., WANG, H. & JIANG, X. 2022a. mTORC1 beyond anabolic metabolism: Regulation of cell death. *J Cell Biol,* 221.

ZHU, X., ZHANG, Y., WU, Y., DIAO, W., DENG, G., LI, Q. & WU, C. 2022b. HMOX1 Attenuates the Sensitivity of Hepatocellular Carcinoma Cells to Sorafenib via Modulating the Expression of ABC Transporters. *Int J Genomics,* 2022**,** 9451557.

ZHU, Y., FUJIMAKI, M., SNAPE, L., LOPEZ, A., FLEMING, A. & RUBINSZTEIN, D. C. 2024. Loss of WIPI4 in neurodegeneration causes autophagy-independent ferroptosis. *Nat Cell Biol,* 26**,** 542-551.

ZILKA, O., POON, J. F. & PRATT, D. A. 2021. Radical-Trapping Antioxidant Activity of Copper and Nickel Bis(Thiosemicarbazone) Complexes Underlies Their Potency as Inhibitors of Ferroptotic Cell Death. *J Am Chem Soc,* 143**,** 19043-19057.

ZILKA, O., SHAH, R., LI, B., FRIEDMANN ANGELI, J. P., GRIESSER, M., CONRAD, M. & PRATT, D. A. 2017. On the Mechanism of Cytoprotection by Ferrostatin-1 and Liproxstatin-1 and the Role of Lipid Peroxidation in Ferroptotic Cell Death. *ACS Cent Sci,* 3**,** 232-243.

ZIMMER, T. S., CIRIMINNA, G., ARENA, A., ANINK, J. J., KOROTKOV, A., JANSEN, F. E., VAN HECKE, W., SPLIET, W. G., VAN RIJEN, P. C., BAAYEN, J. C., IDEMA, S., RENSING, N. R., WONG, M., MILLS, J. D., VAN VLIET, E. A. & ARONICA, E. 2020. Chronic activation of anti-oxidant pathways and iron accumulation in epileptogenic malformations. *Neuropathol Appl Neurobiol,* 46**,** 546-563.

ZOU, Y., PALTE, M. J., DEIK, A. A., LI, H., EATON, J. K., WANG, W., TSENG, Y. Y., DEASY, R., KOST-ALIMOVA, M., DANCIK, V., LESHCHINER, E. S., VISWANATHAN, V. S., SIGNORETTI, S., CHOUEIRI, T. K., BOEHM, J. S., WAGNER, B. K., DOENCH, J. G., CLISH, C. B., CLEMONS, P. A. & SCHREIBER, S. L. 2019. A GPX4-dependent cancer cell state underlies the clear-cell morphology and confers sensitivity to ferroptosis. *Nat Commun,* 10**,** 1617.